Squaramide-Naphthalimide Conjugates as Potential Self-Assembled Materials and as DNA Binders.

A thesis submitted to the National University of Ireland in fulfilment of the requirements for the degree of

Master of Science

By

Ales Grundzi, B.Sc.

Department of Chemistry,

Maynooth University,

Maynooth, Co. Kildare,

Ireland.

2021

Research Supervisor: Dr. Robert Elmes

Head of Department: Prof. Denise Rooney

Declaration

I hereby certify that this thesis has not been submitted before, in whole or in part, to this or any university for any degree and is, except where otherwise stated, the original work of the author.

Signed:  _____ Date:16/04/2021_____

Maynooth University

Acknowledgements

First of all, I would like to thank my supervisor Dr. Robert Elmes for accepting me to do this project with his support, encouragement and knowledge in the past two years. This project would not have been made possible without his continuous help, reassurance and patience. He was very helpful, even during the most challenging moments in this research project.

I would also like to thank all member of the Elmes research group, Luke Marchetti, Luke Brennan, Conor Geraghty, Conor Wynne, Oisín Kavanagh and Hua Tong – thank you all for the good chats and endless laughs that kept me sane even during the most challenging moments in the laboratory. Wishing you all the best in the future!

Thank you to the all postgrads, past and present, including: Muhib, Harlei, Amanda, Kyle, Eoin, Clara, Sinead, Darren, Aoife, Jessica, Kobi, Caytlin, Jason, Grace, Colm, Stephen, Alessandro, Paddy and Lokesh for making my time in the chemistry department an enjoyable and pleasant experience! If I were to include everyone, the list would be endless as there are so many people to thank.

Thanks to all of the academic and technical staff in the department including: Ollie, Barbara, Walter, Anne, Karen, Donna and Carol for their advice and support whenever I needed anything, including chemicals or training. I would especially like to thank Ria for always providing me with anything I needed in the laboratory. I would also like to thank Noel for fixing my computer when I was running tests and I would also like to thank him for always fixing up trolleys whenever we had to perform a solvent run.

I would like to thank my family, especially my parents for their endless emotional, financial and moral support. Thank you so much for always believing in me! This project would not have been possible without you! They were always there for me when I needed care and support. It always makes me happy that you are proud of me as your son.

Last but definitely not least, I would like to thank my girlfriend Holly who was by my side since day one when I started this research project. She always provided me with endless support, understanding and love. She always made sure that I ate healthy and was there for me no matter what and encouraged me to never give up!

Summary

This thesis entitled 'Squaramide-Naphthalimide Conjugates as Potential Self-Assembled Materials and as DNA Binders' is divided in 7 chapters. Chapter 1 presents an introduction to DNA, its function and structure. Various DNA binders were introduced in this section, specifically currently studied naphthalimides as DNA intercalators, with potential as possible treatments for various types of cancers. The H-bonding ability of squaramide and its potential as a DNA binder to the negatively charged sugar phosphate backbone was discussed. Bis-intercalators were also described in detail and their strong DNA bis-intercalating ability was also discussed. The proposed target bis-intercalators were introduced, with multiple modes of binding to DNA, where the naphthalimide moieties would bis-intercalate into DNA, while the squaramide would bind to the negatively charged sugar phosphate backbone of DNA.

In Chapter 2, the design and synthesis of novel compounds are discussed. The syntheses of the desired compounds, the challenges encountered during synthesis and the change in the design of the desired compounds was also described. Each compound was characterised with room temperature NMR and it was concluded that after VT-NMR studies were performed, which clearly indicated self-assembly properties of these novel compounds.

Chapter 3 describes the self-assembly properties of the novel squaramide containing bis-naphthalimides, which will involve various techniques including VT-NMR, UV absorbance time studies, extinction coefficient studies and Scanning Electron Microscopy.

Chapter 4 discusses the possible DNA binding ability of the novel synthesised compounds using UV-Vis absorbance, fluorescence and Ethidium Bromide Assays.

Chapter 5 gives an overall conclusion of the entire work carried out in this research and also provides a perspective with the ideas for future work.

Chapter 6 contains the general experimental procedures including the synthesis and detailed characterisation of each of the synthesised compounds.

Chapter 7, the Appendix section contains all supporting information.

Abbreviations

A-T	Adenine-Thymine
a.u.	arbitrary units
BIMZ	Benzimidazole
C	Carbon
d	doublet
DBD	DNA-binding domain
DCM	Dichloromethane
dd	Doublet of doublets
DMF	*N*, *N*-dimethylformamide
DMSO	Dimethyl sulfoxide
DNA	Deoxyribonucleic acid
EDG	Electron donating group
eq.	Equivalent
ESI	Electrospray ionisation
EtBr	Ethidium bromide
EtOH	Ethanol
EWG	Electron withdrawing group
G-C	Guanine-Cytosine
HCl	Hydrochloric acid
HR-MS	High resolution mass spectrometry
hrs.	Hours
Hz	Hertz
IR	Infrared
J	Coupling constant
K	Kelvin
LCMS	Liquid chromatography-mass spectrometry
MeCN	Acetonitrile
mins.	minutes
N	Nitrogen
NH_3	Ammonia
nm	Nanometre
NMR	Nuclear magnetic resonance

O	Oxygen
PBD	Pyrrolo[2,1-c][1,4]benzodiazepine
Pd/C	Palladium on carbon
PDT	Photodynamic therapy
Pgp	P-Glycoprotein
ppm	Parts per million
q	Quartet
RNA	Ribonucleic acid
ROS	Reactive oxygen species
R_t	Retention time
s	Singlet
SEM	Scanning electron microscopy
t	Triplet
TFA	Trifluoroacetic acid
UV/Vis	Ultraviolet/visible
VT	Variable temperature
δ	Chemical shift
ε	Molar extinction coefficient
λ	Wavelength

Contents

Chapter 1 DNA and DNA targeting synthetic compounds

1.1 Introduction to DNA

Deoxyribonucleic acid (DNA) is a nucleic acid that contains the genetic instructions for the development and function of all living things.[1] DNA is mostly located in the cell nucleus (nuclear DNA) while being less abundant in the mitochondria of a cell (mitochondrial DNA).[2] DNA is a long polymer made up of simple units called nucleotides, which are held together by a backbone of sugars and phosphate groups (Figure 1.1).[3] As originally hypothesised by Watson and Crick, semiconservative DNA replication is carried out by all living organisms.[1] The three molecular fragments that make up the nucleotide are: sugar, heterocycle and phosphate, while the cyclic furanoside deoxyribose sugar is connected with one of the four heterocyclic bases by an 8-glycosyl linkage.[1] The sugar-phosphate backbone runs at the curve of the helix in an antiparallel orientation. The Base-pairs (A-T and G-C) along the centre of the right handed double helix are also presented.[4]

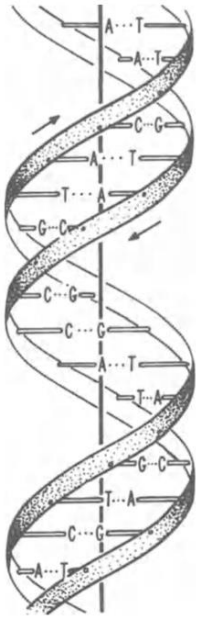

Figure 1.1: Proposed schematic structure of the DNA double helix by Watson and Crick in 1953.[1]

1.2 Structure of DNA

DNA is wound into a right-handed double helix in order to be protected from the outside environment (Figure 1.2).[5] The two grooves in the helix (major and minor) are defined by the right-handed twist of the DNA backbone (in B-form DNA) which are lined by the sugar phosphate backbone.[6] The negatively charged sugar phosphate backbone carries four types of molecules called bases which are: Adenine, Thymine, Guanine and Cytosine and it is the sequence of these four bases that encodes genetic information.[7] It is also important to view the individual components of DNA to truly understand the structure of DNA B-form as well as the various structural variations in the DNA right-handed double helix. There are a number of possible variations in the helical structure of DNA due to numerous possibilities in the structures of the sugars and the bases and to the structural relationship of the bases to the sugars.[8] It is known that DNA (right-handed double helix) is formed by two individual strands which are aligned in an anti-parallel fashion, which means that one strand is oriented from the 5' end to 3' end, while the other strand is oriented from the 3' end to the 5' end, where the adjacent nucleotides are linked due to the formation of phosphodiester bonds, caused by the phosphate group attachment to the 5' end of one nucleotide and the hydroxyl group at the 3' end of another nucleotide.[9] This linkage enables the structural rigidity of DNA due to the sugar-phosphate backbone. The 3-dimensional double helix structure of DNA correctly elucidated by James Watson and Francis Crick. Complementary bases are held together as a pair by hydrogen bonds.[10]

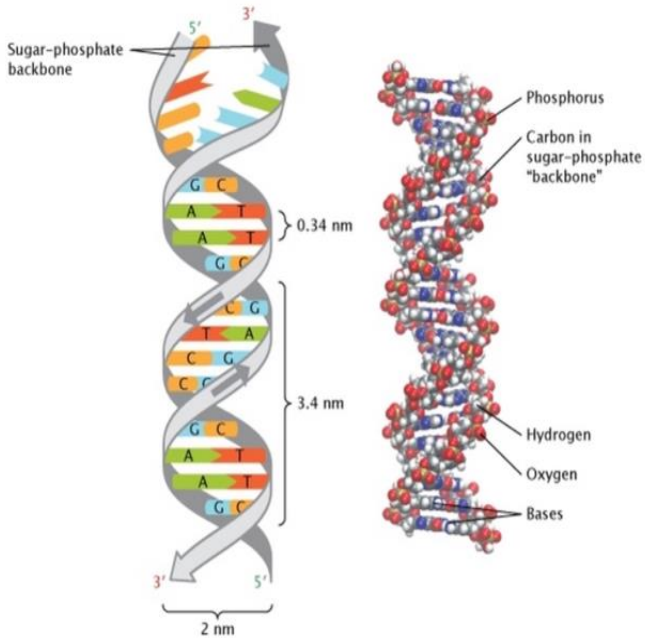

Figure 1.2: The double-helical structure of DNA.[5]

1.3 DNA base pairs

DNA base pairing is the aspect where guanine is always bound to cytosine and adenine is always bound to thymine *via* hydrogen bonding (Figure 1.3). The bond between guanine-cytosine share three hydrogen bonds compared to the adenine-thymine bond which always share two hydrogen bonds.[3] Complimentary purine-pyrimidine base pairing increases the stability of the double helix, as it keeps a constant distance between the two polynucleotide strands.[11] The stability of the double helix is enhanced by the weak and numerous Hydrogen-bonds between the complementary bases. The processes of transcription and DNA replication are made possible by enzymes which are responsible for breaking the Hydrogen-bonds. Complementary base pairing is crucial as it is essential in forming the helical structure of DNA, due to the base pairs having the most stable position.[12] It is also important in replication as it allows semiconservative replication.[13]

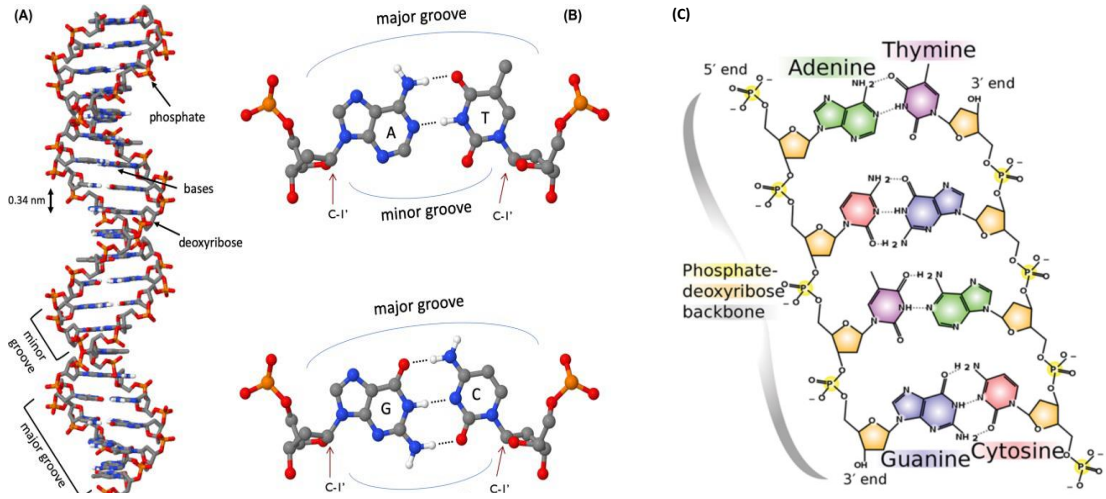

Figure 1.3: DNA structure including the complimentary base pairs.[3]

(A) DNA double helix, containing the nitrogenous bases in the middle, while the negatively charged sugar phosphate backbone is positioned on the outside.

(B) Adenine-Thymine and a Guanine-Cytosine base pairs, where the arrow indicates C1′ of the deoxyribose. The atoms on the lower edge of the base pair face into the minor groove, while the atoms on the upper edge face into the major groove. The C1' of the deoxyribose has been highlighted to be positioned in the same locations of all base pairs. The dotted line also illustrates the hydrogen bonds between the base pairs.[14]

(C) The structure of DNA illustrating the negatively charged sugar phosphate backbone and the base pairs.

1.4 Function of DNA

The major function of DNA is to encode the sequence of amino acid residues in proteins, using the genetic code.[15] Importantly, the covalently bonded sugar-phosphate backbone is responsible for storing the base sequence of genetic information of the cells, while also allowing the shortening of DNA during the process of cell division.[11] The genetic function of DNA can be explained as an alliance of two properties which include: a strand which contains the necessary information which encodes the sequences of RNA molecules and sequences of proteins as well as a polymer which enables the packaging, replication as well as the accessibility of the information, as it exists as a double helical string.[16] Although DNA does indeed play a crucial role as it stores genetic information, it also plays a role of adopting a large variation of possible conformations, which include: cruciforms, quadrupex DNA, intramolecular triplexes and left handed z-DNA to name a few.[8] Another key function of DNA in a cell nucleus is that it also acts as a store of energy in order to enable the transport of DNA and RNA polymerases. It is the double-helical structure of DNA that does indeed enable this process as it can exist in the coiled or supercoiled forms.[17] The stability of the double helix is achieved due to the stacking of the bases and it is known that there are 10-10.5 base pairs per turn of the double helix.[18]

1.5 Negatively charged sugar phosphate backbone

DNA backbone is a negatively charged repetitive chain of interconnected sugar and phosphate groups as it is situated on the outside of the double helix (Figure 1.3).[8] Interconnected sugar and phosphate groups are responsible for making up a repetitive chain of a DNA backbone.[19] The structural frame work of DNA nucleic acids are formed by the sugar-phosphate backbone and this backbone is responsible for defining the directionality of the molecule.[20] DNA-protein interactions are facilitated by the dynamic properties of the DNA backbone.[21] The backbone utilises the control over the base stacking geometries by two crucial mechanisms which are:

1) The sugar-phosphate backbone is well known to have a limited length and thus, it limits the conformational space which is accessed by the bases.

2) The neighboring base pairs in a sequence are held by the backbone in order to embed the structures of the same dinucleotide in different sequence contexts in a series of tetranucleotides, which may enable the possibility of having variable differences.[22] The phosphate backbone provides a means for DNA recognition through electrostatic or H-bond interactions amongst others.

The bases: Adenine, Thymine, Guanine & Cytosine are shown to bind to the negatively charged phosphate backbone. The anti-parallel nature of the two backbones are also displayed, where one strand runs from the 5' end to the 3' end and the other strand runs from the 3' end to the 5' end.[23]

1.6 DNA binding and recognition

A DNA-binding domain (DBD) is a protein that is responsible for recognising single or double stranded DNA as it is known to contain at least one structural motif.[24] A DBD has a general affinity to DNA or it can distinguish a recognition sequence of a specific DNA sequence.[25] An interesting non protein alternative which regulates transcription is the use of synthetic small molecules which are able to bind DNA.[26] Controlling gene expression has successfully proven to be a means of therapeutic development.[27] Both natural and synthetic small molecules that strongly bind in the groves have been designed to inhibit DNA-protein interactions, since these interactions engage contacts in minor and major grooves of DNA.[28] Molecules that fit between DNA base pairs can also directly or allosterically disrupt DNA-protein interactions. Therefore, low molecular weight DNA binders are used in drug discovery projects as they are able to act as inhibitors of gene expression.[28] Small molecule studies, including both current and potential drugs, have shown that they can be classified as intercalators, multi-mode binders, groove binders, multi-mode and single chain ligands.[29-32]

1.7 Binding interactions of synthetic compounds with DNA

The main binding interactions of [small molecules/synthetic compounds/potential drugs etc] can include electrostatic, allosteric, hydrophobic, hydrogen bonding and/or Van der Waals interactions.[29, 30] Previous studies have proven that small molecules with an overall positive charge are very likely to bind to DNA grooves in the initial and the final state (Figure 1.4).[33, 34]

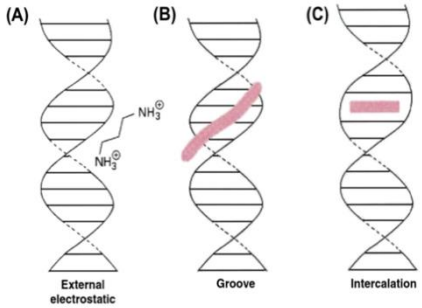

Figure 1.4: Three types of DNA binders including; A=External electrostatic binder, B=Groove binder, C=Intercalator. The drug is represented by the pink bar in each type of binders.[29, 33]

1.7.1 Electrostatic interactions

Ions or small molecules that bind externally with DNA are generally not specific to the sequence and position of the nucleotides. Their distribution is mainly determined by the electrostatic interaction with negatively charged phosphate groups in the DNA backbone.[35] Li^+, Na^+ and K^+ are examples of ions that bind in this non-specific way. However, ions such as Ag^+ and Hg^{2+} are examples of ions that specifically bind to the nucleobase.[36] Cationic polyamines are examples of small molecules that have been examined in a number of studies to externally bind to DNA.[37] External binding is electrostatic in nature and generally is characterised by binding kinetics approaching the diffusion limit of $K_a = 10^7\text{-}10^8$ $M^{-1}s^{-1}$ as it does not require significant DNA structure changes.[35] A number of metal ions bind to DNA *via* an electrostatic bond, also known as an external non-specific external association.[38] Synthetic compounds are able to interact with the electron donating parts of the DNA bases or they can covalently or non-covalently bind to the negatively charged phosphate DNA backbone.[39] The hydrophilic-hydrophobic structure of the molecule, the charge on the compounds and the overall size of the ions determine the intensity of these types of interactions. The DNA double helix structure results in damage following the interaction between the compound and DNA phosphate backbone.[39] Reversible intermolecular interactions including electrostatic bonds result from the interaction between the cations and the negatively charged phosphate on the outer surface of the DNA helix.[40]

There are various different types of molecules that can interact with this outer edge, generally through non-specific electrostatic interactions.[41] Metal ions such as Na^+ and Mg^{2+} are bound in an aqueous solution, but spermine 2 and spermidine 3 are examples polyamines of externally DNA linked differentially methylated genes.[42] Due to the unspecific nature of the binding, the mechanisms of action are unknown. However, polyamines are likely to neutralize negative charges on the DNA phosphate backbone, thereby promoting DNA packaging, which is an essential process for cell proliferation.[43] Polypyridyl metal-ruthenium(II) complexes have been studied and examined in great detail in the past 25 years due to their excellent photophysical properties and their high affinity for binding to DNA.[44, 45] These complexes strongly bind to DNA *via* electrostatic interactions to the phosphate backbone due to their positive charge.[46, 47] These Ru^{2+} complexes can also be varied with ligands which can also intercalate with DNA.[48] *Mihailovic et al.* had synthesized the Ru^{2+} complex, **1** which comprised of bipyridine ligands

for enhanced electrostatic interaction to the DNA, where Ru^{2+} was bound to the backbone of the negatively charged phosphate DNA (Figure 1.5).[49]

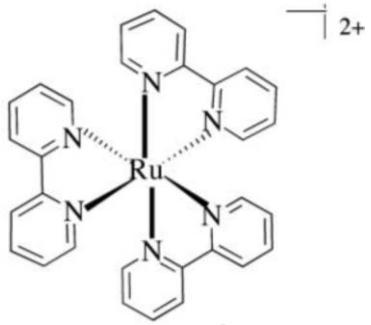

1

Figure 1.5: Synthesised electrostatically DNA binding Ru^{2+} metal complex $[Ru(bpy)3]^{2+}$, **1** by *Mihailovic et. al.*[49]

One of the compounds synthesised by the group showed concentration-dependent cytotoxicity in HeLa cells and mesothelioma cells.[49] The cytotoxicity of the compound against the cell lines was found to be between 8.8 and 43 µM, while also having possible uses as a novel PDT agent.[49]

1.7.2 Allosteric interactions

Allosteric interactions take place when the binding of a ligand to its site on a receptor can alter the binding of another ligand to a topographically different site on the same receptor and *vice versa*.[50] Allosteric mechanisms have many advantages as these interactions make it possible to regulate a specific reaction step by the products of other phases of the reaction pathway or altogether from other reaction pathways.[51] Allosteric interactions also allow specific regulation of an enzyme. For example, it is difficult to directly block a specific ATP binding site by forcing the regulator to compete for the target enzyme at high ATP concentrations and not to bind to multiple ATP binding sites that are linked to other proteins.[51] It is well known that biological systems utilise allosteric regulation, as *Monod* predicted almost 40 years ago.[51] Recent studies have shown that the development of new classes of allosteric drugs can be derived from these natural processes (Figure 1.6).[51, 52]

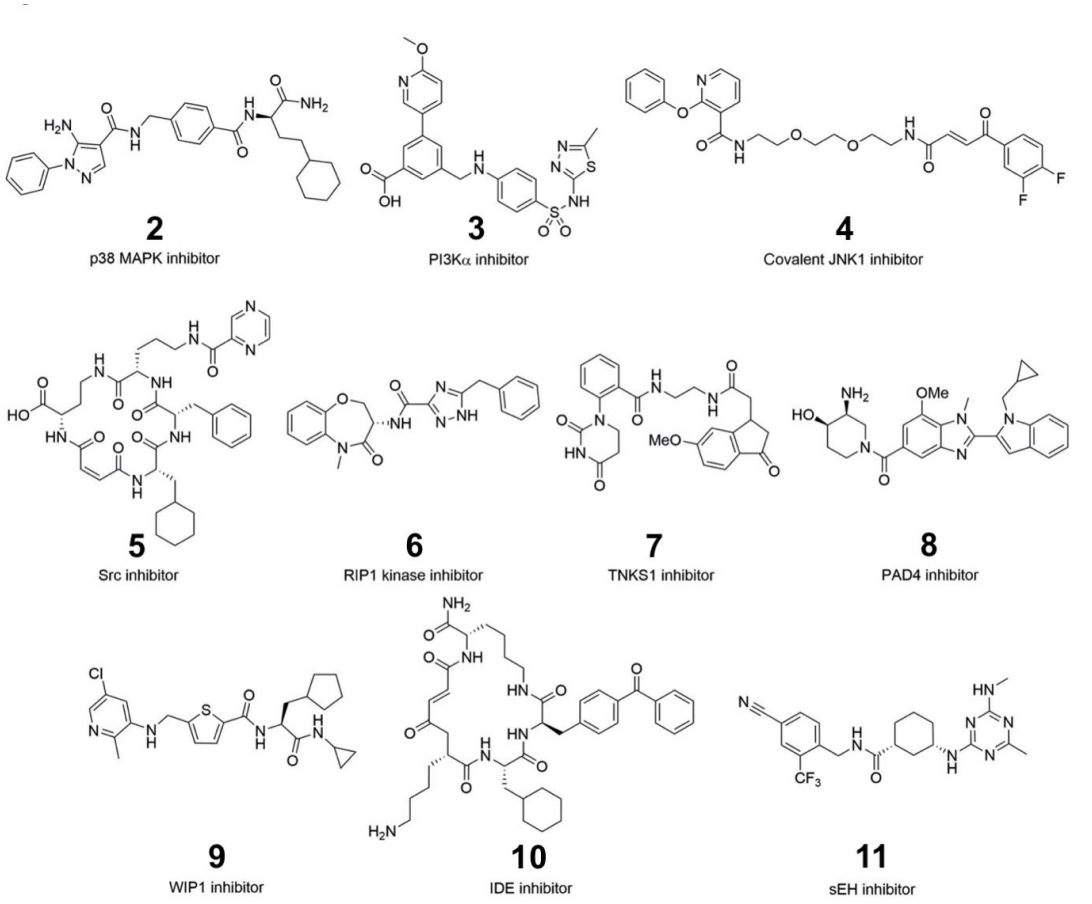

Figure 1.6: Chemical structures of synthesised compounds that bind to DNA with allosteric interactions.

The development of ligands that solely bind to the receptor's orthosteric hormone binding site is the result of numerous attempts to discover various drugs at the β2 adrenergic receptor (β2AR).[53] Nonetheless, there is a vast potential for designing specialised drugs with fewer side effects than orthosteric ligands when targeting the generally unexplored unique allosteric sites.[53] Remarkable isoenzyme selectivity can be demonstrated due to large transfer in the binding site caused by the allosteric binding compounds.[52] Compound **2** hinders p38α MAP kinase in the nanomolar range with stronger selectivity than the kinome, due to its activated adaptive binding mode demonstrated by X-ray crystallography.[54] Phosphoinositide 3-kinase α (PI3Kα) inhibitor **3** is a kinase inhibitor with a different binding mode, as it binds to the ATP binding site.[55] Compound **4**, is known to be selective for closely related members of the Bruton's tyrosin kinase and Cyclin G-associated kinase families.[52] The selection for a completely different class of encoded compounds, namely peptide macrocycles, resulted in compound **5**, the Src allosteric kinase inhibitor.[56, 57] Compound **6**, demonstrated the ability of the inhibitor to block RIP1 kinase hydrolysing ATP to ADP with a cellular potency. It targets

type III allosteric site at the back of the ATP binding, where the benzyltriazole portion is bound in the allosteric lipophilic pocket and the benzoxazepinone heterocycle binding in space that the γ-phosphates of ATP would be present in.[52] Nanomolar potency of **7** has been demonstrated in its inhibition of the poly (ADP-ribose) polymerase Tankyrase 1.[52] Inhibitor **8** utilises selective inhibition of the protein arginine deiminase 4 (PAD4) isoenzymes *via* Induced Fit-Type Mechanism, where the binding of **8** to PAD4 causes a change in the shape of the enzyme in order to inhibit its activity.[58] The Wip1 inhibitor **9** hinders the phosphatase in a non-competitive mechanism of action as it targets a binding site outside the catalytic centre.[52] Insulin Degrading Enzyme (IDE) inhibitor **10** is a macrocycle known for its binding to an allosteric binding site, which eliminates the need for a metal ion binding group leading to off-target activity.[52] IDE inhibition is a possible treatment option for diabetes due to elucidating the role of IDE in metabolising amylin, glucagon and most importantly insulin due to its oral activity.[52]

1.7.3 Hydrophobic interactions

Distamycin, **12** is an antibiotic used to treat fungal infections (Figure 1.7).[59, 60] Predominantly, derivatives of distamycin are well known to have anti-tumour activity.[61, 62] Hydrophobic interactions and hydrogen bonds are the result of Distamycin binding with these DNA A-T rich regions in the minor groove (Figure 1.8).[63] Distamycin is attracted to the negatively charged sugar phosphate backbone of DNA due to its basic terminal amidine group.[64] Distamycin is A-T selective as it is restricted from binding to the minor groove of the G-C base pairs due to steric hindrance.[64]

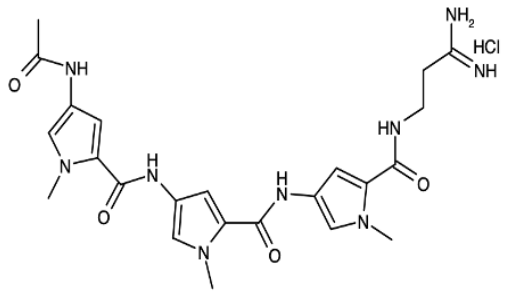

Distamycin A

12

Figure 1.7: Chemical structure of Distamycin A, a polyamide antibiotic.

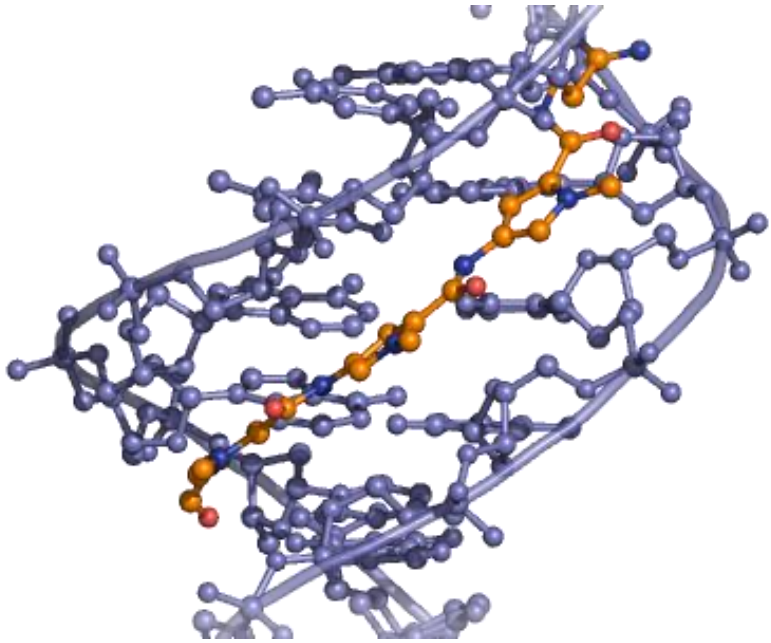

Figure 1.8: DNA binding of Distamycin: View of the DNA duplex strand (purple) and distamycin (orange) binding to the minor groove.

Actinomycins, **13** are a class of antibiotics known for their inhibition of both RNA and DNA syntheses processes by creating a barrier preventing chain elongation, as actinomycins are used in the treatment of Wilms tumour, trophoblastic neoplasm, Ewing's sarcoma and various types of ovarian cancers (Figure 1.9).[65, 66]

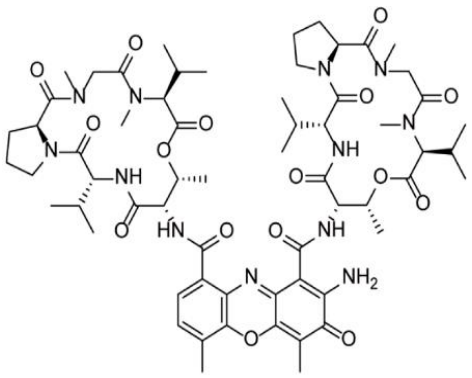

13

Figure 1.9: Chemical structure of Actinomycin-D, a polypeptide antibiotic.

Actinomycins, in contrast to distamycin, require the 2-amino group of guanine for binding in the G-C base pairs.[67] The side chains of the pentapeptides of actinomycins are known for their ability to form hydrogen bonds and hydrophobic interactions in the minor groove of DNA, while the phenoxazone ring intercalates in between the base pairs (Figure 1.10).[63, 64] A very stable complex is formed as a result of both interactions of actinomycin with DNA (minor-groove binding and intercalation).[64]

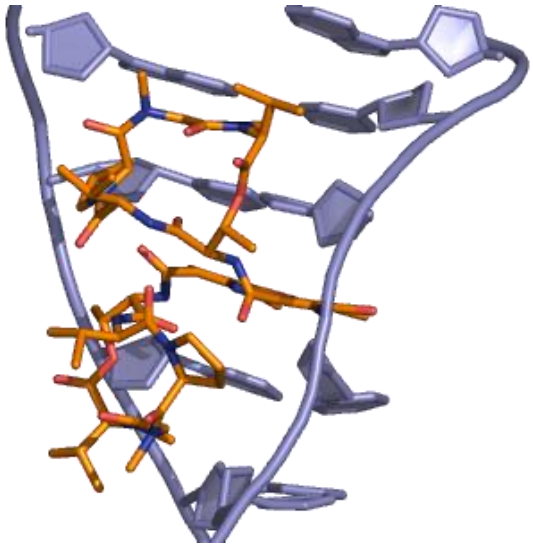

Figure 1.10: DNA binding of Actinomycin: View of the DNA duplex strand (purple) and actinomycin D (orange), where the pentapeptides of actinomycin bind to the minor groove, while the phenoxazone ring intercalates in between DNA base pairs.

1.7.4 Hydrogen bonding interactions

Magnesium ions are known to be essential in both the structure and function of nucleic acids.[68] There is very little known about the interactions of RNA helical regions with magnesium ions, although the process of RNA tertiary folding frequently uses magnesium ions when binding to clustered phosphates of RNA.[68] $[Mg(H_2O)_6]^{2+}$ is known to have two binding modes to both A-DNA and RNA (Figure 1.11).[68]

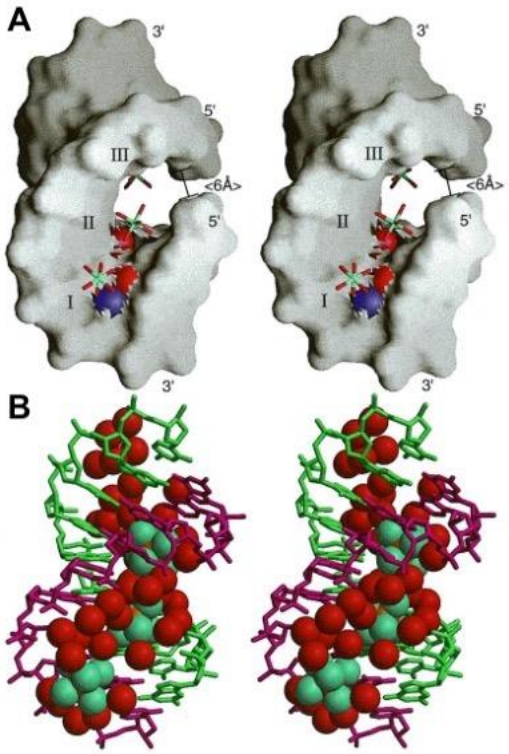

Figure 1.11: (A) $[Mg(H_2O)_6]^{2+}$ and its two binding modes to RNA-DNA duplex of r(GCG)d(TATACGC), where; three Mg^{2+} ions Mg I, Mg II and Mg III labelled (I,II and III) bind directly *via* hydrogen bonding to the O6 and N7 sites of guanine bases (represented by red and blue spheres).
(B) Major groove of DNA being almost entirely filled by the three $[Mg(H_2O)_6]^{2+}$ ions, where the first shell bound aqua regions are located (red).

Three Mg^{2+} ions bind directly *via* hydrogen bonding to the O6 and N7 sites of guanine bases.[69] $[Mg(H_2O)_6]^{2+}$ ions are also very well known to bind to the A-DNA phosphates at the outer part of the A-DNA major groove *via* electrostatic interactions, proven by their presence at the most negative electrostatic potential sections.[68] The $[Mg(H_2O)6]^{2+}$ ion can access the edges of the A-DNA base pairs, although it is much larger (approximately 8Å in diameter) than the outer part of the major groove average width.[68]

1.7.5 Major/Minor-Groove binders

DAPI, **14** (Figure 1.12) selectively binds into the minor groove of DNA with a preference for the adenine-thymine regions, resulting in a decrease of the bending rigidity of DNA.[70-73] Berenil, **15** binds to the minor groove of DNA also *via* attachment to the minor groove of AT-rich domains of DNA helices.[74] Pentadimine, **16** has been widely studied in the treatment for human protozoan infections, where the mechanism of action also involves selective binding to the AT-rich regions of DNA.[75-78] Hoechst 33258, **17** is used as a fluorescent dye, as it binds to DNA by forming extensive van der Waals forces and *via* binding to the minor groove of DNA phosphate backbone (Figure 1.13).[79, 80]

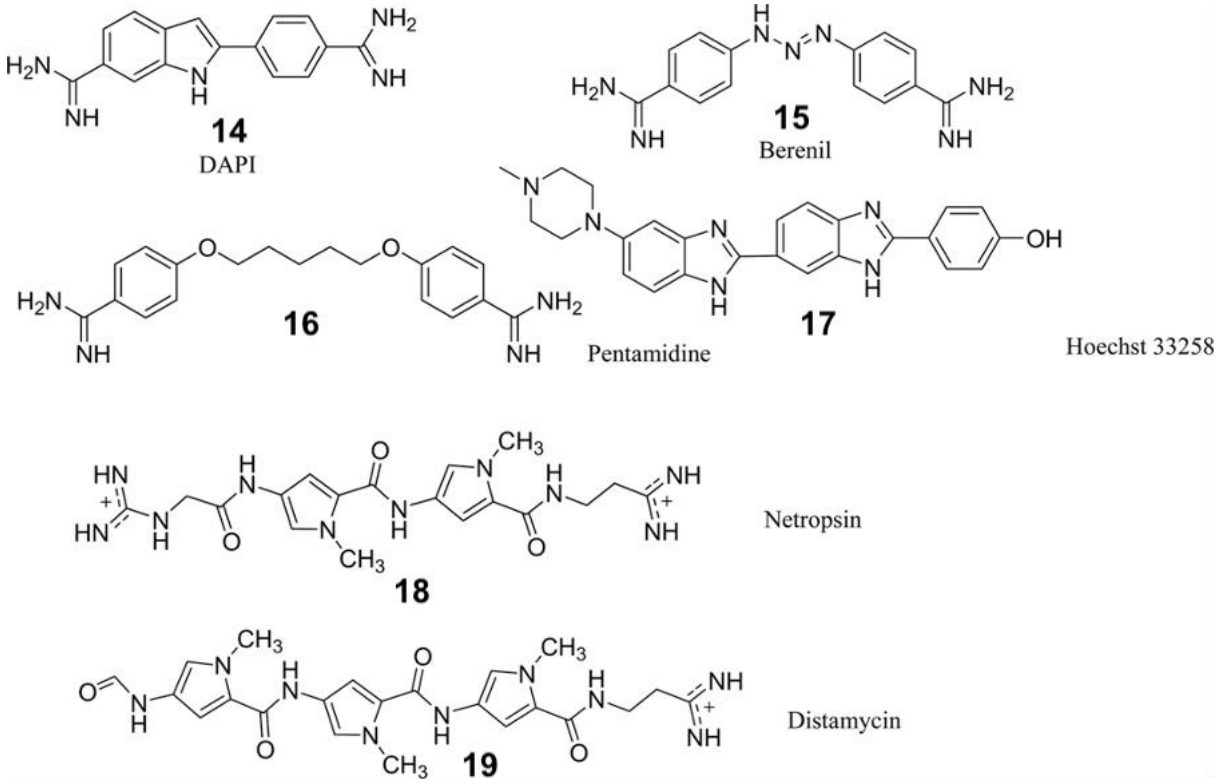

Figure 1.12: Chemical structures of widely used DNA-minor groove hydrogen binders.

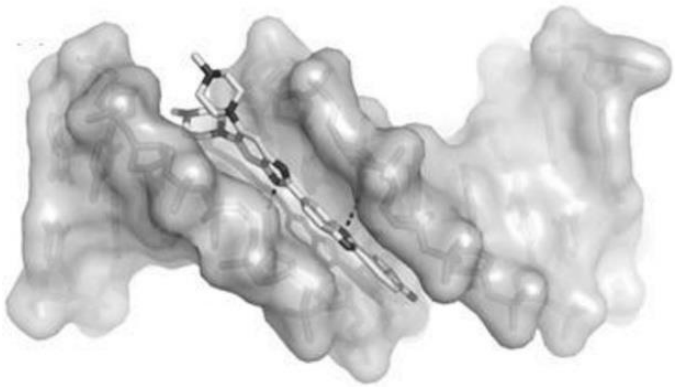

Figure 1.13: Hoechst 33258 bound to DNA [5'-d(CGCGAATTCGCG)$_2$-3'] *via* hydrogen bonds highlighted by the black dashed lines.

Distamycin-DNA and netropsin-DNA interactions rely heavily on H-bonds, although H-bonds do not make an important contribution in recognising Hoechst 33258 with DNA (Figure 1.14).[80] It has been proven that netropsin, **18** forms eight hydrogen bonds when bound to DNA,[80] while distamycin, **19** forms a total of ten hydrogen bonds when bound to DNA.[81]

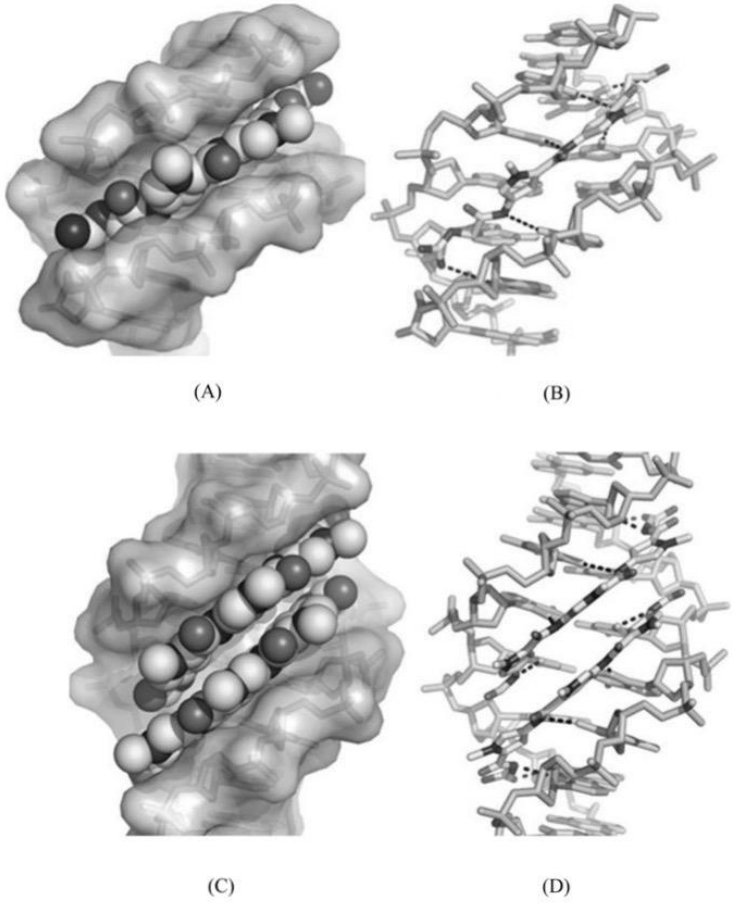

Figure 1.14: Binding of netropsin to DNA [5'-d($C^{5\text{-}Br}$CCCCIIIII)$_2$-3'] *via* van der Waals forces (A) and its binding to DNA *via* hydrogen bonding highlighted by the black dashed lines (B).
Binding of distamycin to DNA [5'-d(GTATATAC)$_2$-3'] *via* van der Waals forces (C) and its binding to DNA *via* hydrogen bonding highlighted by the black dashed lines (D).

In DNA sections, the groove binders have been proven to increase the transitional force of excessive DNA stretching, as both Methyl Green and distamycin, both major and minor groove binders, increased the transition strength, indicating a stabilisation of the DNA double helix.[82] It had also been proven that the DNA melting cooperativity had decreased due to the presence of major groove binders, as the over stretching of a transition force range had been broadened.[83] Intercalation is the final state of the binding modes which is caused by groove binding as it is often an intermediate state.[33]

Berenil is an example of a drug that intercalates DNA at higher concentrations but binds in the minor groove at low concentrations (Figure 1.15).[30, 84] Some small molecules can thread between the DNA base pairs before the process of intercalation takes place, as they have higher orders of complexity of DNA binding intercalation.[85, 86] Although binding to single-stranded DNA (ssDNA) is the least common type of binding, as reported for DNA glyoxal binding,[87, 88] small molecule DNA intercalators are also abundant.

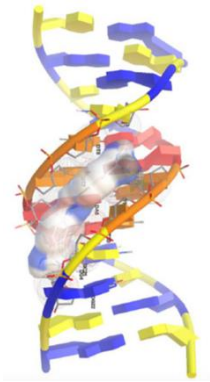

Figure 1.15: Hydrogen bond interaction between DNA and Berenil.

The molecular recognition of B-DNA can be done in five different ways: major groove recognition; minor groove recognition; sugar-phosphate backbone binding; intercalation between the base pairs; covalent binding or metal-coordination to the bases.[89] Developing ways of inhibition of protein-DNA interactions are vital in terms major groove specific ligand-DNA interactions (Figure 1.16).[90, 91]

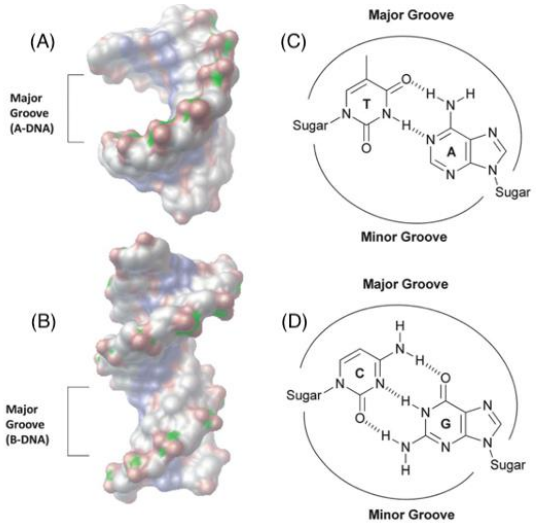

Figure 1.16: (A) DNA double helix representing major groove of A-DNA (PDB ID: 2ANA), (B) DNA double helix representing major groove of B-DNA (PDB ID: 1D98), (C) base pair hydrogen bond donor/acceptor in the major and minor groove of A-DNA and (D) base pair hydrogen bond donor/acceptor in the major and minor groove of B-DNA.

It has been proven that natural molecules such as: ditercalinium, aflatoxin, neocarzinostatin, pluramycin, azinomycin and leinamycin have potential major-groove binding characteristics.[92] Nonetheless, these compounds mainly interact with DNA through the process of intercalation.[91, 93] According to recent studies, aminoglycosides have proven to be promising probes for DNA major groove binders.[91] Nonetheless, major groove binding is an emerging area of interest in DNA interaction, as proteins and many biological macromolecules mostly bind to DNA *via* major groove through a series of hydrogen bonds.[91]

Pluramycin, **20** is a widely used antibiotic in the treatment of various cancers due to their strong biological activity (Figure 1.17).[91, 94] Altromycin B, **21** and Hedamycin, **22** are the most active antitumor antibiotics of the pluramycin family (Figure 1.18).[95, 96]

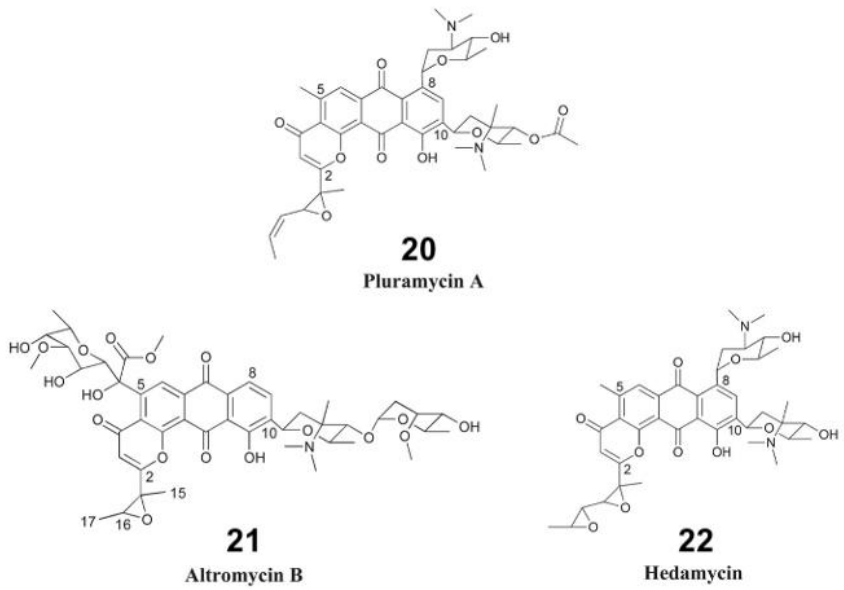

Figure 1.17: Chemical structures of pluramycin A, **20,** altromycin B, **21** and hedamycin, **22**.

The reactivity of pluramycins is intensified by TBP binding to the human myoglobin TATA sequences on DNA.[97] Although pluramycins intercalate between the DNA base pairs, the N7 position of guanine of the purine bases in the major groove become alkylated in the presence of the adjacent epoxide rings of pluramycins, which facilitate covalent bonding (Figure 1.18).[91, 98] The glycosidic substituents regulate the selectivity of sequences, due to the presence of oligonucleotide substrates with altromycin B and hedamycin alkylated complexes.[99, 100] The DNA melting temperature is increased by 20°C due to the presence of hedamycin, which involves reversible and non-reversible binding modes.[101]

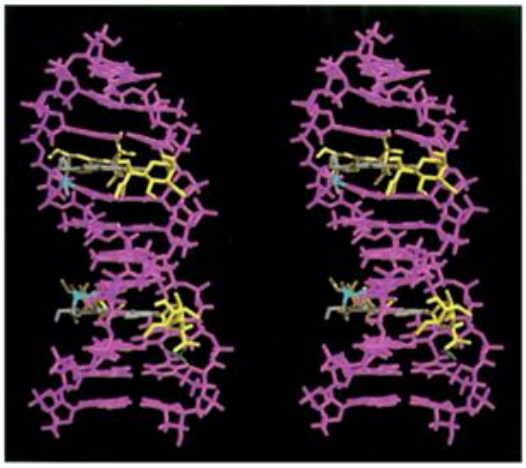

Figure 1.18: Chemical structure of bis-altromycin B with the processes of alkylation at N7 (turquoise), saccharide binding in major and minor grooves of the double helix (yellow) and intercalation of altromycin B with both major groove: top and minor groove: bottom of the DNA strand (grey).

1.7.6 Covalent interactions

The covalent bond in DNA is irreversible and always leads to cell death due to DNA process inhibition.[102] Cis-diamminedichloroplatinum (cis-platin), **23** a very well-known anticancer covalent DNA binder (Figure 1.19).[102] Cis-Platin has been widely used for over 40 years for the treatment of testicular, ovarian, neck and head cancers.[103] Cis-platin uses its chloro groups to form an inter/intrastrand cross-link with the nitrogens on the bases of DNA.[102]

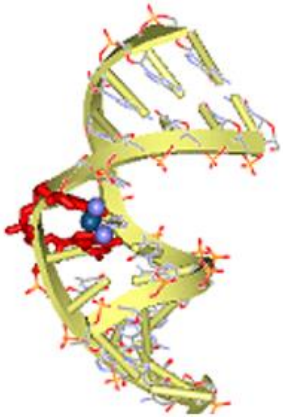

Figure 1.19: Covalent binding of cis-platin with DNA.

Various alkylating agents have been developed in the past twenty years, due their strong anticancer activity.[104] DNA miscoding is the result of alkylating agents suppressing the process

of DNA base pairing, due to binding with the N-3 of adenine and particularly with the N-7 of guanine nitrogen bases of DNA.[105] DNA fragmentation is the result of repair enzymes replacing the alkylated bases of DNA which are a result of cisplatin induced DNA damage.[106] Cross-bridge formation is an additional DNA damage mechanism in which the DNA is prevented from being separated for either transcription or synthesis due to the formation of bonds between the atoms in the DNA.[104] Mutations result from the process of mispairing of nucleotides of DNA, where a particular nucleotide is replaced by another due to errors in DNA replication, caused by alkylating agents. This is known to be the third mechanism of action of alkylating agents.[107]

Monofunctional Pt-DNA adduct is formed as a result of cisplatin initially forming a single covalent bond with DNA.[108] 1,2-Pt-d (GpG) intrastrand crosslink is the most abundant cisplatin formed species, which makes up approximately 60% to 65% of all adducts formed by cisplatin.[109] Both 1,3-Pt-d(GpXpG) and 1,2-Pt-d(ApG) are much less abundant cisplatin formed species, which together make up approximately 30% of all adducts formed by cisplatin (Figure 1.20).[110, 111]

Further DNA strand breaks are caused by transcription inhibition, DNA unwinding, replication inhibition and DNA unwinding caused by the different crosslinks and adducts of cisplatin due to the Pt-d(GG) interstrand crosslinks.[112] Carboplatin, **24** and Oxaliplatin, **25** are the less toxic derivatives of cisplatin developed in recent times which also highlight the success of cisplatin as a strong anticancer agent (Figure 1.21).[113, 114]

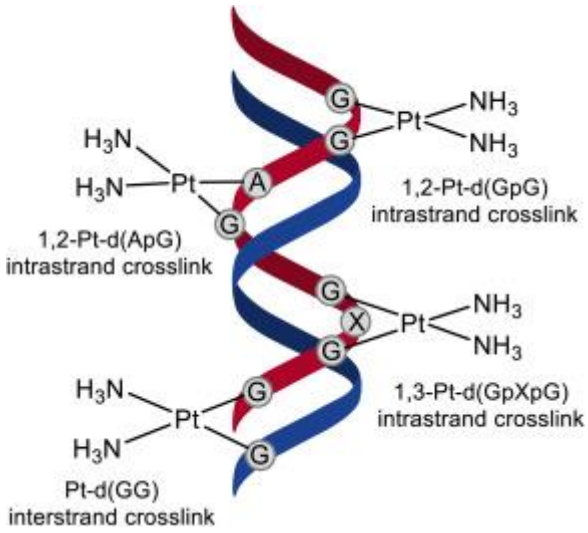

Figure 1.20: Cisplatin-DNA crosslink species, including the platinum atom with two bound amino groups.

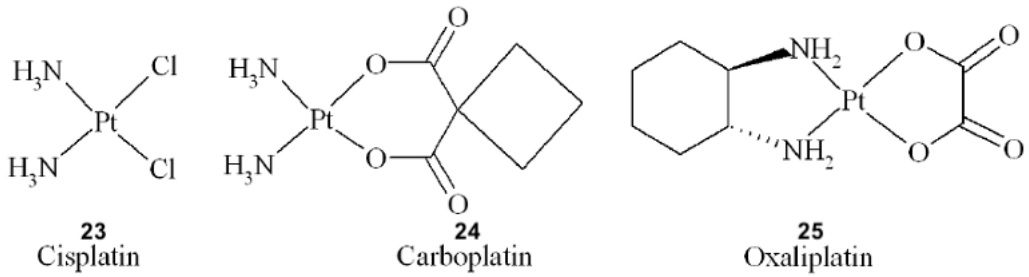

Figure 1.21: Chemical structures of cisplatin, carboplatin and oxaliplatin.

1.7.7 Metal-coordination to the bases

Numerous recently developed metal complexes have become effective chemotherapeutic drugs and diagnostic agents.[115] Using a metal ion to substitute the hydrogen atom in the hydrogen bonded base pairs was the base idea which had led to the development of metal-mediated base pairs due to both accepting lone pairs on the heteroatoms.[116] *Lee et al.* discovered that divalent Zn^{2+} ions stabilise DNA duplexes,[117] where at high pH, they release hydrogen atoms that are bound to the base pairs and the metal ions are responsible for binding to the nucleobases.[118] The development of these metal complexes with stronger anticancer activity and minimal toxicity compared to the standard platinum complexes is one of the main challenges in the therapeutic field.[119] DNA synthesis, energy metabolism and respiration are all functions of numerous enzymes involving the copper metal.[119] This creates the possibility of using other alternative metal complexes exhibiting copper-based antineoplastic activity.[120, 121] Free radicals are generated due to hydrogen peroxide and molecular oxygen being prone to reacting with copper involving redox reactions in these strongly biologically active copper compounds.[122] DNA and RNA are directly cleaved due to the displacement of other metal ions as a result of the ability of copper to produce reactive oxygen species (ROS) and this explains the strong biological activity of copper.[123] Casiopeinas, **26** are a family of compounds synthesised on the basis of designing copper(II) coordination complexes which are known to trigger DNA cleavage.[119, 124, 125] $[Cu(N\text{-}N)(O\text{-}O)]NO_3$ or $[Cu(N\text{-}N)(N\text{-}O)]NO_3$ are the general formulas of these complexes , where N-N represents a 1,10-phenanthroline or a substituted bipyridine; N-O represents a peptide or an a-amino acid, while O-O indicates salicylaldehyde or acetylacetonate (Figure 1.22).[119]

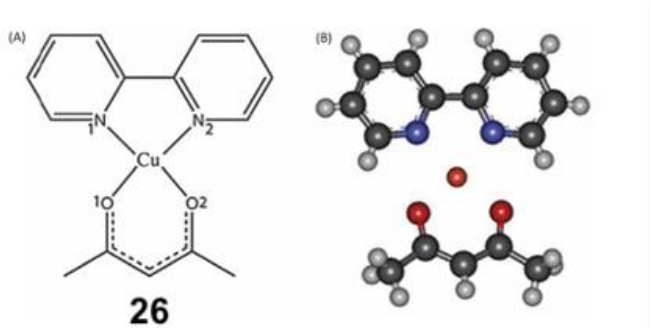

Figure 1.22: (A) Cas ([Cu(2,2'-bipyridine)(acetylacetonate)(H_2O)]+).
(B) CCDC 737505 X-ray structure.

This family of compounds have been classified as genotoxic,[126] cytotoxic in vivo and in vitro[125] with possessing strong antineoplastic activity.[127] Dose-dependent cell death is achieved by apoptosis due to the inhibition of cell proliferation by the Casiopeinas compounds,[128] resulting from mitochondrial toxicity or generations of ROS.[129, 130]

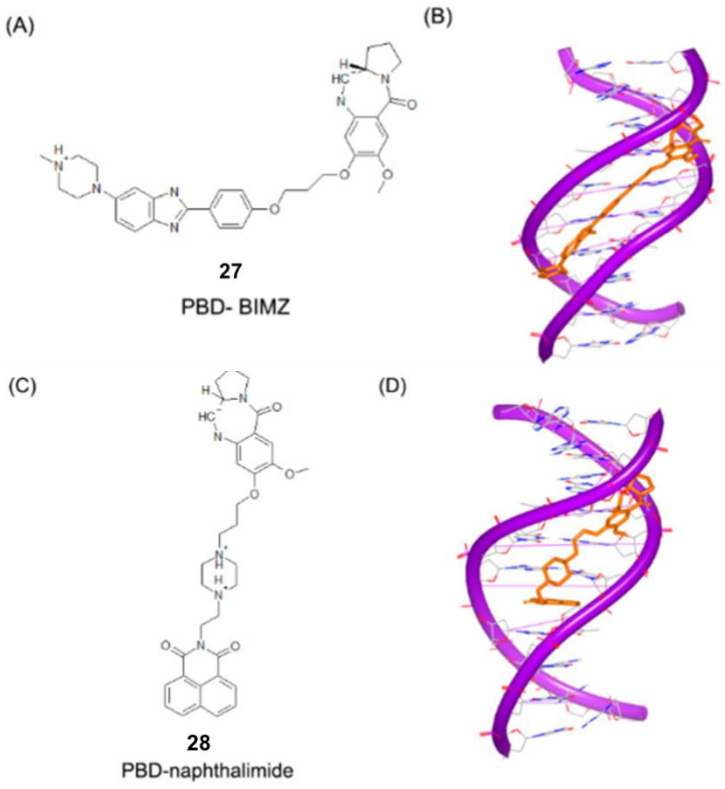

Figure 1.23: Chemical structure of PBD-BIMZ (A), Schematic displaying PBD-BIMZ with bound to DNA duplex (B), Chemical structure of PBD-naphthalimide (C), (D) Schematic displaying PBD-naphthalimide bound to DNA duplex. The synthesised molecule is represented by the orange complex, nitrogen atoms are represented by blue atoms, oxygen atoms are represented by the red atoms and the purple structure represents the negatively charged sugar phosphate backbone.

1.7.8 Interactions by intercalation

Limited intercalation in between two base pairs of particular side-chains of proteins is the result of the critical protein-DNA recognition processes.[131] The β-sheet domain of the TBP protein binds to the minor groove of the DNA TATA-box in addition to the side chains of Phenylalanine residues binding in between the base pairs *via* the process of intercalation.[132] The hinge region is particularly prone to the intercalation of the side chains of Leucine residue between the DNA binding domain (DBD) and the C-terminal ligand-binding domain (LBD), specifically the Lac-repressor between the consensus and non-consensus sequences.[133, 134] DNA-ligand interaction by the process of intercalation between DNA base pairs can therefore be applied to the development of synthetic molecules.[135] DNA bis-intercalation with binding to the major groove of DNA is the binding mode of the XR5944 drug, **29** which possesses strong anti-tumour activity (Figure 1.24).[136, 137] XR5944 was formerly designed as a topoisomerase inhibitor,[138] as it is a DNA bis-intercalating compound that has reached Phase I clinical trials (Figure 1.25).[136, 139]

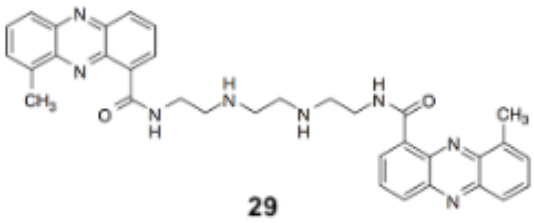

Figure 1.24: Chemical structure of XR5944.

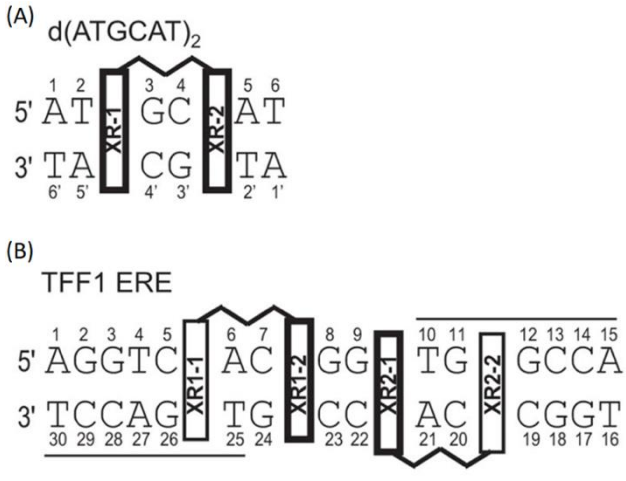

Figure 1.25: (A) Preferred XR5944 DNA binding site on the DNA d(ATGCAT)$_2$ hexamer. (B) Two binding sites of the drug XR5944 on the TFF1 ERE DNA sequences, where the weak bindings sites (XR1-1 and XR2-2) are displayed by the light boxes, while the strong binding sites (XR1-2 and XR2-1) are displayed by the darkened boxes. The solid lines on the sequence represent the ERE half-sites.

Both acridine carboxamides and phenazine carboxamides, which are known to be XR5944 parent compounds are inhibitors of DNA topoisomerase I/II.[140-142] The mechanism of action of XR5944 has been demonstrated by recent studies, which present that it is related to the inhibition of transcription as it is essentially topoisomerase independent,[139, 143] although previous reports illustrated that XR5944 is responsible for disrupting the regular function of topoisomerase I and II *in vitro* (Figure 1.26).[136, 144]

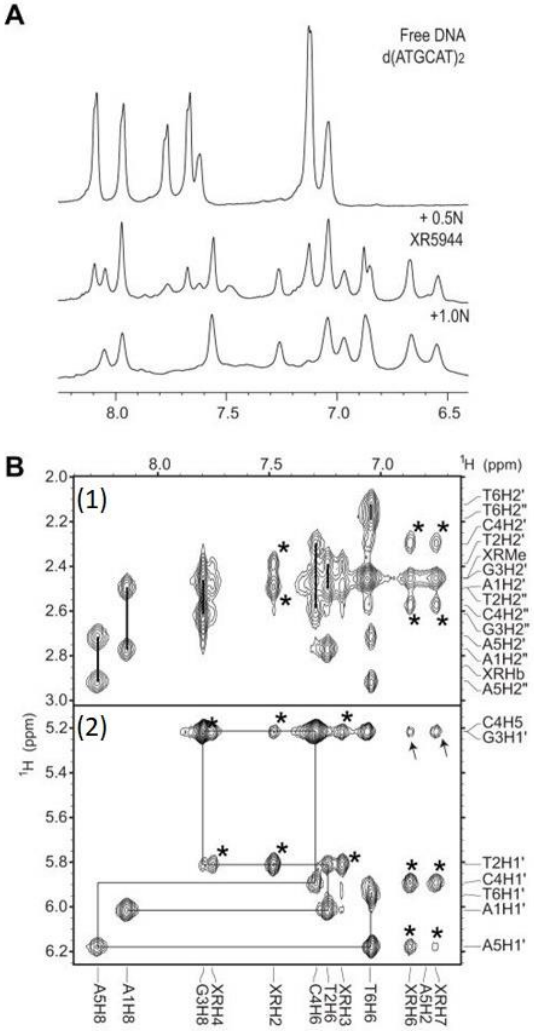

Figure 1.26: (A) NMR spectroscopy determination of XR5944 drug equivalents from 0 (top) to 1 (bottom) binding with d(ATGCAT)$_2$ DNA hexamer. New DNA-Drug complex protons have started appearing, while the free DNA proton peaks have started disappearing according to the increased concentrations of XR5944. Once the XR5944 drug equivalence of 1 is reached, protons representing free DNA disappear entirely. (B) NOESY spectra of XR5944-DNA complex representing the expanded nonexchangeable regions. (1) Aromatic-H2'/H2''/methyl region. Both the (*) and the (↑) (only for C4H5) symbols representing the XR5944 and DNA intermolecular NOE cross-peaks. (2) H1' aromatic region. The serial assigned pathway is represented by the spectra.

XR5944 is considerably more efficacious than doxorubicin and topotecan topoisomerase inhibitors, as XR5944 has displayed remarkably strong activity against both murine and human tumour models both *in vitro* and *in vivo*.[144, 145] XR5944 has also demonstrated strong efficacy both *in vivo* and *in vitro* in both; colon cancer cell lines in conjunction with irinotecan and 5-fluorouracil[146] and in non-small-cell lung carcinoma in conjunction with doxorubicin and carboplatin due to its DNA binding sites (Figure 1.27).[137, 147] This binding mechanism involves the amino alkyl linker binding to DNA *via* major groove binding and the phenazine moieties bis-intercalating (Figure 1.28).

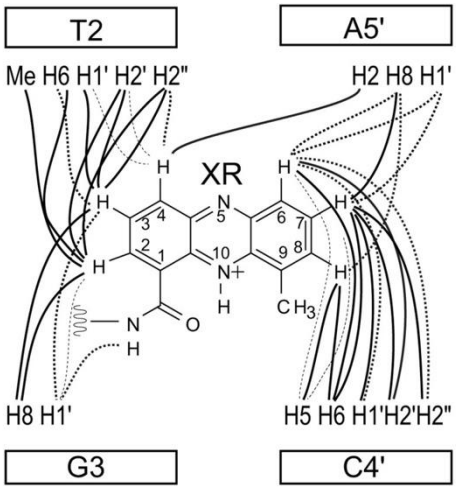

Figure 1.27: XR5944 and the 5'-TpG predominant binding site in the DNA hexamer displaying the intermolecular NOE cross-peaks. The solid lines represent strong intensity for NOEs, the thick dashed lines represent medium intensity for NOEs and the thin dashed lines represent weak intensity for NOEs.

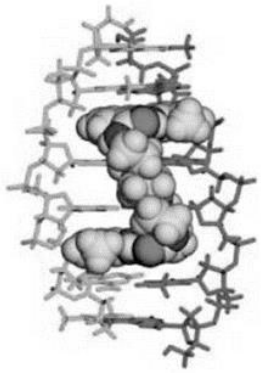

Figure 1.28: DNA-XR5944 complex structure. The amino alkyl linker of XR5944 binds in the major groove of DNA, while both phenazines intercalate into DNA parallel to the base pairs in the CPK model displayed.

XR5944 can bind to number of sites on DNA forming various complexes (Figure 1.29).[136] Drug resistance is minimised with XR5944 due the suppression of ERα activities, which results in the inhibition of ER-ERE binding, as XR5944 binds to the oestrogen response element (ERE) and this also makes XR5944 a potential drug candidate for antioestrogen treatments.[136] ERE-specific bis-intercalators including XR5944 derivatives can be synthesised for specific antioestrogen treatments from the structural information available.

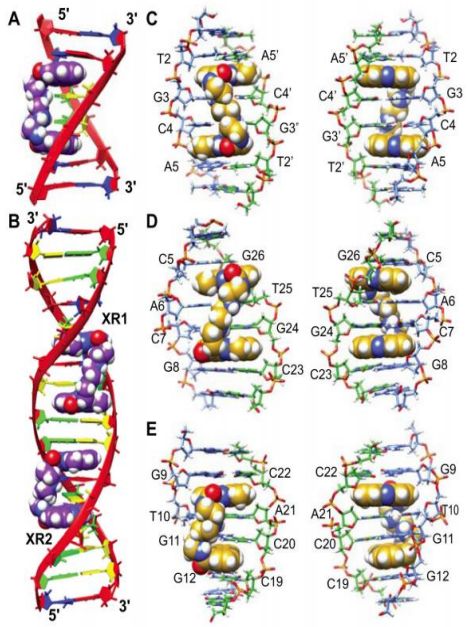

Figure 1.29: 1:1 d(ATGCAT)$_2$-XR5944 complex displayed in (A), 2:1 TFF1-XR5944 complex displayed in (B) Adenine = red, thymine = blue, guanine = green and cytosine = yellow, as the XR5944 molecules are represented by the CPK model. 1:1 d(ATGCAT)$_2$-XR5944 complex represented by (C), XR1 form of attachment of XR5944 with DNA represented by (D) and the second XR2 form of attachment of XR5944 with DNA represented by (E) where the XR5944-TFF1 2:1 complex is formed, which is viewed from the major groove (left) and the minor groove (right).

It has been determined that the binding equilibrium of XR5944 is gradually changed at pH 7 at the NMR time scale upon binding with DNA and forming a 1:1 stable complex with d(ATGCAT).[136] A stable duplex DNA is the result following the process of binding of XR5944 to DNA, due to the previously unseen G$_3$HN1 imino proton at 15°C in the free DNA, now identified at 25°C in the complex.[147]

WP631, **30** is another recently developed bis-anthracycline, which is a strong DNA bis-intercalator, where both anthracycline groups slide between the DNA base-pairs.[148] WP631 demonstrates strong clinical potential, due to initial cytotoxicity studies. The induction of P-glycoprotein causes a higher drug efflux, which results in multidrug resistance (MDR). MDR is well known to minimise the efficacy of various anthracyclines.[149] WP631 is known to surpass MDR, displaying stronger cytotoxicity against MDR in human carcinoma cells than against sensitive cells as it bis-intercalates in the DNA hexamer duplex.[148] 5′-C(1)G-(2)A(3)T(4)C(5)G(6)-3′ on the fist and 5′-C(7)G-(8)A(9)T(10)C(11)G(12)-3′ on the second strand of DNA complex have demonstrated WP631 bis-intercalating between base pairs C(5)-G(8) and G(6)-C(7) and between base pairs C(1)-G(12) and G(2)-C(11).[150] The centre of the DNA complex has displayed the strongest bis-intercalation affinity of WP631. WP631 has stronger efficacy against Jurkat T-cells, MCF7/VP-16 and MCF-7 leukemia cells compared to mono-anthracyclines (Table 1.1).[148, 151] WP631 has also demonstrated 5-8 times stronger efficacy hindering the Jurkat cell growth compared to daunorubicin (Figure 1.30).[148, 151] WP631 is known to bis-intercalate into DNA *via* its anthracycline moieties (Figure 1.31).[150]

Comparative *In vitro* Cytotoxicity of WP631, Daunorubicin and Doxorubicin

Cell line	IC_{50} (μM)		
	Doxorubicin	**Daunorubicin**	**WP631**
MCF-7	0.9 ± 0.5	n.d.	4.8 ± 2.5
MCF7/VP16	14.2 ± 0.8	n.d.	2.5 ± 3.4
Jurkat T	0.13 ± 0.07	0.083 ± 0.009	0.018 ± 0.006

Table 1.1: *In-vitro* cytotoxicity of Doxorubicin, Daunomycin and WP631.

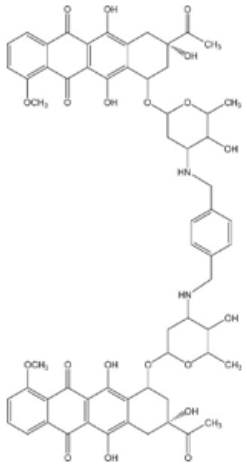

30

Figure 1.30: The structure of this bis-daunomycin molecule, WP631.

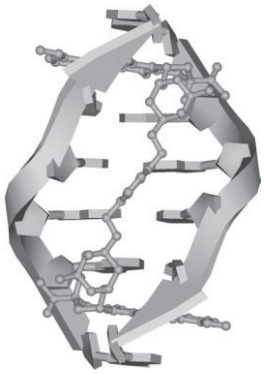

Figure 1.31: The crystal structure of the bis-daunomycin molecule WP631 bound to the duple sequence d(CGTACG), displaying the anthracycline groups bis-intercalating between the DNA base pairs.

These modes of DNA recognition first were discovered in the early 1960s and have become essential in the field of DNA recognition.[89] Proteins are responsible for binding in or around the major groove and creating specific hydrogen-bond interactions to the edges of base pairs, as DNA sequence recognition is accomplished.[131] This is due to the groove having a larger variation in terms of its size and shape or a greater number of hydrogen-bond donor and acceptor units to which binding of the protein can take place.[89] The major groove recognition generally refers to cylindrical alpha helix units. The units are sized and shaped to perfectly fit the main groove and are too large to fit in the minor groove. Helix-turn-helix structures are included by the motifs.[152] Synthetic minor groove regulators and binders have become a popular topic in modern medicine as these agents have various clinical applications as they possess anti-cancerous, antibacterial, antiviral and protozoal properties.[153] Synthetic bisbenzimidazoles (such as Hoechst 33258), diarylamines (including pentamidine, berenyl and pentamidine) and a natural molecule distamycin A are known minor groove binding agents.[153] DAPI has been thoroughly examined as an anti-parasitic agent even though its use is greatly limited due to toxic side effects, therefore its use is more beneficial as a blue-fluorescent stain for studying DNA.[154] It can be easily transported through cell membranes and has proven to be popular in microscopic studies.[155] DAPI is known to inhibit both RNA and DNA polymerase as it binds to the Adenine-Thymine rich regions of double-stranded DNA.[154] The AT regions of DNA B have a smaller, narrow sulcus than the GC regions, in order for the drug can adapt perfectly to the sulcus walls. Synthetic molecules that affect the major DNA groove are rare. Their smaller size, synthetic molecules tend to collect in the small groove or between base pairs. Guanine-Cytosine regions of B-DNA have wider minor groove and therefore the drug cannot fit against the walls of the groove as opposed to Adeninde-Thymine regions which allow

the drug to fit perfectly against the walls of the groove.[156] Synthetic molecules that are either intercalators or minor groove binders are more favoured over molecules that target DNA major groove because of their significantly smaller size.[157]

The DNA transactions in vivo and in vitro are envisaged by DNA intercalators which have a common use as fluorescent probes.[158] They are known to alter the structure and stability of DNA, which in turn can affect the processing of DNA by proteins.[158] DNA intercalators can be linked reversibly between the double-stranded complimentary bases of DNA.[158]

DNA-processing by proteins can be affected as a result of intercalators disrupting DNA structure and stability upon their attachment.[158] Stabilisation, lengthening, stretching, local unwinding and some other structural changes in the DNA are caused by intercalation. Although the general form of B-DNA is preserved, the change in several biological functions results from intercalation.[159-161] Intercalators are clinically used as anticancer, antiparasitic and antibacterial agents[162-164] as they hinder the transcription process, growth and cell division as a result of suppressing DNA replication, which presents them as excellent therapeutic agents.[165] The structure and dynamics of nucleic acids are studied from examining the mechanisms of intercalation agents.[166, 167] Intercalation is known to generally affect cancer cells due to cancer cells being more susceptible to growth, although other normal cells are also affected.[168] One family of strongly DNA binding agents *via* intercalation are naphthalimides due to their anticancer activity through photoinduced DNA damage and their inhibition of Topoisomerase I/II.[169] Previously developed examples of naphthalimides that have proven their efficacy include: Amonafide, Mitonafide and Elinafide.[169]

1.8.1 Naphthalimides as intercalating DNA Binding Agents

Napthalimides consist of a mainly π-deficient aromatic or heteroaromatic region, which is known to intercalate in between the base pairs of the double helix of DNA.[170] Naphthalimides were developed as a result of a combination of structural components of a number of antitumor synthesised compounds which included the basic side chain of CG603 and tilorone, the glutarimide rings of CG603 and cycleheximide and the β-nitronaphthalene of the aristolochic acid.[171] Stacking and charge transfer of napthalimides are the main driving forces for binding to the DNA.[172] The change of degree of rotation between base pairs, and the distortion of the sugar phosphate backbone occurs due to intercalation, which is known to cause the base pairs to separate vertically.[173] The development of bis-intercalating agents is the result of the therapeutic properties of these lead drugs, where two linked Naphthalimides create more possibilities of limiting cytotoxicity and side effects after administration.[174] The derivatives of 1,8-Naphthalimides are effective in a range of applications in medicine due to their strong photostability, electroactivity and fluorescence, as these types of compounds are used as dyes for polymeric matierials,[175-177] chemiluminescent agents[178] as well as synthetic and natural fibres.[175, 179, 180] A number of derivatives of naphthalimides have also been described as molecular probes.[181, 182] Due to their unique properties, naphthalimides have found application in many areas of chemistry, for example in fluorescence sensors, dyes, chemical probes, in the detection of biologically relevant cations and anions, and in pharmacy as cancer treatment (Figure 1.32).[183-185] It is widely acknowledged that the cytotoxic properties of various substituted Naphthalimides have significant antitumor activity.[182] DNA photocleavage is known to result from a number of reactive intermediates as a result of inhibition of both DNA and RNA synthesis, due to the reading errors in the course of the replication process, as a result of an enzymatic restriction caused by the process of DNA intercalation by the naphthalimide derivatives, due to possessing their cytostatic activity.[186, 187]

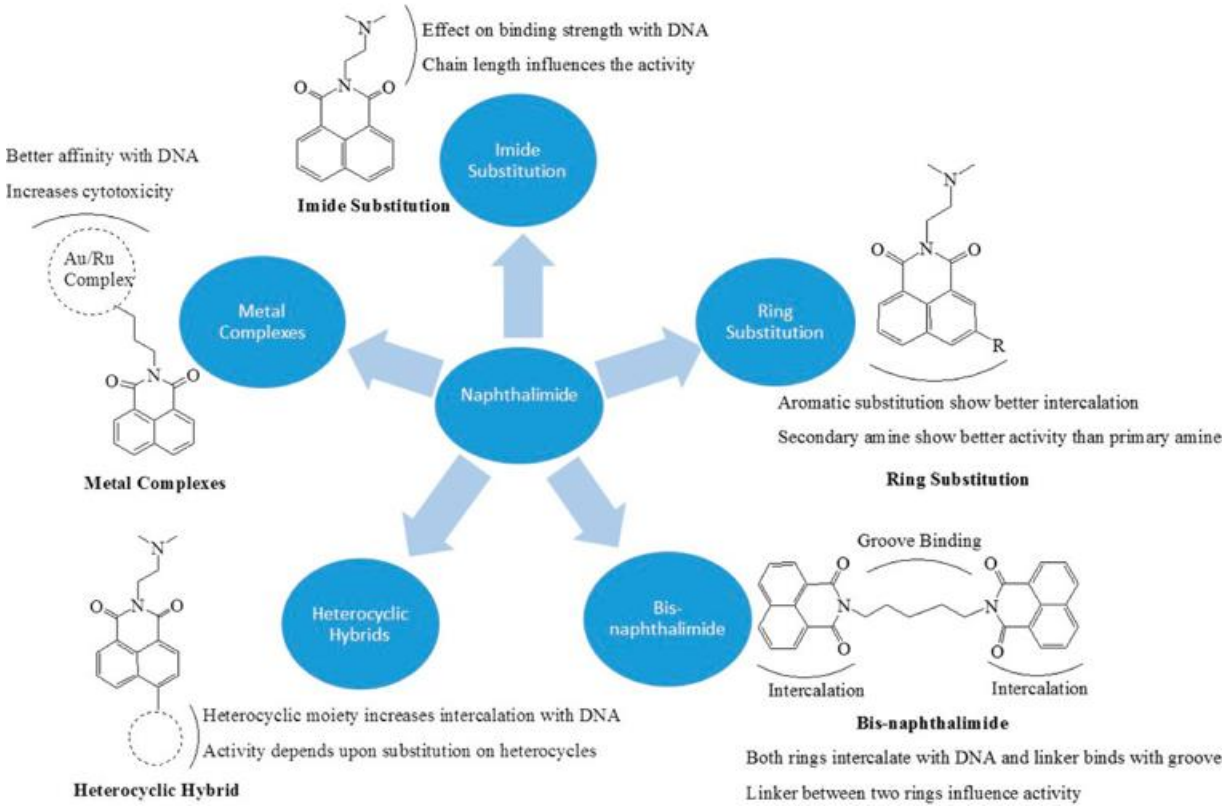

Figure 1.32: Uses of various naphthalimides in different binding modes to DNA.[188]

All clinical trial studies have been abandoned due to toxic side effects of napthalimides, although a number of its derivates have been approved for clinical trials.[189-193] Various changes in the structures of naphthalimides have been made in recent years as several derivatives with different cycle substitutes, side chains and aromatic ring systems were synthesized, to reduce side effects and enhance antitumor activity.[194-197] Naphthalimide dimerisation is a design in which derivatives of 1,8-napthalimides display higher anti-tumour activity in human xenographs, as elinafide (bis-intercalator) has a higher activity compared to monomers and it is therefore a commonly practiced design.[198] Among all sorts of spacers, except Tröger's base moieties,[199-204] *Lin et al.* have studied a spermidine-bound bis-naphthalimide derivative and it had displayed an IC 50 value of 0.15 and 1.64μM for the adenocarcinoma cells HT-29 and Caco-2 in the large intestine and caused intense DNA damage.[205] This compound also displayed an increase in fluorescence upon DNA binding. Intercalators such as bisphenanthridine, bisnaphthalimides and bisphenanazine carboxamides, which are dimers, have also showed a strong anti-tumour potential. The in vivo activities of bis-naphthalimide drugs such as WP631[206] and bisnafide[207] have accelerated the research synthesising new bis-intercalators as DNA binders. The main reason behind the synthesis of dimers is to improve DNA binding affinity and sequence recognition. In some cases, nonetheless, the second

chromophore can serve as a hook to capture cofactors and proteins that bind to DNA but it does not act as an intercalator.[208] The 1,8-naphthalimide derivatives generally show very strong fluorescence and they are universally used as dyes in the polymer industry, fluorescent probes for medical and biological purposes as fluorescent cell markers, n-type materials in the organic light-emitting diodes,[209] anti-HIV drugs and DNA cutting agent, laser dyes and crystal additives.[209] The excellent properties in terms of fluorescence of the commercially available compounds of 1,8-naphthalimide rely heavily on the presence of alkoxy and alkylamine groups at the C-4 position, which are known as strong electron donating groups.[210] As the derivatives of naphthalimides are one of the best examined fluorescent probes owing to their brilliant photophysical properties, these fluorophores are frequently tested in the biological and biochemical disciplines.[211] DNA plays an important role in everyday life and consequently this macromolecule continues to be one of the main molecular targets in the design of antineoplastic agents as naphthalimides are effective intercalators with DNA base pairs and this makes them of the strongly active anticancers drugs.[188] Amonafide, a novel topoisomerase ll inhibitor was first developed almost 40 years ago.[212] As an evidence of marked antineoplastic efficacy in preclinical trials of cancer, the drug was selected for further investigation and testing due to its ability to form a ternary drug-DNA-topoisomerase complex, with the side chain interacting with the enzyme of the DNA and the planar ring interacting with the DNA/protein interface.[213] Amonafide, **31** had specifically been used against secondary treatment-associated acute myeloid leukemia (AML), as amonafide was resistant to Pgp-mediated efflux mechanisms, as Between 50 and 70% of blasts examined from treatment-resistant, relapsed and secondary AML (sAML) were found to be positive for Pgp,[214, 215] as its usefulness in the treatment of various solid malignancies proved limited.[193] After Phase I studies of amonafide in solid tumors identified myelosuppresion as the most significant dose-limiting toxicity (DLT).[216] Mitonafide, **32** intercalates the double stranded DNA, it induces single strand breaks in DNA and hinders the incorporation of DNA precursor into the acid-soluble fraction.[217] Mitonafide is known to induce specific DNA cleavage at a single major site on pBR 322, while it also stabilises a reversible enzyme-DNA as it is a topoisomerase II inhibitor.[218] Mitonafide has shown in vitro toxicity against cells such as KB cells, HeLa cells and other tumoral cell lines, while also showing an in vivo antineoplastic activity against L1210 and P388 leukemias, Lewis lung carcinoma, rat Yoshida carcinoma and Erlich ascites carcinoma.[207, 217] Elinafide, **33** differs from both amonafide and mitonafide as it is a bis-napthalimide (contains two naphthalimide groups) had been tested in a number of tumours including breast cancer, and mesothelioma, breast cancer and ovarian cancer,[219] as it had shown partial regressions or complete regressions

inLOX (melanoma), CX-1 (colon), LX-1 and DLD (colon) xenografts.[174] Elinafide is responsible for bis-intercalating DNA *via* the major groove, where bis-intercalating is a process of intercalation using two links, or a double bond.[220, 221] Elinafide treatment had resulted in tumour regression and tumour growth inhibition and even tumour free survivors in a number of these models.[219] Elinafide is known to form a complex that is sequence-specific which includes the hexanucleotide d(ATGCAT)2, where two naphthalimide groups bis-intercalate with the DNA molecule.[219] In vivo, Elinafide is very effective against tumour xenographts, as tumour xenographts are models of cancer where the cells or tissues from a tumour of a patient are introduced into an immunodeficient or humanised mouse.[198] One of the striking differences between Amonafide and Mitonafide compared to Elinafide is the inclusion of a second naphthalimide moiety: so-called bis-naphthalimides (Figure 1.33).[196, 222] A number of bis-naphthalimides have been reported, where they show strong DNA binding ability coupled with high cellular cytotoxicity.[203]

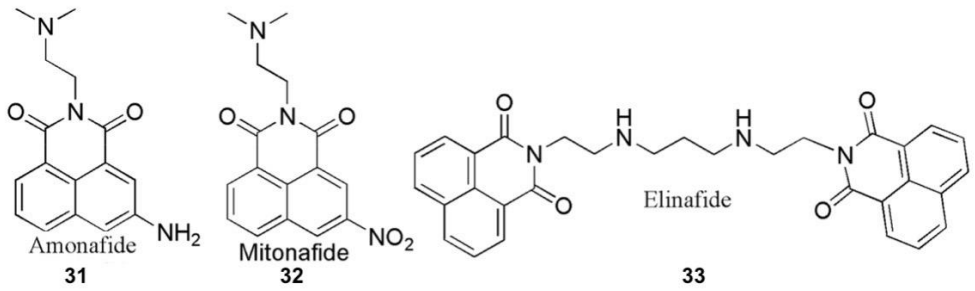

Figure 1.33: Chemical structures of mono-naphthalimide derivatives: Amonafide, Mitonafide and a bis-naphthalimide derivative: Elinafide.

1.8.2 Bis-Naphthalimides as intercalating DNA Binding Agents

A recently reported example of bis-naphthalimides containing a Pt(II) linker, **34** and **35** display high cytotoxicity against MCF-7 breast cancers, while having strong binding ability due to Pt(II) additionally binding to the negatively charged sugar phosphate backbone *via* electrostatic interactions (Figure 1.34).[190]

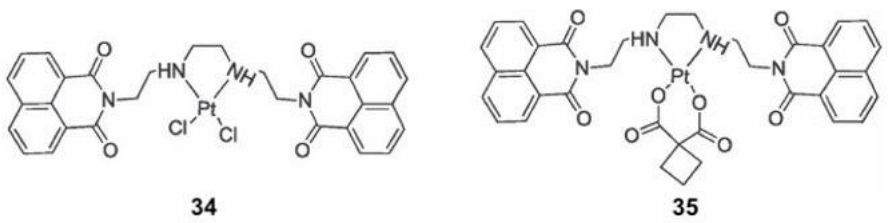

Figure 1.34: Pt(II) bis-naphthalimide family of compounds, which display stronger cytotoxicity and DNA binding over cisplatin in MCF-7 breast cancer cells.

These agents also display excellent results in minimising resistant cisplatin-resistant cells lines.[190] Transition metal complexes have sparked a lot of interest in recent years as chemotherapeutic anti-cancer agents in recent years.[223] *Perez et al.* have synthesised various novel Pt-bis naphthalimide conjugates in order to minimise cellular resistance, while enhancing cytotoxicity and DNA binding ability *via* bis intercalation (from both naphthalimide groups) and platinization of DNA bases by Pt(II).[224] Both 4-N,N-dimethylamino-1,8-naphthalimide and terpyridyl are incorporated by the Pt(II) based bifunctional DNA binder, recently synthesised by *Banerjee et al.*, displaying stronger (IC_{50} 18 mM) toxicity against MCF-7 breast cancer cell lines and stronger DNA binding affinity in comparison to the commercially available cis-platin.[225]

Due to the kinetic and chemical inertness, water solubility and spectroscopic properties such as photoluminescence and visible light absorbance, Ru(II)-polypyridyl complexes demonstrate their uses in modern therapeutic treatments.[44, 226, 227] These complexes have displayed their internalisation mechanisms *via* passive diffusion, endocytosis and active transport, as well as *via* the use of polypeptides for cell internalisation.[228-238] Electrostatic interactions, intercalation, and groove binding are examples of modes of Ru(II)-polypyridyl binding to DNA.[44] Both Ru.Nap, **36** and Ru.2Nap, **37** have strong DNA binding properties due to their CD activity in the presence of DNA (Figure 1.35).[239]

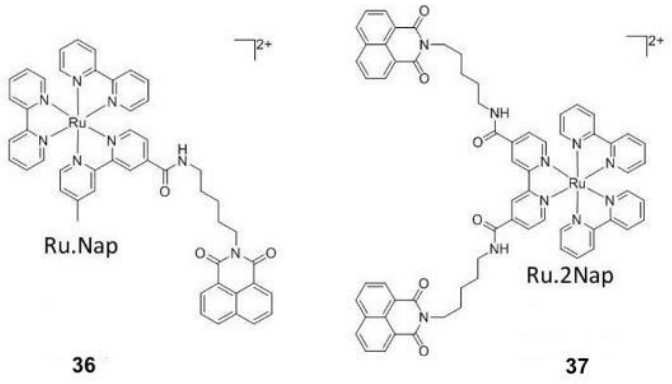

Figure 1.35: Chemical structures of DNA binders: Ru.Nap and Ru.2Nap.

The naphthalimide moiety of **36** displayed binding to DNA *via* the process of intercalation, proven by the substantial negative band in the LD.[239] Proven by the small LD signal of the naphthalimide region, **37** had displayed binding to DNA in a more complex way. Both naphthalimide regions of **37** have intercalated into DNA, which caused the Ru(II)-polypyridyl centre shift in its position at the negatively charged DNA sugar phosphate backbone.[239]

Compound **37** had displayed poor cleavage of plasmid DNA upon light activation when compared to **36**. Compound **37** was nontoxic when introduced to HeLa cells, as it had significantly reduced viability of the HeLa cell after photoactivation.[239] It was concluded that the presence of a second naphthalimide strengthened the binding ability of **37** compared to single naphthalimide moiety in **36**, while not increasing its toxicity and this information is detrimental as such complexes have the potential for the uses as therapeutic agents.[239] This creates the possibility to use a different linker in potential bis-naphthalimide agents, which has the ability to bind to the negatively charged sugar phosphate backbone of DNA. One method of conjugation that has garnered significant interest recently is the use of the squaramide moiety to act as a linker between two molecules. With excellent H-bonding ability coupled with synthetic versatility, the squaramide seems an obvious choice in linking two naphthalimide structures.

1.9 Squaramides

Squaramides, a family of cyclic derivatives of the rigid form of cyclobutene, are rapidly gaining interest in research in various fields of chemical and biological science.[240-243] This small molecular scaffold consists of two carbonyl hydrogen bond acceptors close to two N-H hydrogen bond donors and benefits from unique physical and chemical properties that make it exceptionally useful in various areas such as self-assembly, catalysis, bioconjugation and molecular recognition.[240] The process of delocalisation of a nitrogen lone pair in the cyclobutenedione ring system, gives the four-membered ring its aromatic character (Huckel's rule: electrons [4n + 2] p, n = 0).[241] Furthermore, the ability of squaramides to form strong hydrogen bonds that simultaneously improve the aromaticity of the four-membered ring is extremely beneficial, as the molecular recognition and self-assembly processes can take advantage of the thermodynamic stability caused by the aromatic gain.[244, 245] Squaramides are predominantly known to be favourable in asymmetric synthesis as chiral ligands and H-binding catalysts,[246-249] but are also very useful as building blocks in the field of medicinal chemistry. Navarixin (chemokine receptor antagonists 1 and 2)[250] and Perzinfotel (NMDA receptor antagonist)[251] are examples of small molecules with an embedded squaramide structure that have reached the various stages of clinical studies. One of the main reasons why squaramides are considered as a motif of interest is due to their ability to donate H-Bonds to various functional groups such as ureas, amino and carboxillic acids, cyanoguanidine, guanidine and various phosphate groups make squaramides very attractive in medicinal chemistry.[241] In the recent years, derivatives of mono- and bis-squaramides have been studied for the treatment of Malaria,[252] Chagas disease[253] and Leishmania,[254] which are diseases transmitted by insects. A high affinity for hydrogen bonding is caused by a simultaneous increase in the aromaticity of the cycle. This hydrogen bond and aromatic change in combination with structural rigidity has been used in many Squaramide applications.[241] The simultaneous gain of the aromaticity of the ring causes strong hydrogen bonding affinity and this enabled the use of this aromatic change and aromatic switching together with structural rigidity has been used in many squaramide applications.[241] In a series of articles, Deya, Frontera and their colleagues have examined the physical properties of squaramides and their derivatives with cations and anions.[241] It was acknowledged that secondary squaramides provide donors, acceptors and donor-acceptor groups with a high possibility of forming hydrogen bonding to acceptors suaramides.[241] An investigation of the configuration of artificial squaramide receptors for the detection of cations has shown that squaramide receptors have a strong acceptance of hydrogen bonds in the

detection of ammonium ions.[241] It has been shown that the excellent hydrogen bonding and acceptance of squaramides (Figure 1.36)[241] can be described by an improvement in the aromaticity during the development of hydrogen bonds, which differentiates them from the urea-based groups.[255]

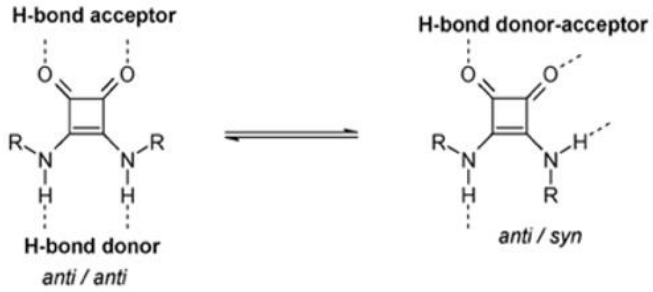

Figure 1.36: Squaramides displaying the ability to act as hydrogen bond donors-acceptors in both anti/anti and anti/syn configurations.

Hence, squaramides have been utilised as an alternative to (thio) urea in the process of organocatalysis.[256] The process of self-aggregation of squaramides generates low solubility and thus possible precipitation, which is created by a multitude of links from head to tail *via* double hydrogen bonds.[257] Low solubility of squaramides in non-polar solvents, reduced the ability to regulate the pK_a of the donor hydrogens and the limited solubility in non-polar solvents restrict the performance in a number of reactions.[257]

Recently, the area of anion detection has grown significantly, and much research has been performed in the field of anion sensors,[258, 259] anion receptors.[260] The first revolutionary work by Costa and colleagues in the field of anion detection with squaramides[261, 262] was followed by a report by *Fabbrizzi et. al*, in which the ability to detect urea anions was compared with a squaramide which had identical aromatic substituents.[255]

Numerous biological processes are dependent on the process of molecular recognition between a substrate and the associated enzyme.[263] Hydrogen, π-π, cation-π, and anion-π, van der Waals, hydrophobic and electrostatic interactions are responsible for holding substrates with the associated enzymes.[264] Derivatives of squaramides have been precisely studied as receptors for numerous anions including: sulphate,[246] chloride,[241] benzoates[265] and carboxylates[241] due to the strong interactions of the hydrogen bond with the anions (Figure 1.37).

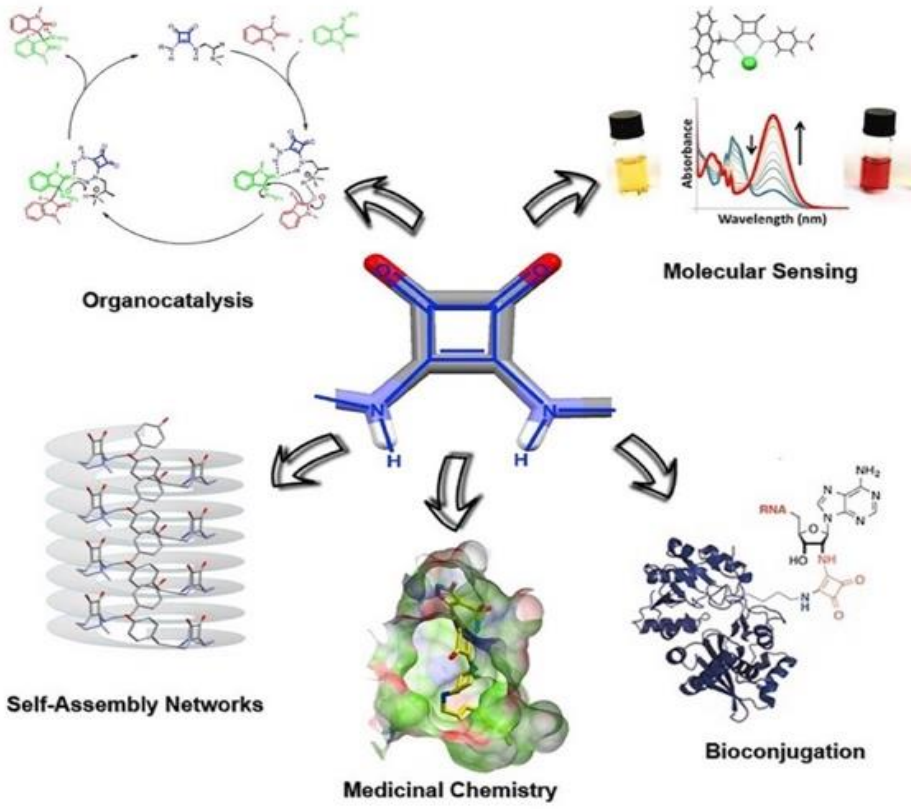

Figure 1.37: Squaramides displaying their ability in various beneficial applications.

While the use of squaramides has attracted a lot of research attention in recent years, they have not yet been exploited in the field of DNA recognition. Given their known ability to bind to anionic species, this is surprising, particularly given the anionic nature of the DNA-phosphate backbone. This project will aim to explore the potential of squaramides to improve DNA binding ability, specifically in this case taking advantage of the naphthalimide moiety. The following section will outline the specific aims and objectives for the project.

1.10 Aims and Objectives

As part of this project, we aim to design and synthesise a range of squaramide based bis-naphthalimides (Figure 1.38). The general design strategy is outlined as a schematic in Figure 1.38. This will include a central squaramide unit conjugated to two naphthalimide units *via* aliphatic linker. Two main variables will be introduced, whereby the linker length will be varied from 2 carbons to 8 carbons. Similarly, the orientation and substitution pattern of the naphthalimides will be varied to provide a range of photophysical properties and DNA binding characteristics. Given the ability of Elinafide to bind strongly to DNA, we expected that the inclusion of a squaramide moiety would improve DNA binding ability given its known propensity for strong H-bonding. This is particularly important given the negatively charged sugar-phosphate DNA backbone. We will synthesise a series of bis-naphthalimides, where we will vary the linker length that separates the squaramide (H-bonding ability) from the naphthalimides (intercalation). This creates the possibility that the bis-naphthalimide linker will bind to the negatively charged sugar phosphate backbone of DNA *via* hydrogen bonding, while the naphthalimides will engage in DNA intercalation.

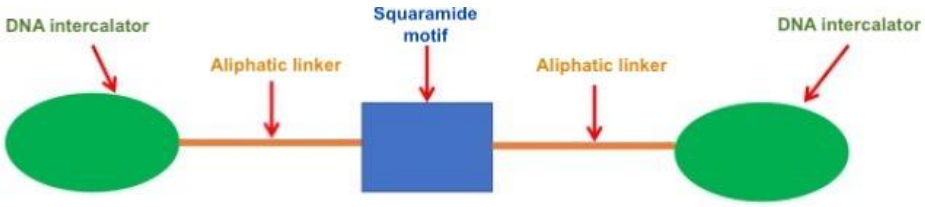

Figure 1.38: General schematic of proposed synthetic compounds.

We have designed compounds **38-46** (Figure 1.39), a family of squaramide-naphthalimide conjugates, where both the linker length and substitution pattern of the naphthalimide will be varied. *Elmes et. al* have previously synthesised a series of naphthalimide-squaramide conjugates that efficiently assembled in solution, where self-assembly was reversed as soon as the H-bonding network was disrupted by anion addition.[266] The squaramide position relative to the naphthalimide was varied at either the head or the tail of the structure, as the design included a short linker with a strongly hydrophobic side arm, which was believed to support the sensor's aggregation behaviour in polar solvents.[267] These important results will be used to inform experimental design for this project. **38-40** are composed of naphthalimides without substitution, this was chosen for the ease of synthesis and also the observing the fluorescent properties, DNA binding properties and the possibility of synthesis of substituted naphthalimides, where **41-43** contain an amino naphthalimide. The 4-amino naphthalimide was

chosen as this substitution of naphthtalimide describes the possibility of an increase in emission an important consideration, when designing squaramide containing bis-naphthalimides. Upon binding to DNA, it is expected that these compounds would be strongly fluorescent prior to DNA interaction, with a large shift in fluorescence change after DNA interaction, enabling the determination of DNA binding due to this change in emission. Thirdly, **44-46** included an alternative attachment point to the naphthalimide, where the linker was incorporated at the 4-carbon position. It was expected that this may affect the DNA binding properties for these conjugates, as Gunnlaugsson *et al.* previously reported the importance of the substitution of the tail-to-head attachment of naphthalimides.[268]

Once successful synthesis and characterisation has been carried out, we will investigate the photophysical properties, the self-assembly behaviour as well as the DNA binding ability of each compound.

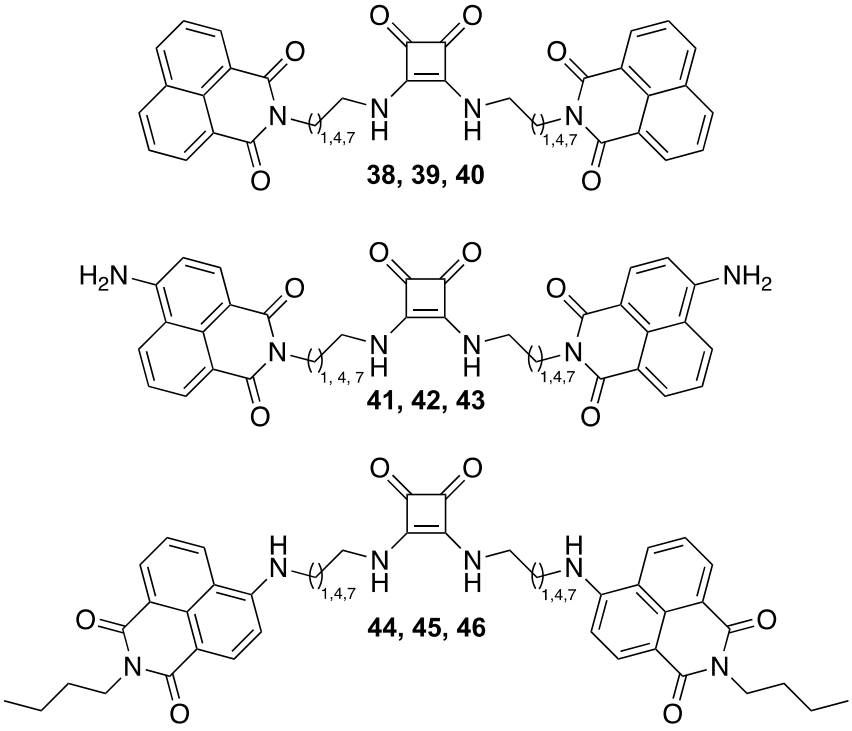

Figure 1.39: Proposed synthetic compounds **38-46**.

Chapter 2 Synthesis

2.1 Introduction

As discussed in the previous chapter, naphthalimides are a class of polycyclic imides that comprise of π-deficient planar aromatic or heteroaromatic ring systems.[188] 1,8-naphthalimides and their derivatives have displayed excellent physicochemical and biological properties. Most of 1,8-naphthalimides display a broad range of biological activities as they show strong antiviral, antibacterial and anticancer activity.[171] 1,8-Naphthalimides are especially known to inhibit tumour growth and tumour metastasis, due to their strong DNA intercalation.[188] For instance, as previously discussed in Chapter 1, Elmes *et al.* reported a group of naphthalimide-based ruthenium compounds as DNA binders. The scientific community has made several attempts to enhance the naphthalimide moieties to promote their DNA antitumor and photocleaving abilities, by synthesising bis-naphthalimides which increase their DNA binding ability.[174, 222, 269] Naphthalimides have found application in a variety of areas of chemistry, from their use as anticancer, antiviral, anti-inflammatory, antiprotozoal and antidepressant agents to novel DNA intercalators in medicinal chemistry.[171] Research by the Elmes group has focused on the development of squaramide-naphthalimide scaffolds with potential applications in a variety of biomedical and anticancer treatments.[240] The aim of this chapter is to synthesise squaramide, bis-naphthalimide conjugates, which were varied in the aliphatic chain lengths and electron donating group presence, squaramide absence in a bis-naphthalimide and squaramide absence in a mono-naphthalimide. Below, we will outline the synthetic approach to make compounds **38-46** using various known and new synthetic transformations.

2.1.2 Varying the linker

Three different lengths of linkers (2-carbon, 5-carbon and 8-carbon) were exploited in the design of the novel squaramide-naphthalimide conjugates (Figure 2.1). A 2-carbon linker was introduced into the design of the novel compounds to promote potential stacking interactions *via* increased structural rigidity, which is ascribed to the reduced degrees of rotation by the presence of the two carbon groups. The linker of 5-carbons was introduced into the design of the novel compounds to act as a comparison for the linker containing 2-carbons, which is more prone to aromatic stacking. The main objective was observing whether the bis-intercalation into DNA by the naphthalimide motifs of the molecule were more intense, due to the varied lengths of the aliphatic moiety. The linker of 8-carbons was synthesised to observe whether this squaramide-naphthalimide conjugate is even more likely to bis-intercalate into DNA, due

to its longer distance from the squaramide motif compared to the previously synthesised 2-carbon and 5-carbon length squaramides.

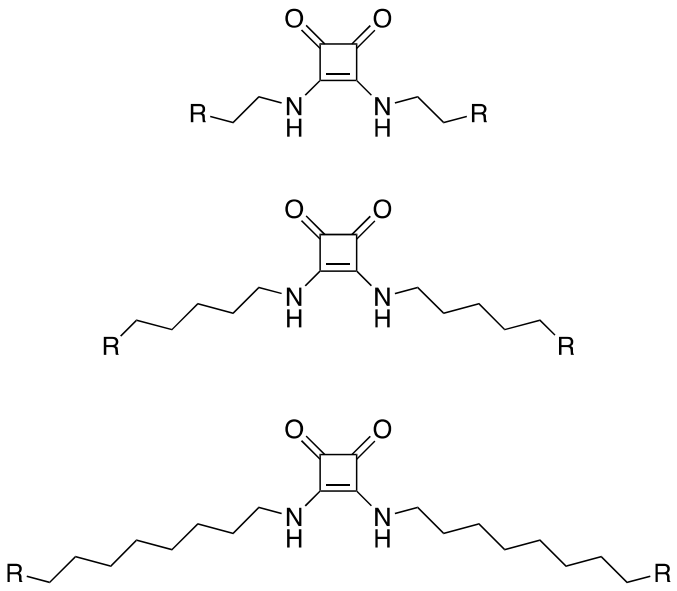

Figure 2.1: Structure of linkers exploited in the design of the potential bis-intercalators.

2.1.3 The squaramide motif

Squaramides have the capacity for selectively binding into the negatively charged sugar phosphate backbone of DNA *via* their acidic N-H groups resulting in the formation of H-bonds.[240, 266] Squaramide scaffolds have the ability to undergo π-π interaction between the cyclobutenedione rings, due to their properties of aromaticity and planarity.[240] In the design of our novel squaramide-naphthalimide conjugates, we foresaw the π-π interaction between the cyclobutenedione rings. We have also foreseen the remarkable hydrogen bonding donor ability of the squaramide motif could be utilised to use these squaramide-naphthalimide conjugates as DNA binders.

2.1.4 Varying the Substitution Patterns

These reports indicate that 1,8-naphthalimide derivatives are not only capable of cleaving DNA photochemically but that, depending on the substitution pattern, hydrogen abstraction atoms from deoxyribose, or from thymine methyl groups, can result in site selective photocleavage.

2.1.5 The Binding Site Position

In the design of our novel squaramide-naphthalimide conjugates (Figure 2.2), we envisaged to synthesise squaramide-naphthalimide conjugates with a non-substituted naphthalimide, 4-nitro bis-naphthalimide to yield the desired 4-amino bis-naphthalimide. The fluorescence properties of naphthalimides can also be modulated by the nature of the substitution pattern. This substitution was varied due to the synthetic pathway leading to the synthesis of the 4-nitro bis-naphthalimide derivatives, which are not fluorescent due to the electron withdrawing nitro group presence. These compounds will be further reduced into the 4-amino bis-naphthalimide derivatives, with an electron donating group. 4-amino bis-naphthalimides are known for their strong emission and fluorescence properties. These compounds have strong green-fluorescence properties and after intercalation into DNA, their fluorescence undergoes a red-shift.[270] This would make it easier to determine their binding into DNA *via* intercalation.

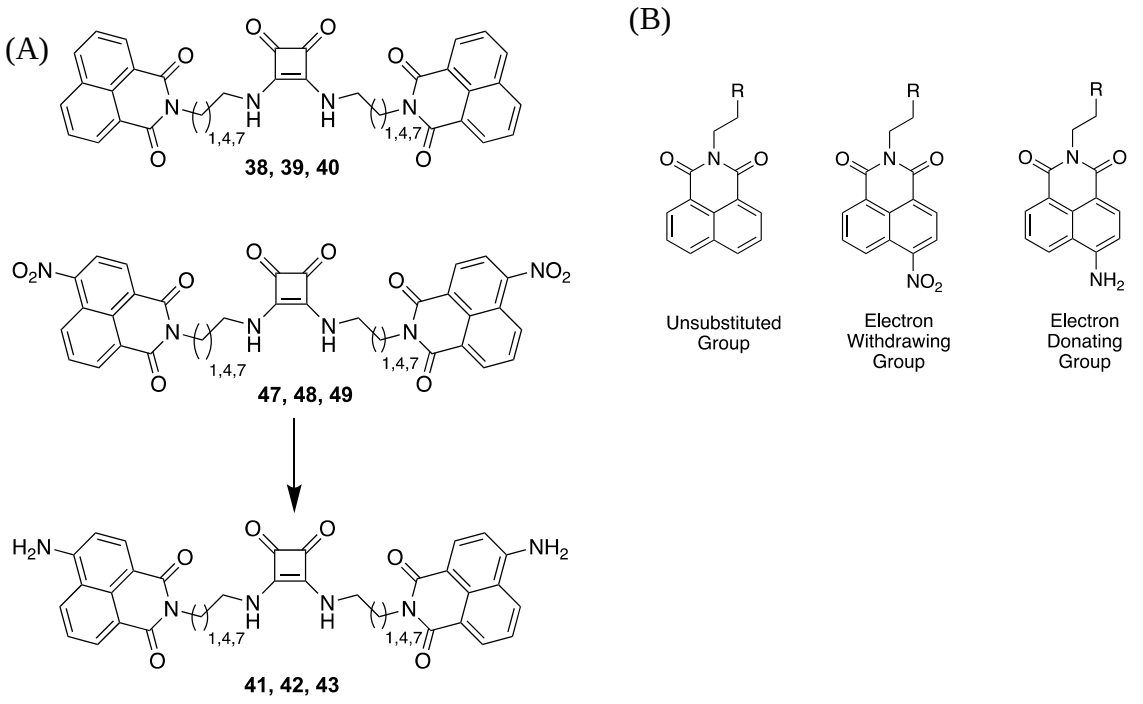

Figure 2.2: (A) Structures of target compounds with unsubstituted, electron withdrawing and electron donating naphthalimide moieties. (B) Variations of synthesising possible 1,8-naphthalimide derivatives.[271, 272]

2.2 Synthesis

The target compounds **38-40, 47-49, 97** and **98** were synthesised from commercially available starting materials. All intermediate and target compounds were fully characterised using ^{1}H NMR, ^{13}C NMR, high resolution mass spectrometry and infrared spectroscopy. In this chapter, the description of the synthesis and characterisation of each synthesised compounds **38-40, 47-49, 97** and **98** and the attempted syntheses of compounds will be given.

The proposed synthetic pathway will firstly involve the mono-boc protection of the aliphatic linker, followed by the reaction with naphthalene-1,8-dicarboxylic anhydride, which will be deprotected with trifluoroacetic acid in dichloromethane and the resulting trifluoroacetic salt will be reacted with diethyl squarate to yield the desired compounds **38-40** (Figure 2.3)**.**

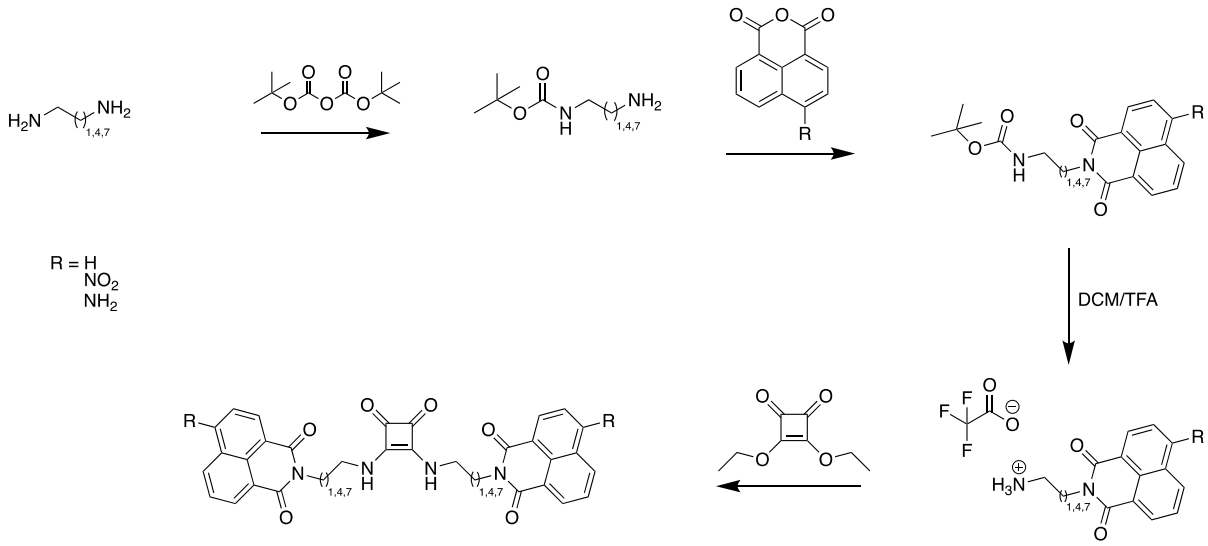

Figure 2.3: Initially proposed synthetic pathway of compounds **38-46.**

2.2.1 Synthesis of 50

The synthesis of diethyl squarate, **50** (See Appendix) was achieved using intermediates in the synthetic pathway as outlined in scheme 2.1. 3,4-dihydroxycyclobut-3-ene-1,2-dione was dissolved in ethanol followed by an instant addition of triethylorthoformate. The mixture was allowed to reflux at 85°C for 48 hours.[273] The product was concentrated in-vacuo to afford the crude material. The desired product was purified *via* column chromatography to afford a yellow oil, which was the pure product with a yield of 82%.

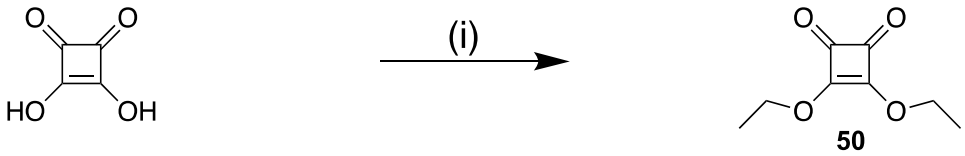

Scheme 2.1: Synthesis of **50.**

i) Triethylorthoformate, ethanol.

2.2.2 Synthesis of 51, 52 and 53

The next step involved synthesising aliphatic linkers of appropriate lengths. The syntheses of compounds **51**, **52** and **53** involved a mono-boc protection of ethane-1,2-diamine, pentane-1,5-diamine and octane-1,8-diamine by a dropwise addition of di-*tert*-butyl dicarbonate, while allowing it to stir at 0°C for 3 hours.[274] After letting the reaction reach room temperature overnight while stirring, the mixtures were each washed with water and with brine, dried over $MgSO_4$ and the products were concentrated in-vacuo to afford a colourless oil in all three cases. The afforded yields in all three reactions were 90% for **51**, 85% for **52** and 91% for **53.**

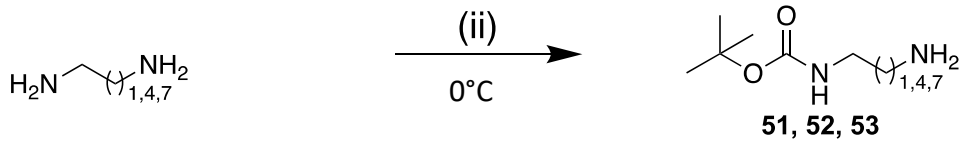

Scheme 2.2: Syntheses of **51**, **52** and **53**.

ii) Chloroform, di-*tert*-butyl dicarbonate.

2.2.3 Synthesis of 54, 55 and 56.

Naphthalene-1,8-dicarboxylic anhydride was dissolved in toluene with triethylamine. The appropriate diamines were all added into each separate reaction. All three reactions were allowed to reflux at 125°C for 12 hours accordingly following the standard method.[275] The reaction times were also monitored by TLC and ^{1}H NMR analyses. The solvent was removed in-vacuo to afford the crude products. The desired products were purified *via* column chromatography to afford white solids **54**, **55** and **56** with yields of 89%, 84% and 77%. ^{1}H NMR analysis of **54** (Figure 2.4) had further confirmed the purity of the compound, where the naphthalimide moiety was represented by the signals at 8.49, 8.45 and 7.87 ppm, while the N-H was represented by a signal at 6.88 ppm, the aliphatic CH_2s were represented by the signals at 4.14 ppm and 3.25 ppm and the boc-protecting group was represented by the singlet signal

at 1.02 ppm. Similar results were obtained for **55** and **56** with only additional aliphatic CH_2 signals (2.0-5.0 ppm) depending on the length of the aliphatic chain for each compound.

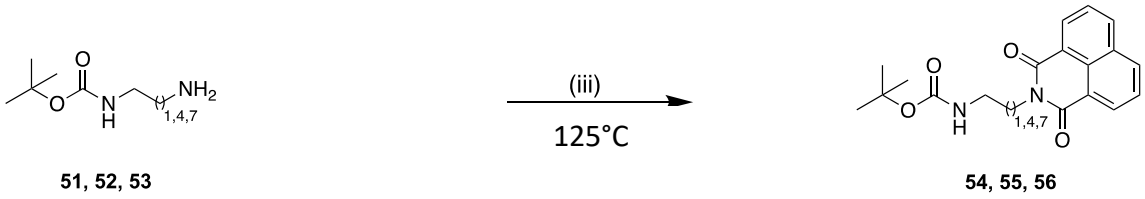

51, 52, 53 **54, 55, 56**

Scheme 2.3: Syntheses of **54**, **55** and **56**.

iii) Ethanol, triethylamine, naphthalene-1,8-dicarboxylic anhydride

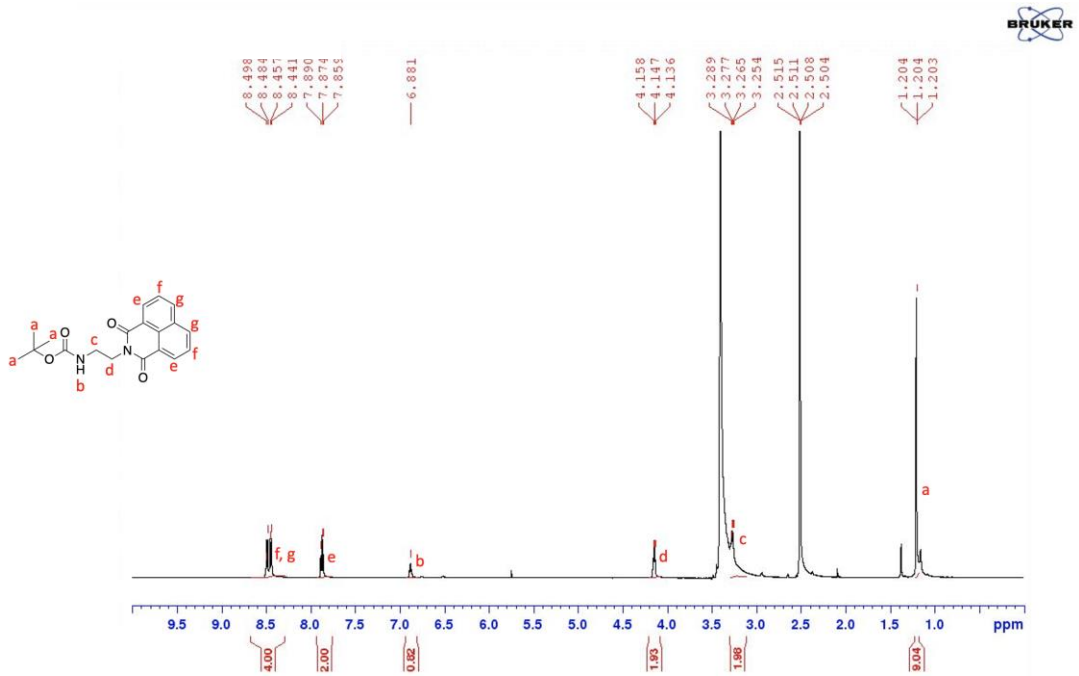

Figure 2.4: The ^{1}H NMR Spectrum of **54** (500 MHz, DMSO-d_6, 298 K.)

54, **55** and **56** were each dissolved in dichloromethane and trifluoroacetic acid (50:50). All three reactions were allowed to stir at room temperatures. The reduction of **54** required 2 hours to form the product TFA salt **57**. The reduction of **55** required 3 hours to form the product TFA salt **58** and the reduction of **56** to form the product TFA salt **59** required 12 hours. The solvent was removed with N_2 and in-vacuo. The title compounds appeared as brown residues in all three cases and were used directly without further purification closely mirroring the reaction done previously by *Kamal et. al*.[276] The LCMS (Figure 2.5) demonstrated the purity of **57,** with a single peak of the compound, without any other impurities, where the TFA peak is not observed due to TFA being used as an ion-pairing reagent in the mobile phase of the analysis.

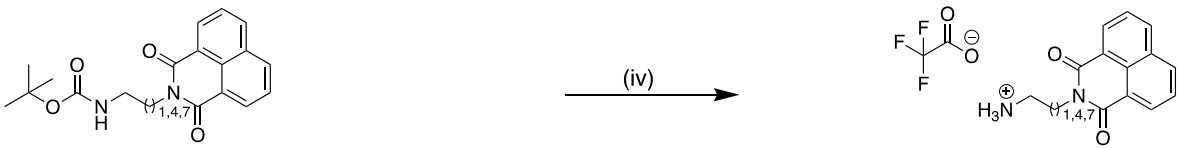

54, 55, 56

57, 58, 59

Scheme 2.4: Syntheses of **57**, **58** and **59**.

iv) Dichloromethane, trifluoroacetic acid

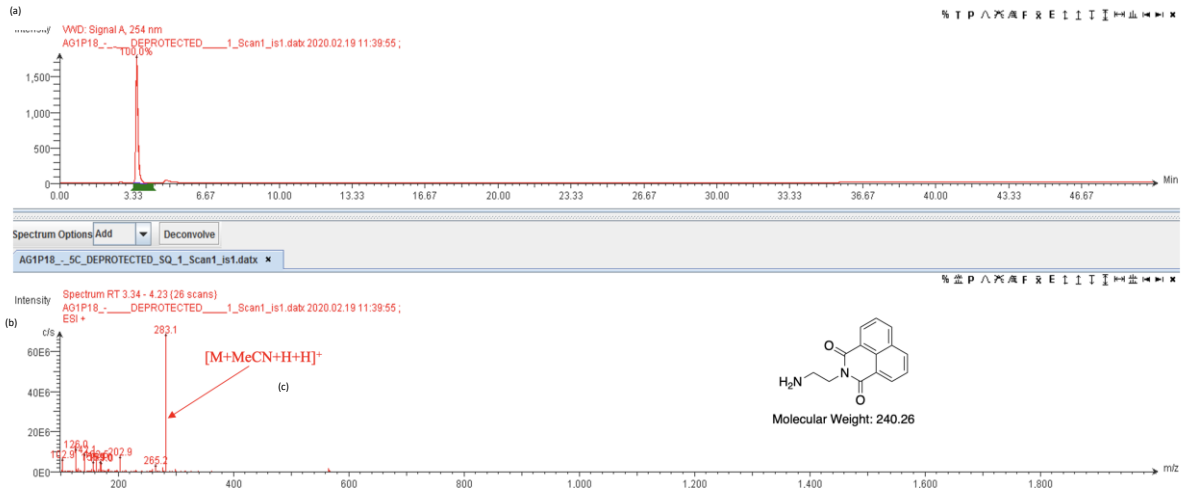

Figure 2.5: LCMS Characterisation of **57:** (a) Analytical HPLC trace of purified **57**; R_t = 3.0 mins (0-100% MeCN over 30 mins, λ = 254 nm). (b) Extracted Ion Chromatogram for 241.26 $[M + H]^+$. (c) Mass Spectrum detected between R_t = 3.0-4.0 mins (157 scans); Calculated for $[M + H]^+$ = 241.3; Mass Found (ESI^+) = 283.1 $[M + MeCN+H+H]^+$.

It was theorised that once **57**, **58** and **59** were each dissolved in ethanol first and the solvents mentioned were added after using ethanol with a slow addition of **50**, the desired products would be achieved, as previously done with naphthalimide urea derivatives.[275] Triethylamine was added in all three reactions until completely dissolved. **50** was added into the reactions individually. All three reactions were allowed to reflux at 85°C for 12 hours. The reactions all formed precipitates, which were filtered and centrifuged in ethanol and diethyl ether. Unfortunately, upon NMR analysis (Figure 2.6), it was clearly observed that the precipitates formed were not the desired compounds but were the result of mono-substitution (Scheme 2.5).

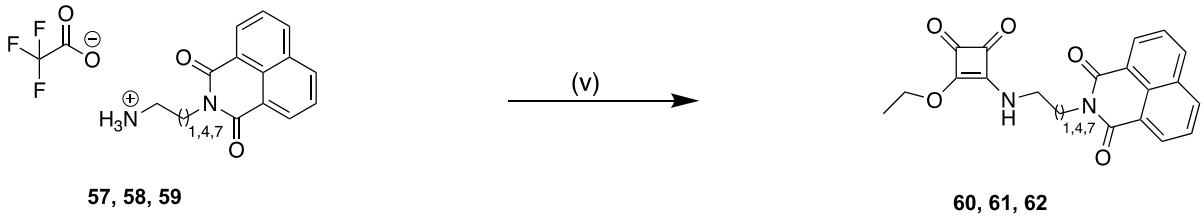

57, 58, 59 60, 61, 62

Scheme 2.5: Syntheses of **60**, **61** and **62**.

v) Triethylamine, 3,4-diethoxycyclobut-3-ene-1,2-dione, Attempted to synthesise the target compounds in Ethanol first and after numerous failed attempts: Methanol, Toluene, Dichloromethane, Dimethylformamide, Tetrahydrofuran have been used, similarly done in the following attempted final product reactions.

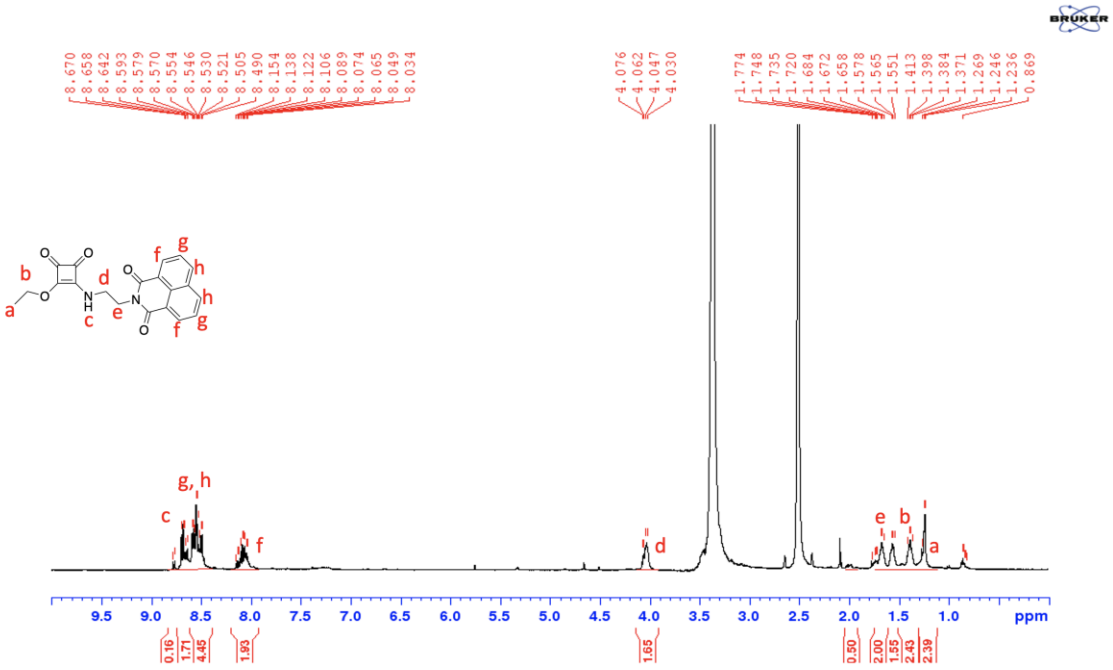

Figure 2.6: The ^{1}H NMR Spectrum of **60** (500 MHz, DMSO-d_6, 298 K.)

^{1}H NMR analysis of **60** (Figure 2.6) had further confirmed the mono-substitution of the starting materials, where the naphthalimide moiety was represented by the signals at 8.56, 8.51 and 8.09 ppm, while the N-H was represented by a signal at 8.63 ppm, the aliphatic CH_2s were represented by the signals at 4.05, 1.71 and 1.60 ppm, while the methyl CH_3 region was represented by the singlet signal at 1.25 ppm. Similar results were obtained for **61** and **62** with only additional aliphatic CH_2 signals depending on the length of the aliphatic chain for each compound.

The challenges encountered, when reacting **57, 58** and **59** with 3,4-diethoxycyclobut-3-ene-1,2-dione resulting in **60, 61** and **62** due to these compounds forming a precipitate when the squaramide became mono-substituted. Despite several unsuccessful attempts at this approach, it was evident that a different approach of synthesis had to be explored.

Throughout the synthesis of the target compounds, we encountered challenges. The main challenges faced were: solubility of intermediates, purification of both intermediates, target compounds and reduced reactivity of the starting materials. We therefore proposed to change the synthetic pathway. The new proposed synthetic pathway entailed the mono-boc protection of the aliphatic linker, followed by the reaction with diethyl squarate to form the di-substituted derivative. This was followed by the deprotection and the final reaction with the naphthalene-1,8-dicarboxylic anhydride (Figure 2.7). We hoped that this would yield our desired compounds.

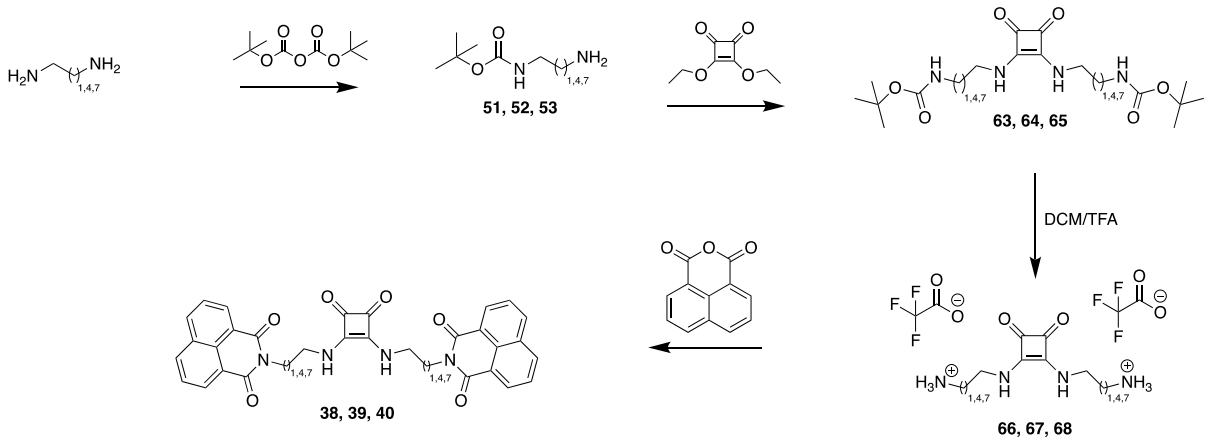

Figure 2.7: Novel proposed synthetic pathway of compounds **38-46**.

2.2.4 Synthesis of 63, 64 and 65

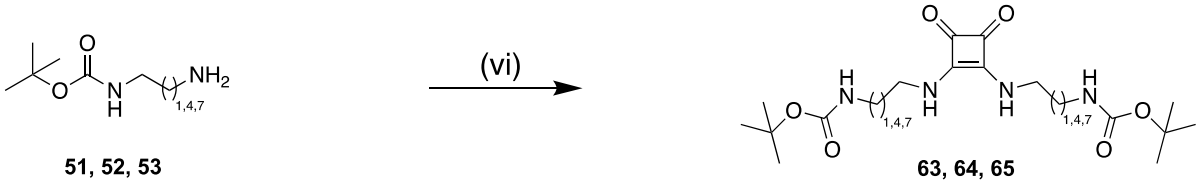

Scheme 2.6: Syntheses of **63**, **64** and **65.**

vi) 3,4-diethoxycyclobut-3-ene-1,2-dione, ethanol.

The following steps involved the conjugation of the various linkers to the central squaramide moiety. The syntheses of **63**, **64** and **65** involved dissolving **51**, **52** and **53** respectively in ethanol, followed by a dropwise addition of 3,4-diethoxycyclobut-3-ene-1,2-dione and allowing the mixtures to reflux at 85°C for 12 hours. The products were concentrated in-vacuo to afford the crude material. **63** and **64** title compounds were purified *via* column chromatography to afford two products which appeared as white solids with yields of 88% and 81% respectively, while **65** had precipitated when the reaction had undergone completion and was isolated by filtration with a yield of 79%. The ^{1}H NMR of compound **63** is shown in Figure 2.8 as an example. As can be seen, the broad singlet at 7.5 ppm indicates the presence of an N-H of the squaramide moiety, while the peak at 6.9 ppm indicated the presence of another N-H, which was assigned to the boc protecting group. There was a signal integrating to two at 3.5 ppm, which was indicative of aliphatic CH_2 next to the squaramide, while another signal represented two protons at 3.1 ppm which was indicative of the aliphatic CH_2 next to the boc-protecting group, which integrated to nine at 1.3 ppm. LCMS analysis was also conducted (Figure 2.9), which displayed a presence of a single compound and with hits for $[M+H]^+$ and $[M+Na]^+$, confirming both the purity and the identity of our proposed compound.

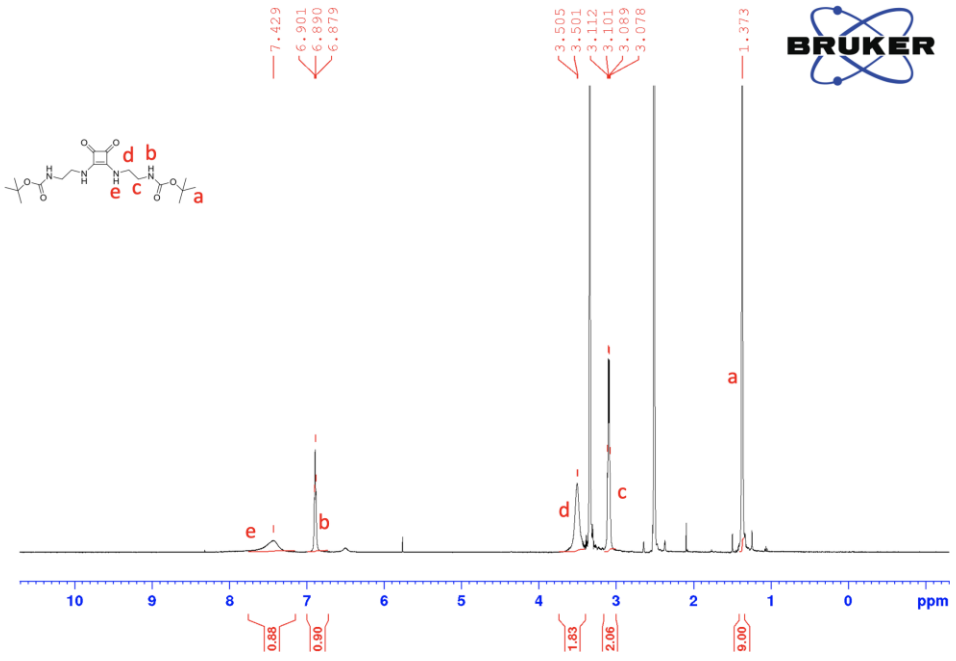

Figure 2.8: The ^{1}H NMR Spectrum of **63** (500 MHz, DMSO-d_6, 298 K.)

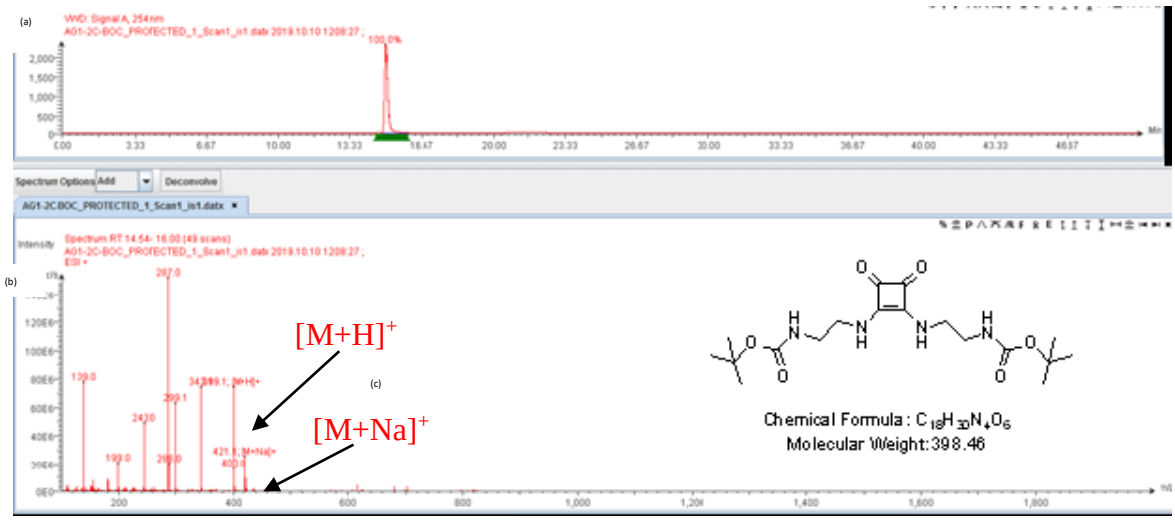

Figure 2.9: LCMS Characterisation of **63:** (a) Analytical HPLC trace of purified **63**; R_t = 15.0 mins (0-100% MeCN over 30 mins, λ = 254 nm). (b) Extracted Ion Chromatogram for 398.46 $[M + H]^+$. (c) Mass Spectrum detected between R_t = 14.6-16 mins (157 scans); Calculated for $[M + H]^+$ = 399.4; Mass Found (ESI^+) = 399.1. Also Found 421.1 $[M + Na]^+$.

2.2.5 Synthesis of 66, 67 and 68

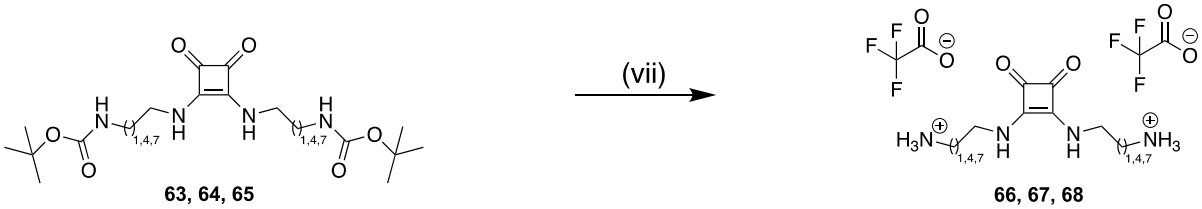

Scheme 2.7: Syntheses of **66**, **67** and **68**.

vii) Dichloromethane, trifluoroacetic acid

The syntheses of **66**, **67** and **68** involved dissolving **63**, **64** and **65** in dichloromethane. Trifluoroacetic acid was added into all three mixtures respectively, while they were allowed to stir at room temperatures for 2, 5 and 12 hours respectively, as previously done with naphthalimide urea derivatives.[275] The solvent was evaporated with N_2 and in-vacuo. The title compounds appeared as brown residues in all three cases and were used directly without further purification. The LCMS (Figure 2.10) demonstrated the synthesis of **67,** with a single peak of the compound, without any other impurities, where the TFA peak is not observed due to TFA being used as an ion-pairing reagent in the mobile phase of the analysis.

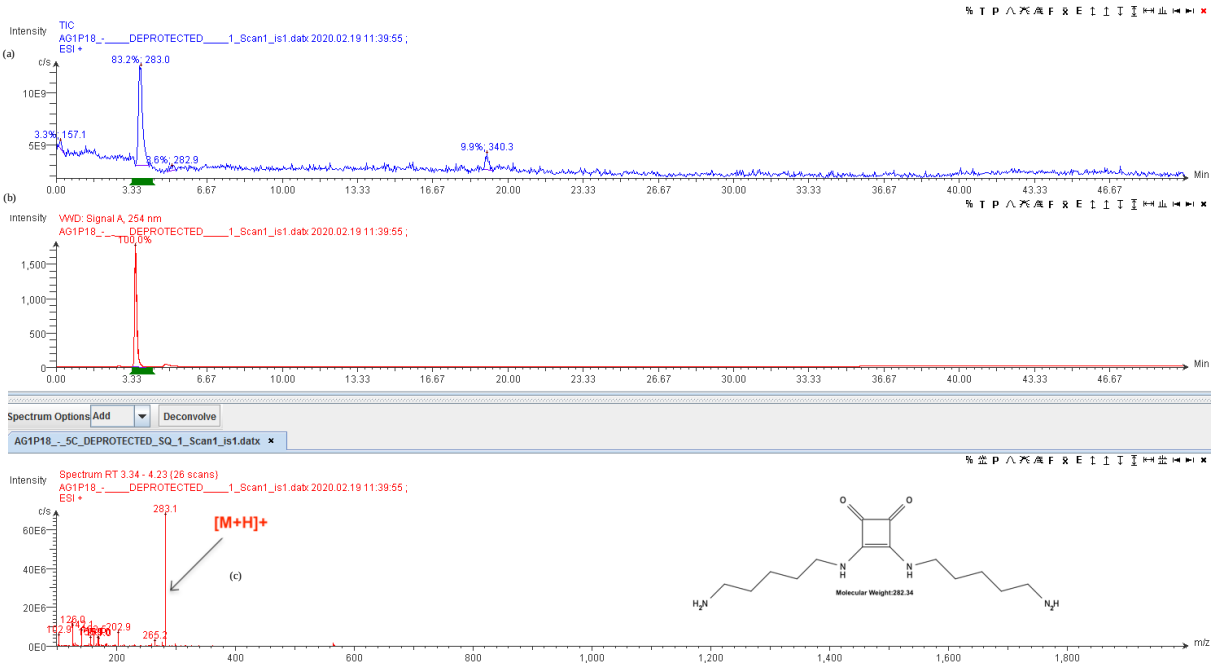

Figure 2.10: LCMS Characterisation of **67:** (a) Analytical HPLC trace of **67**; R_t = 3.0 mins (0-100% MeCN over 30 mins, λ = 254 nm). (b) Extracted Ion Chromatogram for 283.34 $[M + H]^+$. (c) Mass Spectrum detected between R_t = 3.0-4.0 mins (157 scans); Calculated for $[M + H]^+$ = 283.34; Mass Found (ESI^+) = 283.1.

2.2.6 Synthesis of 38, 39 and 40

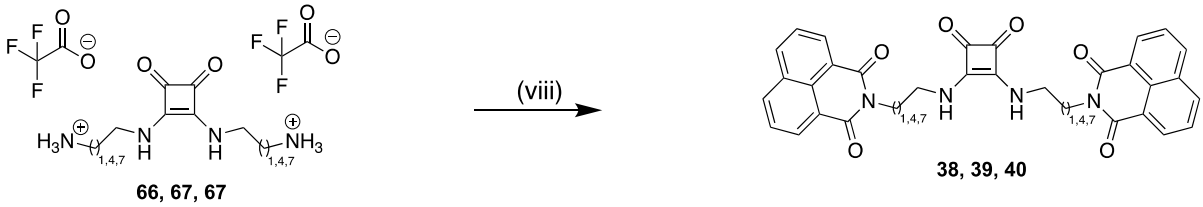

Scheme 2.8: Syntheses of **38**, **39** and **40.**

viii) Ethanol, triethylamine, naphthalene-1,8-dicarboxylic anhydride

Having successfully synthesised **66, 67** and **68,** the final step was to incorporate the naphthalimide structure to synthesise compounds **38, 39** and **40.** The syntheses involved dissolving naphthalene-1,8-dicarboxylic anhydride with triethylamine respectively in ethanol. **66, 67** or **68** were added into all three reactions accordingly, once the starting materials had completely dissolved. The reaction was allowed to reflux at 85°C for 12 hours. The title compounds appeared as precipitates with yields of 84% for **38**, 89% for **39** and 77% for **40**. The afforded precipitates were purified *via* trituration and centrifuging in ethanol and diethyl ether. The room temperature ^{1}H NMR of compound **38** is shown in Figure 2.11 as

an example. As can be seen from Figure 2.11, the ^{1}H NMR of compound **38** was poorly resolved and resulted in broadening of all peaks. This is an indication that self-assembly behaviour may be occurring under these conditions. In order to probe whether this was the case, a series of VT-NMR experiments were also conducted, which will be further discussed in Chapter 3. As can be seen, the peaks at higher temperature became more clearly resolved with increasing temperature indicating some degree of self-assembly. Importantly, upon cooling of the NMR sample, peak broadening was again observed suggesting that this process is reversible. As can be seen in Figure 2.12, ^{13}C NMR also confirmed the presence of the final compound according to peaks at 183.3 ppm, which is indicative of a carbonyl carbon on the squaramide moiety and 168.6 ppm and 164.0 ppm, which indicate the carbonyls on the naphthalimide moiety with peaks representing both the aliphatic region (49.0 and 19.0 ppm) and the naphthalimide region (122.0, 127.4, 127.8, 131.0, 131.5, 134.6 ppm). The purity of the compound was also confirmed by the LCMS analysis (Figure 2.13). Similar behaviour was seen in all cases for compounds **38-40** (See Appendix). As compounds **38-40** were novel final compounds, their self-assembly and DNA binding characteristics will be discussed in the following chapters.

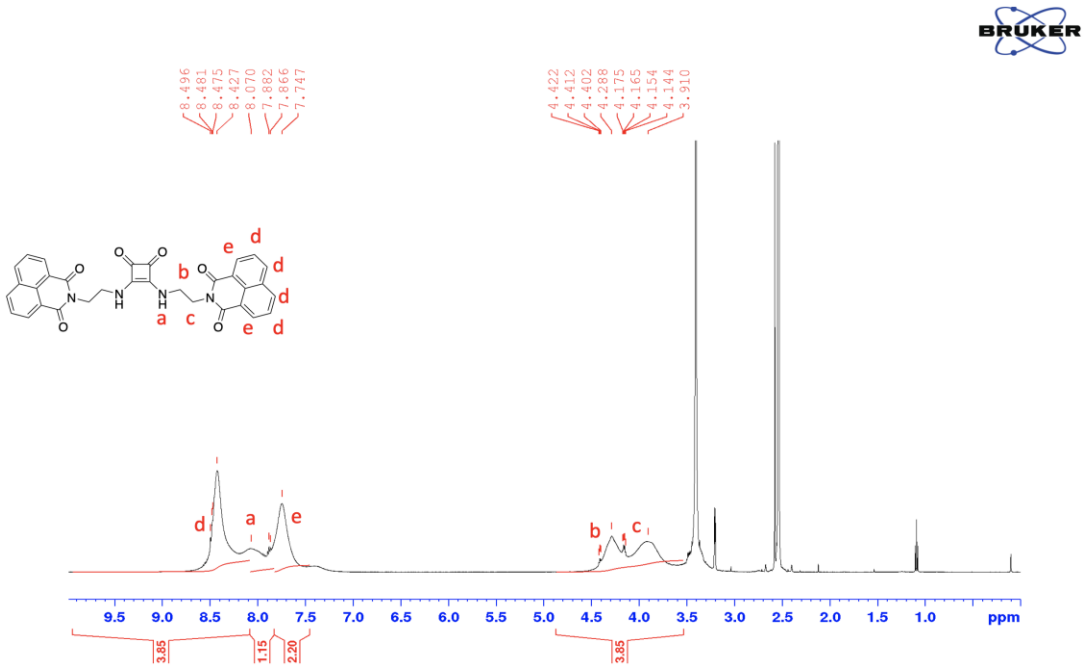

Figure 2.11: The ^{1}H NMR Spectrum of **38** (500 MHz, DMSO-d_6, 298 K.)

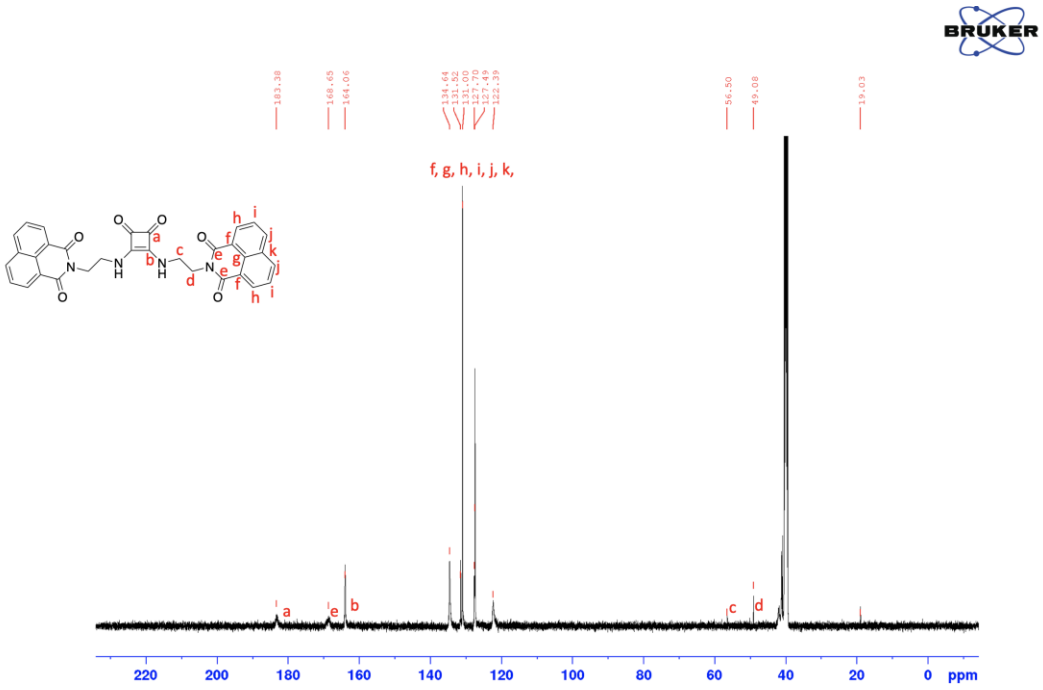

Figure 2.12: The ^{13}C NMR Spectrum of **38** (126 MHz, DMSO-d_6, 298 K.)

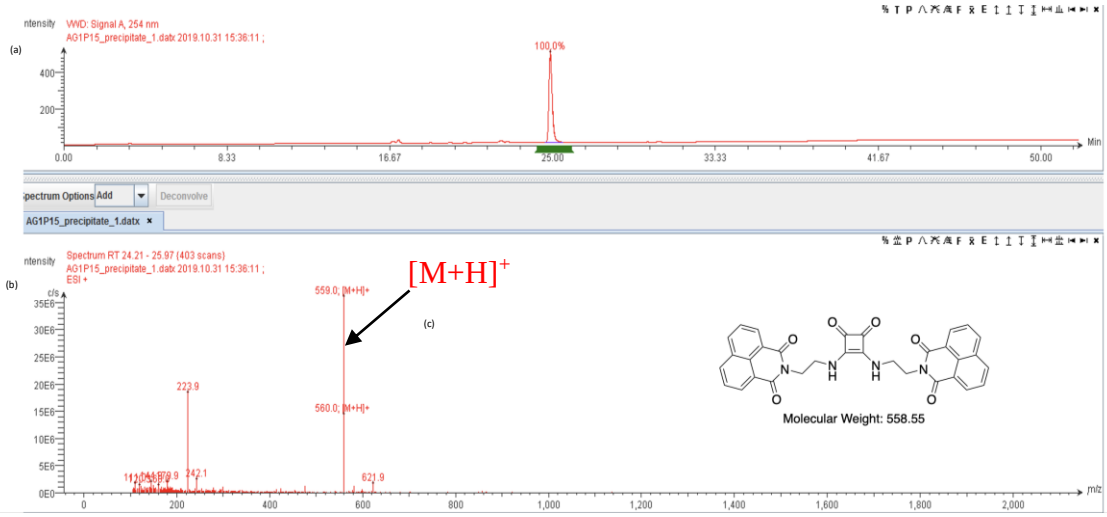

Figure 2.13: LCMS Characterisation of **38:** (a) Analytical HPLC trace of purified **38**; R_t = 25.0 mins (0-100% MeCN over 30 mins, λ = 254 nm). (b) Extracted Ion Chromatogram for 559.0 $[M + H]^+$. (c) Mass Spectrum detected between R_t = 24.0-26.0 mins (157 scans); Calculated for $[M + H]^+$ = 559.5; Mass Found (ESI^+) = 559.0 $[M+H]^+$.

2.2.7 Synthesis of 41, 42 and 43

The next step of the synthesis was to obtain the 4-amino derivatives of squaramide containing bis-naphthalimides, which involved synthesising compounds **47, 48** and **49**. This involved firstly following a similar approach that was used with **38, 39** and **40.** However, the synthesis

will involve 4-nitronaphthalene-1,8-dicarboxylic anhydride, which will yield 4-nitro derivatives of the squaramide containing bis-naphthalimides, which we hope to reduce into the 4-amino forms *via* reduction reactions (Figure 2.14).

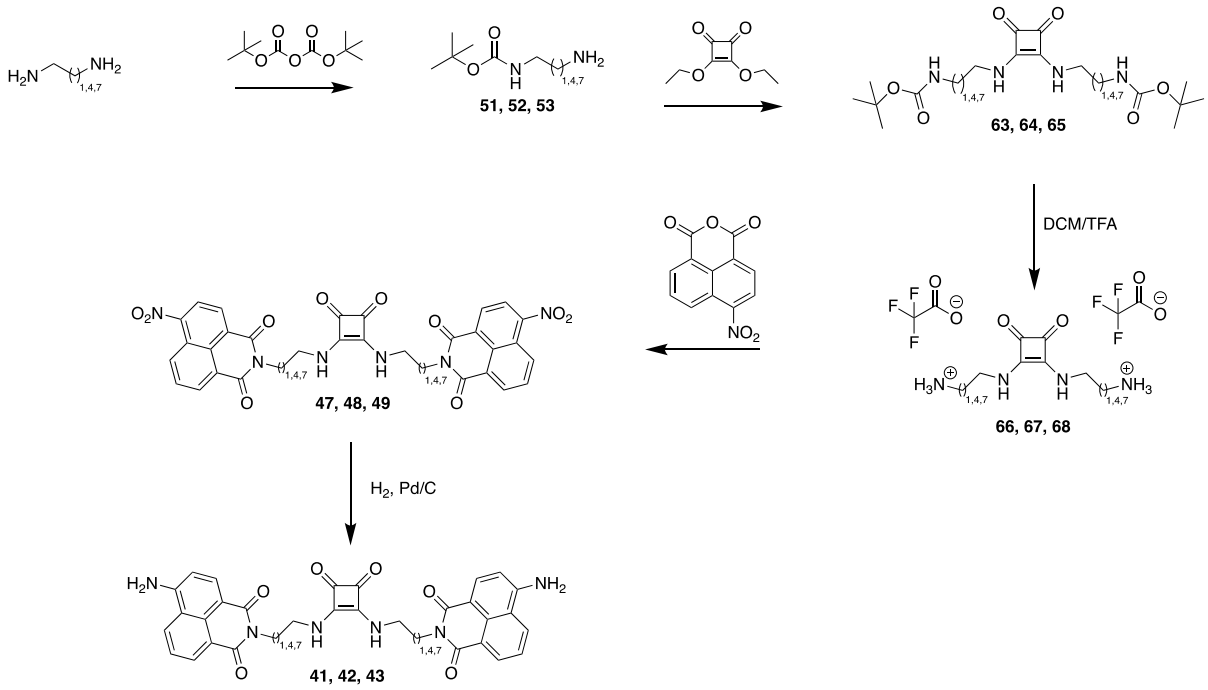

Figure 2.14: First synthetic pathway to obtain **41, 42** and **43.**

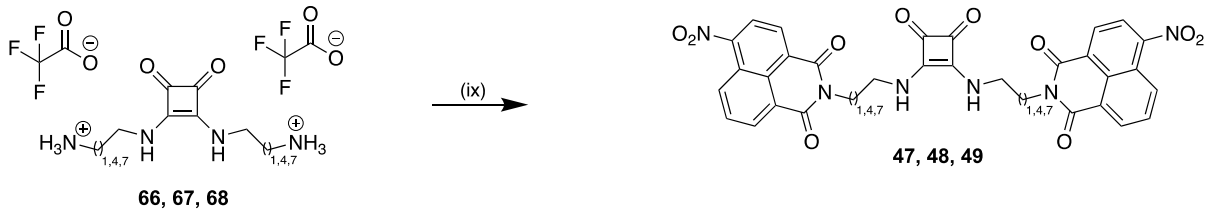

Scheme 2.9: Syntheses of **47**, **48** and **49**.

ix) Ethanol, triethylamine, 4-nitronaphthalene-1,8-dicarboxylic anhydride

The syntheses of **47**, **48** and **49** involved dissolving 4-nitronaphthalene-1,8-dicarboxylic anhydride in all three cases and fully dissolving **66**, **67** and **68** separately in ethanol. Once dissolved, triethylamine was added into all three reactions individually. The reaction was allowed to reflux at 85°C for 12 hours. The title compounds appeared as orange precipitates with crude yields of 86% for **47**, 88% for **48** and 79% for **49**. The precipitates were purified *via* trituration and centrifuging in ethanol and diethyl ether. HRMS data suggested that all compounds were successfully synthesised. However, the characterisation data for each

compound was difficult to obtain due to insolubility issues. The ^{1}H NMR of compound **47** is shown in Figure 2.15.

As can be seen, we clearly demonstrated the correct signals for the aliphatic region and the naphthalimide region. However, it was difficult to draw firm conclusions based on the level of purity as we were unable to obtain pure LCMS and the NMR was inconclusive. Unfortunately, reliable purity information could not be obtained by LCMS due to insolubility in all suitable mobile phases. Due to the difficulties in characterisation, we decided to continue with the synthesis. ^{1}H NMR of compound **47** is shown in figure 2.15. As can be seen, the signals were in the correct range of chemical shifts. However, at room temperature all peaks were poorly resolved as previously observed for compounds **38-40**. VT-NMR studies were again carried out and improved resolution considerably (Figure 2.16). Due to overlapping signals in the aromatic region, full assignment of all signals was not possible. Similarly, reliable purity information could not be obtained by LCMS due to insolubility in all suitable solvents (Figure 2.17). The HR-MS however did indicate the presence of **47** (Figures 2.18 and 2.19) Given the limited characterisation, we decided to continue with the synthesis regardless, in the hope that reduction of the NO_2 to NH_2 may result in improved solubility. The following section describes the attempted syntheses of compounds **41-43.**

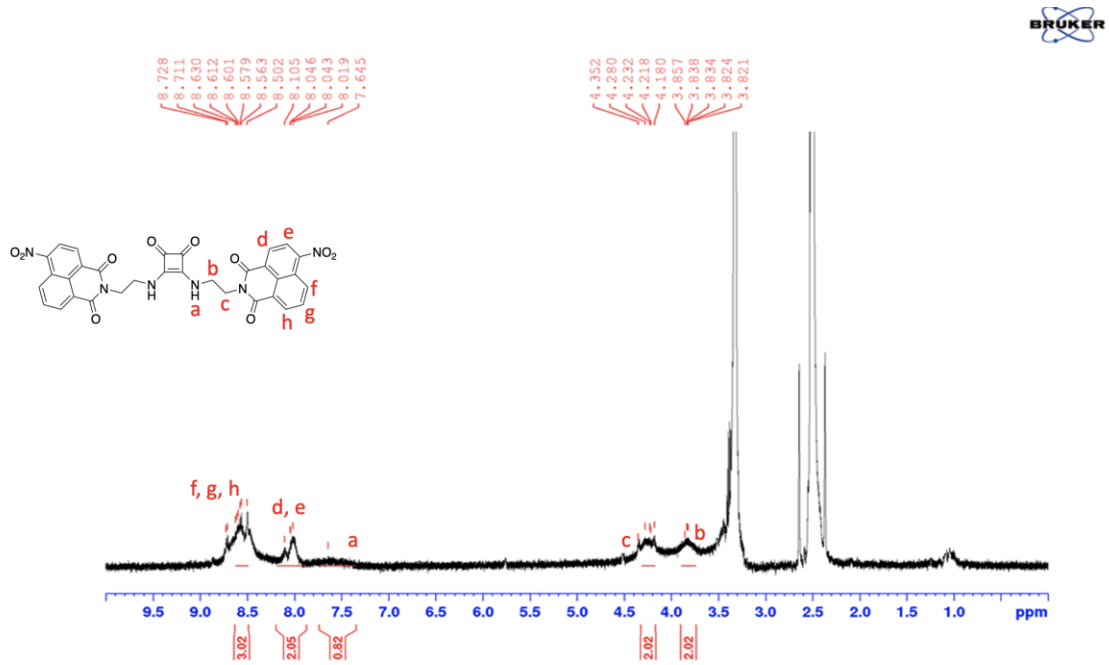

Figure 2.15: The ^{1}H NMR Spectrum of **47** (500 MHz, DMSO-d_6, 298 K.)

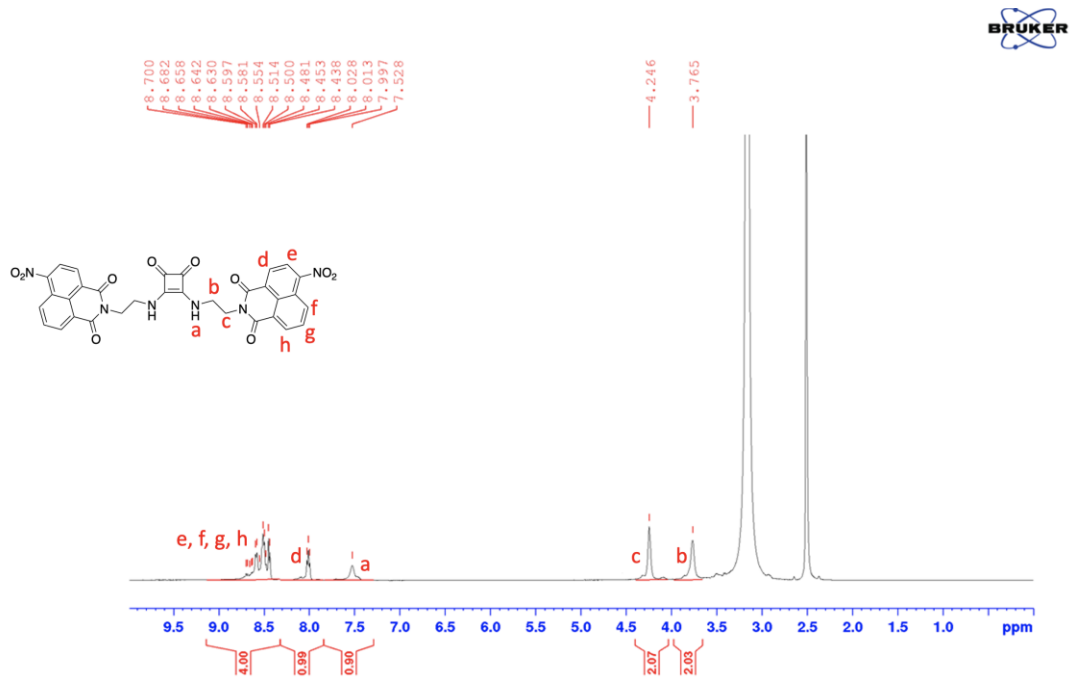

Figure 2.16: The ^{1}H NMR Spectrum of **47** at 358 K (500 MHz, DMSO-d_6, 358 K.)

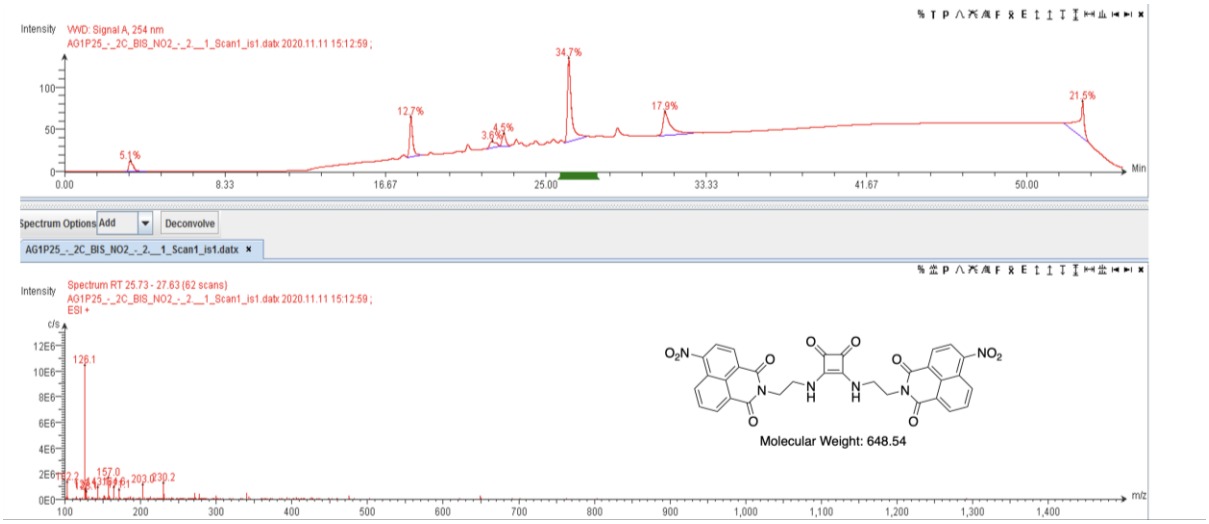

Figure 2.17: LCMS Characterisation of **47**.

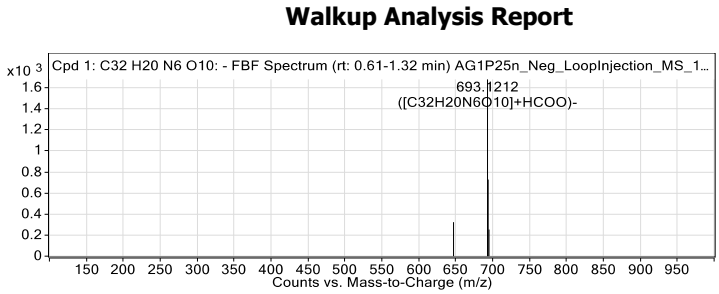

Figure 2.18: HRMS spectrum of **47**.

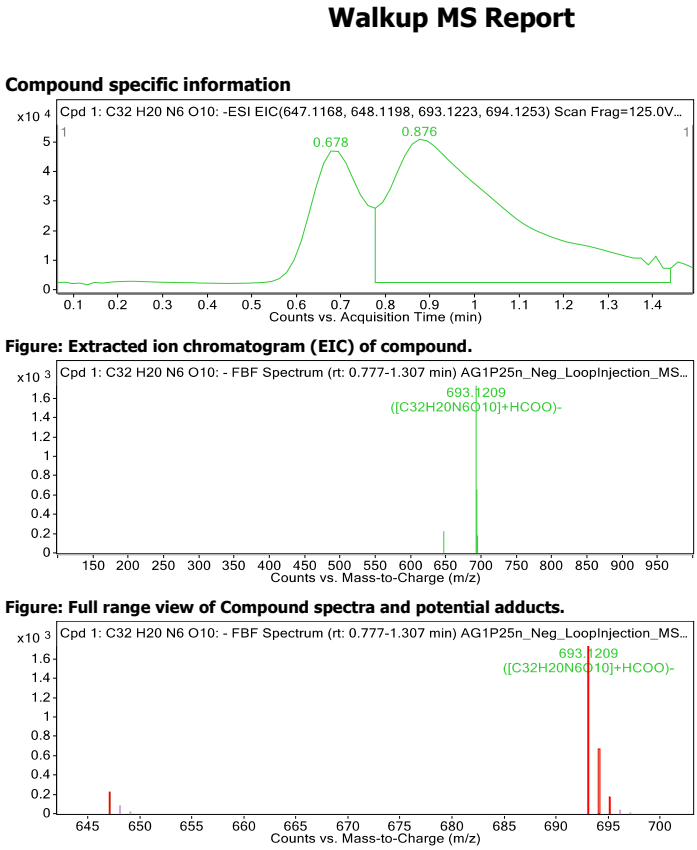

Figure 2.19: HRMS spectrum of **47**.

Multiple attempts to synthesise **41**, **42** and **43** were made. **47**, **48** and **49** were dissolved in ethanol, while 20% palladium on carbon was added into each reaction. More solvent was added to prevent **47**, **48** and **49** from precipitating. However, in each case **47**, **48** and **49** had precipitated no matter how much solvent was added into each reaction. The solvents were removed *via* Büchner filtration after 12 hours. The precipitates were analysed by ^{1}H NMR and LCMS and it was concluded that the reaction had not proceeded in each case.

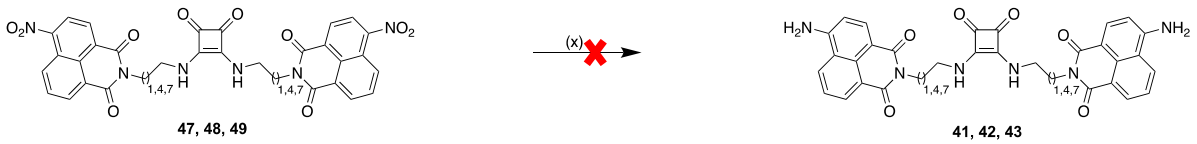

Scheme 2.10: Attempted syntheses of **41**, **42** and **43**.

x) Ethanol/Methanol/Toluene/Dichloromethane/Dimethylformamide/ Tetrahydrofuran, H_2, Pd/C

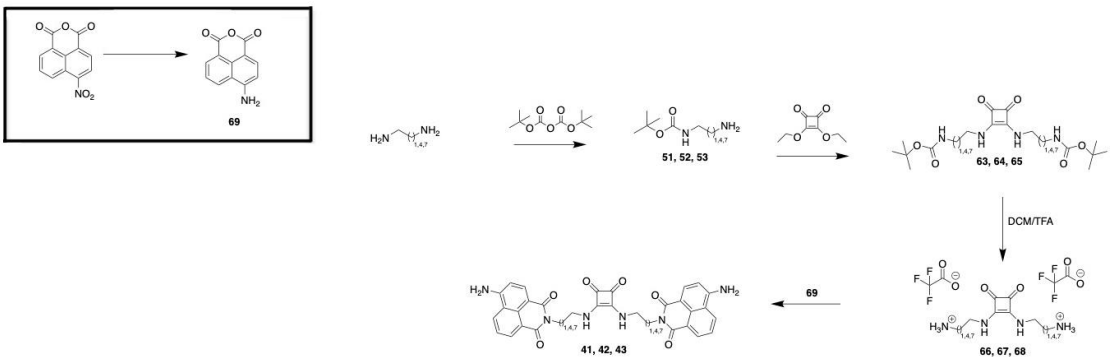

Figure 2.20: Second synthetic pathway of yielding compounds **41-43.**

Another approach was therefore explored (Figure 2.20), where 4-nitronaphthalene-1,8-dicarboxylic anhydride could be firstly reduced into **69** as previously reported.[277] 4-nitronaphthalene-1,8-dicarboxylic anhydride was added into ethanol. 20% palladium on carbon (Pd/C) was added into each solution while stirring. The reaction was allowed to stir at room temperature under a hydrogen atmosphere for 4 hours. Once the 4-nitronaphthalene-1,8-dicarboxylic anhydride had dissolved in ethanol and had undergone a transfer into **69**, the reaction became fluorescent under a UV torch. The solution was filtered through a celite plug. The solvent was removed in-vacuo to afford **69**, with a yield of 82%. The ^{1}H NMR of compound **69** is shown in Figure 2.21. As can be seen, the naphthalimide moiety is represented by signals at 8.7, 8.4, 8.2, 7.6 and 6.9 ppm, while the peak at 7.8 ppm indicated the presence of another NH_2, further indicating successful completion of the reaction. The LCMS (Figure 2.22) had also displayed purity of **69** following the reduction of 4-nitronaphthalene-1,8-dicarboxylic anhydride**.**

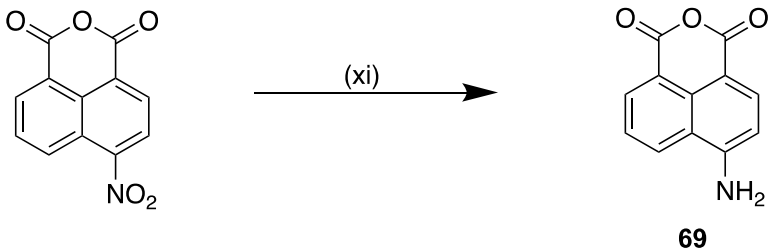

Scheme 2.11: Synthesis of **69**.

xi) Ethanol, H_2, Pd/C

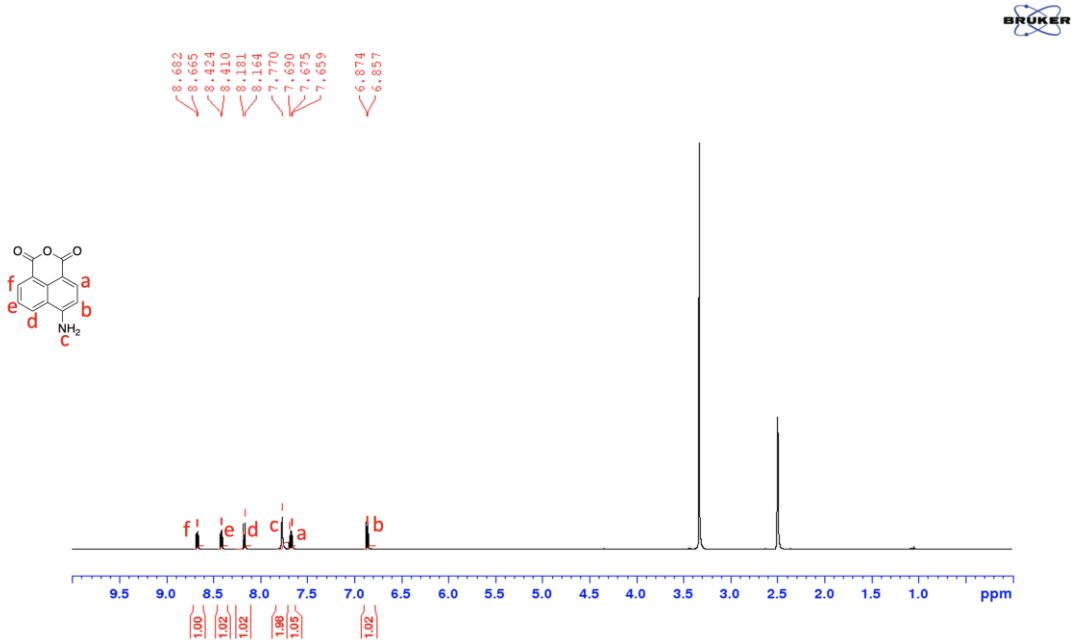

Figure 2.21: The ^{1H}NMR Spectrum of **69** (500 MHz, DMSO-d_6, 298 K.)

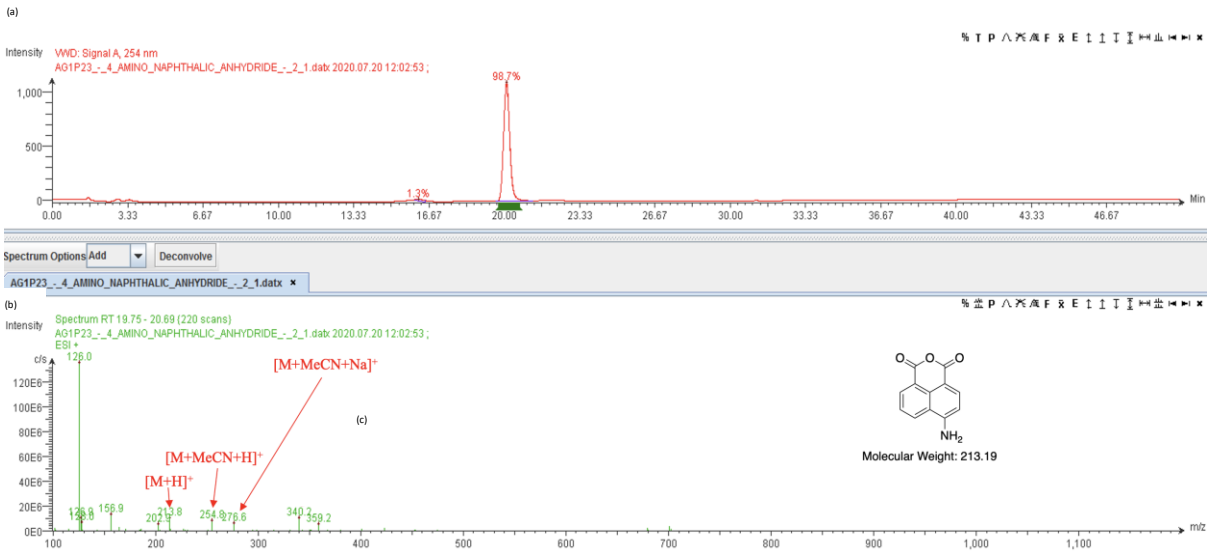

Figure 2.22: LCMS Characterisation of **69:** (a) Analytical HPLC trace of pure **69**; R_t = 20.0 mins (0-100% MeCN over 30 mins, λ = 254 nm). (b) Extracted Ion Chromatogram for 214.2 $[M + H]^+$. (c) Mass Spectrum detected between R_t = 19.0-21.0 mins (157 scans); Calculated for $[M + H]^+$ = 214.2; Mass Found (ESI^+) = 213.8 $[M + H]^+$. Also Found 254.8 $[M + MeCN + H]^+$, 276.6 $[M + MeCN+Na]^+$.

66, **67** and **68** were dissolved in ethanol separately. Triethylamine was added into each reaction with appropriate quantities of **69**. All three reactions were allowed to reflux at 85°C for 12 hours respectively. The solvents in all three reactions were removed in-vacuo to afford white solids. The products were analysed by ^{1}H NMR and LCMS and it was evident that the starting materials were returned in each case. Various solvents were used when repeating the reaction. However, in all cases the starting materials had not reacted to form the desired products. The free amine products were returned as the reaction had not proceeded further.

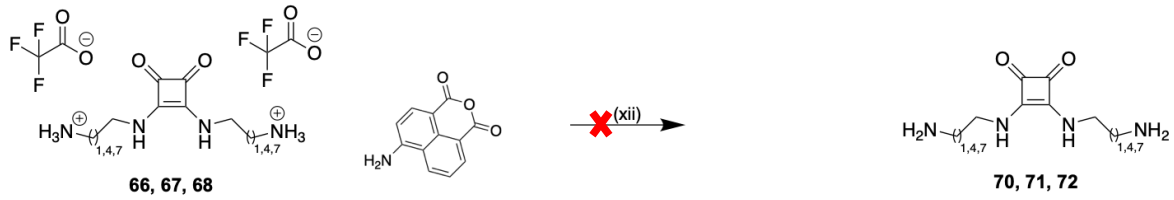

Scheme 2.12: Syntheses of **70**, **71** and **72**.

xii) Ethanol/Methanol/Toluene/Dimethylformamide/Dichloromethane/Chloroform/ Tetrahydrofuran, H_2, Pd/C

The third proposed synthetic pathway (Figure 2.23) was to firstly involve the mono-boc protection of the aliphatic linker, followed by the reaction with 4-nitronaphthalene-1,8-dicarboxylic anhydride, which will be reduced into 4-aminonaphthalene-1,8-dicarboxylic anhydride, which will be deprotected with trifluoroacetic acid:dichloromethane (50:50) and the resulting trifluoroacetic salt will be reacted with diethyl squarate to yield the desired compounds **41-43.**

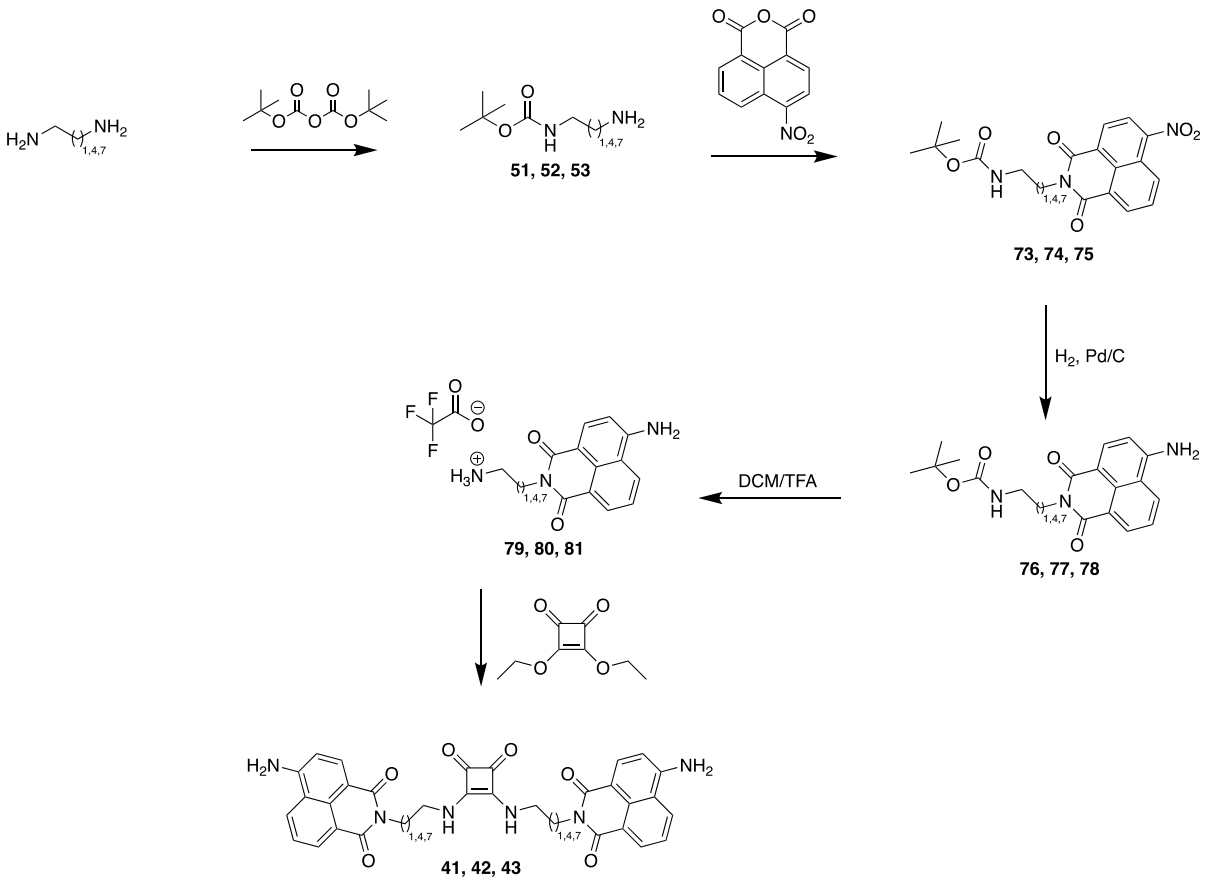

Figure 2.23: Third proposed synthetic pathway of compounds **41-43.**

51, **52** and **53** were dissolved in toluene with triethylamine before the addition of 4-nitronaphthalene-1,8-dicarboxylic anhydride. All three reactions were allowed to reflux at 85°C for 12 hours. The solvents in all three reactions were removed in-vacuo to afford crude white solids in all three reactions. All three crude products were purified *via* column chromatography to afford the products **73**, **74** and **75** with yields of 90%, 83% and 80%, as previously reported by *Guo et al.*[278] ^{1}H NMR confirmed the successful outcome of the reaction (See Appendix).

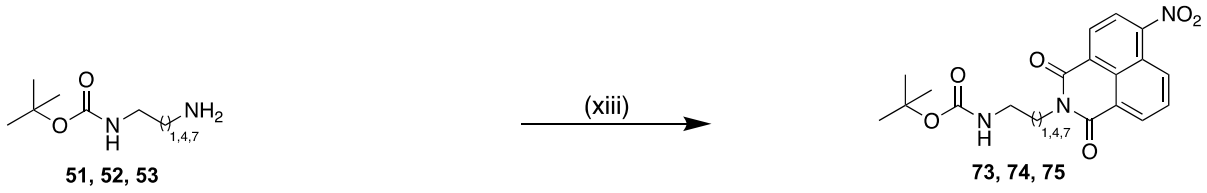

Scheme 2.13: Syntheses of **73**, **74** and **75**.

xiii) Toluene, triethylamine, 4-nitronaphthalene-1,8-dicarboxylic anhydride

The next step involved the reduction of the NO_2 group. **73**, **74** and **75** were all dissolved in ethanol before 20% of palladium on carbon (Pd/C) were added into all three reactions and the reactions were allowed to stir for 4, 6 and 12 hours under H_2 atmosphere. Once the reactions had completed, the solutions were filtered through a plug of celite and the solvents were removed in-vacuo to afford yellow solids **76**, **77** and **78**, as reported by *Andersen et. al.*[279] The yields for **76**, **77** and **78** were 89%, 84% and 81% respectively. The ^{1}H NMR of compound **77** is shown in Figure 2.24. As can be seen, the naphthalimide moiety is represented by signals at 8.6, 8.4, 8.2, 7.6 and 6.9 ppm, the N-H peak was visible at 6.7 ppm, the aliphatic peaks were visible on the ^{1}H NMR spectrum at 4.3, 2.8, 1.59, 1.41 and 1.0 ppm, the boc-protecting group was visible at 1.39 ppm, while the peak at 7.4 ppm indicated the presence of NH_2, further indicating successful completion of the reaction.

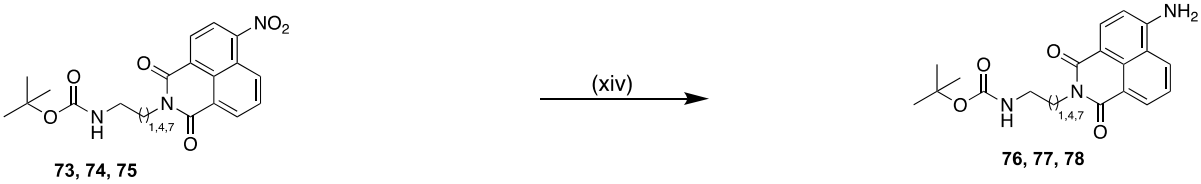

Scheme 2.14: Syntheses of **72**, **73** and **74**.

xiv) Ethanol, H_2, Pd/C

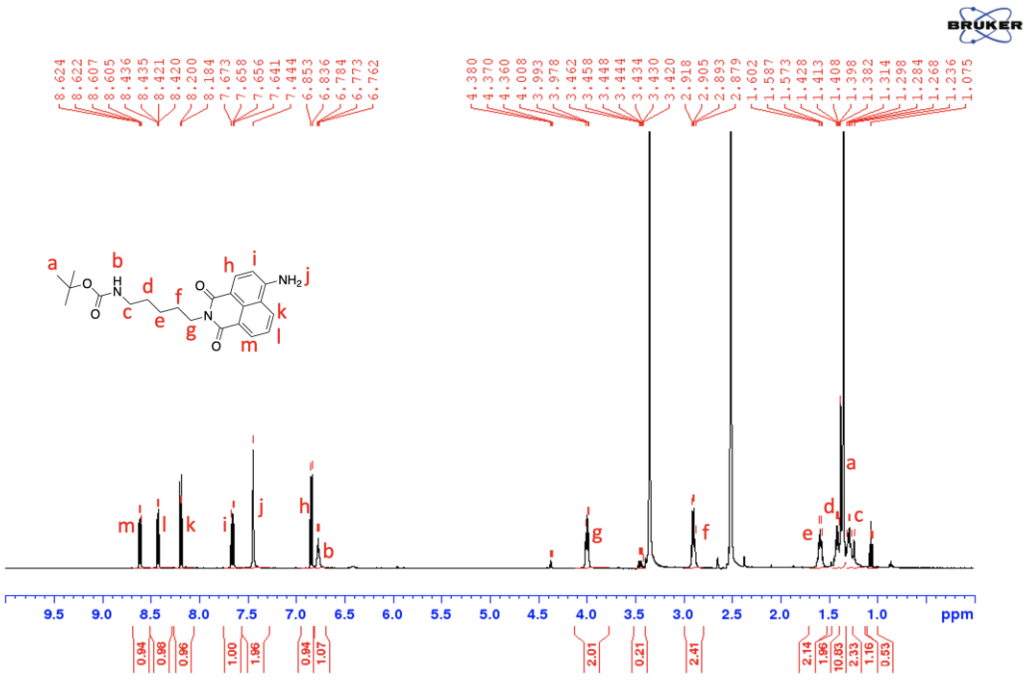

Figure 2.24: The ^{1}H NMR Spectrum of **77** (500 MHz, DMSO-d_6, 298 K.)

76, **77** and **78** were each dissolved in dichloromethane and trifluoroacetic acid (50:50). All three reactions were allowed to stir at room temperature. The deprotection of **76** required 1 hour to form the product **79**. The reduction of **77** required 2 hours to form the product **80** and the reduction of **78** required 4 hours to form the product **81**. The solvent was removed with N_2 and in-vacuo. The title compounds appeared as orange residues in all three cases and were used directly without further purification.

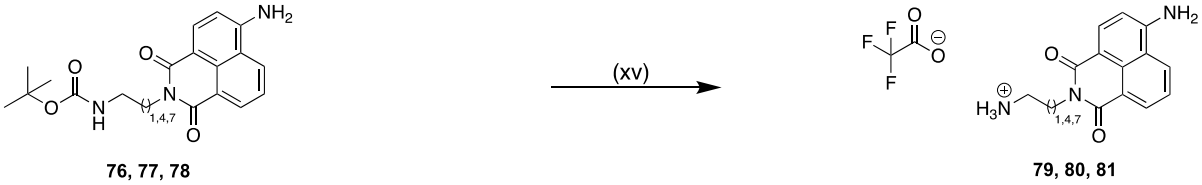

76, 77, 78 **79, 80, 81**

Scheme 2.15: Syntheses of **79**, **80** and **81**.

xv) Dichloromethane, trifluoroacetic acid

The final step in this proposed synthesis involved the reaction with diethyl squarate, **50**. **79**, **80** and **81** were separately dissolved in ethanol before the addition of triethylamine. Once **79**, **80** and **81** had fully dissolved, 4-diethoxycyclobut-3-ene-1,2-dione was added into each reaction. After 12 hours, the solvent was removed from each reaction in-vacuo to afford yellow solids. The yellow solids were analysed by ^{1}H NMR and LCMS analysis and it was evident that the starting materials were returned and the reactions had not formed the desired products. Various solvents were used in theses reactions. However, the starting materials were returned as the reaction had not proceeded in each case, as the free amine starting materials were returned.

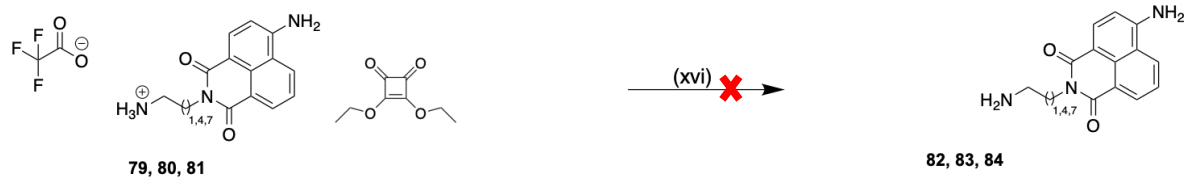

79, 80, 81 **82, 83, 84**

Scheme 2.16: Syntheses of **82**, **83** and **84**.

xvi) Ethanol/Toluene/Dimethylformamide/Dichloromethane/Chloroform/Tetrahydrofuran, triethylamine, 4-diethoxycyclobut-3-ene-1,2-dione

The fourth proposed synthetic pathway (Figure 2.25) entailed the mono-boc protection of the aliphatic linker, followed by the reaction with diethyl squarate to form the di-substituted derivative. This was followed by the deprotection and the final reaction with the 4-bromonaphthalene-1,8-dicarboxylic anhydride. We envisaged that this bromo-derivative could be reacted with ammonia to yield the desired amino substituted products.

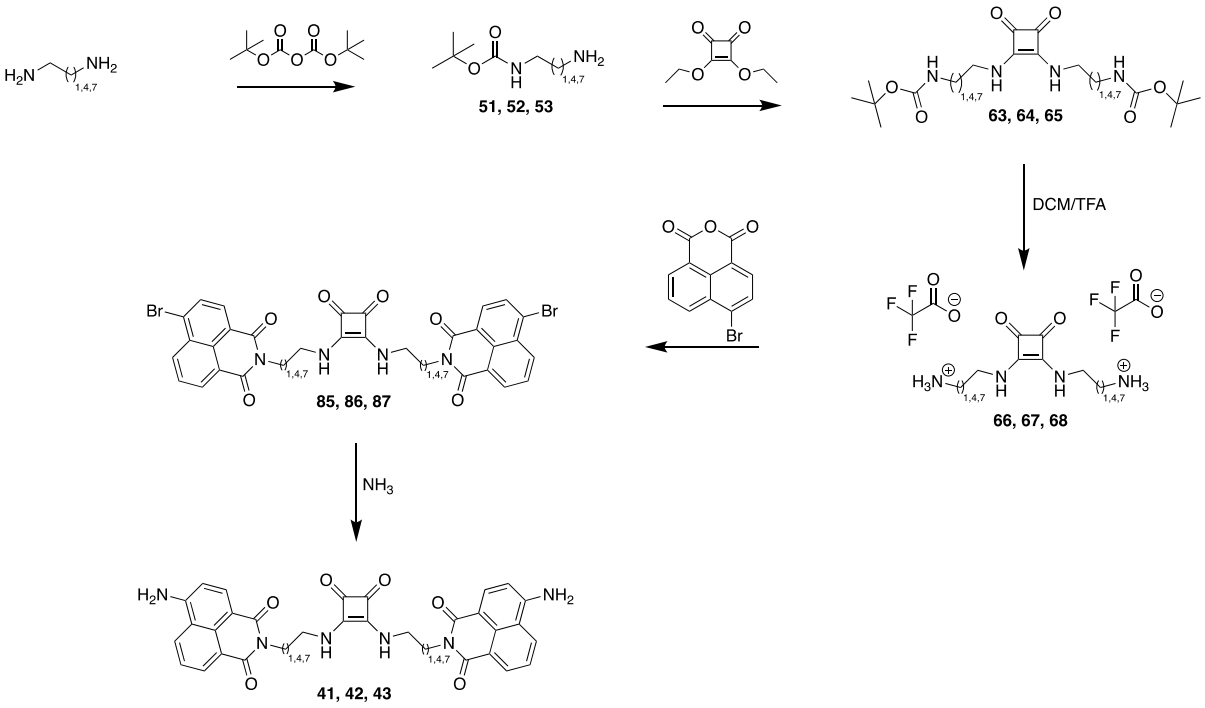

Figure 2.25: Fourth proposed synthetic pathway of synthesising compounds **41-43.**

66, **67** and **68** were separately dissolved in ethanol before the addition of triethylamine in each reaction. 4-bromonaphthalene-1,8-dicarboxylic anhydride was added into each reaction until fully dissolved. All three reactions were allowed to reflux at 85°C for 12 hours, as previously reported by O' Malley.[280] The solvent from each reaction was removed in-vacuo to afford three crude products. All three crude products were purified *via* column chromatography to afford pure products, which appeared as yellow solids, with yields of 89%, 92% and 81%. The ^{1}H NMR confirmed the purity of **85** as each signal corresponded to each proton. However, as previously observed, the spectra were significantly broadened (Figure 2.26). LCMS confirmed the successful formation of the desired compounds (Figure 2.27).

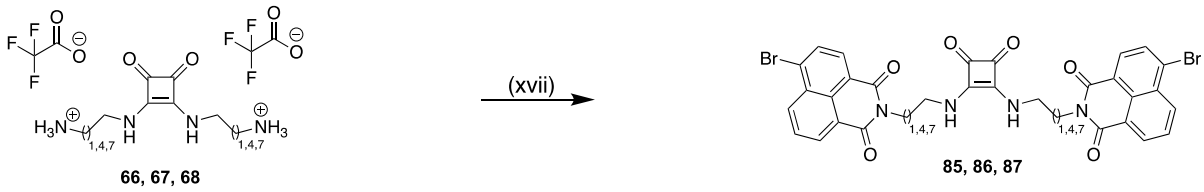

Scheme 2.17: Syntheses of **85**, **86** and **87**.

xvii) Ethanol, triethylamine, 4-bromonaphthalene-1,8-dicarboxylic anhydride

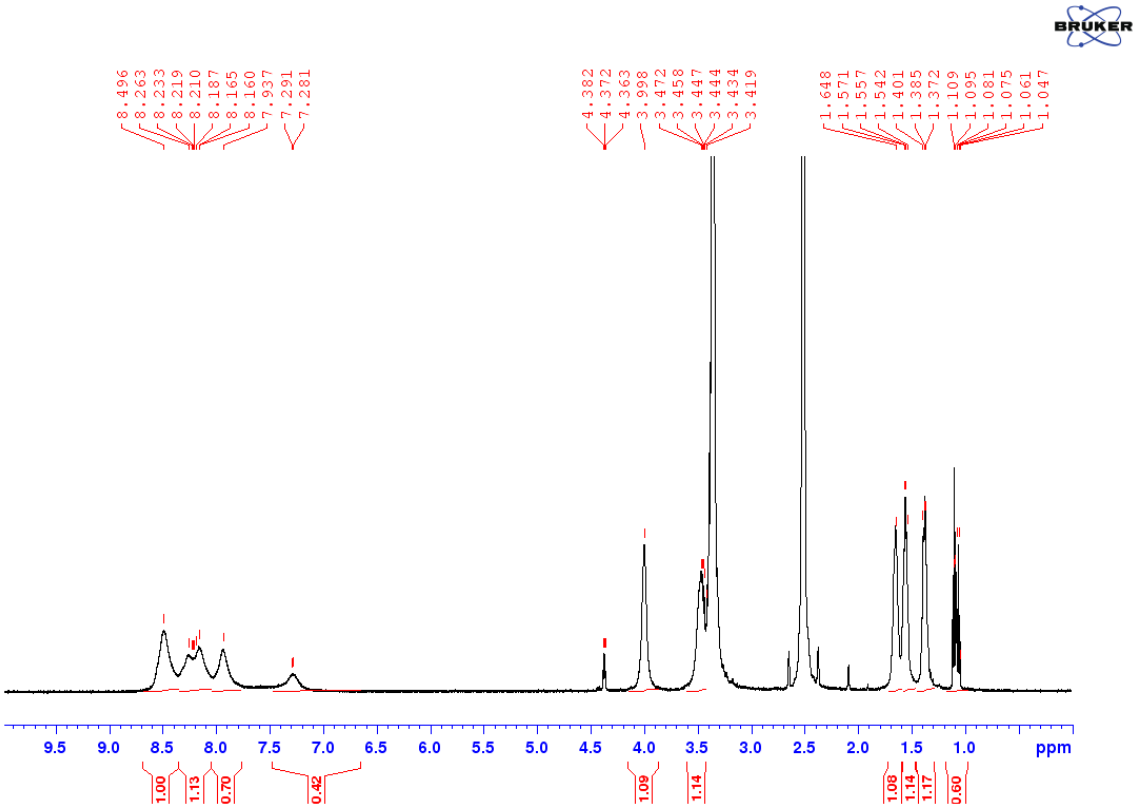

Figure 2.26: The ^{1}H NMR Spectrum of **87** (500 MHz, DMSO-d_6, 298 K.)

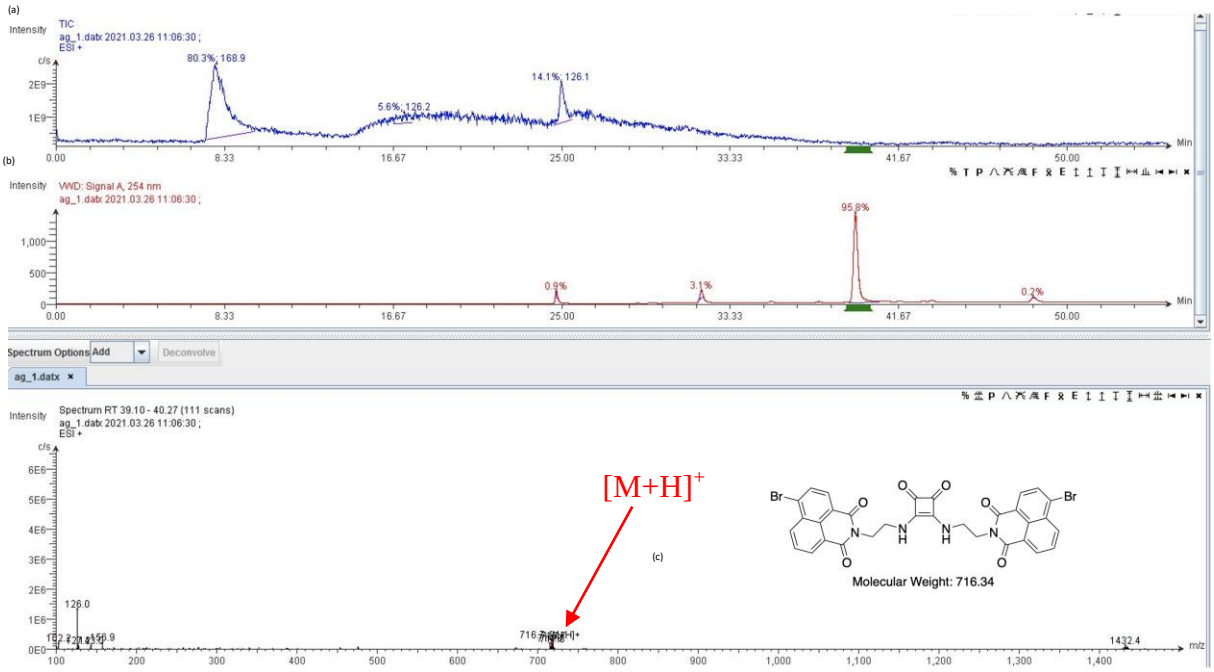

Figure 2.27: LCMS Characterisation of **85:** (a) Analytical HPLC trace of pure **85**; R_t = 38.0 mins (0-100% MeCN over 30 mins, λ = 254 nm). (b) Extracted Ion Chromatogram for 717.3 $[M + H]^+$. (c) Mass Spectrum detected between R_t = 37.0-39.0 mins (157 scans); Calculated for $[M + H]^+$ = 717.3; Mass Found (ESI^+) = 716.7 $[M + H]^+$.

The final step involved conversion of the bromo-naphthalimides to the amino-naphthalimides by reaction with ammonia. **85**, **86** and **87** were dissolved in ethanol with 20% ammonia. All three reactions were allowed to reflux at 85°C for 12 hours. The solvents from each reaction were removed in-vacuo to afford yellow solids. Each solid was analysed and it was evident that the reactants were returned. Neat ammonia was also used as a solvent under more harsh reaction conditions to force conversion. However, in all cases, starting materials were returned according to ^1H NMR and LCMS analysis.

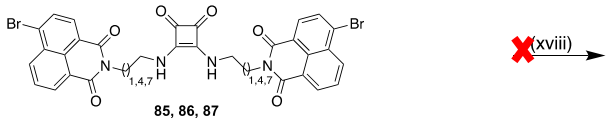

Scheme 2.18: Syntheses of **88**, **89** and **90**.

xviii) Ethanol/Toluene/Dimethylformamide/Dichloromethane/Chloroform/ Tetrahydrofuran, Ammonia

The fifth proposed synthetic pathway saw a slight variation of the design, whereby a butylamine would be substituted at the 4-position of the naphthalimide. This entailed the mono-boc protection of the aliphatic linker, followed by the reaction with diethyl squarate to form the di-substituted derivatives. This was followed by the deprotection and the final reaction with the 4-bromonaphthalene-1,8-dicarboxylic anhydride. We envisaged that this could be reacted with n-butylamine to yield the desired products (Figure 2.28).

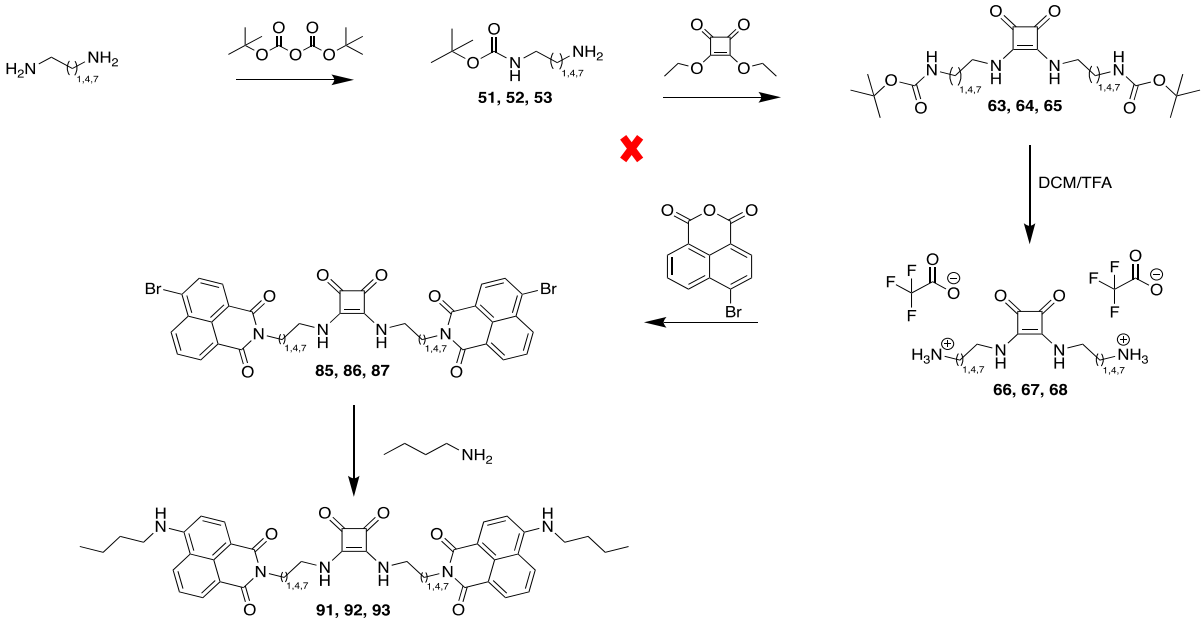

Figure 2.28: Proposed synthetic pathway of yielding compounds **91-93.**

85, **86** and **87** were dissolved in ethanol and 20% n-Butylamine was added into each reaction accordingly. All three reactions were allowed to reflux at 85°C for 12 hours. The solvents from each reaction were removed in-vacuo to afford yellow solids. Each solid was analysed by ^{1}H NMR and LCMS and it was evident that the reactants were returned in each case. After all solvents have been used in this reaction, **85**, **86** and **87** were dissolved in pure n-Butylamine. All three reactions were allowed to reflux at 85°C for 12 hours respectively. The solvent from each reaction was removed in-vacuo to afford yellow solids. Each product was analysed by ^{1}H NMR and LCMS and that the starting materials were returned, as the reaction had not proceeded further.

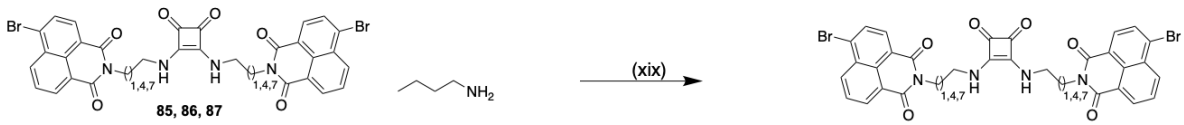

Scheme 2.19: Syntheses of **94**, **95** and **96**.

xix) Ethanol/Toluene/Dimethylformamide/Dichloromethane/Chloroform/ Tetrahydrofuran.

The sixth explored option to attempt to synthesise the desired products was *via* Tin(II) chloride reduction of the previously discussed nitro-derivatives, which is a softer method of reduction (Figure 2.29). **47**, **48** and **49** were dissolved in 10N hydrochloric acid, acetic acid before the addition of tin(II) chloride/iron. Ethanol and H_2O were added into the reaction as solvents. The three reactions were allowed to reflux at 85°C for 12 hours. The solutions were filtered through a celite plug and the solvents were removed in-vacuo to afford orange solids. The solids were analysed by ^1H NMR and LCMS and it was clear that the desired products had not formed in these reactions.

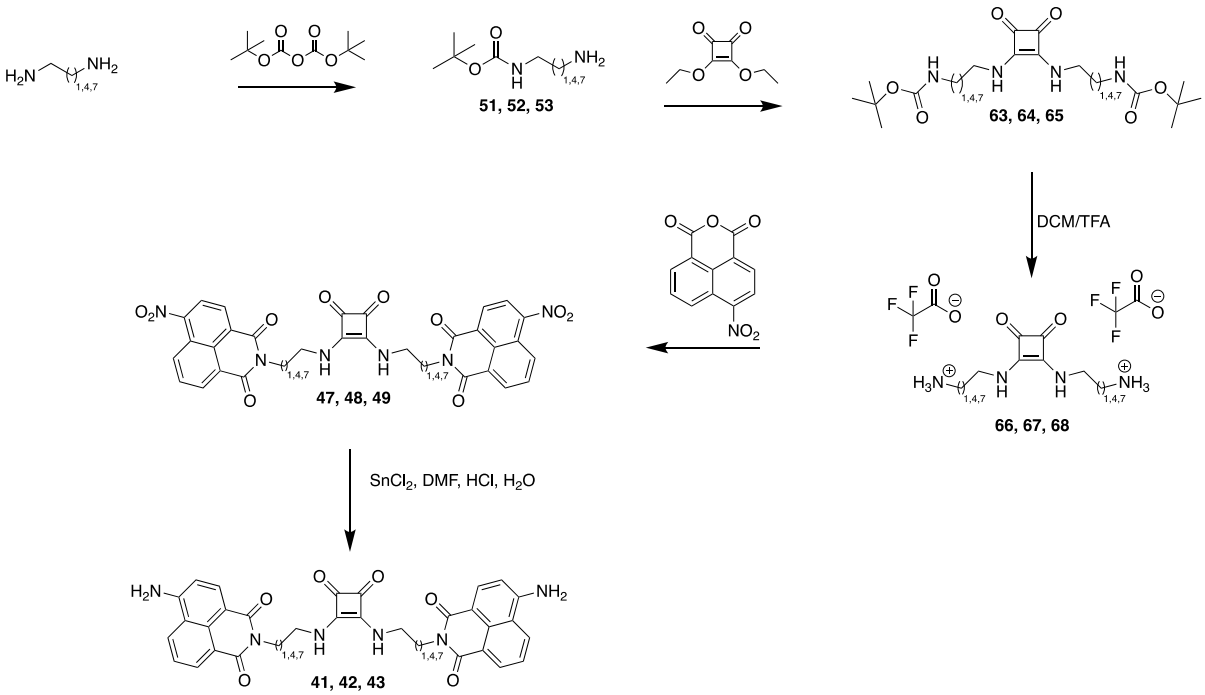

Figure 2.29: Sixth synthetic pathway of compounds **41-43.**

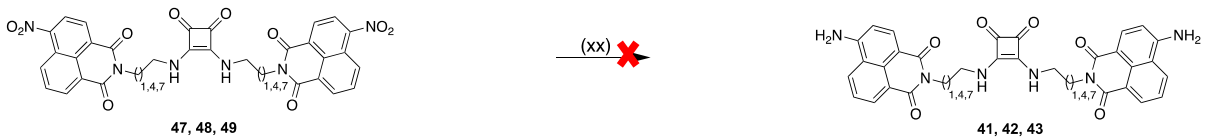

Scheme 2.20: Attempted syntheses of **41, 42** and **43**.

xx) Ethanol/Toluene/Dimethylformamide/Dichloromethane/Chloroform/ Tetrahydrofuran, Tin(II) chloride/iron, hydrochloric acid, water

The final proposed synthetic step attempted involved the synthesis of compounds **44-46**, where the naphthalimide is substituted at the 'tail' (Figure 2.30). This synthetic pathway entailed the mono-boc protection of the aliphatic linker, followed by the reaction with diethyl squarate to form the di-substituted derivatives. This was followed by the deprotection and the final reaction with the 4-Bromo-N-n-butyl-1,8-naphthalimide to yield the desired products **44-46.**

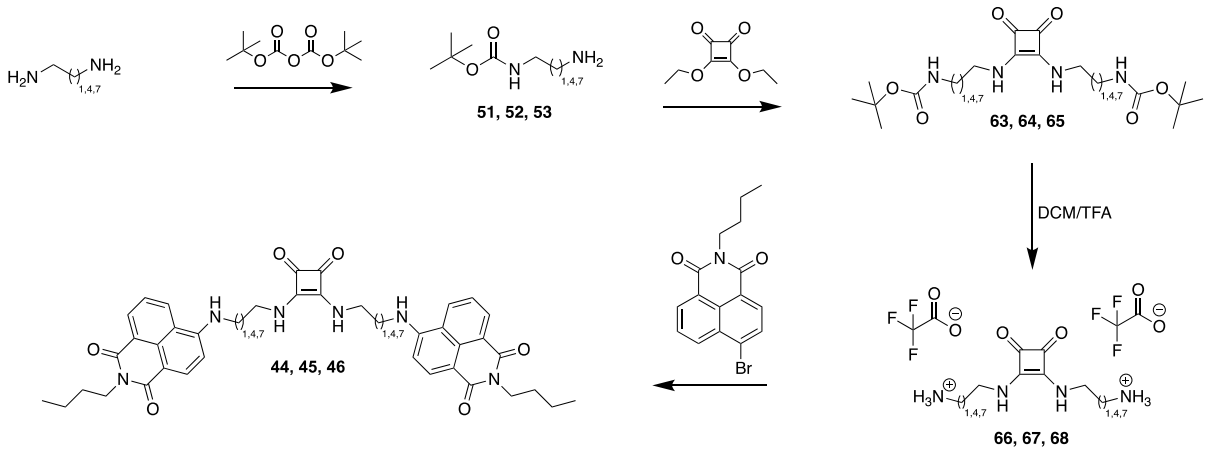

Figure 2.30: Proposed synthetic pathway of compounds **44-46.**

66, **67** and **68** were dissolved in ethanol with H_2O before the addition of triethylamine. 4-bromo-N-n-butyl-1,8-naphthalimide were added into each reaction until dissolved. All three reactions were allowed to reflux at 85°C for 12 hours. The solvents were removed in-vacuo to afford a yellow solid. The solids were analysed by ^{1}H NMR and LCMS analysis and suggested that starting materials were returned in each case as well as other side products that could not be identified. Both ^{1}H NMR and LCMS did not show any evidence of successful compound formation (Figures 2.31 and 2.32), as this spectrum resembles the starting material. This suggested a mixture of starting materials and side products.

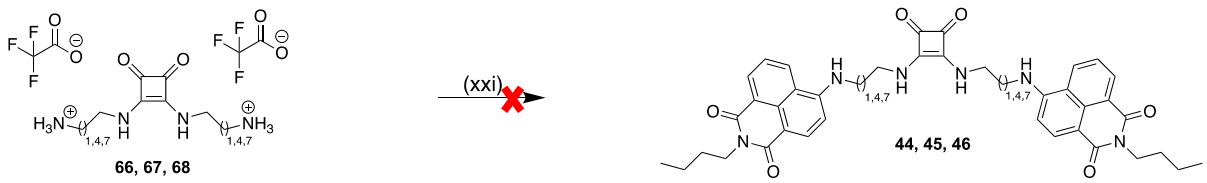

Scheme 2.21: Syntheses of **44**, **45** and **46**.

xxi) Ethanol/Methanol/Toluene/Dimethylformamide/Dichloromethane/Chloroform/Tetrahydrofuran, 4-Bromo-N-butyl-1,8-naphthalimide

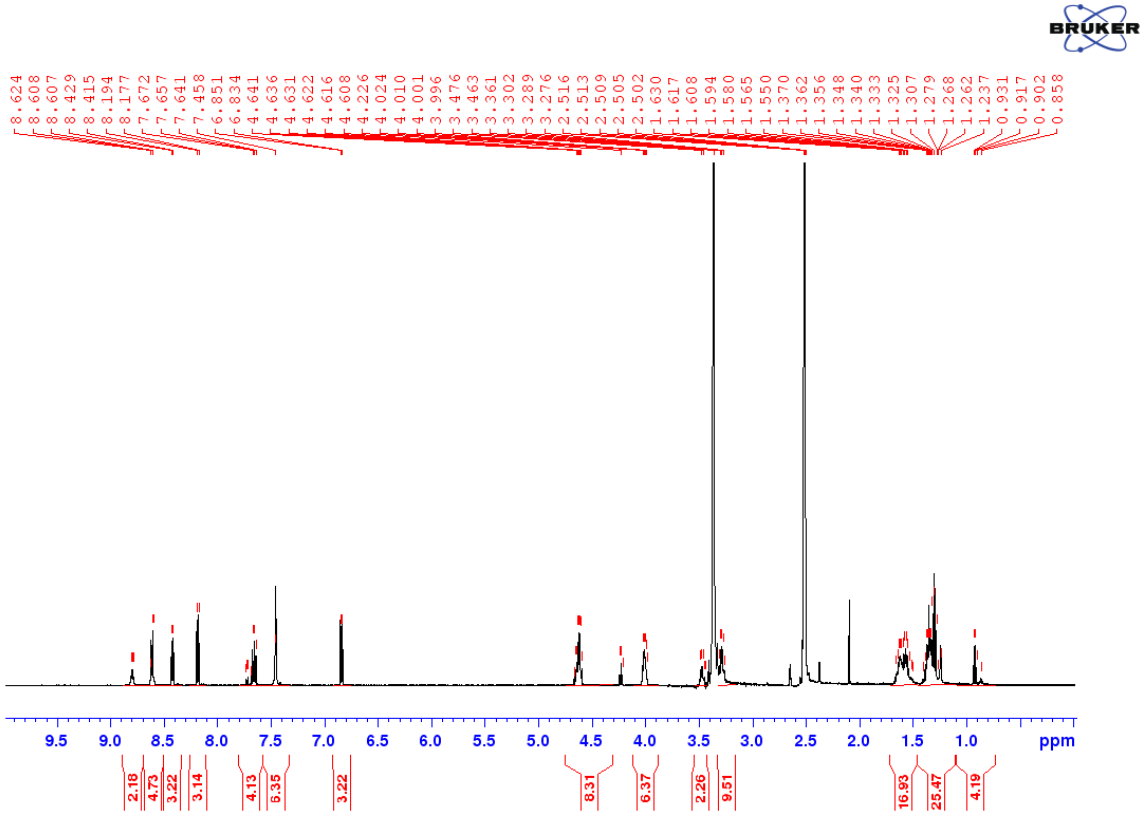

Figure 2.31: The ^{1}H NMR Spectrum of **44** (500 MHz, DMSO-d_6, 298 K.)

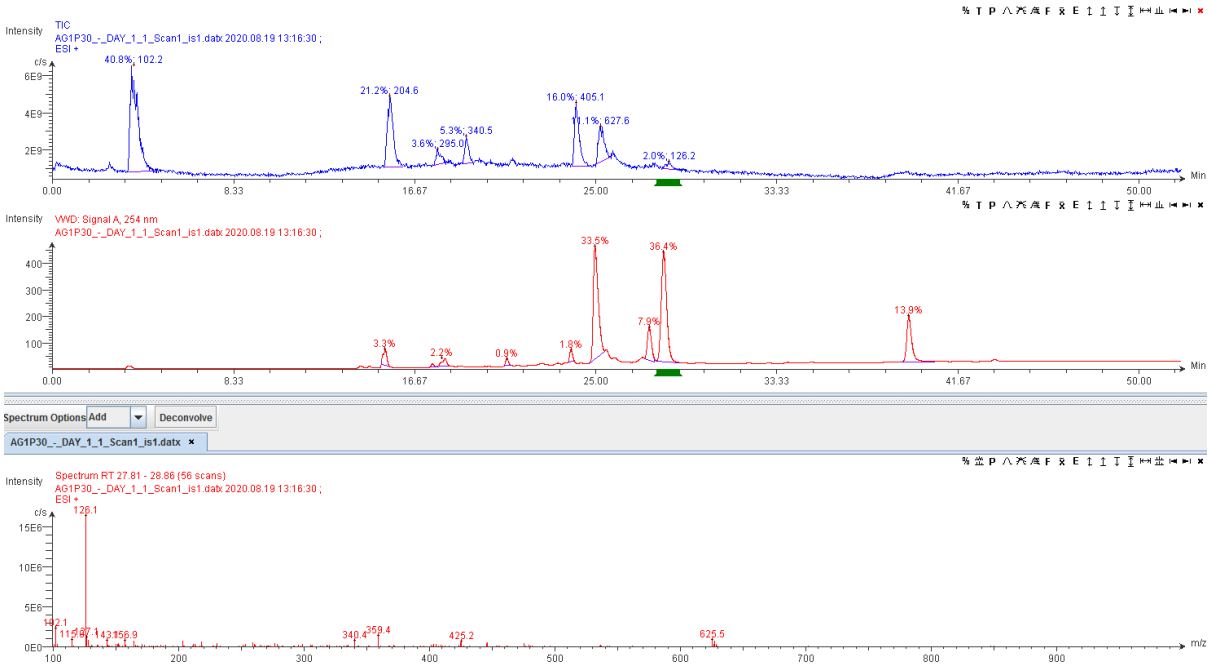

Figure 2.32: The LCMS Spectrum of **44**, where neither the starting material nor the product was observed**.**

2.2.8 Synthesis of 97

In order to provide a comparison of compounds that either contain 1 or 2 naphthalimides with or without a squaramide, compound **97** and **98** as previously reported were also synthesised as model compounds, where the syntheses have followed the procedures previously conducted in order to obtain the desired products.[281, 282] The spectroscopic data of both synthesised model compounds match the spectroscopic data obtained in the previous studies. The spectroscopic data of both synthesised model compounds match the spectroscopic data obtained in the previous studies.[281, 282]

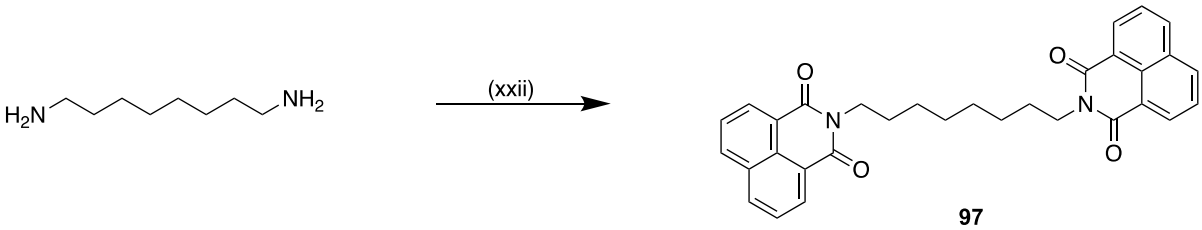

Scheme 2.22: Synthesis of **97**.

xxii) Ethanol, triethylamine, naphthalene-1,8-dicarboxylic anhydride

The synthesis of **97** involved dissolving naphthalene-1,8-dicarboxylic anhydride in ethanol and triethylamine, followed by an addition of 1,8-octanediamine. The reaction was allowed to reflux at 85°C for 12 hours. The solvent was removed in-vacuo to afford the crude product. The desired product was purified *via* column chromatography to afford a white solid, which was the pure product with a yield of 84%. The final compound was made according to the ^{1}H NMR (Figure 2.33), where the naphthalimide region peaks were represented by the peaks at 8.49, 7.71 and 7.68 ppm. The aliphatic region was represented by the peaks at 4.22, 2.08 and 1.34 ppm. The process of aggregation was evident, when the ^{1}H NMR at 358 K had indicated clearer proton signals (Figure 2.34). The process of aggregation was also evident in the solubility issues which prevented the possibility of collection of reliable ^{13}C NMR spectrum. The presence of the compound was also confirmed by the HR-MS (Figure 2.35).

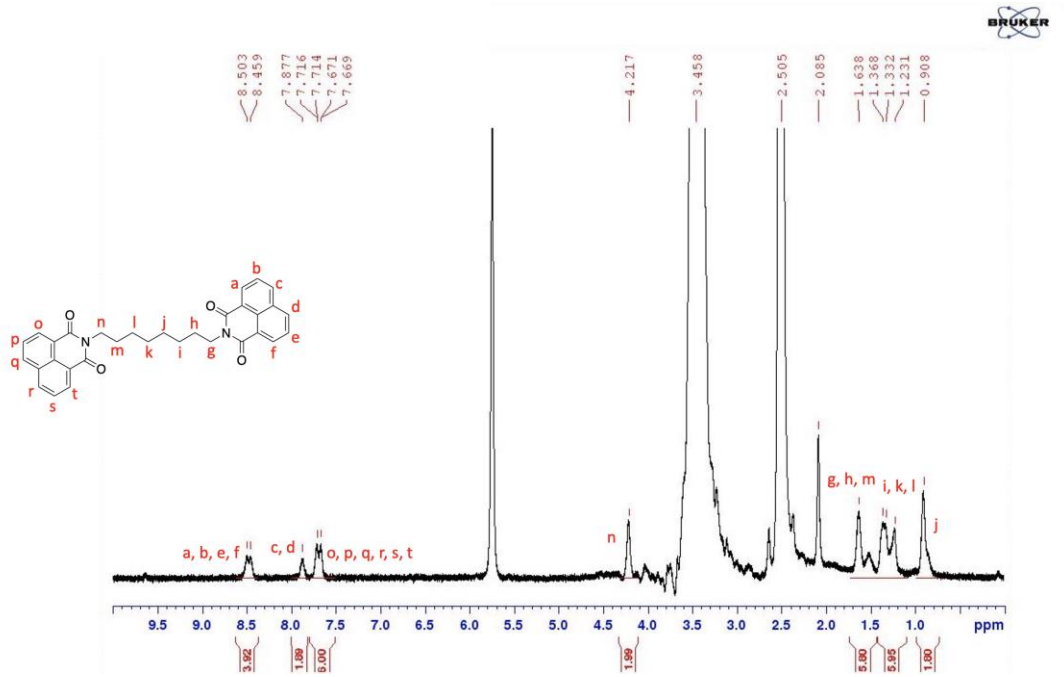

Figure 2.33: The ^{1}H NMR Spectrum of **97** (500 MHz, DMSO-d_6, 298 K.)

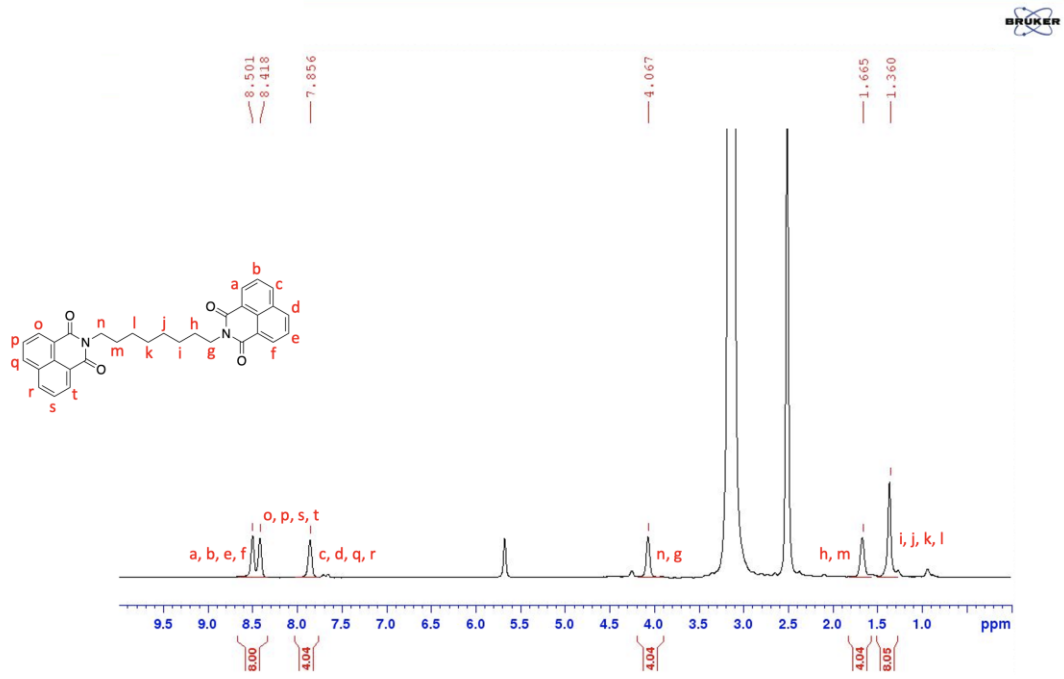

Figure 2.34: The ^{1}H NMR Spectrum of **97** at 358 K (500 MHz, DMSO-d_6, 358 K.)

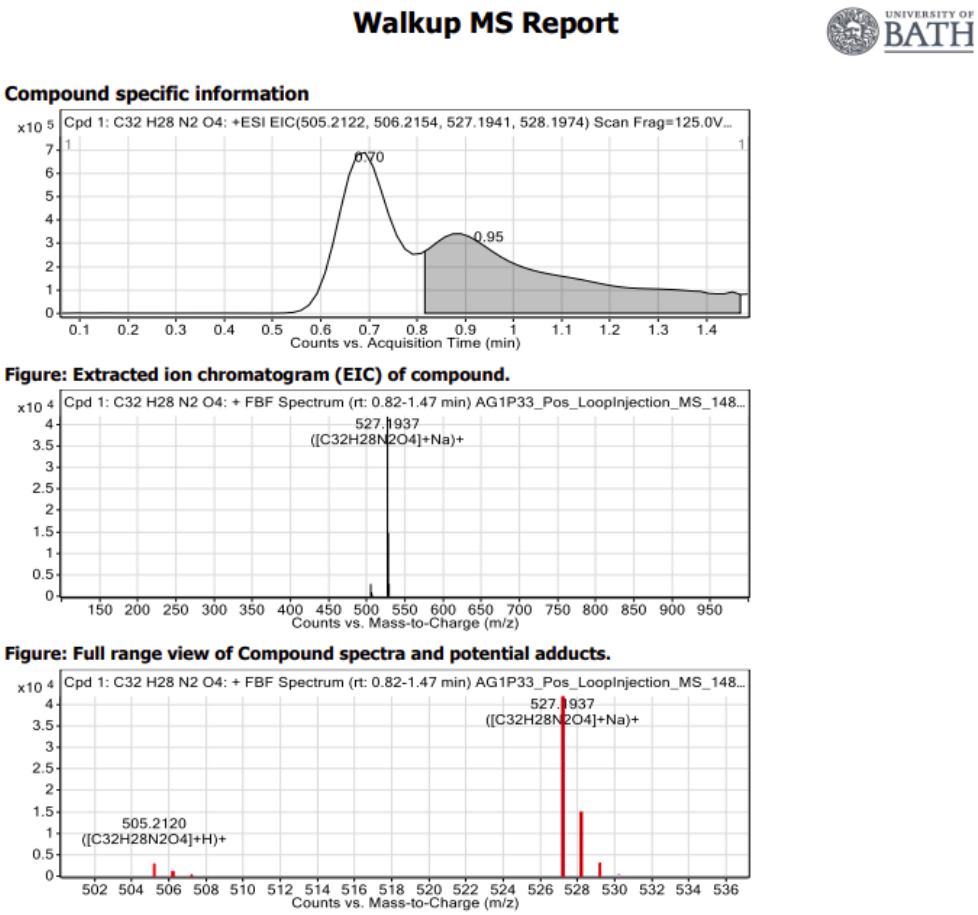

Figure 2.35: HRMS spectrum of **97.**

2.2.9 Synthesis of 98

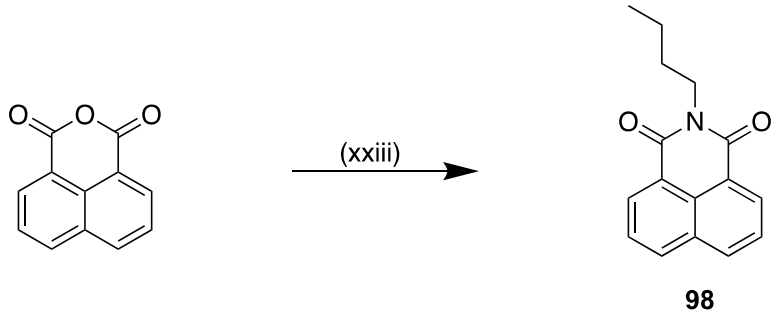

98

Scheme 2.23: Synthesis of **98**.

xxiii) Ethanol, triethylamine, 1-aminobutane

The synthesis of **98** involved dissolving naphthalene-1,8-dicarboxylic anhydride in ethanol and triethylamine, followed by the addition of 1-aminobutane. The reaction was allowed to reflux at 85°C for 12 hours. The solvent was removed in-vacuo to afford the crude product. The desired product was purified *via* column chromatography to afford a white solid, which was

the pure product with a yield of 81%. ^{1}H NMR confirmed the purity of **98** (Figure 2.36)**,** where the proton signals at 8.40 and 7.8 ppm both represented the protons in the naphthalimide moiety. The aliphatic region protons were represented by the signals at 4.0, 1.5, 1.3 and 0.9 ppm. The purity of the compound **98** was also confirmed by the LCMS analysis (Figure 2.37).

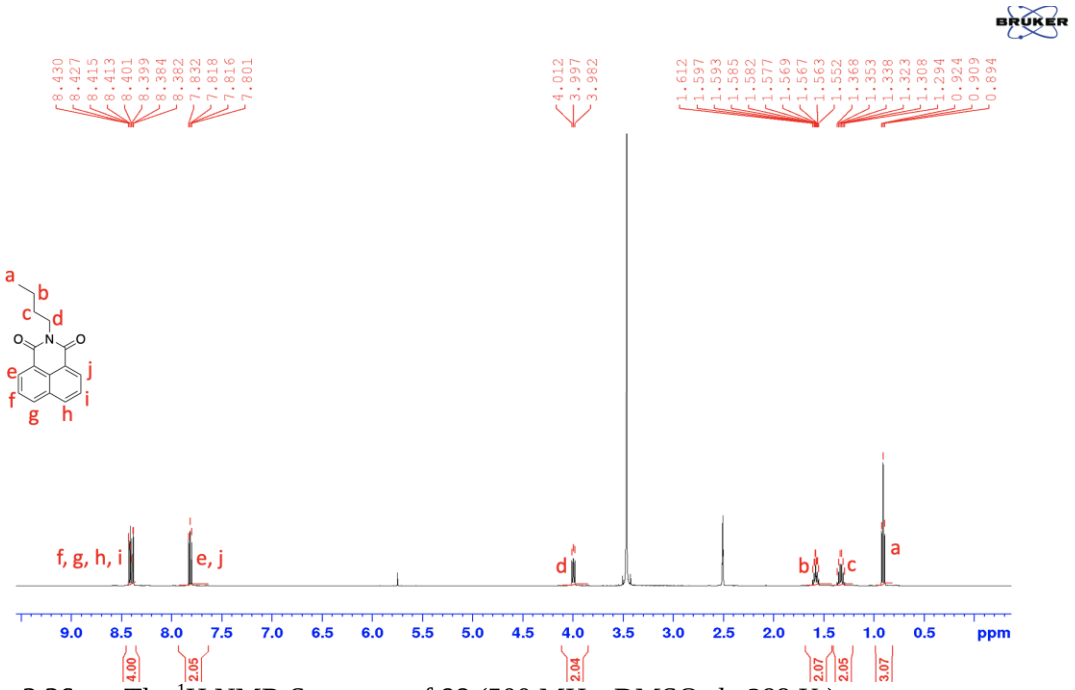

Figure 2.36: The ^{1}H NMR Spectrum of **98** (500 MHz, DMSO-d_6, 298 K.)

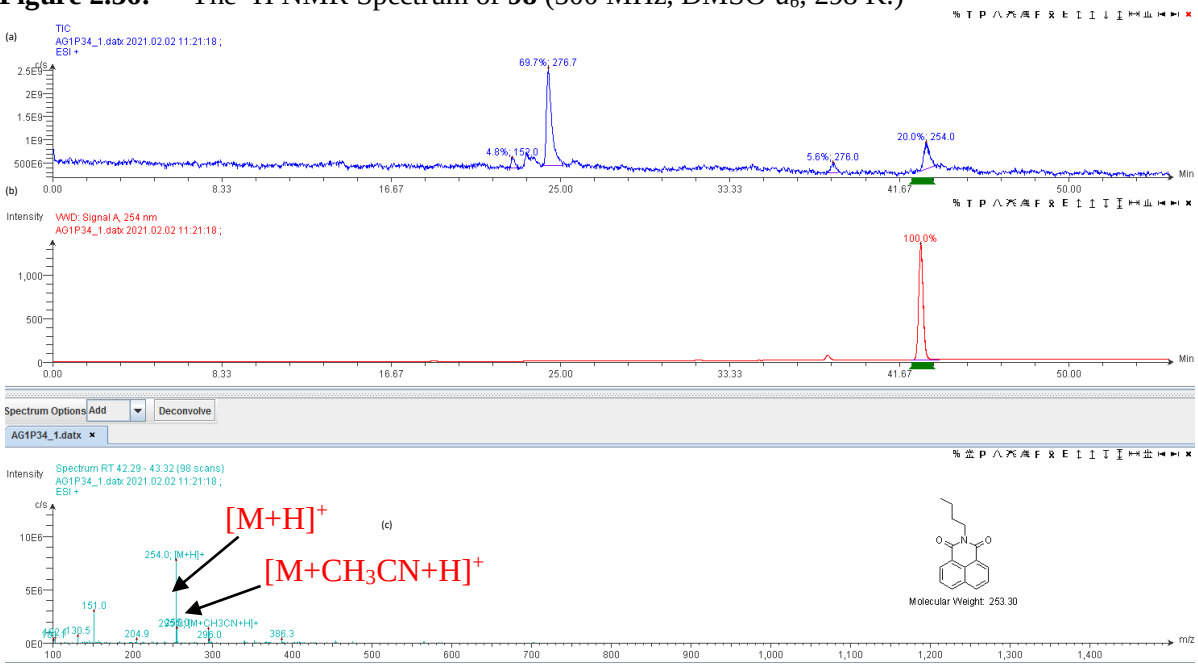

Figure 2.37: LCMS Characterisation of **98:** (a) Analytical HPLC trace of purified **98**; R_t = 42.0 mins (0-100% MeCN over 30 mins, λ = 254 nm). (b) Extracted Ion Chromatogram for 254. $[M + H]^+$. (c) Mass Spectrum detected between R_t = 42.0-43.5 mins (157 scans); Calculated for $[M + H]^+$ = 254.3; Mass Found (ESI^+) = 254.0 $[M+H]^+$. Also Found 295.0 = $[M+MeCN+H]^+$

2.3 Conclusion

In conclusion, we have successfully synthesised a family of compounds **38-40, 47-49, 97** & **98** based on the squaramide-naphthalimide moiety, where the new compounds were characterised by various techniques including: ^{1}H NMR, ^{13}C NMR, high resolution mass spectrometry and infrared spectroscopy.

Different synthetic pathways have been explored to synthesise the desired target compounds. The initial pathway when synthesising 1,8-naphthalimides with different aliphatic chain lengths have been explored. However, when diethyl squarate was added in the further steps, the reactions had only worked partially, where one side of the diethyl squarate had reacted to form 1,8-naphthalimide bound to the mono-squaramide. This occurred with the naphthalimides of different aliphatic chain lengths: 2-carbons, 5-carbons and 8-carbons. It was concluded that only one side of diethyl squarate had reacted to form a mono-naphthalimide, which precipitated immediately out of the reaction and the lack of solubility of mono-naphthalimide prevented the reaction proceeding further.

Another approach that was explored to synthesise the final desired compounds was reacting: diethyl squarates with mono-boc protected amines with the lengths of 2-carbons, 5-carbons and 8-carbons aliphatic chains. These reactions had formed the desired mono-boc protected squaramides with aliphatic chains of three different lengths. These squaramides were deprotected and reacted with 1,8-naphthalic anhydride respectively to form the desired final products, which were purified *via* centrifuging in ethanol and diethyl ether to afford the yellow solids. The key findings in this approach had also highlighted the stronger reactivity of the di-substituted derivatives, where the desired products were made using this method, compared to the first attempt.

The exact same approach was used with 4-nitro naphthalic anhydride to synthesise the desired products with a 4-nitro moiety on the 4-carbon position of the naphthalimide. Multiple attempts were made to synthesise 4-amino bis-naphthalimides as our desired compounds. It was first attempted to reduce 4-nitro bis-naphthalimides with palladium on carbon under a hydrogen atmosphere. Due to this reaction not being successful, due to the lack of solubility of 4-nitro bis-naphthalimides, we have changed the approach to first reduce the commercially available 4-nitro naphthalic anhydride to 4-amino naphthalic anhydride, where the ^{1}H NMR and LCMS data highlighted the formation and the purity of the 4-amino naphthalic anhydride made. The deprotected squaramides that were previously made were reacted with 4-amino naphthalic

anhydride. Solubility issues were the main factor preventing this reaction from proceeding further. It was only possible to dissolve 4-amino naphthalic anhydride in dimethylformamide. However, when the squaramide was added into the reaction, the reaction did not proceed any further, which indicated no reactivity, even with 10 equivalent excess of 4-amino naphthalic anhydride. This was also supported by the ^{1}H NMR and LCMS, where the starting materials were returned, which further concluded their low solubility.

Another approach that was explored was reacting the mono-boc protected amines with three different aliphatic chain lengths with commercially available 4-nitro naphthalic anhydrides to synthesise 4-nitro naphthalimides. The 4-nitro naphthalimides were purified *via* column chromatography. These 4-nitro naphthalimides were reduced with palladium on carbon under hydrogen atmosphere into 4-amino naphthalimides, once the reactions had undergone completion. The newly formed 4-amino naphthalimides were then deprotected and reacted with diethyl squarate in all three cases. However, this reaction was not successful, due to no reactivity of diethyl squarate in this reaction, which was supported by ^{1}H NMR and LCMS. Another approach we tried was reacting the commercially available 4-bromo naphthalic anhydride with the three different deprotected squaramides. The reactions were successful and the three desired 4-bromo squaramide-naphthalimide conjugates were synthesised. The 4-bromo squaramide-naphthalimide conjugates were purified *via* column chromatography. Various attempts have been made to aminate this family of compounds into the desired products *via* the addition of ammonia and even as a last resort using ammonia as the solvent. The starting materials were returned and the desired compounds were not made, due to the low reactivity of 4-bromo squaramide-naphthalimide conjugates. Another approach that was explored involved using the previously synthesised 4-bromo squaramide-naphthalimide conjugates and reacting them with n-butylamine in different solvents. This was not successful and the last attempt was using n-butylamine as a solvent and the reaction had failed to undergo completion to synthesise the desired compounds. This further proved that 4-bromo squaramide-naphthalimide conjugates had no reactivity.

Another approach we tried was reacting the 4-nitro squaramide-naphthalimide conjugates with Tin (II) Chloride, hydrochloric acid, water and acetic acid. This was also unsuccessful and the starting materials were returned as analysed, due to no solubility. The last resort explored, involved reacting 4-Bromo-N-n-butyl-1,8-naphthalimide with **66, 67** and **68** in different solvents. The starting materials were not reactive and the desired products were not obtained.

As a result, we have synthesised a bis-naphthalimide without a squaramide moiety which involved using 1,8-naphthalic anhydride and reacting it with 1,8-diaminooctane. This reaction was successful and the crude product was obtained. The crude product obtained was purified *via* column chromatography. We have also synthesised a mono-naphthalimide *via* reacting n-butylamine with 1,8-naphthalic anhydride. This reaction was also successful and it generated the desired crude product. The crude product was purified *via* column chromatography to obtain the pure desired product. Both the desired compounds and their syntheses had to be altered in this chapter due to reduced reactivity of starting materials and solubility issues.

Although the syntheses of these products were very challenging, we were successfully able to form 6 novel squaramide-containing bis-naphthalimides and 2 model naphthalimide compounds. During their syntheses, several interesting experimental observations led us to conclude that self-aggregation in solution appears to be a significant factor in the behaviour of this family of compounds in solution. The properties of these novel compounds will be discussed in further detail in the following chapters.

Chapter 3 Self-Assembly properties of the novel compounds

3.1 Introduction

In recent years, 4-substituted-1,8-naphthalimide derivatives have increased scientific interest due to their potential use as polymerizable fluorophores for synthetic polymers.[283] Various different naphthalimide derivatives have been synthesised recently due to their potential uses as DNA binders but also due to their self-assembly properties.[284] Similarly, squaramide based compounds are known for their self-assembly and molecular recognition properties.[240] In the previous chapter, we discussed the synthesis of several squaramide-naphthalimide conjugates. Precipitation of these compounds was common, due to the novel squaramide-naphthalimide conjugates undergoing self-aggregation, as previously observed with similar analogues.[266] It was also concluded that this resulted in their low reactivity in a number of reactions and their low solubility in nonpolar solvents. Although, significant difficulty was encountered in the synthesis of this family of compounds, 6 novel compounds **38-40, 47-49,** and 2 model compounds **97, 98** were successfully reported. During the characterisation of compounds **38-40**, we observed significant broadening of the ^{1}H NMR spectra and this led us to suspect some level of compound self-assembly was occurring in solution. Thus, as part of this chapter, we will investigate this behaviour using a series of spectroscopic techniques such as temperature dependent NMR, UV/Vis and fluorescence time studies, UV/Vis and fluorescence concentration studies as well as scanning electron microscopy (SEM).

3.2 Variable temperature studies

Prior to performing variable temperature experiments in the appropriate solvent, the optimised temperature range for VT-NMR studies was determined. DMSO-*d6* was chosen for these tests, due to its high boiling point. ^{1}H NMR spectra were collected every 10 minutes with 10 K temperature intervals ranging from 298 K to 358 K (Figure 3.1). At low temperature of 298 K, the NMR appears broad and it is very challenging to depict and assign each signal to the corresponding proton on the chemical structure. However, when the temperature was raised to at least 328 K, the corresponding proton peaks had cleared up significantly and it started becoming easier to assign each corresponding proton of **38**. When the temperature probe had reached its highest point of 358 K, each proton appeared very clear on the NMR spectrum and it was evident that the target compound **38** was made. The proton resonances that were broadened by the self-assembly process included the signals at 8.4, 8.5, 7.7 ppm in the

naphthalimide moiety, 7.4 ppm representing the N-H, 3.7 and 4.2 ppm representing both CH_2s in the aliphatic region, where these signals had a much improved resolution when ^{1}H NMR was taken at 358 K. This had indicated that these compounds underwent de-stacking when the temperature of the ^{1}H NMR was increased, which was consistent with the previous findings observed with similar compounds.[266] Moreover, when the sample was returned to 298 K, the spectrum was observed to undergo broadening again. These results are a clear indication that this compound had undergone the process of self-assembly. See Figures 3.2 and 3.3 for a direct comparison in the case of compound **38**. Similar ^{1}H NMR experiments were performed for the remaining bis-naphthalimides at 298 K and 358 K. The spectra showed significant broadening in each case and seemed to be unaffected by linker length. As an example, see Figures 3.4 and 3.5 for the corresponding experiments with compound **39**. The remaining spectra are shown in the Appendix.

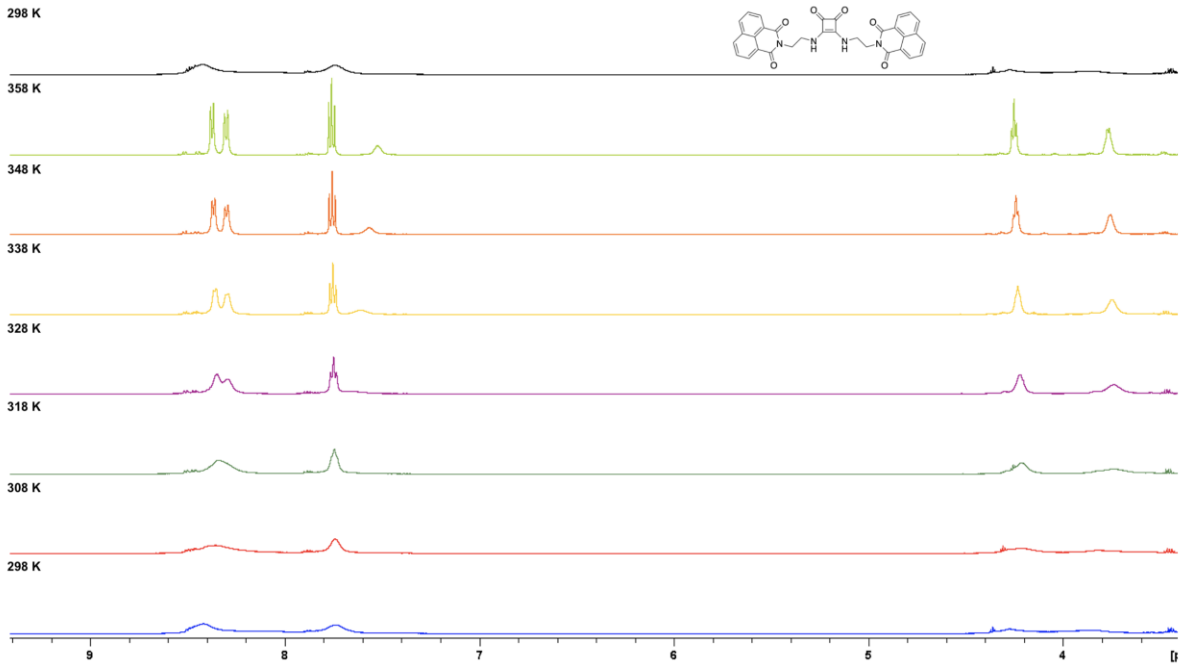

Figure 3.1: Variable temperature ^{1}H NMR (500 MHz, DMSO-d6) of **38**. Room temperature: 298 K (blue), 308 K (red), 318 K (teal), 328 K (violet), 338 K (yellow), 348 K (orange), 358 K (light green), returned to 298 K (black).

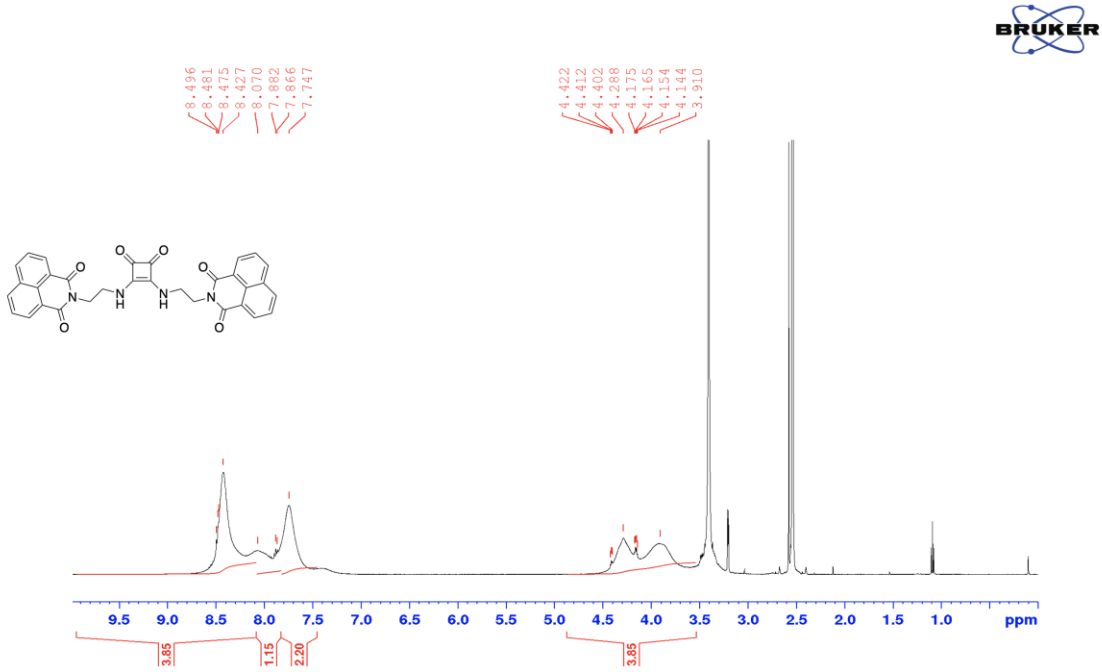

Figure 3.2: ^{1}H NMR (500 MHz, DMSO-d6) of **38** at 298 K.

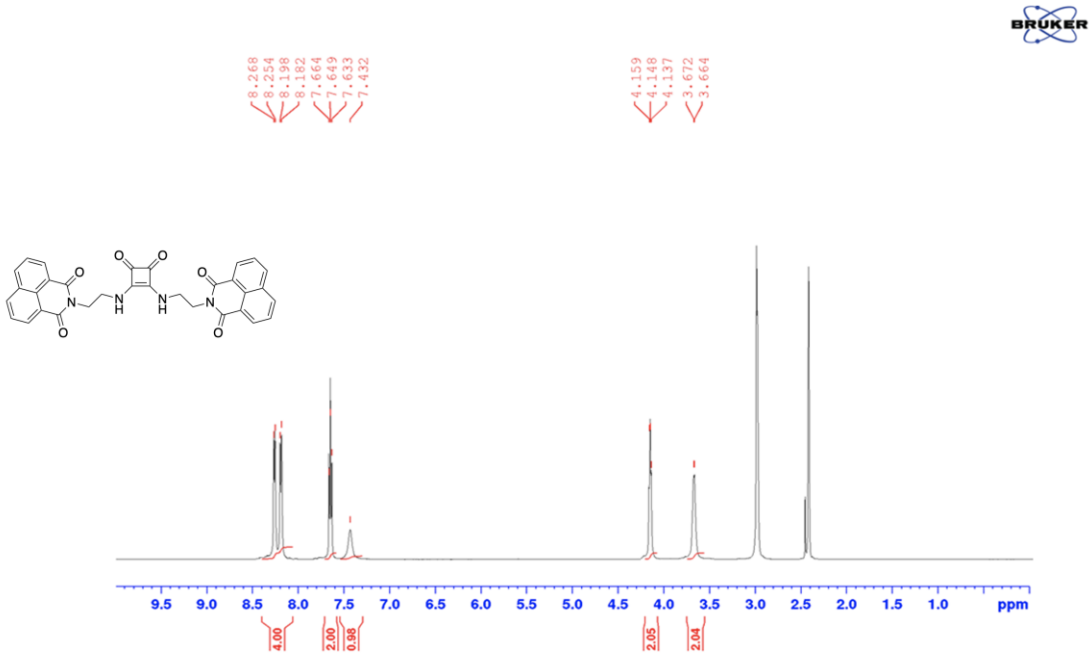

Figure 3.3: ^{1}H NMR (500 MHz, DMSO-d6) of **38** at 358 K.

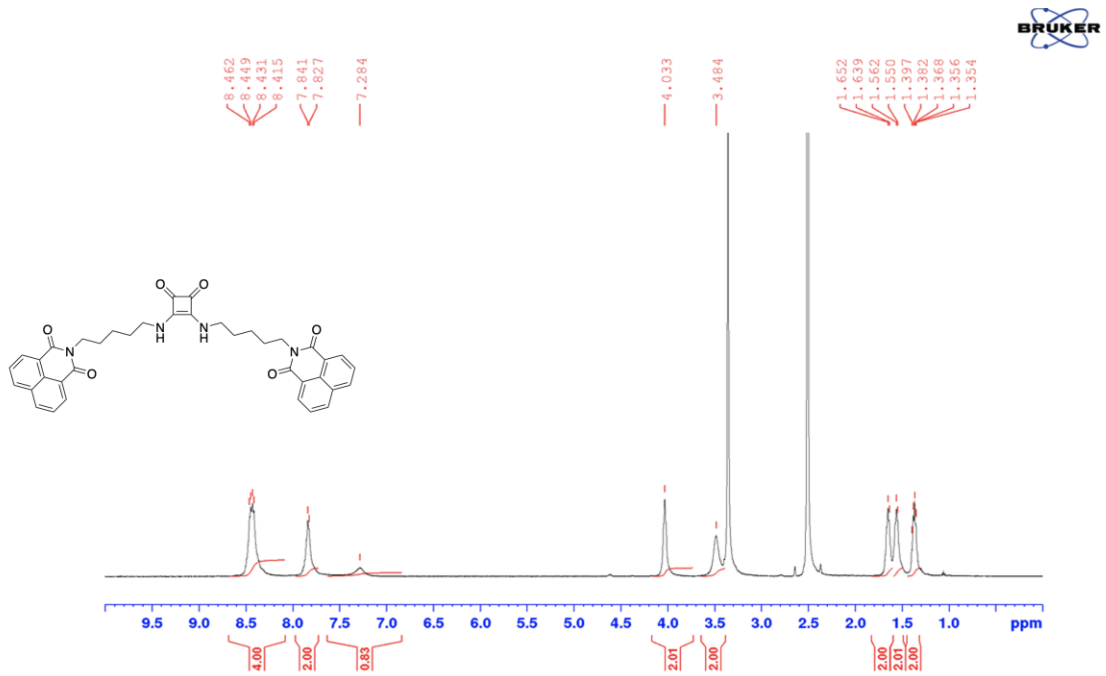

Figure 3.4: ^{1}H NMR (500 MHz, DMSO-d6) of **39** at 298 K.

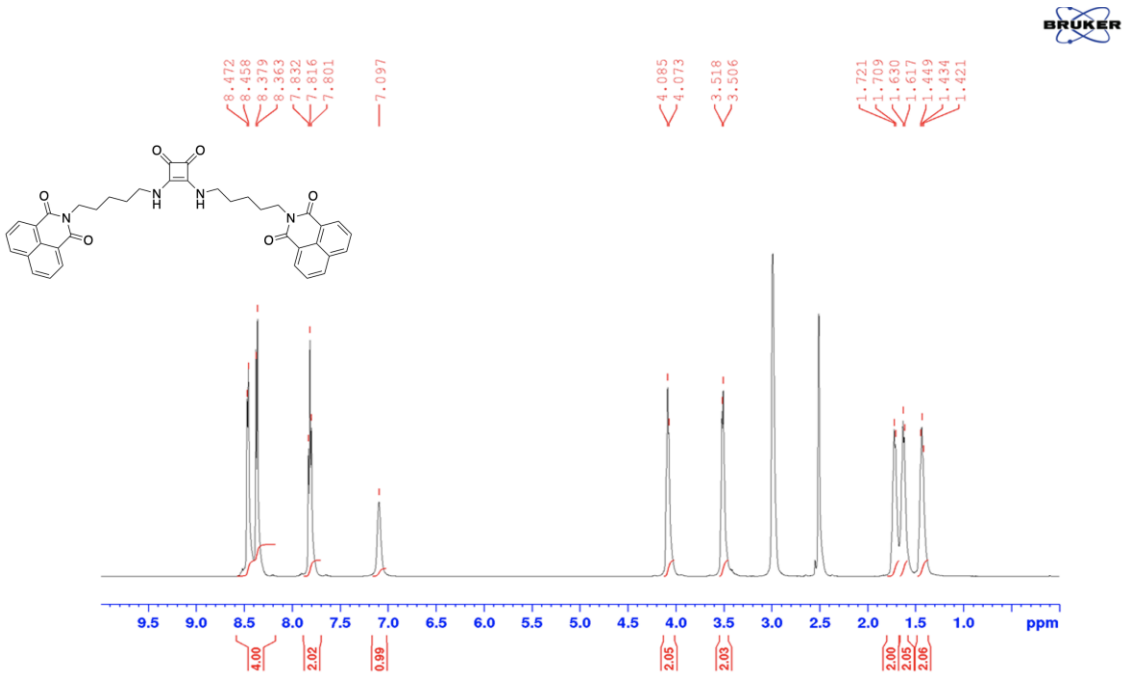

Figure 3.5: ^{1}H NMR (500 MHz, DMSO-d6) of **39** at 358 K.

3.3 UV-Vis and Fluorescence time studies

All of the above data indicates the process of self-assembly taking place, where the novel squaramide-naphthalimide conjugates undergo stacking or intermolecular H-bonding in solution. To confirm the results of the ^{1}H NMR experiments, UV-Vis dilution studies were also conducted and will be further discussed in the following section. UV-Vis dilution will be closely analysed and discussed according to the Beer-Lamber Law[285] (Figure 3.6). The compounds have demonstrated that they do not obey the Beer-Lambert Law, where there is no linear relationship between the concentration and the absorbance of the solutions of each compound in DMSO (Table 3.1), which further demonstrated the process of self-assembly taking place. UV-Vis data was recorded using a Varian Cary 50 UV-Vis Spectrophotometer at 25°C with the initial concentration of each compound at 100μM and the final concentration of each compound at 20μM after a total of 6 serial dilutions. The absorbance was recorded from 200 nm to 900 nm.

$$A = \varepsilon c l$$

A	Absorbance	
ε	Molar absorption coefficient	$M^{-1}cm^{-1}$
c	Molar concentration	M
l	optical path length	cm

Figure 3.6: Beer-Lamber Law equation.

Sample	Dilution factor	Initial Concentration (M)	Final Concentration (M)	R^2 at (295 nm ± 15 nm)	R^2 at (335 nm ± 15 nm)	Molar Extinction Coefficient ($M^{-1}cm^{-1}$) at (295 nm± 15 nm)	Molar Extinction Coefficient ($M^{-1}cm^{-1}$) at (335 nm± 15 nm)
38	3	$100x10^{-6}$	$13.1x10^{-6}$	0.999	0.999	3661.8	2639.9
39	3	$100x10^{-6}$	$13.1x10^{-6}$	0.999	0.999	3502.7	2529.6
40	3	$100x10^{-6}$	$13.1x10^{-6}$	0.999	1.000	4476.9	1063.9
47	3	$100x10^{-6}$	$13.1x10^{-6}$	1	/	1709.7	/
48	3	$100x10^{-6}$	$13.1x10^{-6}$	0.997	/	3638.3	/
49	3	$100x10^{-6}$	$13.1x10^{-6}$	0.996	/	4568.9	/
97	3	$100x10^{-6}$	$13.1x10^{-6}$	0.996	/	3280.7	/
98	3	$100x10^{-6}$	$13.1x10^{-6}$	0.997	/	1525.2	/

Table 3.1: Table of all UV-Vis concentration studies performed.

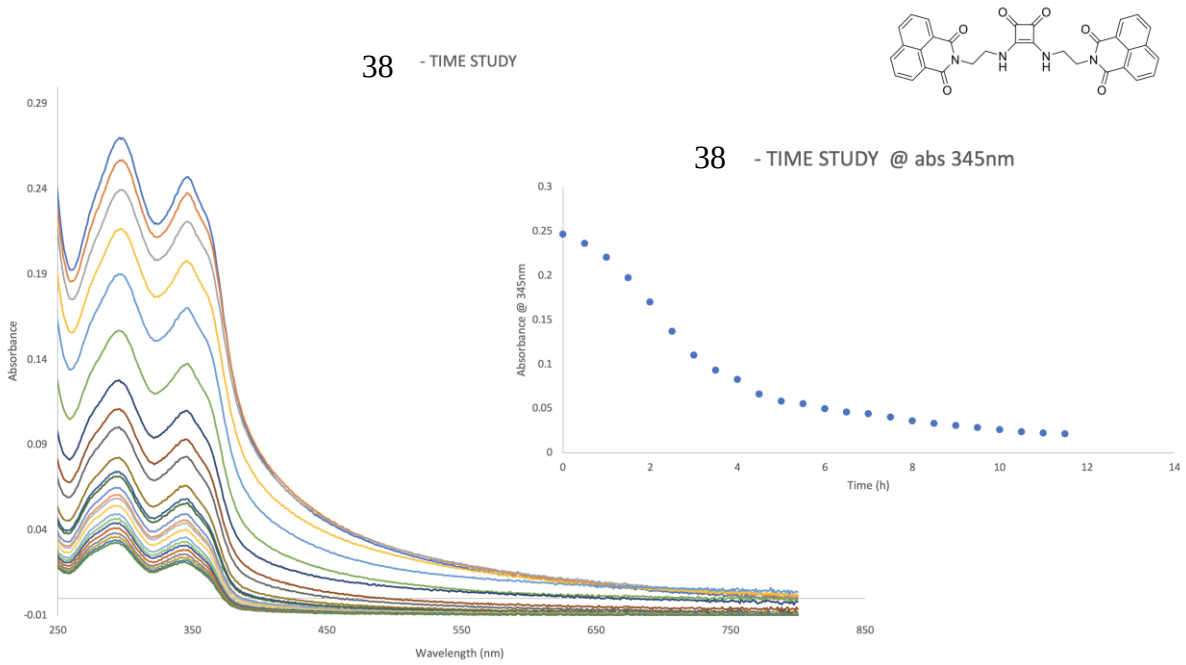

Figure 3.7: UV-Vis absorbance time study of **38** over the course of 12 hours in DMSO.

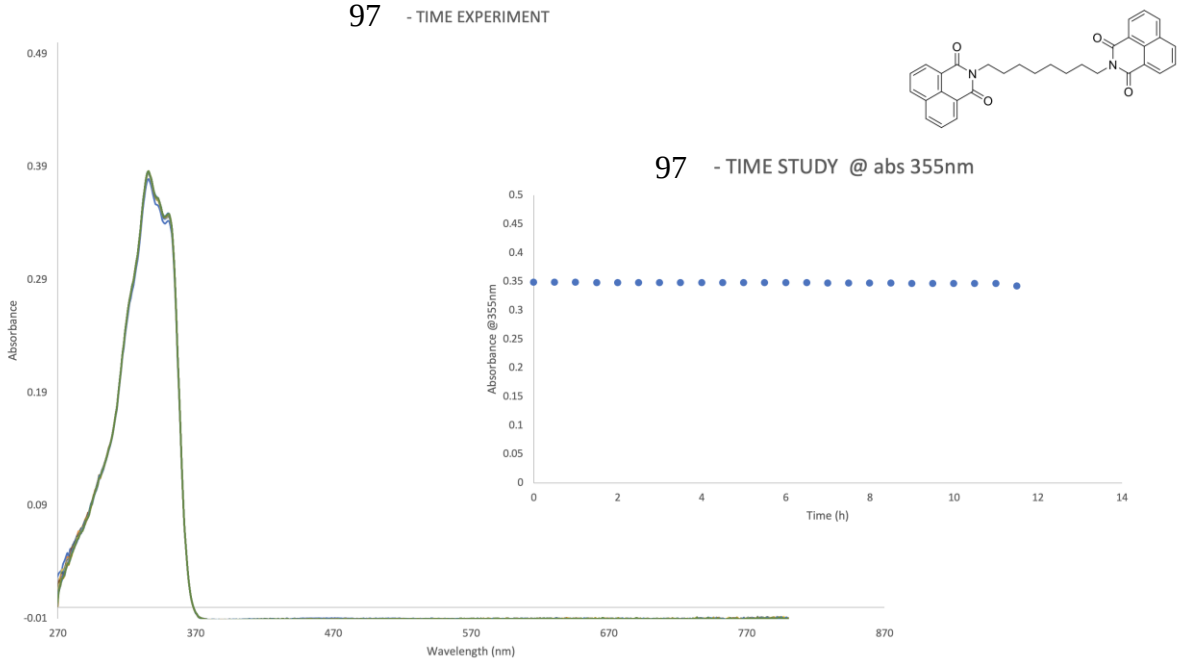

Figure 3.8: UV-Vis absorbance time study of **97** over the course of 12 hours in DMSO.

UV-Vis time studies of **38-40, 47-49, 97** and **98** were carried out in DMSO. **38-40** UV-Vis spectra time studies showed a dramatic decrease in UV absorbance over time. This indicates that due to the presence of a squaramide moiety in unsubstituted bis-naphthalimides, the squaramide may be responsible for these aggregation processes. The UV-Vis absorbance of **38** is shown in Figure 3.7 and had dropped significantly at its λ_{max} of 345 nm over the course of

12 hours as indicated. Although **39** had also dropped in UV absorbance at its λ_{max} of 345 nm over the course of 12 hours, the percentage decrease in absorbance was 45% less than seen with **38** (See Appendix). The UV absorbance percentage decrease of **40** at its λ_{max} of 345 nm was approximately 80% less than seen with **38**. These results can conclude that the further the squaramide moiety is from the naphthalimide moiety, the process of self-aggregation is less significant. Aggregation would be expected to result in a decrease in absorbance, due to their decreased solubility as observed with other similar derivatives.[266, 286] It was evident that **47-49** all had a λ_{max} of 350 nm but with no decrease in absorbance in the time study. It was also observed that **97** and **98** had a λ_{max} of 350 nm (See Appendix), where these compounds did not undergo decrease in UV-Vis absorbance over time, and this suggests that the self-assembly was not occurring for compounds **47-49**, **97** and **98.** See Figure 3.8 for the corresponding spectrum for compound **97** which does not contain a squaramide.

In contrast to the UV/Vis time studies, the fluorescence time studies did not indicate any changes in fluorescence intensity over time at 25°C. The characteristic fluorescence for naphthalimides is at 445 nm, where the fluorescence time study of **38** is shown (Figure 3.9). Even though there were large changes in UV-Vis time studies, these were not mirrored in the fluorescence studies. This suggested that fluorescence was not able to observe the self-assembly formation of the final compounds due to their weak fluorescence. Furthermore, in bis-naphthalimides containing a squaramide moiety, this self-assembly behaviour is not observed *via* their fluorescence. This can be described by the squaramide possibly quenching the fluorescence of the naphthalimide moiety. Concentration dependent studies were suggested to observe the expected decrease in both UV-Vis absorbance and fluorescence with the decreasing concentration of each synthesised compound.

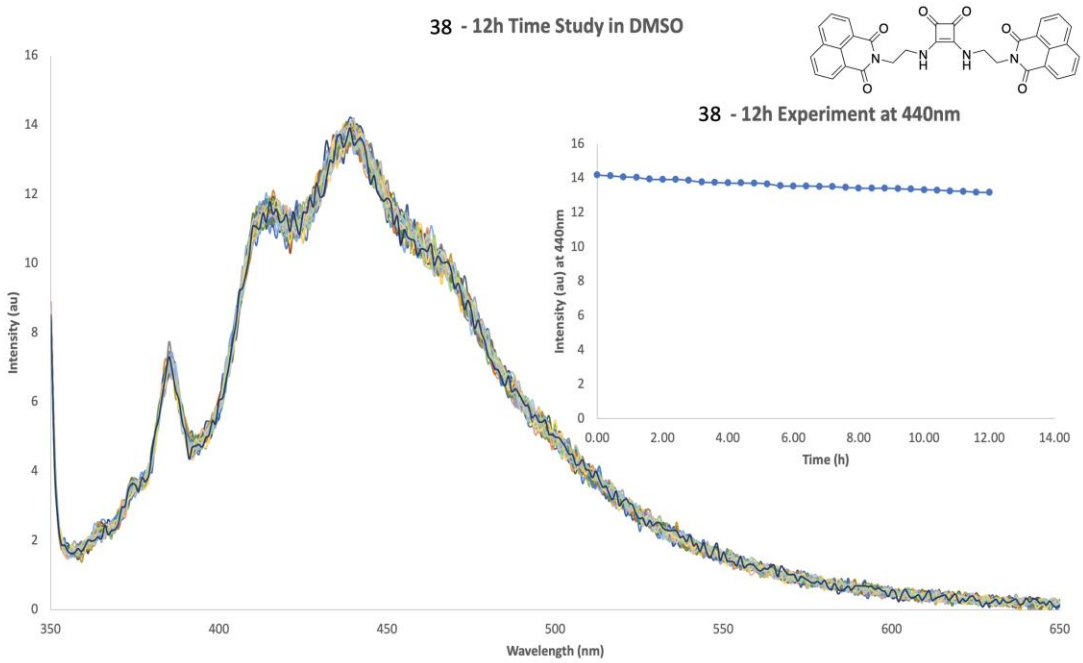

Figure 3.9: Fluorescence intensity (au) time study of **38**, with an excitation wavelength at 440 nm over the course of 12 hours in DMSO.

3.4 Extinction coefficient studies

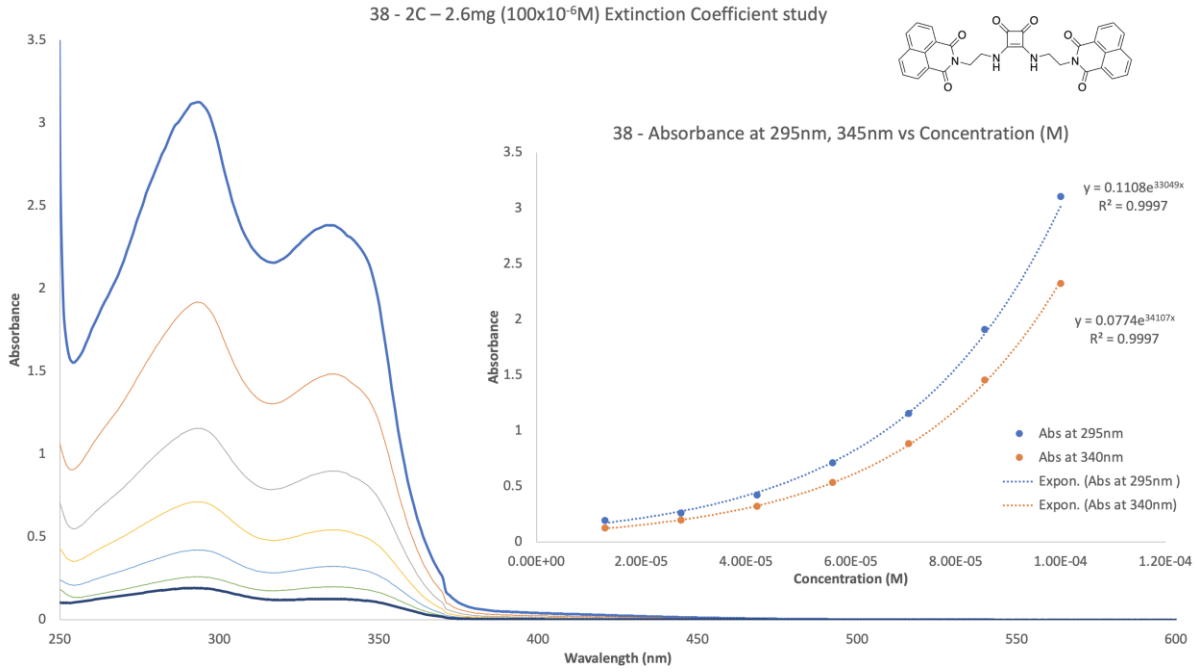

Figure 3.10: UV-Vis Absorbance of 2.6 mg of **38** and its absorbance at 345 nm vs the concentration (M) of **38** in DMSO.

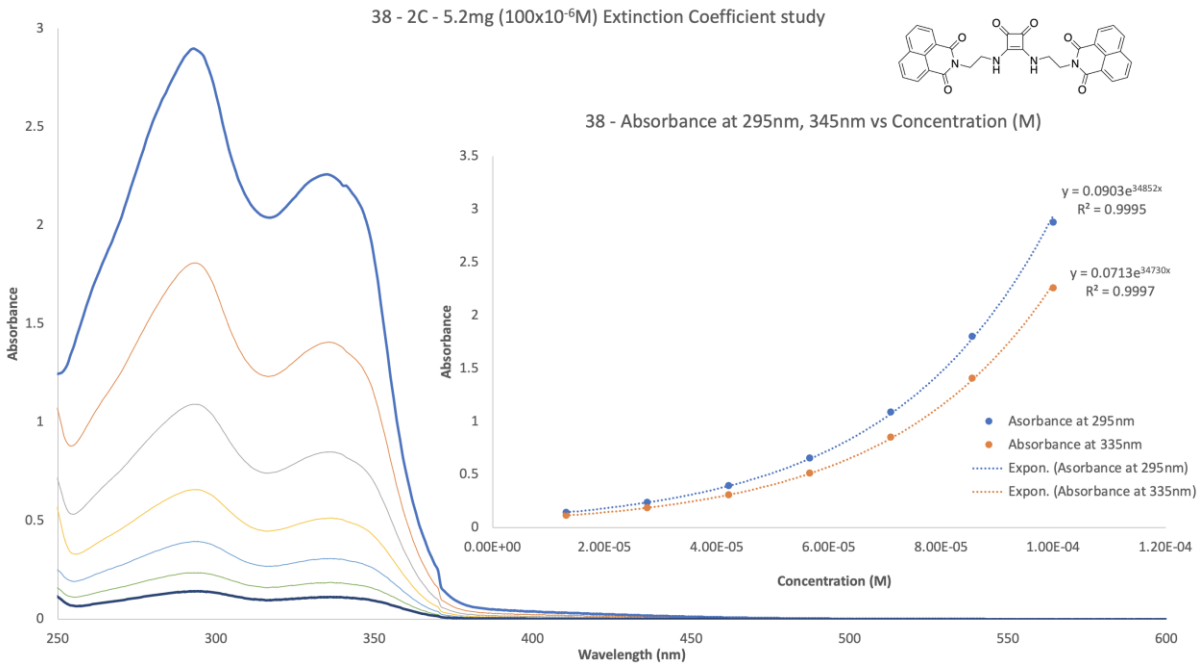

Figure 3.11: UV-Vis Absorbance of 5.2 mg of **38** and its absorbance at 345 nm vs the concentration (M) of **38** in DMSO.

The extinction coefficients were taken immediately after dissolving each compound in DMSO. The UV-Vis concentration study had revealed that with decreasing concentration, each compound had decreased in terms of their UV light absorbance. This decrease was exponential for all compounds. This exponential decrease was observed from the molar extinction coefficient study starting from a $100x10^{-6}$ M concentration of each compound in DMSO with $14.5x10^{-6}$ M decrease of concentration for each run for a total of 6 runs, with the final concentration being $13.1x10^{-6}$ M. The exponential decrease was observed at the highest UV-Vis absorbance wavelength for each compound, as it differed in each case. The exact same concentrations of $100x10^{-6}$ M for each compound were tested under the fluorescence spectrometer to see the same decrease in terms of their light emittance. Each compound concentration was again reduced by $14.5x10^{-6}$ M for a total of 6 times from the initial $100x10^{-6}$ M concentration, with the final concentration being $13.1x10^{-6}$ M as tested previously with UV light absorbance experiments. The same effect of decrease of fluorescence was observed for all compounds. However, both the decrease in intensity and the decrease in concentration at the highest wavelengths for all compounds emitting light (435-440 nm) was exponential. This concludes that both the UV light absorbance and fluorescence of these compounds are concentration dependent. These compounds had a stronger UV light absorbance and emittance of light with higher concentrations and weaker UV light absorbance and emittance of light in lower concentrations.

3.5 Scanning electron microscopy studies

Having observed the aggregation in these compounds in the UV-Vis and the proton VT-NMR studies, we have also decided to observe this process in the solid state using Scanning Electron Microscopy.

The morphological features of **38-40, 97** and **98** in both DMSO and DMSO:water (50:50) was measured upon dropcasting the samples onto silica support using 1 µM stock solutions of each structure. The samples were allowed to dry in air and under vacuum prior to imaging.

In DMSO, all compounds demonstrated the formation of compact films. **38** appears to form quite complex structures in Figure 3.12. Compound **39** also showed the formation of complex structures in Figure 3.13. This further supports the fact that these compounds are undergoing self-assembly in DMSO due to aggregation of naphthalimide and squaramide moieties. However, more fibrillar networks were particularly visible in the case of **97** in Figure 3.14, where only the naphthalimide moieties underwent self-aggregation, while no fibrillar networks were visible in **98** due to no self-assembly taking place (See Appendix). When the experiments were repeated in DMSO:water (50:50), there was an element of formation of fibrillar fine structure forming in each case, suggesting that upon the addition of water, self-assembly was still seen to occur. This will be an important factor in the proceeding sections that will discuss DNA binding behaviour.

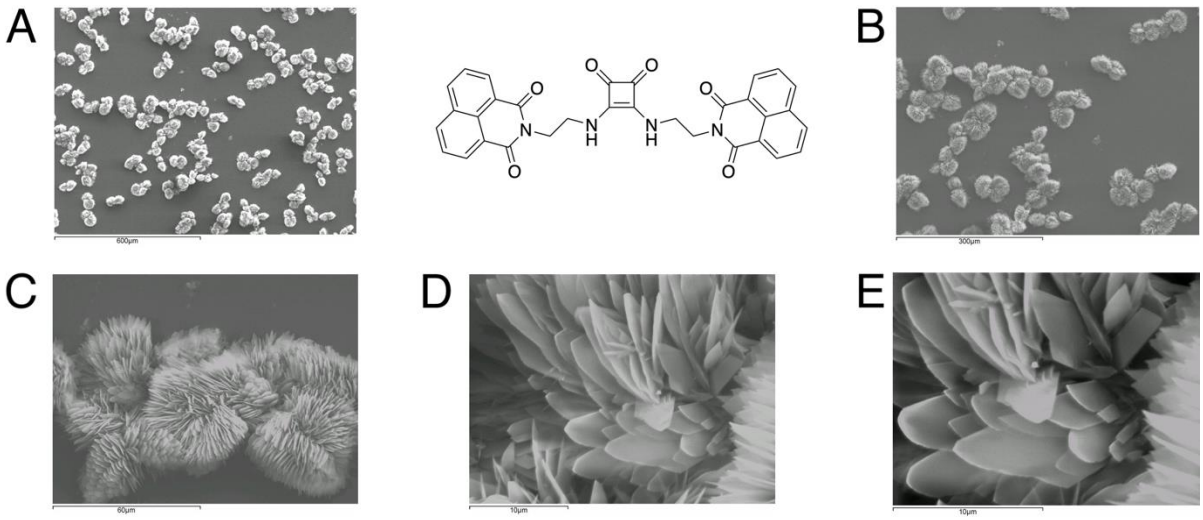

Figure 3.12: Scanning electron microscopy (SEM) images of compound **38** spotted with Au in DMSO, **(A):** Mag x 100; **(B):** Mag x 200; **(C):** Mag x 1000; **(D):** Mag x 4000; **(E):** Mag x 6000.

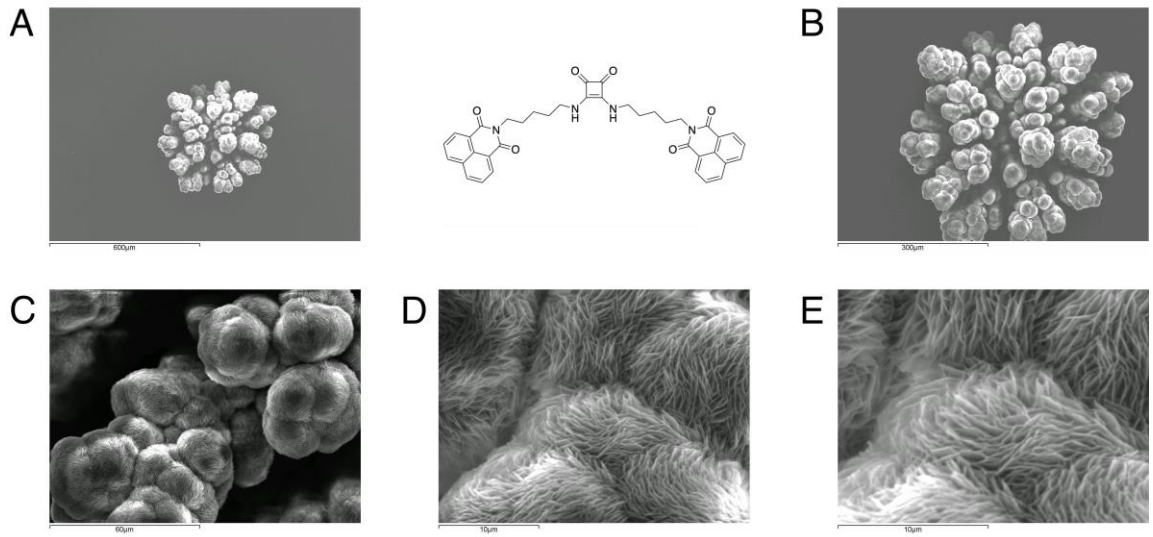

Figure 3.13: Scanning electron microscopy (SEM) images of compound **39** spotted with Au in DMSO, **(A):** Mag x 100; **(B):** Mag x 200; **(C):** Mag x 1000; **(D):** Mag x 4000; **(E):** Mag x 6000.

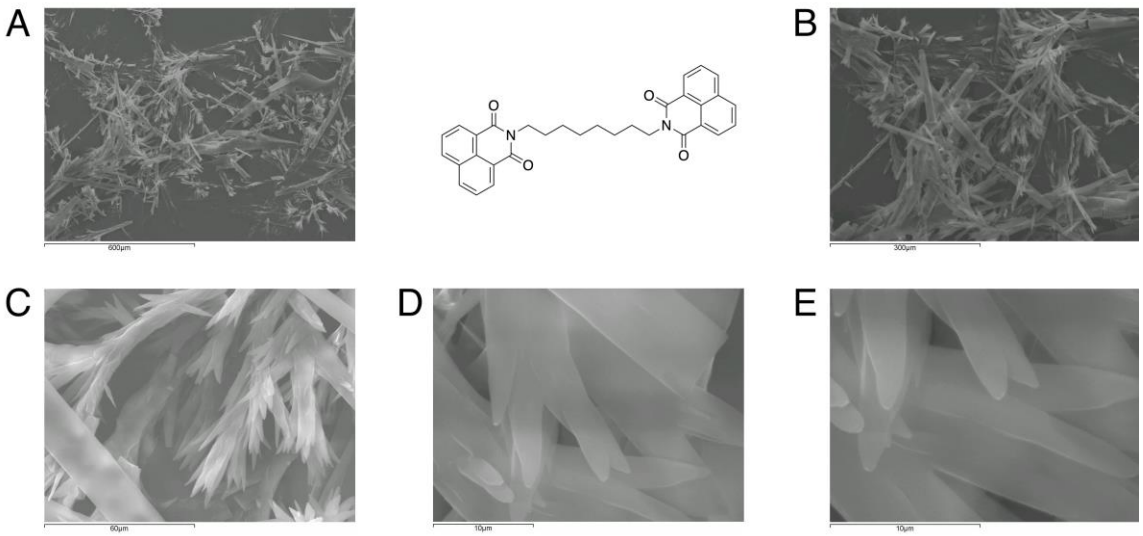

Figure 3.14: Scanning electron microscopy (SEM) images of compound **97** spotted with Au in DMSO, **(A):** Mag x 100; **(B):** Mag x 200; **(C):** Mag x 1000; **(D):** Mag x 4000; **(E):** Mag x 6000.

38-40 and **97** have displayed processes of aggregation, as these compounds underwent π-π stacking interactions, which involved the naphthalimide moiety due to its aromatic nature and the squaramide aromatic moiety also being involved in π-π stacking in compounds **38-40**. It was evident that **38-40** formed quite complex structures, which appeared as sponge like structures when zoomed in under a high magnification in pure DMSO. **98** had appeared as fibrillar structures, which did not display the process of self-assembly taking place. The SEM study was repeated in DMSO:water (50:50) solution.

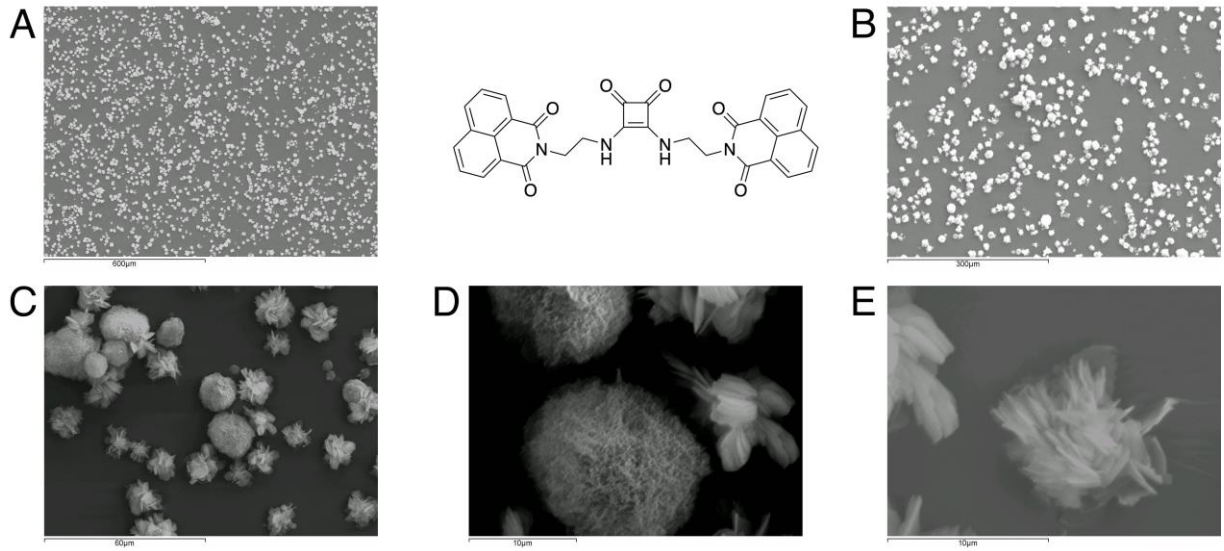

Figure 3.15: Scanning electron microscopy (SEM) images of compound **38** spotted with Au in DMSO:H_2O 50:50, **(A):** Mag x 100; **(B):** Mag x 200; **(C):** Mag x 1000; **(D):** Mag x 4000; **(E):** Mag x 6000.

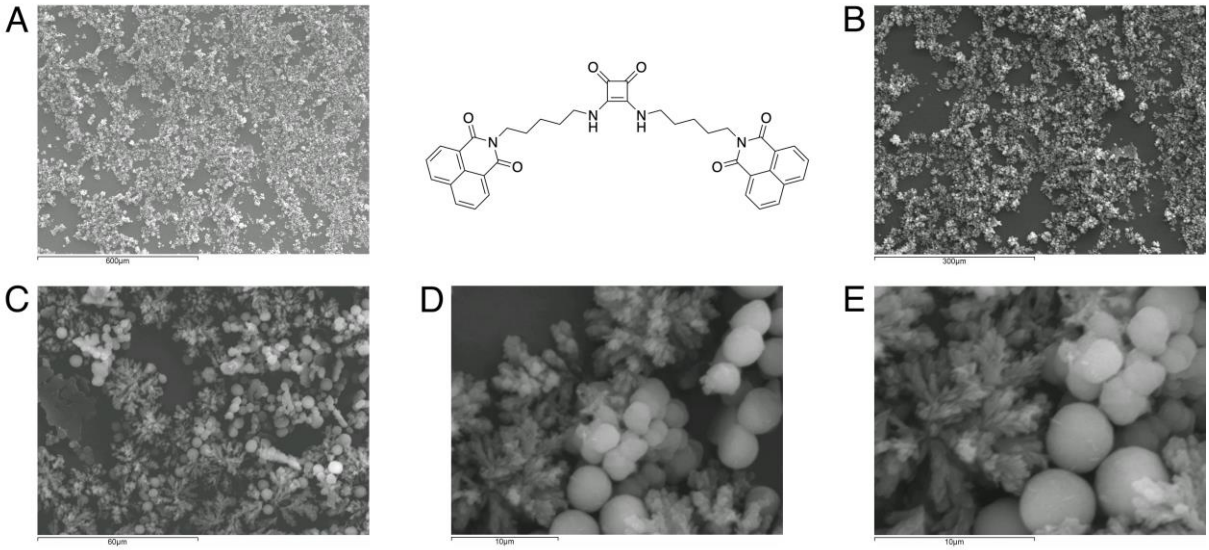

Figure 3.16: Scanning electron microscopy (SEM) images of compound **39** spotted with Au in DMSO:H_2O 50:50, **(A):** Mag x 100; **(B):** Mag x 200; **(C):** Mag x 1000; **(D):** Mag x 4000; **(E):** Mag x 6000.

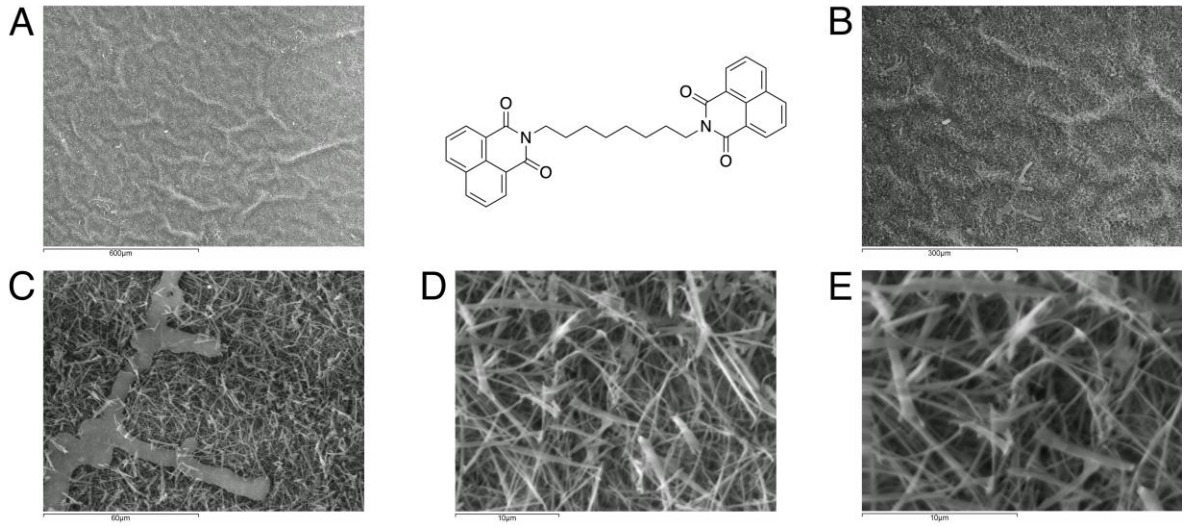

Figure 3.17: Scanning electron microscopy (SEM) images of compound **97** spotted with Au in DMSO:H_2O 50:50, **(A):** Mag x 100; **(B):** Mag x 200; **(C):** Mag x 1000; **(D):** Mag x 4000; **(E):** Mag x 6000.

38-40 have formed similar complex structures in DMSO:Water, (50:50) which highlighted the process of self-aggregation of both squaramide and naphthalimide moieties also taking place in this solvent combination. **97** had formed similar fibrillar structures in DMSO:Water (50:50), which indicated that these compounds had undergone π-π stacking interactions in the naphthalimide moieties, without the presence of the squaramide. It was also reported that **38-40** formed nanofilaments, which appeared as sponge like structures and **97** (Figure 3.17) had formed fibrillar structures in DMSO:water (50:50) when zoomed in under a high magnification. We have attempted to grow crystals from DMSO solution for the novel synthesised compounds. However, the novel compounds had formed amorphous solids, as they did not crystallise.

3.6 Conclusion

In this chapter, we described the processes of self-assembly of the novel bis-naphthalimides using techniques such as: Variable Temperature ^{1}H NMR, UV-Vis Absorption Spectroscopy, Fluorescence Spectroscopy and Scanning Electron Microscopy. These processes had further concluded that self-aggregation of the novel synthesised bis-naphthalimides had taken place. Variable temperature ^{1}H NMR have revealed the process of self-aggregation of all synthesised bis-naphthalimides. Increased temperatures caused the broad spectra of the synthesised bis-naphthalimides to become better resolved in sharper proton signals, enabling us to observe disaggregation with increasing temperatures. It is possible to characterise all ^{1}H signals at a

higher temperature spectrum, especially at 358 K in all synthesised bis-naphthalimides. The signals representing the naphthalimide moiety protons have also become more resolved with the increased temperature. The N-H signals in the squaramide moiety in all synthesised bis-naphthalimides containing this moiety were not well resolved at 293 K. However, as the temperature was increased to 358 K in all cases, the signal representing the N-H of the squaramide moiety had become much sharper and more intense, enabling us to fully characterise the squaramide containing bis-naphthalimides. When the ^{1}H NMR was taken at 298 K following these variable temperature spectra, the spectra collected had broadened again, indicating self-assembly of these novel bis-naphthalimides taking place.

38-40, **47-49, 97** and **98** were all examined using UV/Vis spectroscopy and fluorescence emission spectrometry. **38-40**, which were the unsubstituted bis-naphthalimides had shown a significant decrease in UV light absorbance over the time of 12 hours. This also indicates a process of self-assembly taking place.

Scanning Electron Microscopy (SEM) was used to analyse the morphological features of these compounds. SEM was performed both in pure DMSO and DMSO:H_2O (50:50) solution. In summary, SEM analyses have revealed the presence of self-assembly interaction of all the synthesised bis-naphthalimides. **38-40** and **97** have shown significant processes of aggregation. **38-40** planar compounds have all underwent π-π stacking interactions, which involved both the squaramide and naphthalimide moieties due to their aromatic nature at a room temperature. **97** had also formed fibrillar structures, due to π-π stacking interactions taking place only in the naphthalimide moieties, as no squaramide moiety was present. **38-40** and **97** formed nanofilaments when zoomed in under a high magnification, which showed sponge like structures when zoomed out on the SEM. Although, the exact mechanism of self-assembly undergoing molecular interaction giving these compounds their morphology is not clear, it is evident that high degree of aggregation is taking place that appears to be organised to give rise to such patterns. **97** was another novel bis-naphthalimide compound synthesised, without the squaramide moiety and it was also examined under the SEM, along with a previously synthesised mono-naphthalimide. Compound **97** had formed nano fibres in high density also indicating self-assembly taking place. No fibres or nanofilaments in high density were visible for **98**, which indicated no self-assembly taking place, as the compound was not a bis-naphthalimide and it did not contain a squaramide moiety. The properties of **38-40, 47-49**, **97** and **98** binding to DNA are examined in the following chapter to observe whether these compounds can bind to DNA, while undergoing the process of self-assembly.

Chapter 4 DNA binding studies

4.1 Introduction

In the previous sections of this thesis, squaramide containing bis-1,8-naphthalimide derivatives **38-40**, **47-49**, bis-1,8-naphthalimide without squaramide moiety **97** and a mono-naphthalimide **98** (Figure 4.1) were designed and synthesised and an evaluation of their self-assembly behaviour was undertaken. Overall, it was anticipated that possible noncovalent binding interactions of these compounds may allow binding to DNA *via* various interactions including intercalation, groove-binding (major and minor) and H-bonding to the negatively charged sugar phosphate backbone.[287] Synthesising these planar structures was a necessary feature for the likelihood of intercalation, while keeping a squaramide moiety aiding the H-bonding interactions with DNA. Squaramide containing bis-1,8-naphthalimides were chosen because of the naphthalimides having DNA bis-intercalating properties, while their squaramide moieties have the ability to bind to DNA *via* H-bonding interactions (Figure 4.2). Compounds **97** and **98** were synthesised as control compounds, where **97** was a bis-naphthalimide without a squaramide moiety, where it was compared to compounds **38-40, 47-49.** Compound **98** was a mono-naphthalimide, which was compared to **38-40, 47-49** and **97**, which were all bis-naphthalimides. The final two compounds were compared to the model squaramide containing bis-naphthalimides **38-40, 47-49.**

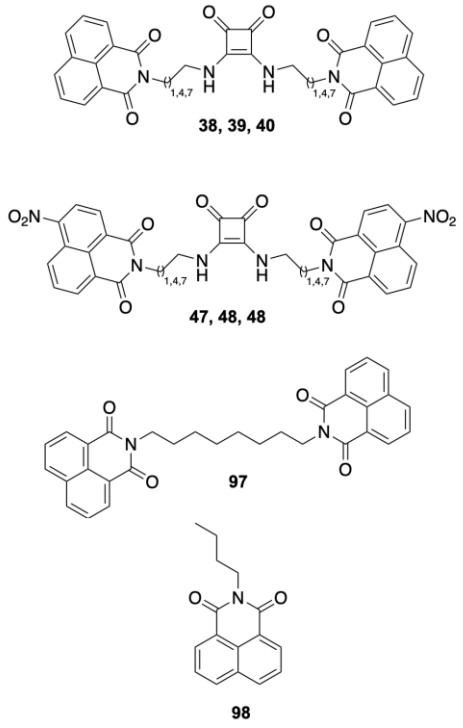

Figure 4.1: Structures of the squaramide containing bis-1,8-naphthalimides **38-40, 47-49,** bis-1,8-naphthalimide without squaramide moiety **97** and a mono-1,8-naphthalimide **98**.

In Chapter 3, the photophysical properties of these molecules in DMSO were investigated, along with their self-assembly properties *via* UV-Vis, Fluorescence studies and Scanning Electron Microscopy. In this chapter, their ability to bind to DNA in buffered aqueous solutions will be explored *via* UV-Vis absorbance and Fluorescence emission DNA interaction studies, along with Ethidium Bromide assays.

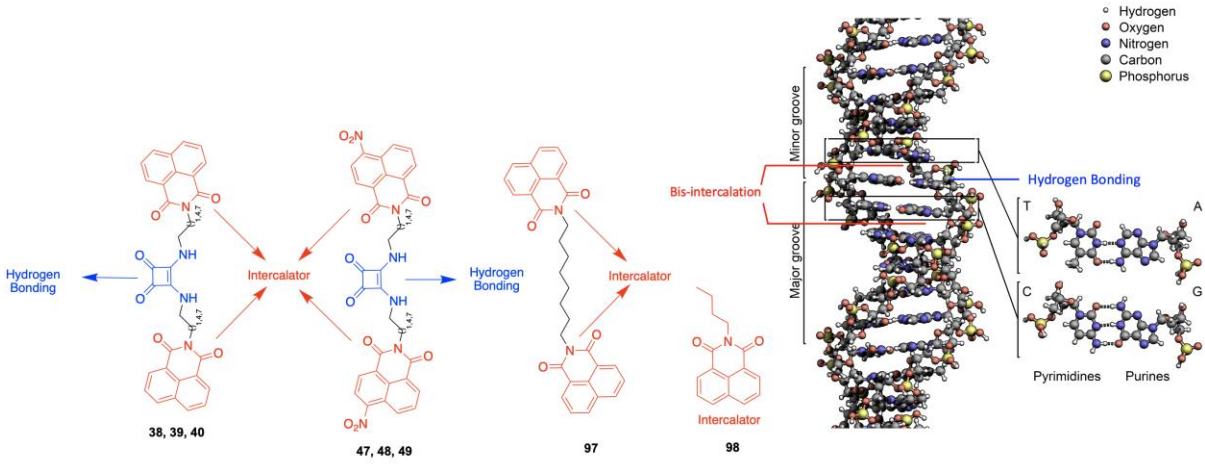

Figure 4.2: Rationale in the design of **38-40, 47-49, 97** and **98** as DNA binding agents, and schematic of methods of binding to DNA helix.

As a means of evaluating the DNA-binding affinity of **38-40, 47-49, 97** and **98**, the following methods were chosen. Firstly, UV-Vis and fluorescence titration studies were used to determine whether there was any interaction between these synthesised compounds and DNA. Taking advantage of the inherent photophysical properties of the 1,8-naphthalimide fluorophore, Ethidium Bromide displacement assays were also carried out in order to have a comparative method that should provide complimentary evidence of DNA binding, after both UV-Vis absorbance and fluorescence emission tests were performed.

4.2 UV-Vis DNA titrations

As shown in Chapter 3, the naphthalimide conjugates of **38-40, 47-49, 97** and **98** absorb in the 350-500 nm region of the electromagnetic spectrum. The nucleobases of DNA absorb at *cca.* 250-260 nm. Therefore, any changes in the absorbance spectra of these molecules upon interacting with DNA can be easily followed. The possible noncovalent binding interactions of the synthesised compound when binding to DNA include intercalation, groove-binding (major and minor) and H-bonding to the negatively charged backbone.

These changes could involve a shift in the wavelength of maximum absorbance (hypsochromic or bathochromic shifts) and most importantly a decrease in the absorption intensity (hypochromism). Any decrease of maximum absorbance after the introduction of DNA would indicate our target compounds binding with DNA.

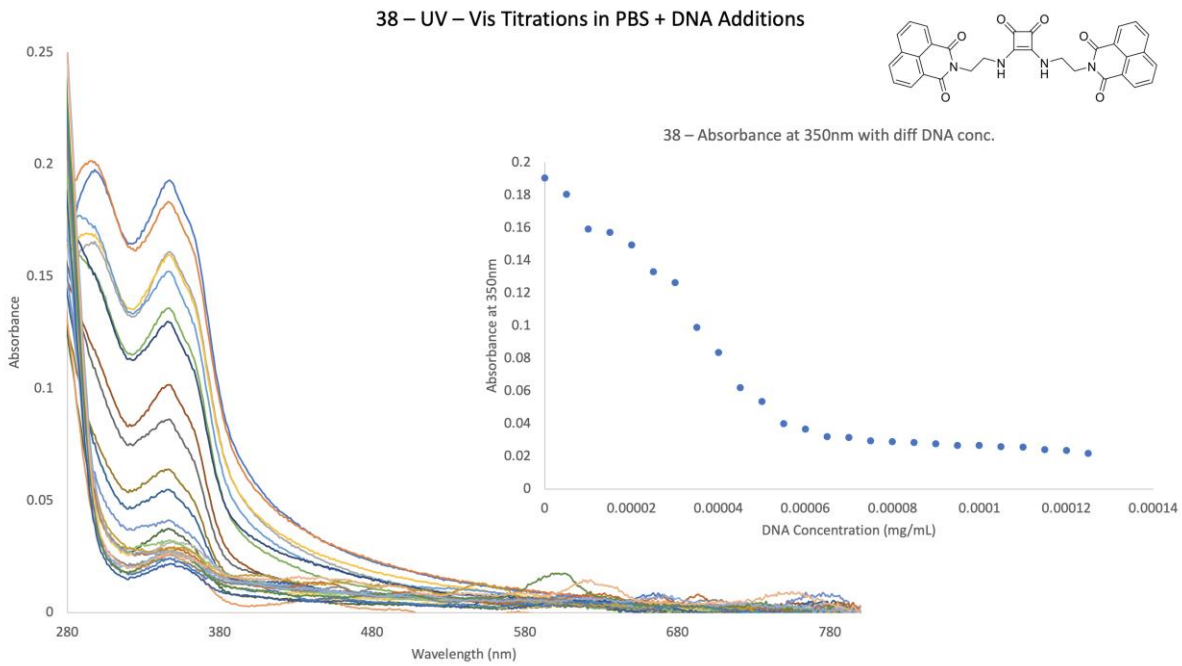

Figure 4.3: UV-Vis absorbance of **38**, with DNA concentration increases of (0.00005 mg/mL) for a total of 25 runs with DNA.

The UV-Vis absorbance of **38-40** was measured with different concentrations of DNA in PBS and it was evident that there was decrease of ~90% of UV absorbance of **38** (Figure 4.3) with increased DNA concentrations. This had corresponded to the possibility of **38** binding to DNA. Smaller decrease of ~40% in UV absorbance was observed for compound **39** and even a smaller decrease of ~25% in UV absorbance was observed for compound **40** with the same increased DNA concentrations (See Appendix). Control experiments have been done after 12 hours with each compound to observe different behaviour in binding to DNA and no change was observed. The control experiments could unfortunately not be done in PBS due to all compounds not being soluble in this solvent. This suggests that binding of **38, 39** and **40** with DNA was taking place.

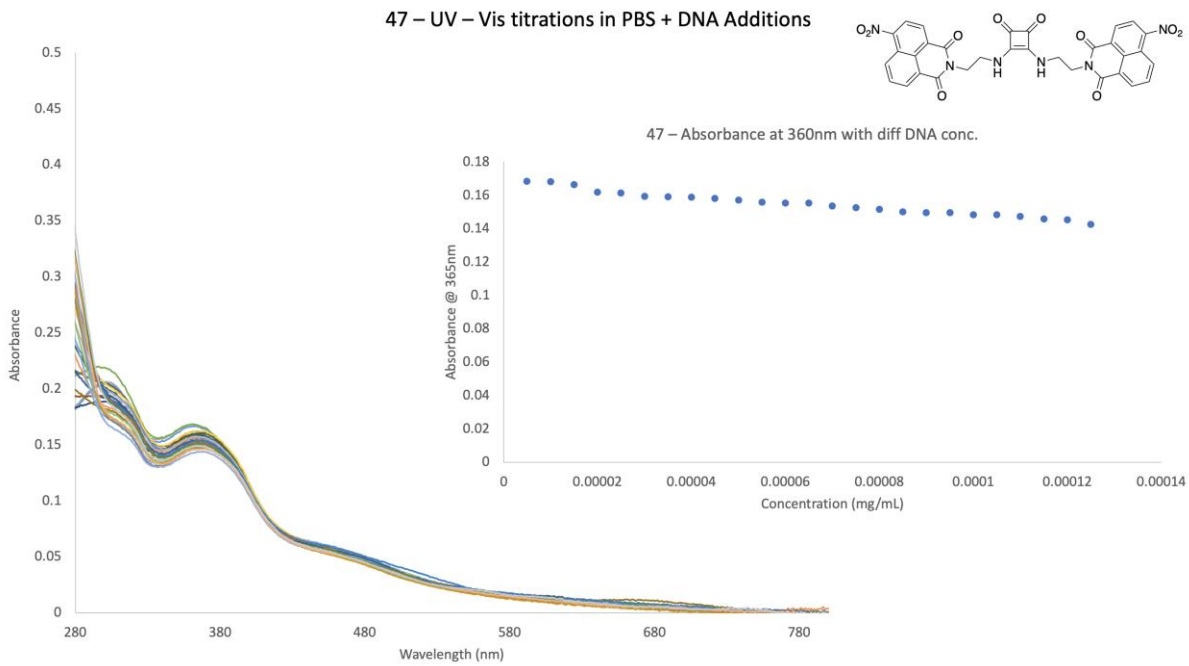

Figure 4.4: UV-Vis absorbance of **47**, with DNA concentration increases of (0.00005 mg/mL) for a total of 25 runs with DNA.

The UV-Vis absorbance of compounds **47-49** was measured with different concentrations of DNA in PBS and it was visible that there was a only a very small decrease in UV absorbance of **47** (Figure 4.4) with increased DNA concentrations. However, very small decreases in UV-Vis absorbance were also evident for compounds **48** and **49** with the same increased DNA concentrations (See Appendix). This indicates that limited binding to DNA was taking place.

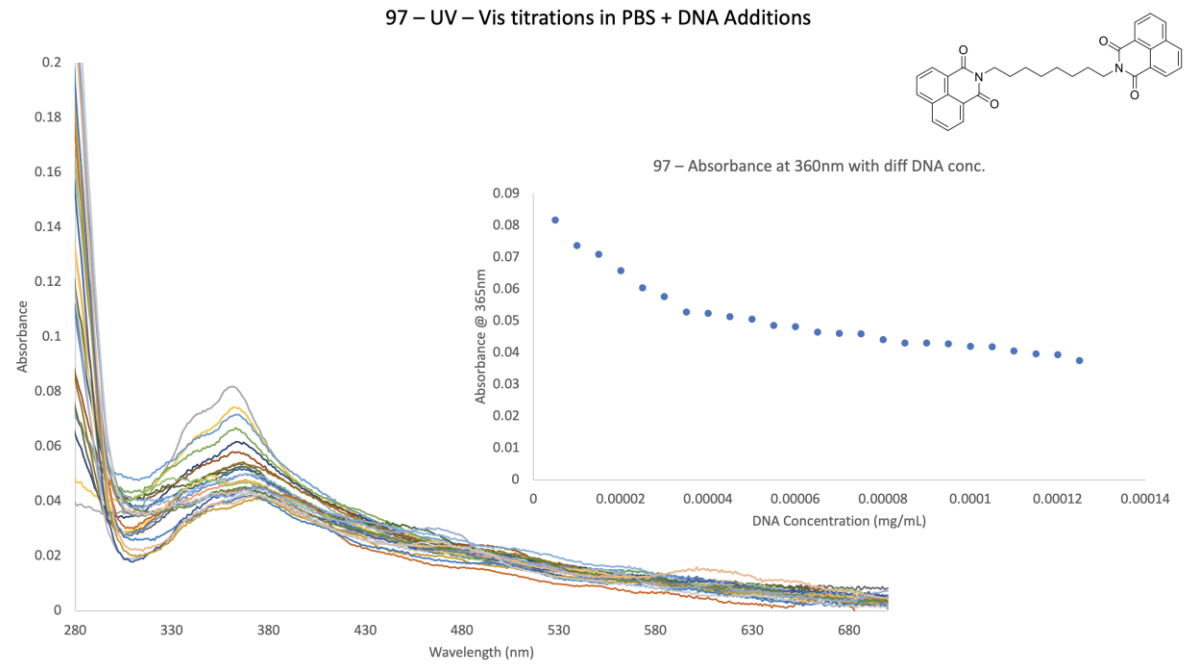

Figure 4.5: UV-Vis absorbance of **97**, with DNA concentration increases of (0.00005 mg/mL) for a total of 25 runs with DNA.

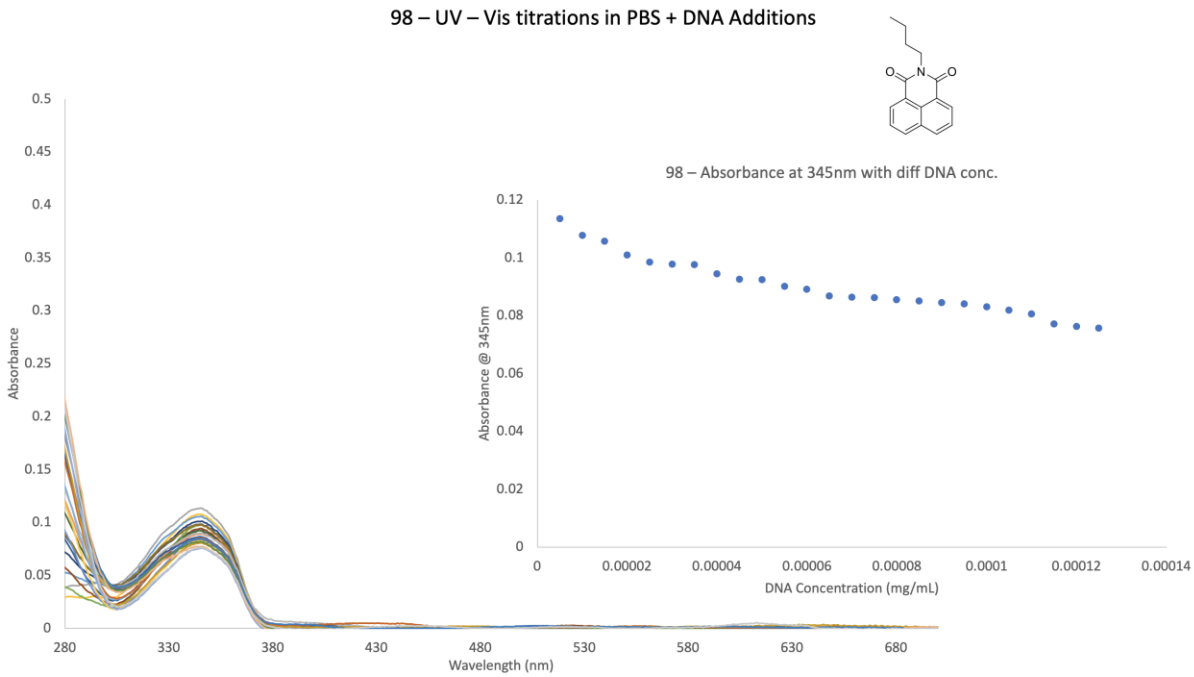

Figure 4.6: UV-Vis absorbance of **98**, with DNA concentration increases of (0.00005 mg/mL) for a total of 25 runs with DNA.

The UV-Vis absorbance had also slightly decreased for compounds **97** and **98** with increased DNA concentrations. Both compounds did not contain a squaramide moiety. This also indicated that weak DNA interaction was taking place for these compounds.

To further investigate, UV-Vis titration control experiments were also conducted, in which buffer was added instead of DNA. It was expected that no changes would occur in this case. However, due to the propensity of the molecules to self-assemble in solution, we wished to ensure that the observed changes were due to DNA binding and not self-assembly. However, this time PBS was added instead of DNA, where 0.5 μL equivalents of PBS were added into the solution each time, as the overall volume of the cuvette did not lead to dilution effects. Similarly the exact UV-Vis absorbance experiments were again conducted for **39** and **40**.

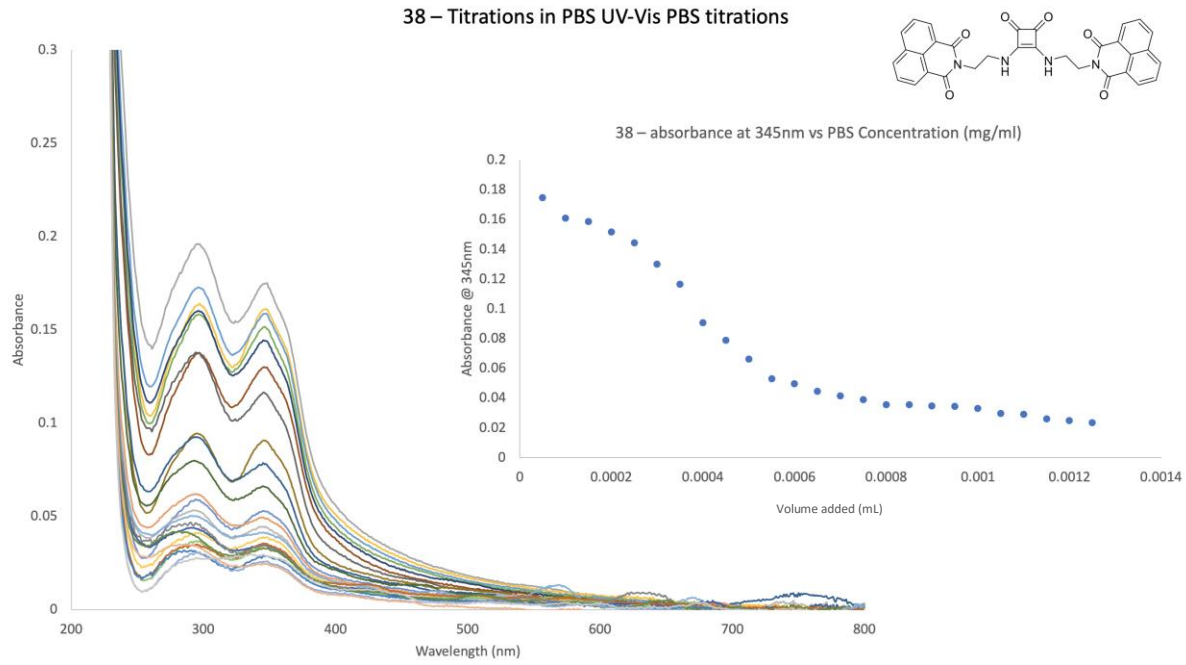

Figure 4.7: UV-Vis absorbance of **38**, with PBS equivalents of DNA concentration increases of (0.00005 mL) for a total of 25 runs with PBS.

Unfortunately, as can be seen with Figure 4.7, the absorbance spectrum of compound **38** tend to decrease and with the addition of PBS and the absence of DNA. The results have mirrored mostly the results of the same experiment conducted with DNA addition (Figure 4.3). The UV absorbance had also identically decreased with the equivalent PBS instead of DNA and mirrored the DNA equivalent addition. These results suggest that the observed changes may not be due DNA binding but to self-assembly or a combination of both. Thus these experiments are unlikely to give reliable DNA binding information for compounds **38, 39** and **40**.

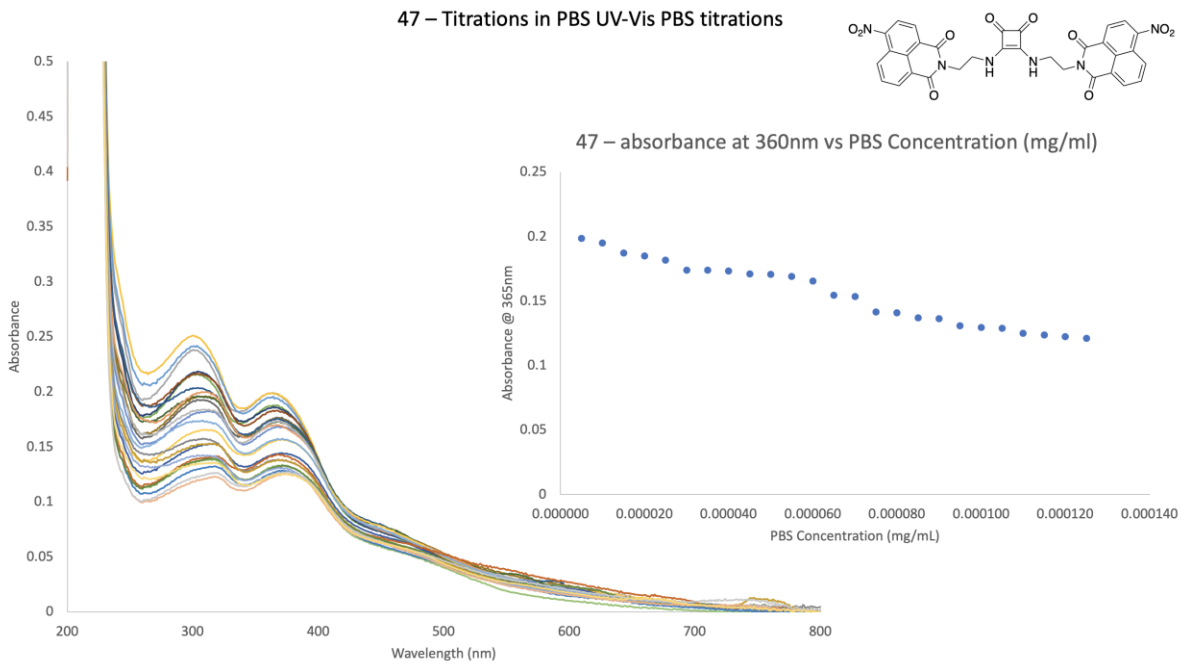

Figure 4.8: UV-Vis absorbance of **47**, with PBS equivalents of DNA concentration increases of (0.00005 mL) for a total of 25 runs with PBS.

The absorbance spectrum of compound **47 (**Figure 4.8) had decreased only slightly and underwent significant hypochromism with the addition of PBS and the absence of DNA. The results have mirrored mostly the results of the same experiment conducted with DNA addition (Figure 4.4). The UV absorbance had also identically decreased with the equivalent PBS instead of DNA and mirrored the DNA equivalent addition, which indicated that very limited DNA binding was taking place for compounds **38, 39** and **40**.

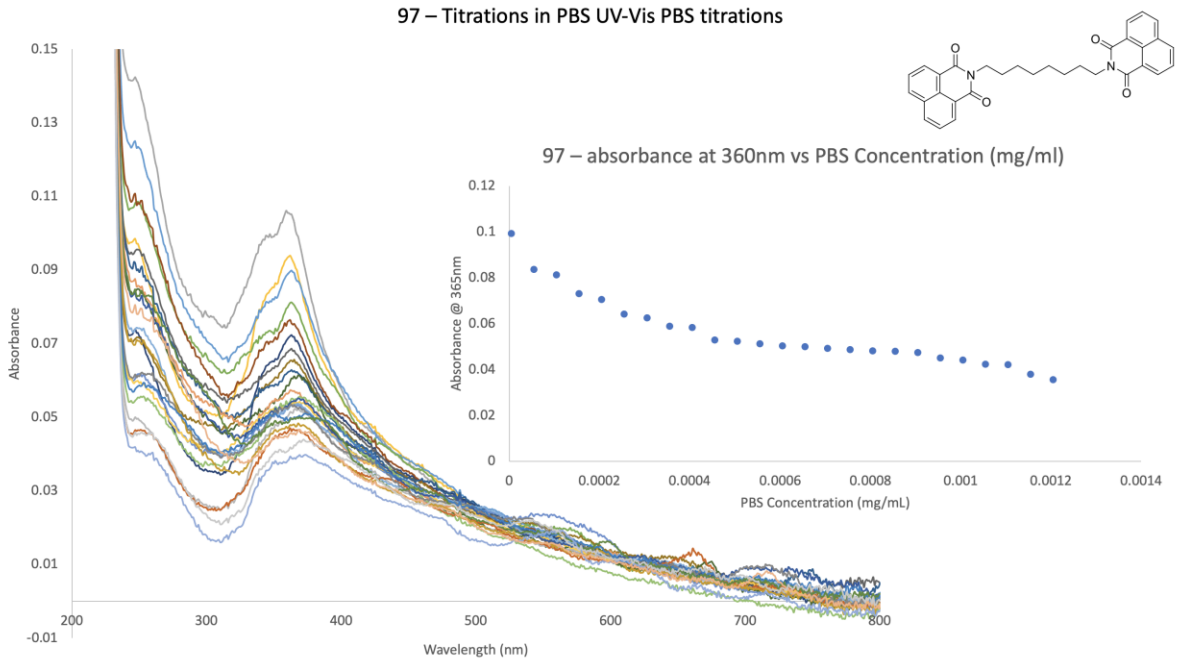

Figure 4.9: UV-Vis absorbance of **97**, with PBS equivalents of DNA concentration increases of (0.00005 mL) for a total of 25 runs with PBS.

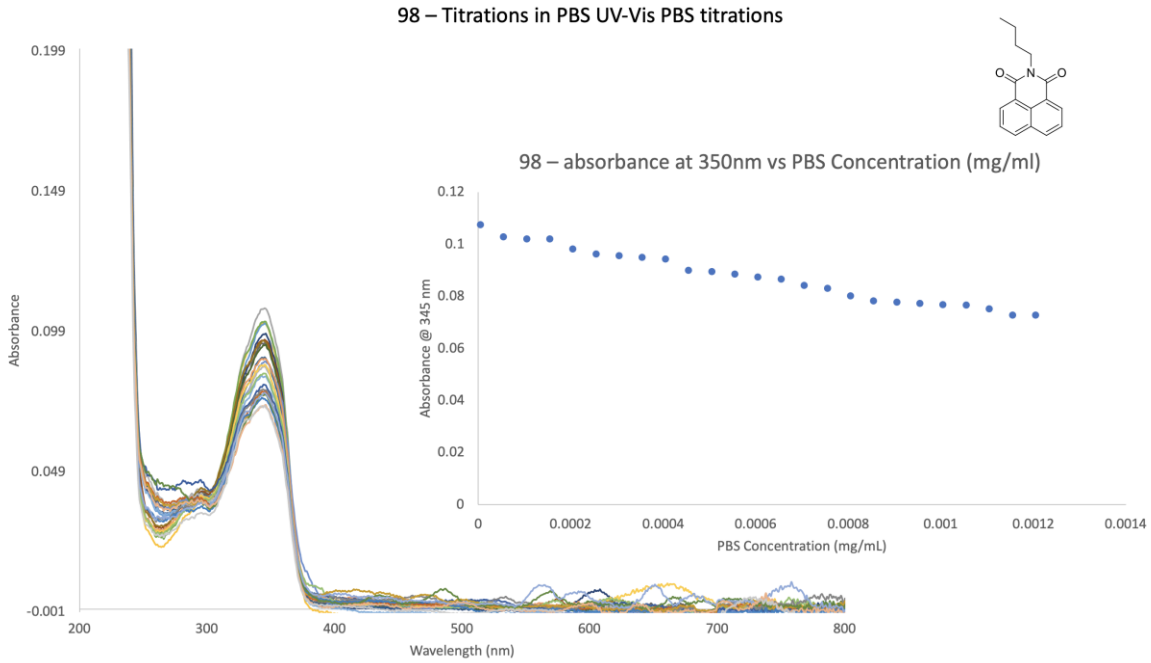

Figure 4.10: UV-Vis absorbance of **98**, with PBS equivalents of DNA concentration increases of (0.00005 mL) for a total of 25 runs with PBS.

Similar results were also observed for compounds **39** and **40**, where the DNA titration experiments, and PBS control experiments did not differ (See Appendix). The DNA UV-Vis titration studies in which DNA concentration was increased in the presence of **38-40** were conducted. The dramatic decrease in UV-Vis absorbance at *cca.* 350 nm, in response to DNA concentration increase. Interestingly, a trend appeared to show the greatest decrease of compound **38**, with the smallest changes occurring in compound **40** (see figure 4.3 and Appendix). This indicates, that although DNA was introduced into the compound in PBS, the drop in UV-Vis absorbance exactly mirrored the drop in UV-Vis absorbance when PBS equivalent was introduced in the test. Almost identical decreases of UV-Vis absorbance for compounds **39** and **40** were also observed with both DNA additions and PBS equivalent additions. For compounds **97** and **98,** a drop in UV absorbance had also very closely resembled the DNA additions when PBS equivalents were added. These results suggested that the data from UV-Vis titrations may not be reliable in probing DNA binding ability and as such further investigation was required. In the next section, the fluorescence emission titrations will be discussed in which DNA concentration was increased in the presence of **38-40, 97** and **98**.

4.3 Fluorescence emission studies in presence of DNA

The emission spectra of **38-40, 47-49, 97** and **98** (10 µM, 10 mM phosphate buffer, pH 7.4) were taken in the absence and presence of DNA (P/D = 0-25) upon excitation at 350 nm. The fluorescence emission studies were carried out to observe whether the synthesised compounds bound to DNA upon introduction. In contrast to the UV-Vis absorbance drop after the introduction of both DNA and PBS equivalents, it was expected that the fluorescence intensity of the synthesised compounds would undergo an increase in intensity, also indicating the process of intercalation taking place of the naphthalimide moieties of the synthesised compounds. Compounds **47-49** showed no fluorescence with and without the presence of DNA due to its electron withdrawing group being present on the naphthalimide moiety thus this method was not used for these compounds.

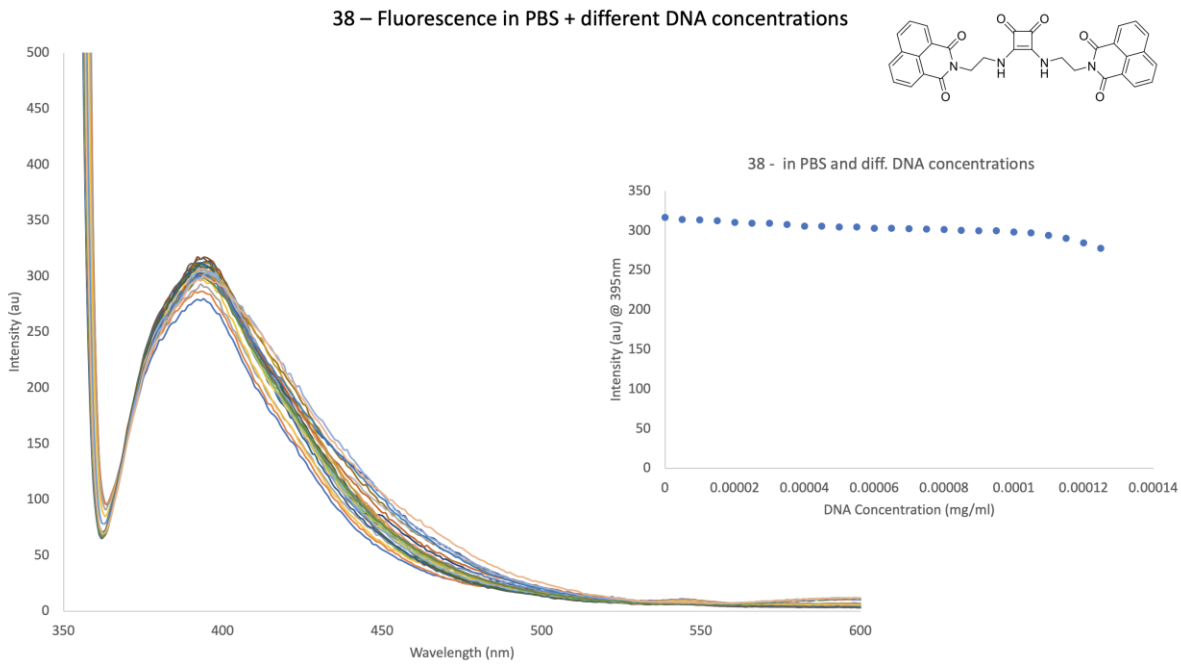

Figure 4.11: Fluorescence intensity of **38**, with an excitation wavelength at 400 nm, with an increased DNA concentration of (0.00005 mL) for a total of 25 runs in PBS.

The fluorescence emission spectrum of compound **38** (Figure 4.11) had decreased only slightly with the addition of identical DNA concentration used in the UV absorbance tests. The results for **39** and **40** had also shown this decrease, indicating minimal DNA binding (See Appendix).

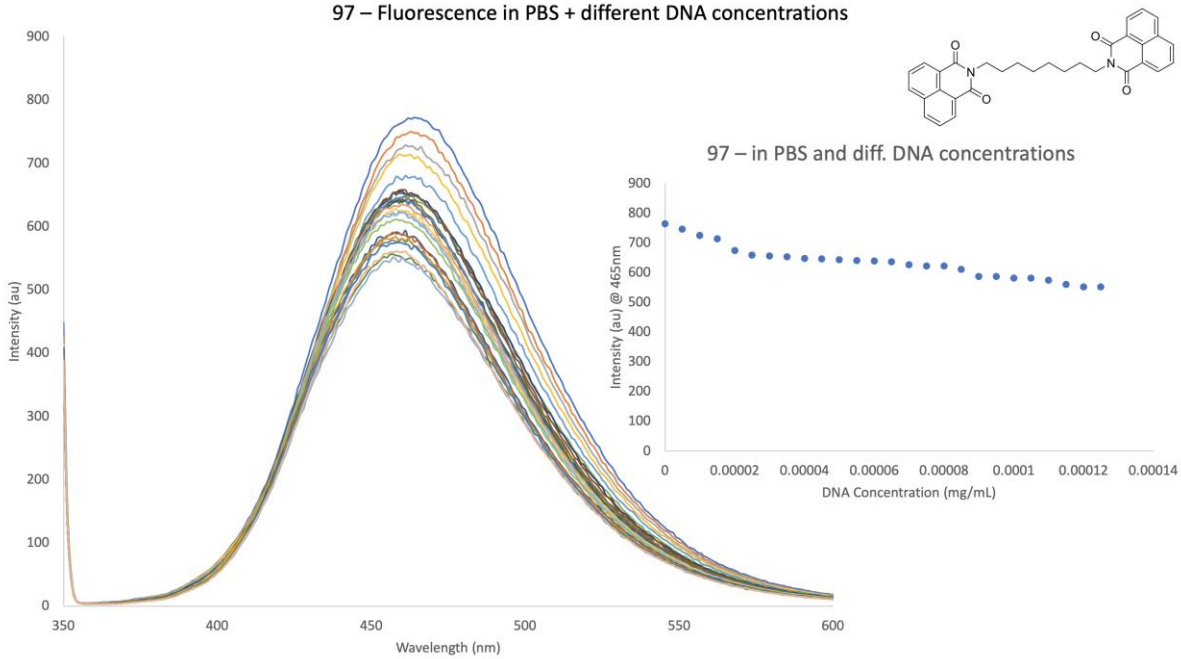

Figure 4.12: Fluorescence intensity of **97**, with an excitation wavelength at 460 nm, with an increased DNA concentration of (0.00005 mL) for a total of 25 runs in PBS.

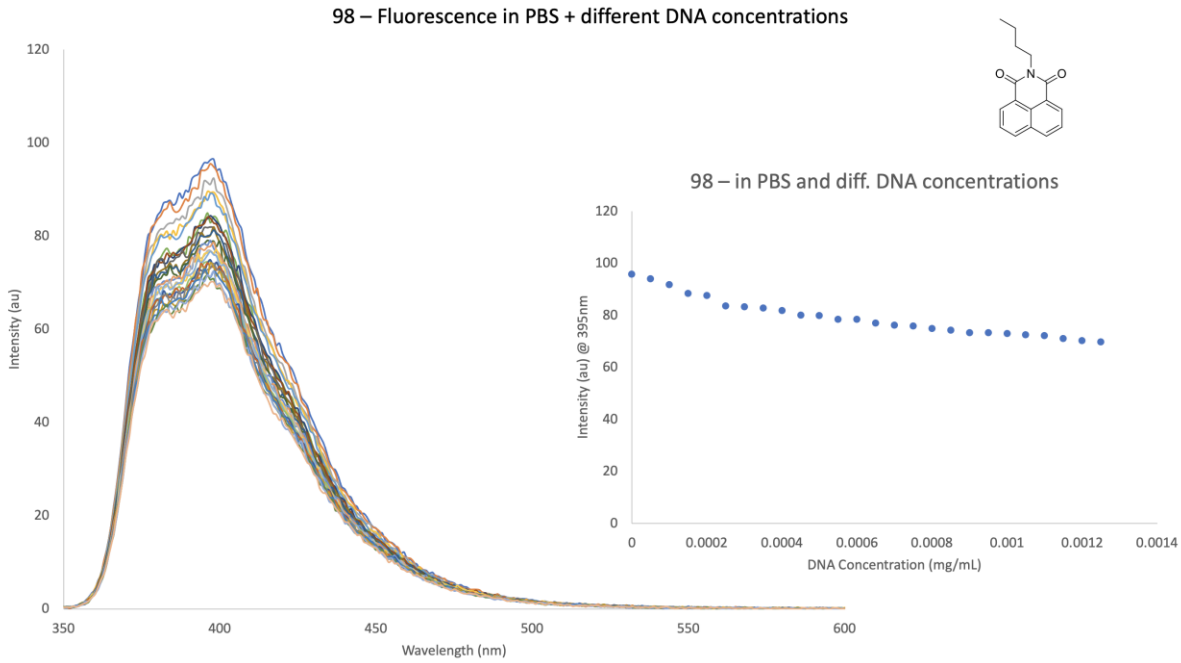

Figure 4.13: Fluorescence intensity of **98**, with an excitation wavelength at 450 nm, with an increased DNA concentration of (0.00005 mL) for a total of 25 runs in PBS.

The fluorescence emission spectrum of control compounds **97** (Figure 4.12) and **98** (Figure 4.13) had a much more significant decrease in fluorescence emission with the addition of identical DNA concentration used in the UV absorbance tests; a clear indication that DNA binding may be occurring for these compounds. Further control experiments were conducted, where again the PBS equivalents of DNA concentrations were added and the fluorescence emission of compounds **38-40**, **47-49**, **97** and **98** was measured.

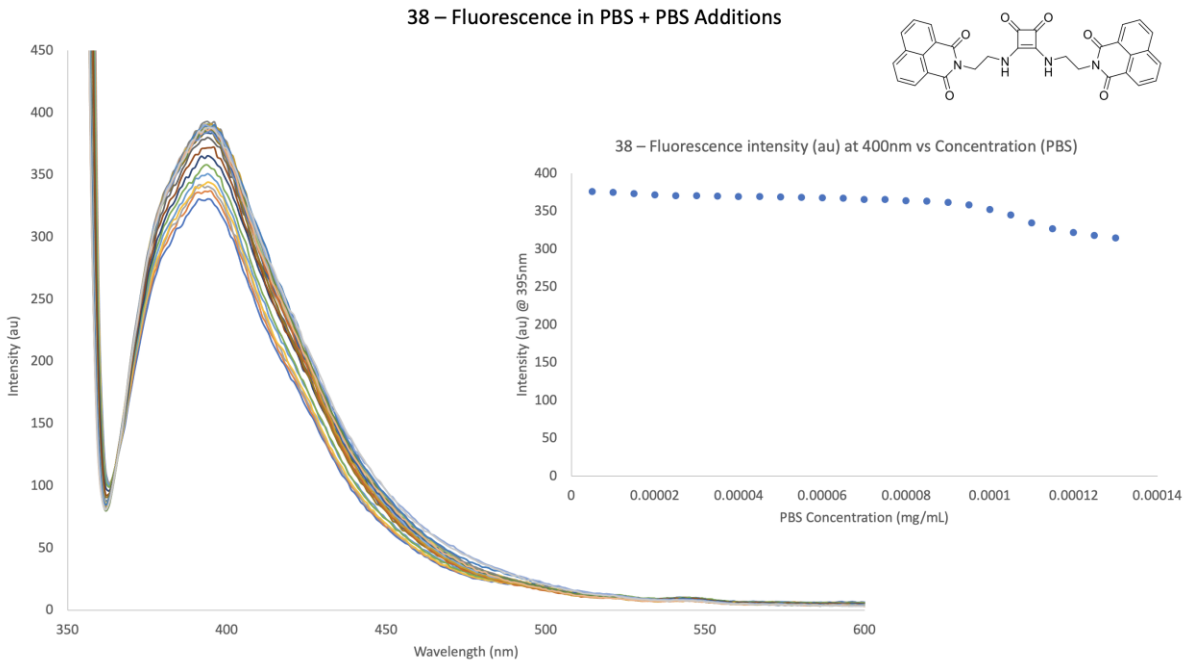

Figure 4.14: Fluorescence intensity of **38** with an excitation wavelength at 400 nm, with PBS equivalents of DNA concentration increases of (0.00005 mL) for a total of 25 runs with PBS.

Unfortunately, as can be seen with Figure 4.14, the emission spectrum of compound **38** was shown to decrease with the addition of PBS and the absence of DNA. The results have mirrored mostly the results of the same experiment conducted with DNA addition (Figure 4.11). The UV absorbance had also identically decreased with the equivalent PBS instead of DNA and mirrored the DNA equivalent addition, which indicated that very limited DNA binding was taking place for compounds **38, 39** and **40**.

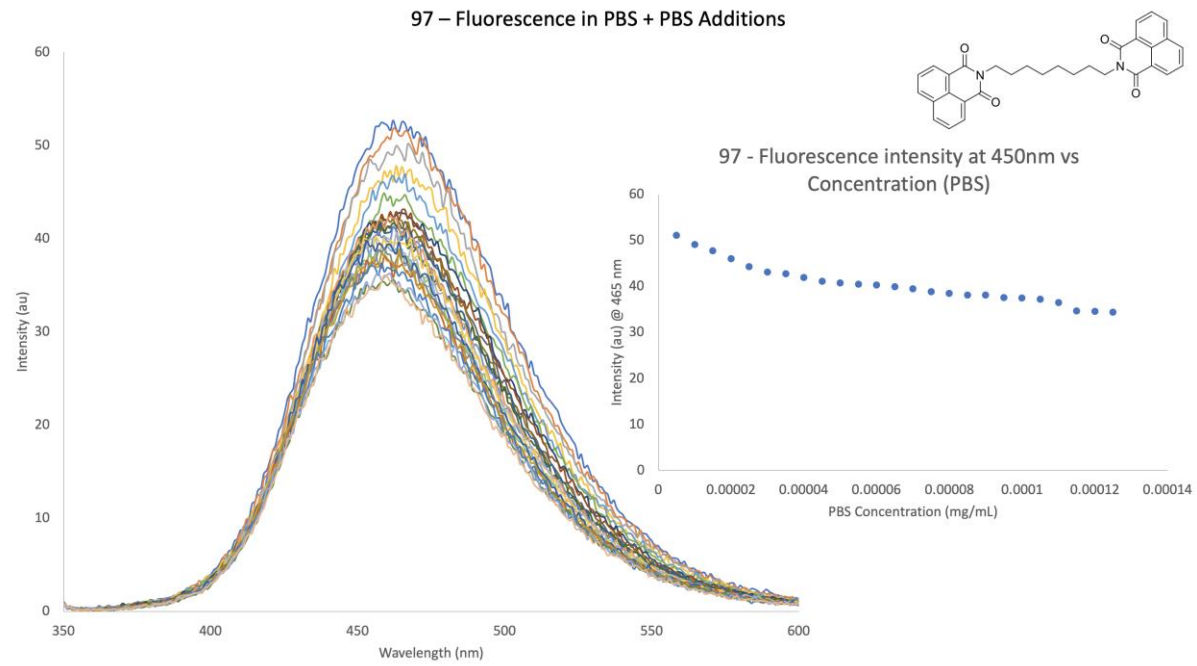

Figure 4.15: Fluorescence intensity of **97** with an excitation wavelength at 450 nm, with PBS equivalents of DNA concentration increases of (0.00005 mL) for a total of 25 runs with PBS.

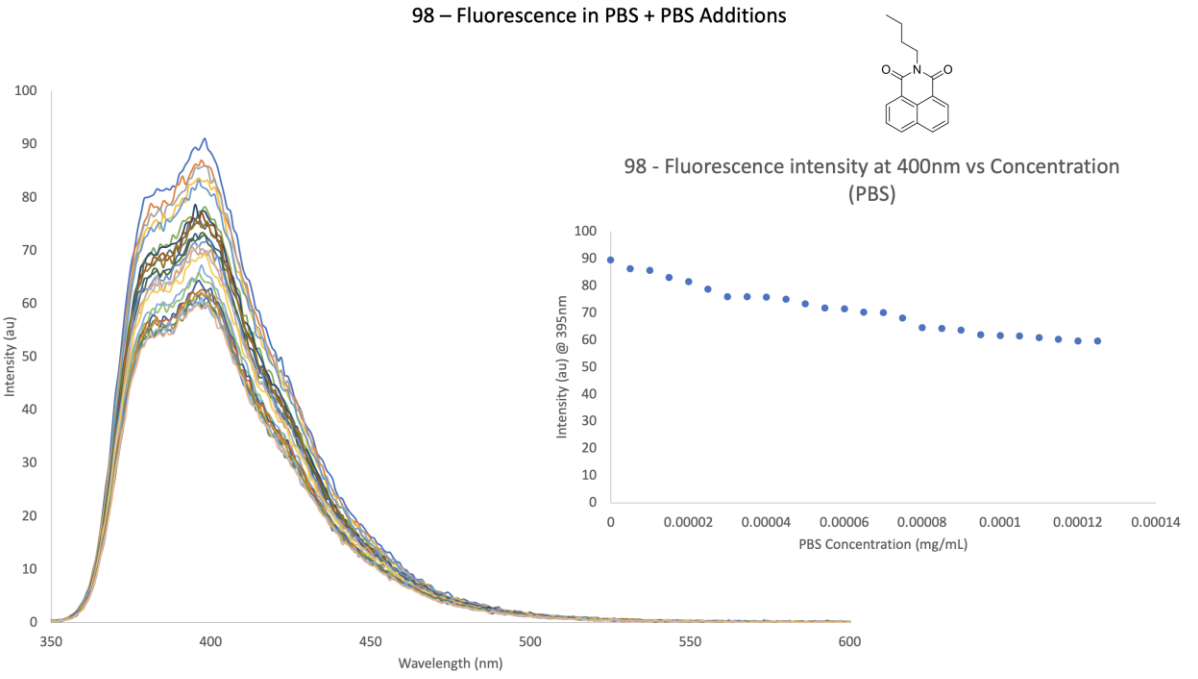

Figure 4.16: Fluorescence intensity of **98**, with an excitation wavelength at 400 nm with PBS equivalents of DNA concentration increases of (0.00005 mL) for a total of 25 runs with PBS.

Both **97** and **98** had displayed a more significant drop of fluorescence compared to **38**, **39** and **40**. However, the decrease in fluorescence for PBS equivalent increase was identical to the DNA concentration increase. This had indicated that these tests were not sufficient enough to note any binding to DNA. It was therefore concluded that Ethidium Bromide displacement measurements should be conducted as an alternative method to measure DNA binding.

The emission spectra of **38** (10 µM, 10 mM phosphate buffer, pH 7.4) in the absence and presence of DNA were shown in Figure 4.19 and Figure 4.24 respectively. When **38-40, 97** and **98** were excited at 345 nm and upon the titration with DNA, the emission spectra displayed almost an identical decrease in both fluorescence intensity and UV absorbance for PBS equivalents in all compounds tested. Taken together the results of these experiments are largely inconclusive, where the observed changes may be a result of either DNA binding or self-assembly or a combination of both processes occurring in solution. The decrease of fluorescence intensity with and without DNA introduction for all synthesised compounds was not greater than 30% in all cases and this may indicate that even if DNA binding is occurring, it is not happening to a large extent.

4.4 Displacement Assays using Ethidium Bromide

In a final attempt to determine reliably whether DNA binding was occurring or not, we decided to conduct Ethidium Bromide displacement assays (Figure 4.17).[288] This method was first introduced by LePecq and Paoletti[289] and is commonly used to evaluate the efficiency of both intercalative and non-intercalative drugs.[290, 291] Ethidium Bromide assays do not rely on the photophysical properties of the naphthalimides, but instead on the inherent fluorescence changes observed for ethidium bromide upon displacement from DNA.[292] Ethidium Bromide is known to be strongly emissive when bound to DNA. The changes in the emission of Ethidium Bromide due to the synthesised intercalator displacing Ethidium Bromide in DNA can be monitored to obtain the C_{50} value. 50% reduction of DNA bound Ethidium Bromide fluorescence intensity, is described by the C_{50} value.[47] DMSO was chosen as the solvent for these tests, as it was the only solvent in which all synthesised compounds did not precipitate out of solution, where it is a standard used solvent for compounds that precipitate in PBS.

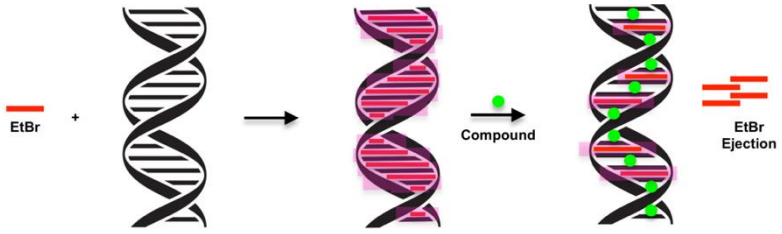

Figure 4.17: Ethidium Bromide Displacement Assay schematic.

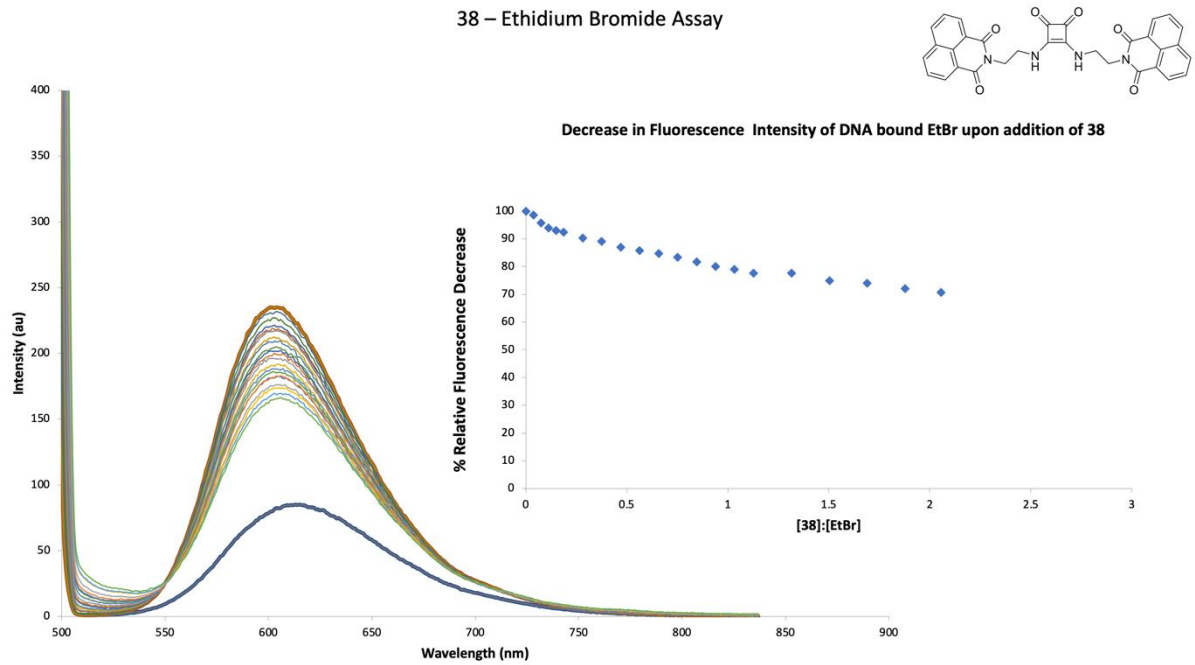

Figure 4.18: Ethidium Bromide displacement of various concentration of **38**, in DMSO with DNA, where the blue trace indicates the EtBr and DMSO solution without DNA and **38** with excitation at 445 nm.

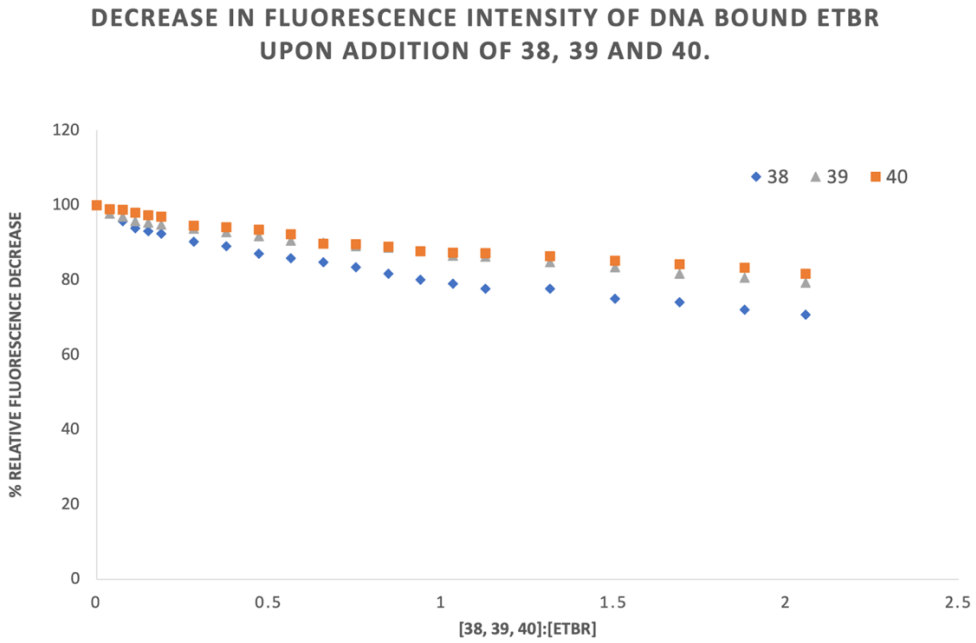

Figure 4.19: Ethidium Bromide displacement assays of various concentrations of **38, 39** and **40**, in DMSO with DNA.

The Ethidium Bromide Displacement Assays of **38** (Figure 4.18), **39** and **40** (See Appendix) have all displayed a decrease in fluorescence. **38** had displayed the most significant fluorescence decrease percentage, compared to compounds **39** and **40** (Figure 4.19). However, the relative fluorescence decrease for **38-40** was not significant, which highlights the weak DNA binding affinity (See Appendix).

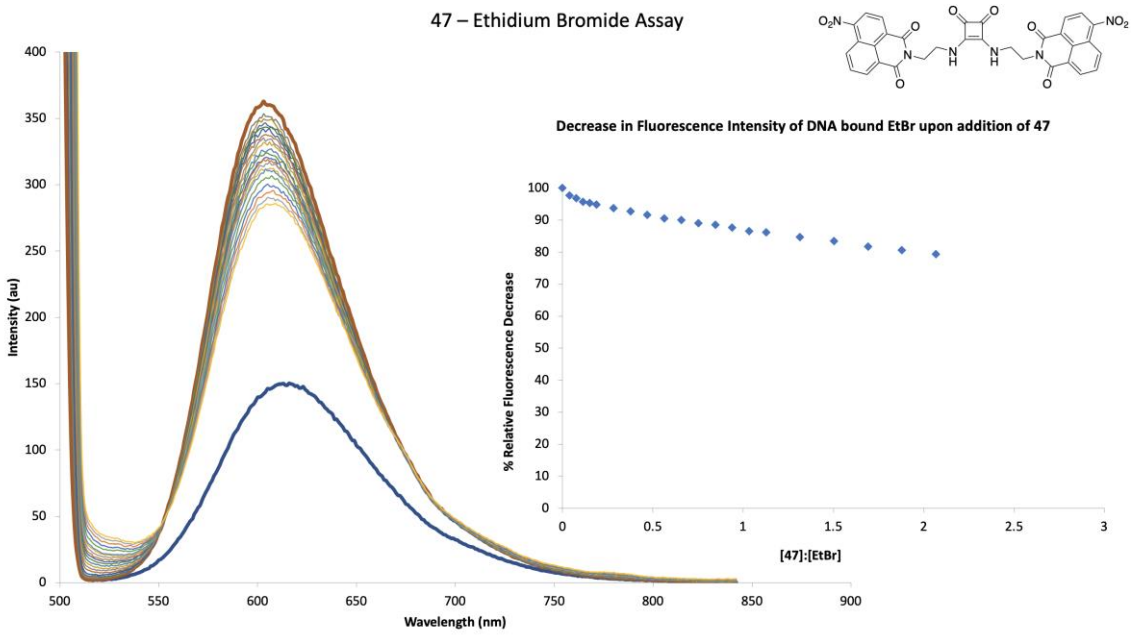

Figure 4.20: Ethidium Bromide displacement of various concentration of **47**, in DMSO with DNA, where the blue trace indicates the EtBr and DMSO solution without DNA and **47** with excitation at 445 nm**.**

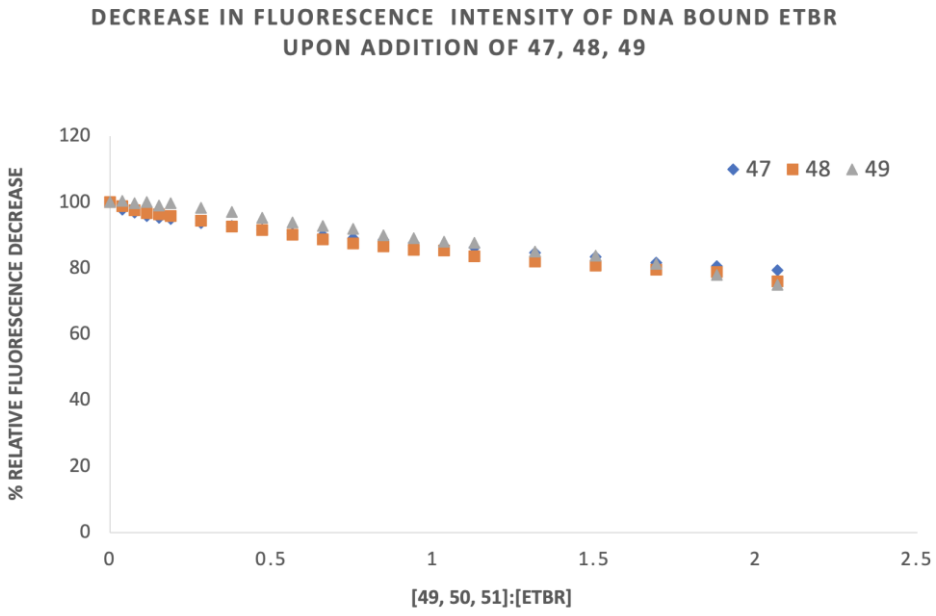

Figure 4.21: Ethidium Bromide displacement assays of various concentrations of **47, 48** and **49**, in DMSO with DNA.

The Ethidium Bromide Displacement Assays of **47** (Figure 4.20), **48** and **49** (See Appendix) have all displayed a small decrease in fluorescence. **47-49** had all displayed almost identical decrease in the relative fluorescence decrease percentage (Figure 4.21). This had also highlighted the weak DNA binding affinity of these compounds.

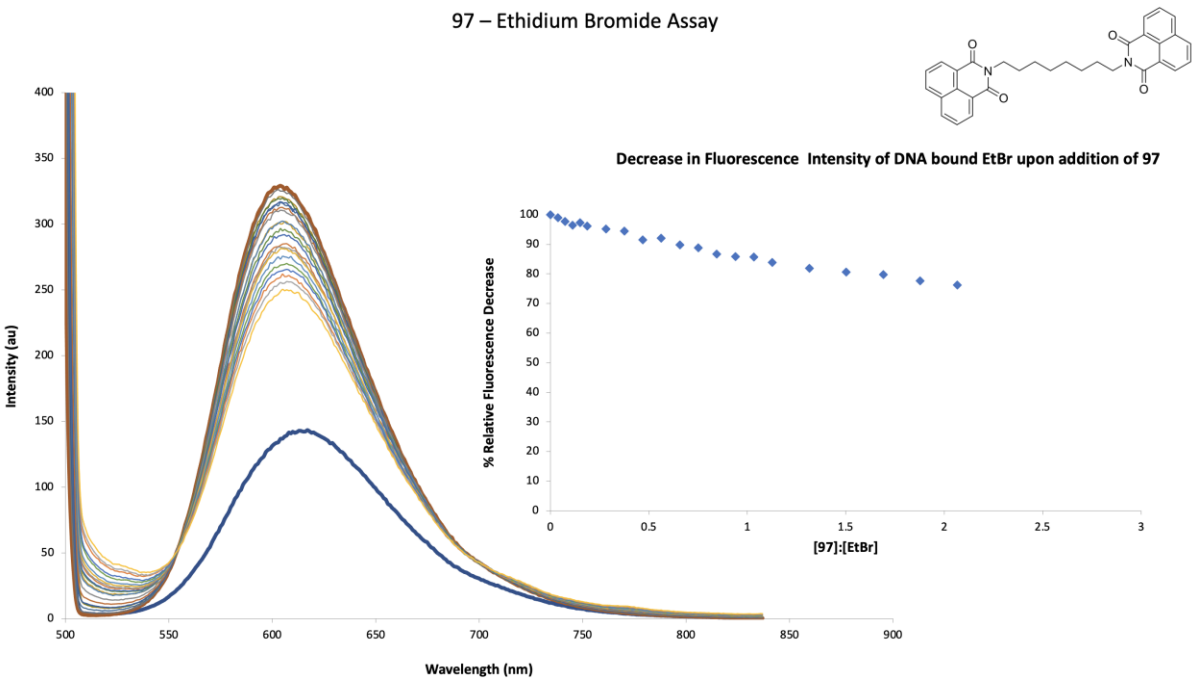

Figure 4.22: Ethidium Bromide displacement of various concentration of **97**, in DMSO with DNA, where the blue trace indicates the EtBr and DMSO solution without DNA and **97**, with excitation at 445 nm.

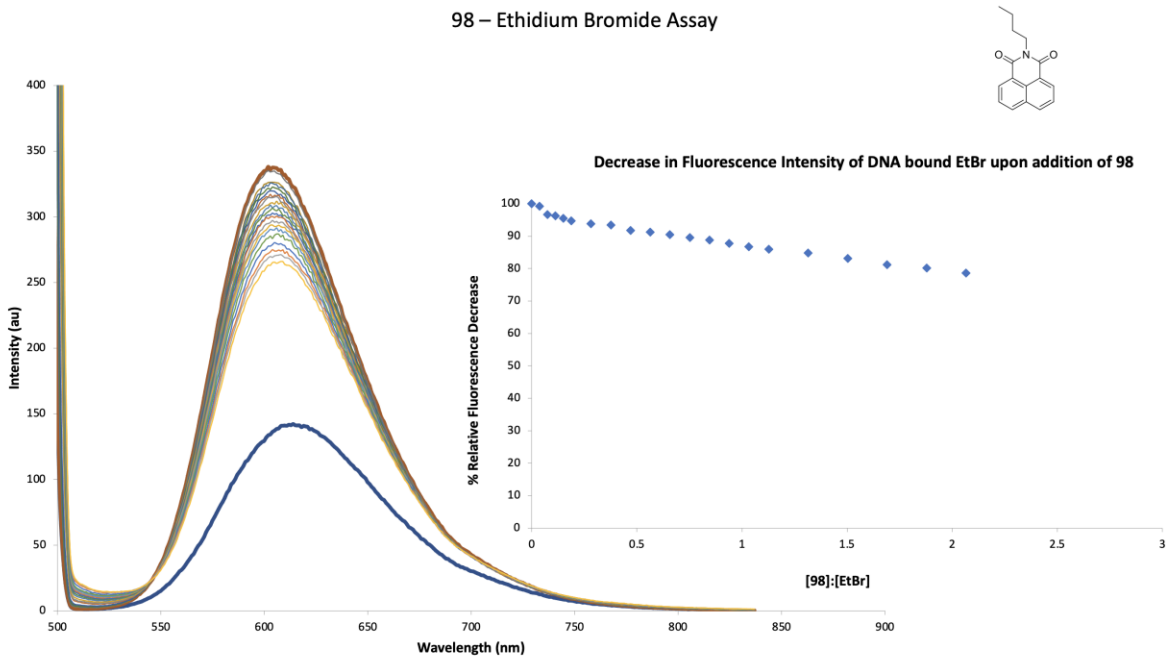

Figure 4.23: Ethidium Bromide displacement of various concentration of **98**, in DMSO with DNA, where the blue trace indicates the EtBr and DMSO solution without DNA and **98**, with excitation at 445 nm.

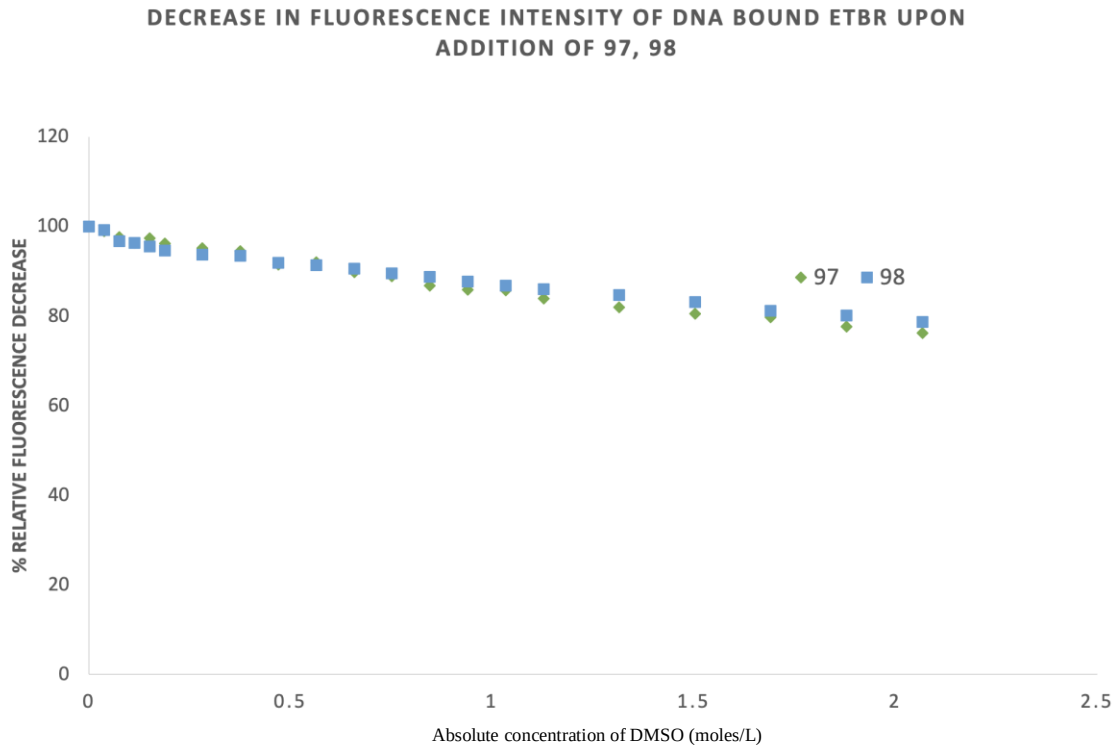

Figure 4.24: Ethidium Bromide displacement assays of various concentrations of **97** and **98** in DMSO with DNA.

Model compounds **97** (Figure 4.22) and **98** (Figure 4.23) have also displayed a small decrease in fluorescence. Both **97** and **98** had displayed almost identical decrease in the relative fluorescence decrease percentage (Figure 4.24), which also demonstrated the weak DNA binding affinity of the model compounds. It was therefore decided that a control experiment will be undertaken where the same volumes of pure DMSO were added, without any naphthalimide compound dissolved. Unfortunately, when the DMSO control experiment was conducted, the relative fluorescence decrease was much more significant. This had proven that the synthesised compounds **38-40**, **47-49**, **97** and **98** had very limited DNA binding affinity and no firm conclusion could be drawn. It may be concluded that the use of DMSO may have affected the results. However, due to being unable to dissolve the compounds tested in PBS, the method utilised by Boger *et al.*, had to be used in order to run the EtBr assays in pure DMSO due to DMSO being the only suitable solvent from which these compounds have not precipitated out.[290]

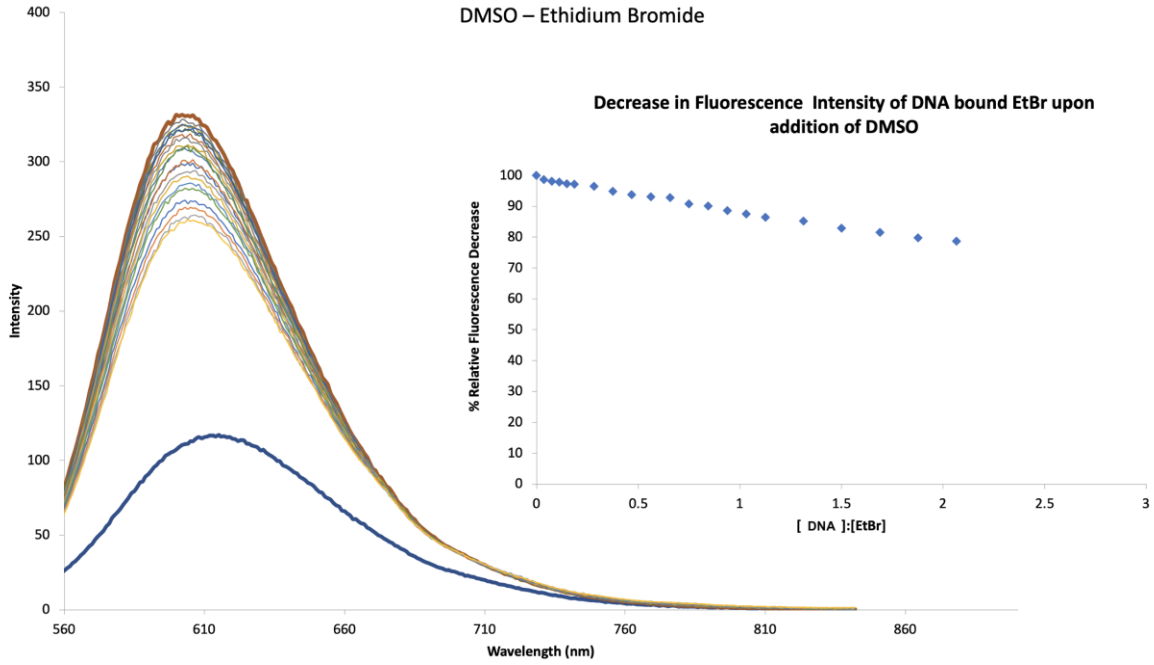

Figure 4.25: Ethidium Bromide displacement of various concentration of DMSO with DNA, where the blue trace indicates the EtBr and DMSO solution without DNA, with excitation at 445 nm.

We conducted Ethidium Bromide Assays, but unfortunately the results were inconclusive and couldn't conclusively tell us whether these compounds are capable of binding to DNA. In both cases, when control experiments were conducted, the results mirrored closely the results seen when DNA was added and at this point no firm conclusion can be drawn on whether these companies are capable of binding to DNA.

The results from the Ethidium Bromide displacement assays with DNA had indicated a decrease in fluorescence emission for compounds **38-40, 47-49, 97** and **98** in DMSO, indicating the process of DNA interaction. However, when the exact same study was performed as a DMSO dilution equivalent, the decrease in fluorescence was even more significant. This corresponds to the compounds having very little affinity for DNA binding, as they are undergoing the process of self-assembly. It was therefore concluded that the synthesised compounds predominantly undergo the process of self-assembly over DNA binding, as indicated by the studies performed.

Examples of other techniques include DNA Melts, Viscometry, Circular Dichroism and various other experiments. However, these experiments were not undertaken due to restrictions enforced by COVID-19. These experiments will be conducted by members of the Elmes lab in due course.

Chapter 5 Summary and Conclusion

The work carried out in this research project had the overall goal of synthesising a family of squaramide containing bis-naphthalimides and investigating their self-assembly and DNA binding properties.

Chapter 1 gave an introduction to the field of DNA binding molecules and outlined the rationale for our compound design.

Chapter 2 detailed the synthesis and attempted synthesis of several families of squaramide bis-naphthalimide conjugates and outlined the various challenges encountered in synthesis. Solubility issues, reduced reactivity, difficulties with isolation and purification hampered advances in synthesis and several different approaches were outlined in this chapter. However, 8 final compounds were successfully isolated and characterised. These compounds included the unsubstituted squaramide containing bis-naphthalimides **38-40**, 4-nitro containing bis-naphthalimides **47-49**, a bis-naphthalimide without a squaramide moiety **97** and a mono-naphthalimide **98**.

In Chapter 3, the potential self-assembly properties of **38-40**, **47-49**, **97** and **98** were examined and discussed in detail using VT-NMR and a range of spectroscopic techniques. High temperature NMR displayed improved resolution of all ^{1}H NMR signals and suggested that a significant amount of self-assembly behaviour is likely for these compounds. The UV-Vis absorbance and fluorescence emission time studies also displayed dramatic decreases of UV-Vis absorbance over time, particularly compounds containing a squaramide moiety. Extinction coefficient studies were also performed and showed that these compounds all obey the Beer Lambert Law, where their absorbance is proportional to their concentration in solution. Scanning Electron Microscopy tests have also been undertaken for compounds both in DMSO and DMSO:water (50:50) solution. All compounds containing a squaramide moiety had formed films in both solutions, while the compounds without a squaramide moiety had formed fibrillar networks. These results had strongly indicated the process of self-assembly taking place in the squaramide containing bis-naphthalimides.

In Chapter 4, all compounds were examined for their DNA binding ability using a range of spectroscopic techniques. These techniques included UV-Vis absorbance and fluorescence emission titrations with DNA where initially it was concluded that DNA binding was giving

rise to hypochromism in the absorbance spectrum. However, after conducting control experiments, it became clear that these changes were inconclusive and may be a result of self-assembly. Ethidium Bromide assays were also carried out for all synthesised compounds. Again, the assays were inconclusive as control experiments were conducted, it was not possible to discern with certainty whether DNA binding was occurring. It was evident that self-assembly was a predominant feature of these novel compounds and may be preventing DNA binding to any meaningful extent. Further techniques are required in this context and may shed light on whether or not these molecules are useful as DNA binders.

The future work to continue this project should examine these compounds with previously mentioned DNA binding techniques, where the possibility of DNA binding could be more easily distinguished from the self-assembly properties. Improving the synthesis and compound design to result in a much stronger DNA binding ability could also be explored.

Improving compound design of the desired products could involve the incorporation of urea-based bis-naphthalimides, where the urea moiety would also bind to DNA phosphate backbone through H-bonding due to its strong H-bonding ability. Different linker units in synthesising the desired compounds could be substituted, such as ethylene glycol linkers instead of the alkyl linkers used, as alkyl linkers are insoluble in water. Ethylene glycols would likely increase the water solubility of the target compounds. Changing the DNA binding moiety of the target compounds could also aid an improved DNA binding ability. Incorporating pyrene into the target structure instead of a naphthalimide moiety would improve the DNA binding ability, as it is known to be a strong intercalator. Anthracene could also be used as a substitute for the naphthalimide moiety, as it is also a strong intercalator and additionally could be examined through other biological tests, as it has strong antibacterial activity against both Gram-positive and Gram-negative bacteria. Additionally, acridine derivatives could also replace naphthalimides in the design of the desired compounds, due to the derivatives of acridine having both strong DNA intercalating ability, gram positive and also gram negative antibacterial ability. For the proposed compound structures, see Figure 5.1.

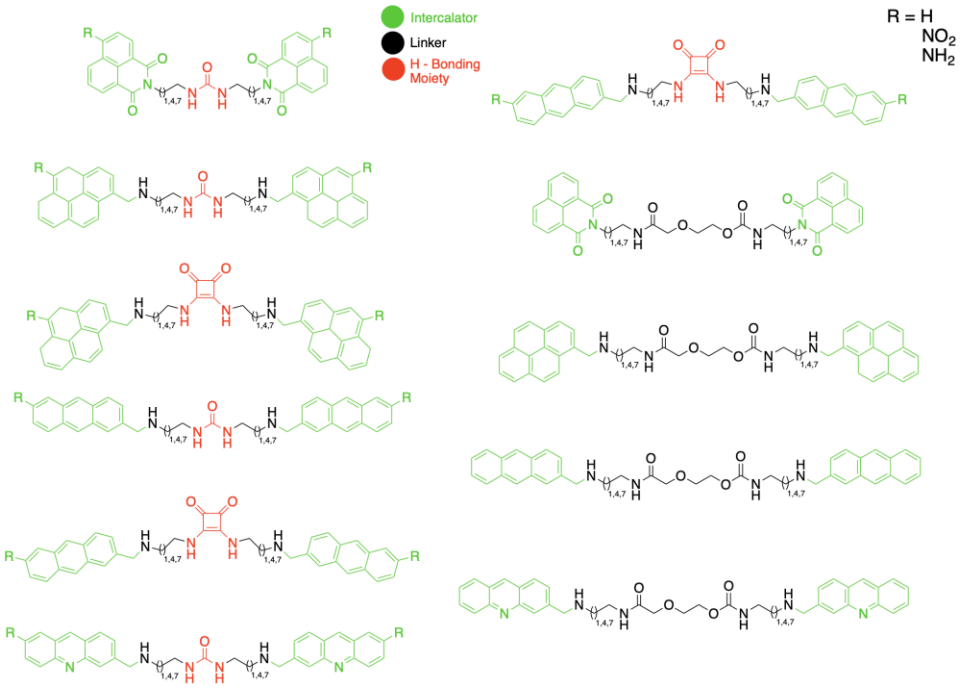

Figure 5.1: Novel bis-intercalator derivatives in the future.

Chapter 6 Experimental

6.1 General remarks

^{1}H NMR spectra were recorded using a Bruker Avance III 500 at a frequency of 500.13 MHz, and chemical shifts (δ) are reported in parts per million (ppm) with either DMSO-d_6 δ_H 2.50 ppm) or $CDCl_3$ (δ_H 7.26 ppm) as an internal reference. The data are reported as chemical shift (δ), multiplicity (br = broad, s = singlet, d = doublet, t = triplet, m = multiplet), coupling constant (*J* Hz) and relative integral. ^{13}C NMR spectra were recorded using a Bruker Avance III 500 at a frequency of 125.76 MHz and are reported as parts per million (ppm) with either DMSO-d_6 (δ_H 39.5 ppm) or $CDCl_3$ (δ_H 77.2 ppm) as an internal reference. High resolution ESI spectra were recorded on an Agilent 6319 LCMS TOF. Analytical TLC was performed using pre-coated silica gel plates (Merck Kieselgel 60 F254). Column chromatography was performed using high-purity grade silica gel (0.2-0.5 mm). The instrumentation used for IR Spectroscopy was Nicolet^{TM} iS50 FTIR Spectrometer. Microwave irradiation of reaction mixtures was performed using a CEM Discover SP microwave controlled by Synergy^{TM} software. Commercial materials were supplied by TCI Europe or Sigma Aldrich and were used without further purification. HPLC grade solved were used as received.

6.2 UV/Vis Measurements

UV-visible absorption spectra and optical density were recorded by means of a Varian CARY 50 Spectrophotometer. 5 mg of each compound tested were dissolved in 5 mL of DMSO to make each stock solution. Each stock solution was further diluted, where 100 *μM stock solution for each compound tested in both 12 hour time studies and UV-Extinction Coefficient studies, where the path length of the cuvette was 10 mm, as was done with the fluorescence measurements* The solutions were measured in 3 cm^3 (10 mm x 10 mm) cuvettes. The wavelength range was 200-900 nm with a scan rate of 600 nm min^{-1}.

In UV absorbance DNA tests, pH 7.4, 0.01 M PBS solution was made from dissolving 1 tablet obtained from Sigma Aldrich in 200 mL deionised H_2O, also containing 137 mM NaCl, 2.7 mM and the PBS solutions used in DNA testing were HPLC grade. Each stock solution was made in PBS, where each compound's concentration was 10 *μM*. Baseline correction measurements were used for all spectra. All solutions were prepared freshly prior to measurement. The pH 7.4 of the DNA unbuffered solutions was determined using Jenway 3305 pH Meter.

For DNA testing, deoxyribonucleic acid sodium salt (Sigma Aldrich) (10 mg) was dissolved in deionised H_2O (20 mL). The solution was divided into 40 Eppendorf tubes (0.5 mL each). They were stored at -20 °C to prevent bacterial growth. The concentrations of DNA were accurately determined by quantification by UV-Vis analysis. Detection for the presence of contaminant proteins in DNA was performed through UV-Vis analysis, where the absorption ration A_{260nm}/A_{280nm} must be greater than 1.8 for protein-free DNA. The DNA concentration per nucleotide was determined spectrophotometrically using the molar extinction coefficient, 6600 $M^{-1}cm^{-1}$ at 260 nm for DNA. Each control experiment was carried out with a stock PBS blank equivalent solution to observe any changes in UV absorbance with and without the presence of DNA.

6.3 Fluorescence Measurements

Fluorescence measurements were made with a Varian Cary 50 UV-Vis spectrophotometer equipped with a 1.0 cm path length quartz cell. The solvents used were of HPLC grade. The concentrations of the compounds under investigation were the same as those used for the UV-Visible absorption measurements, as detailed in Chapter 3 and Chapter 4. In fluorescence emission DNA tests, 0.01 M PBS solution was made from dissolving 1 tablet in 200 mL deionised H_2O. PBS solution was used in DNA testing were HPLC grade. Each stock solution was made in PBS, where each compound's concentration was 10 μM. Each control experiment was carried out with a stock PBS blank equivalent solution to observe any changes in UV absorbance with and without the presence of DNA as previously done.

A stock solution of ethidium bromide was prepared by dissolving ethidium bromide (2.5 mg, 0.63 mmol) in 0.01 M PBS solution (1.0 mL), giving a solution with a concentration of 10 M. Assays were carried out by adding 2.1 μL of the stock solution into the cuvette. This was followed by the addition of 21 μL of DNA from an Eppendorf made, which was further diluted in DMSO to make a 10 μM *stock solution for each compound tested*. These additions were (4 μL for the initial 5 runs, 10 μL for the next 10 runs and 20 μL for the last 5 runs).

6.4 Synthesis and Characterisation of Compounds Described in Chapter 2

3,4-Diethoxy-3-cyclobutene-1,2-dione (50)

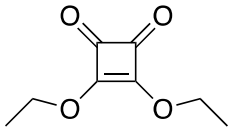

3,4-dihydroxycyclobut-3-ene-1,2-dione (2.00 g, 44.0 mmol) was dissolved in EtOH (100 mL) followed by a dropwise addition of triethylamine (7.33 mL, 219 mmol). The reaction mixture was allowed to reflux at 85 °C for 48 hrs. The product was concentrated in-vacuo to afford the crude material. The title compound was purified *via* column chromatography with 100 % DCM to afford a yellow liquid (1.55 g, 39 mmol, 88 %). **^{1}H NMR** (500 MHz, DMSO-d_6, 298 K, ppm) δ 6.67 (q, J = 14 Hz, 2H), 3.40 (t, J = 14 Hz, 3H). **^{13}C NMR** (126 MHz, DMSO-d_6, 298 K, ppm) δ 189.3, 184.2, 70.6, 15.6, with $CDCl_3$ at 77 and EtOH at 55 ppm.

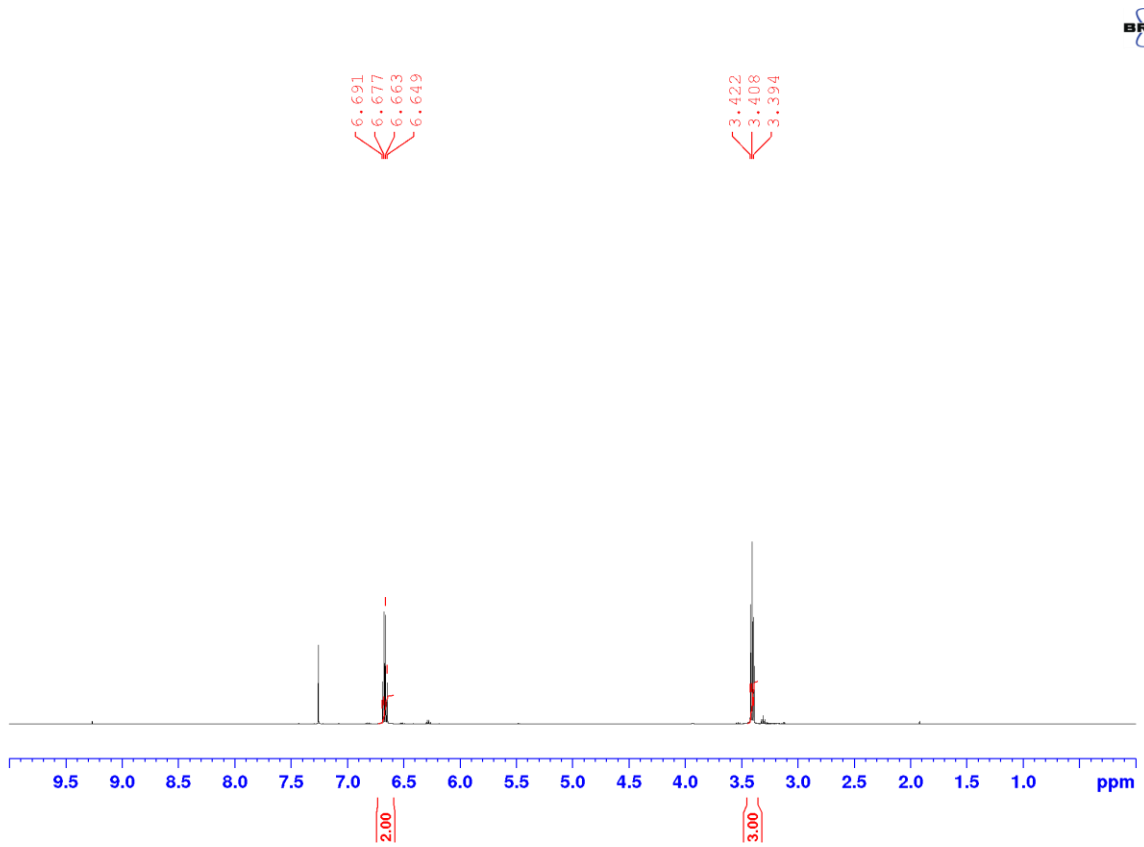

Figure 6.1: The ^{1}H NMR Spectrum of **50** (500 MHz, DMSO-d_6, 298 K.)

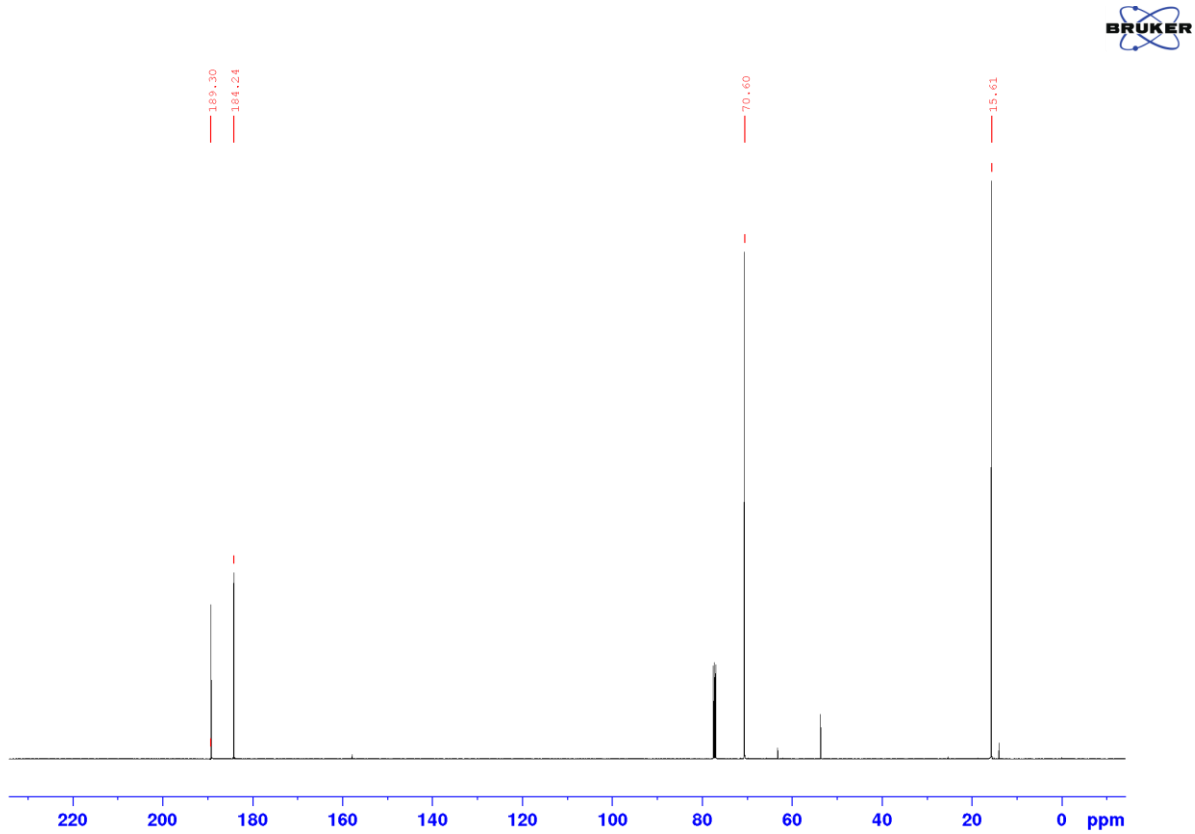

Figure 6.2: The ^{13}C NMR Spectrum of **50** (126 MHz, DMSO-d_6, 298 K.)

***tert*-Butyl *N*-(2-aminoethyl)carbamate (51)**

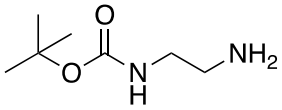

Ethane-1,2-diamine (28 mL, 25.2 g, 400 mmol) was dissolved in $CHCl_3$ (200 mL) followed by a dropwise addition of di-*tert*-butyl dicarbonate (8.74 g, 40 mmol) in $CHCl_3$ (50 mL) over the course of 1 hour. The reaction mixture was allowed to stir at 0° C for 3 hrs. After stirring at ambient temperature for 16 hrs, the mixture was washed 3x with water and 2x with brine, dried over $MgSO_4$. The product was concentrated in-vacuo to afford a colourless oil (5.80 g, 36 mmol, 90 %). **^{1}H NMR** (500 MHz, DMSO-d_6, 298 K, ppm) δ 5.08 (br s, 1H), 3.14 (m, 2H), 2.88 (t, J = 12 Hz, 2H), 1.70 (s, 1H), 1.40 (m, 3H). **^{13}C NMR** (126 MHz, DMSO-d_6, 298 K, ppm) δ 156.3, 79.3, 79.2, 43.2, 41.8, 40.8, 31.2, 28.4, 28.4, 28.2, with $CDCl_3$ at 77 ppm.

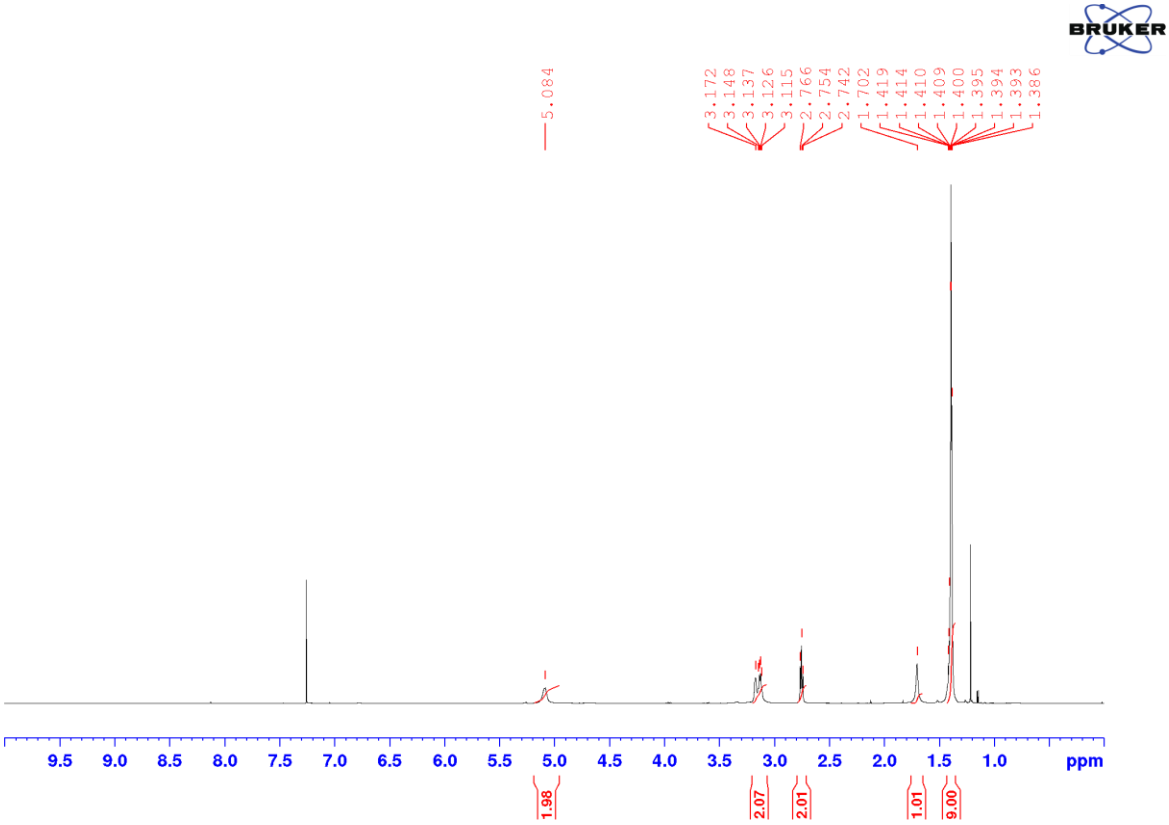

Figure 6.3: The ^{1}H NMR Spectrum of **51** (500 MHz, DMSO-d_6, 298 K.)

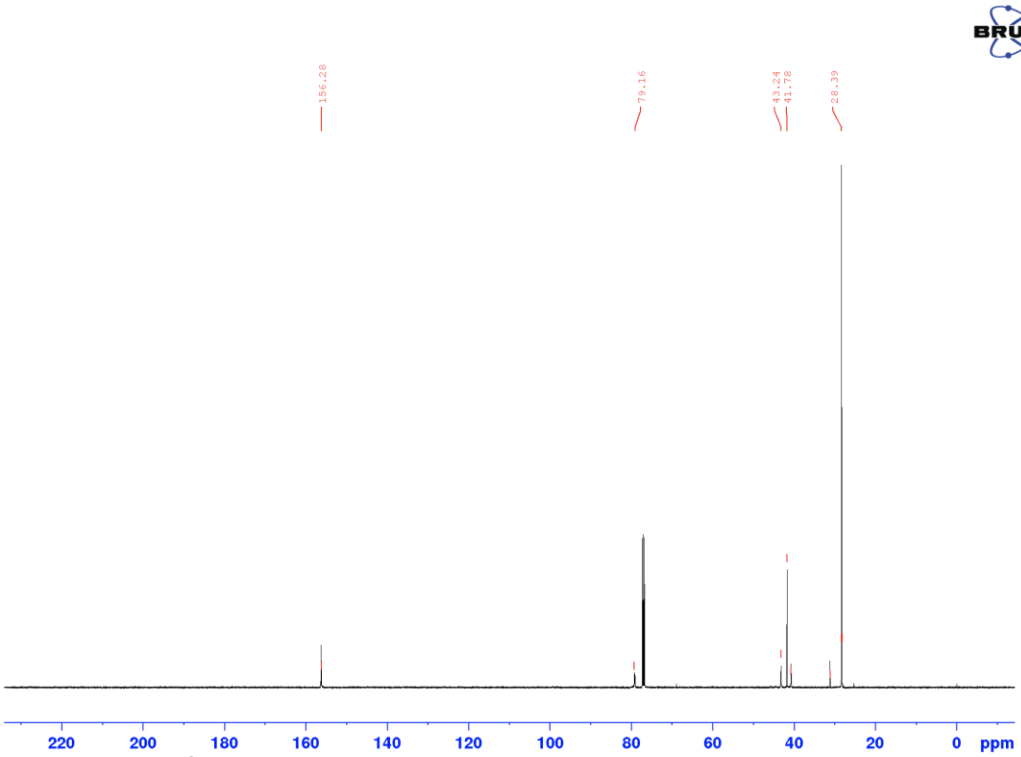

Figure 6.4: The ^{13}C NMR Spectrum of **51** (126 MHz, DMSO-d_6, 298 K.)

5-Aminopentylamino-*tert*-butylformylate (52)

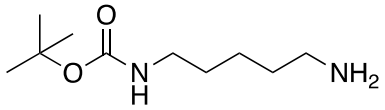

Pentane-1,5-diamine (3.51 mL, 3.06 g, 30 mmol) was dissolved in $CHCl_3$ (150 mL) followed by a dropwise addition of di-*tert*-butyl dicarbonate (1.31 g, 6 mmol) in $CHCl_3$ (50 mL) over the course of 1 hour. The reaction mixture was allowed to stir at 0° C for 3 hrs. After stirring at ambient temperature for 16 hrs, the mixture was washed 3x with water and 2x with brine, dried over $MgSO_4$. The product was concentrated in-vacuo to afford a colourless oil (1.03 g, 5.09 mmol, 85 %). **^{1}H NMR** (500 MHz, DMSO-d_6, 298 K, ppm) δ 4.544 (br s, 1H), 3.65 (q, J = 7 Hz, 2H), 3.12 (q, J = 7 Hz, 2H), 2.78 (s, 2H), 1.52-1.44 (m, 2H, 3H), 1.4 (m, 2H), 1.3 (m, 2H). **^{13}C NMR** (126 MHz, DMSO-d_6, 298 K, ppm) δ 79.1, 64.4, 40.5, 30.9, 29.9, 29.7, 28.4, 25.4, 24.1, 0, with $CDCl_3$ at 77 ppm.

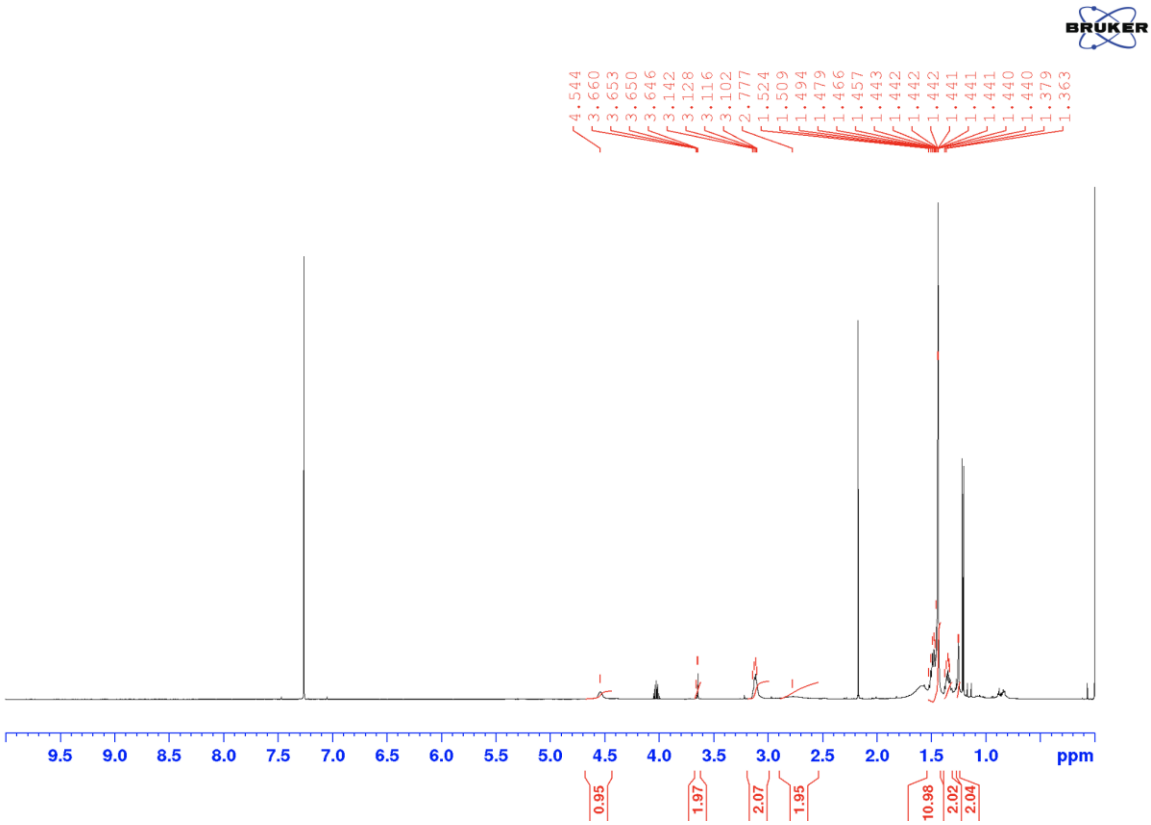

Figure 6.5: The ^{1}H NMR Spectrum of **52** (500 MHz, DMSO-d_6, 298 K.)

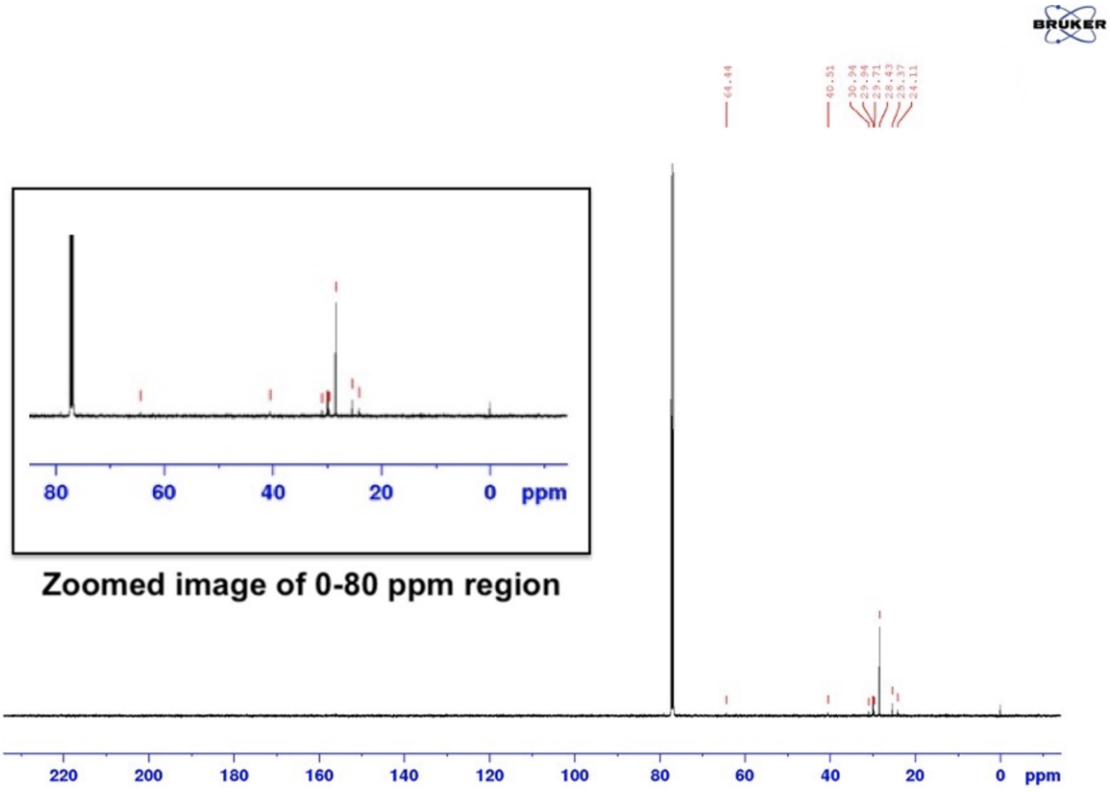

Figure 6.6: The ^{13}C NMR Spectrum of **52** (126 MHz, DMSO-d_6, 298 K.)

8-Aminooctylamino-*tert*-butylformylate (53)

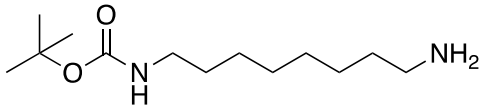

Octane-1,8-diamine (15.0 g, 104 mmol) was dissolved in $CHCl_3$ (150 mL) followed by a dropwise addition of di-*tert*-butyl dicarbonate (2.95 g, 14.0 mmol) in $CHCl_3$ (50 mL) over the course of 1 hour. The reaction mixture was allowed to stir at 0° C for 3 hrs. After stirring at ambient temperature for 16 hrs, the mixture was washed 3x with water and 2x with brine, dried over $MgSO_4$. The product was concentrated in-vacuo to afford a colourless oil (3.74 g, 15.3 mmol, 90 %). **^{1}H NMR** (500 MHz, DMSO-d_6, 298 K, ppm) δ 5.26 (br s, 1H), 2.79 (s, 1H), 2.39 (m, 2x2H), 1.16 (t, J = 12.5 Hz, 4x2H), 1.13 (d, J = 7 Hz, 3H), 1.04 (q, J = 7.5 Hz, 2x2H). **^{13}C NMR** (126 MHz, DMSO-d_6, 298 K, ppm) δ 155.9, 78.3, 51.3, 42.0, 40.3, 33.6, 30.6, 29.8, 29.2, 29.1, 28.2, 26.6, 18.0, with $CDCl_3$ at 77 ppm.

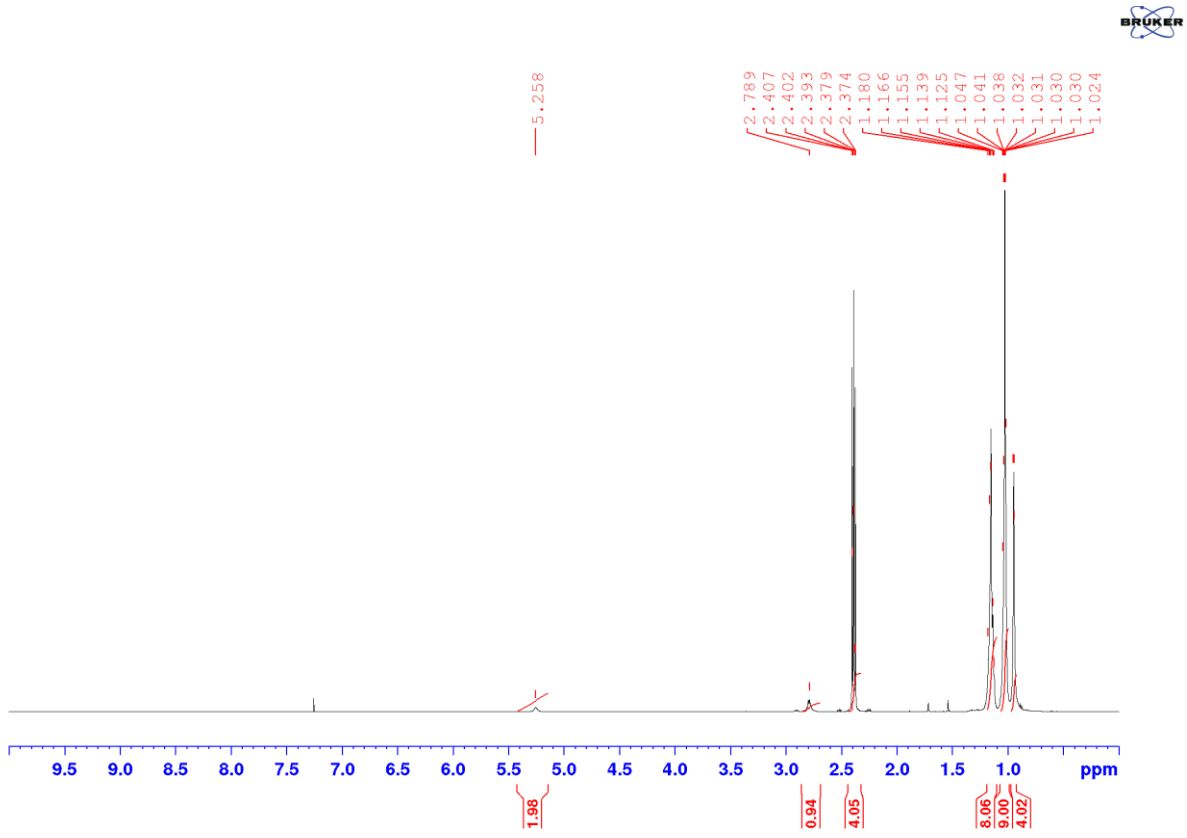

Figure 6.7: The ^{1}H NMR Spectrum of **53** (500 MHz, DMSO-d_6, 298 K.)

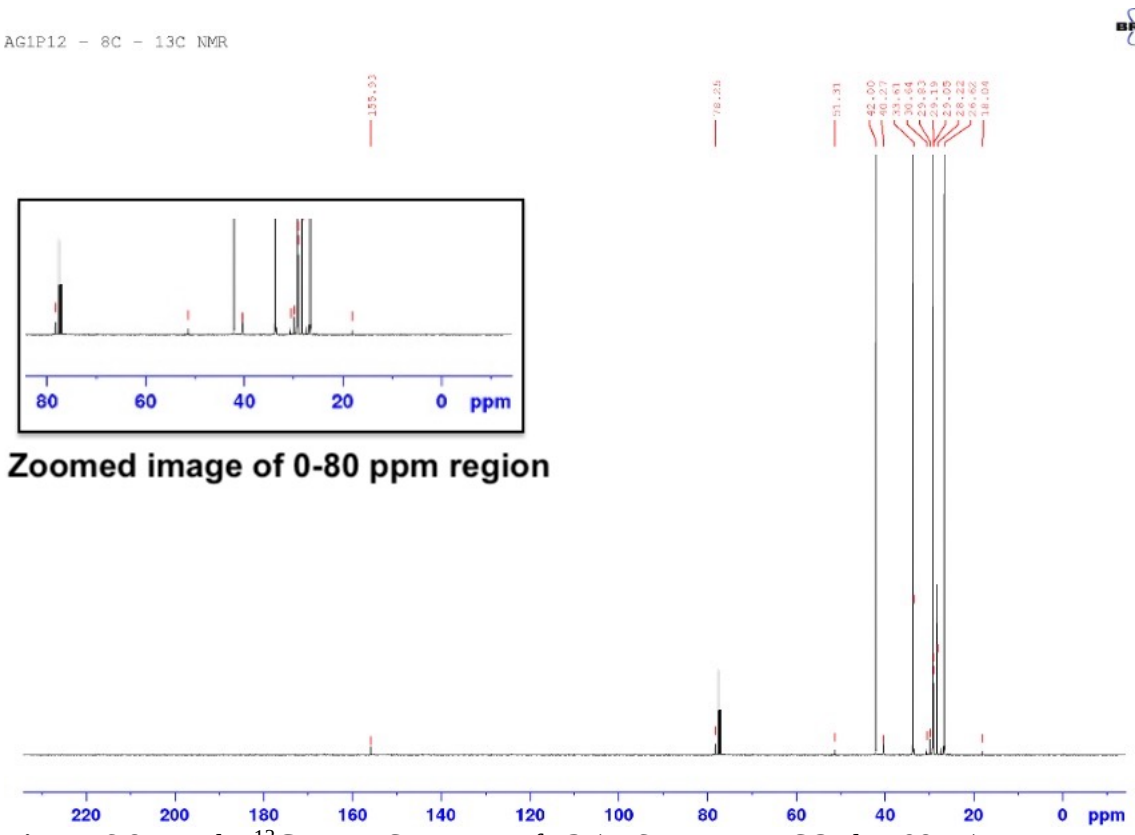

Figure 6.8: The ^{13}C NMR Spectrum of **53** (126 MHz, DMSO-d_6, 298 K.)

2-{2-[2-(*tert*-Butoxycarbonylamino)ethylamino]-3,4-dioxo-1-cyclobuten-1-ylamino}ethylamino-*tert*-butylformylate (63)

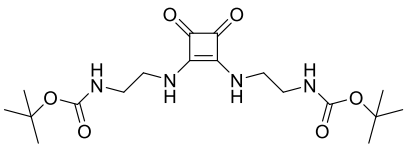

tert-butyl (2-aminoethyl)carbamate (1.00 g, 6.24 mmol) was dissolved in EtOH (50 mL) followed by a dropwise addition of 3,4-diethoxycyclobut-3-ene-1,2-dione (185 µL, 1.25 mmol) dissolved in 2 mL of EtOH. The reaction mixture was allowed to reflux at 85 °C for 12 hrs. The product was concentrated in-vacuo to afford the crude material. The title compound was purified *via* column chromatography with 94% DCM & 6% MeOH to afford a yellow solid (0.44 g, 1.10 mmol, 88 %). M.p. 183-185 °C. **^{1}H NMR** (500 MHz, DMSO-d_6, 298 K, ppm) δ 7.43 (br s, 1H), 6.89 (br t, J = 10 Hz, 1H), 3.50 (d, J = 5 Hz, 2H), 3.10 (q, J = 15 Hz, 2H), 1.37 (s, 3H). **^{13}C NMR** (126 MHz, DMSO-d_6, 298 K, ppm) δ 183.0, 156.2, 78.3, 43.6, 41.6, 28.6, with DMSO-d6 at 40 ppm. **IR** (film) ν_{max} (cm^{-1}): 3341, 2975, 1803, 1691 (C=O stretch), 1646 (C=O stretch), 1558, 1523, 1448, 1389, 1363, 1271, 1250, 1165, 966, 870, 745, 606, 586, 576,

569, 549, 541, 532, 525. **HRMS** (ESI^+): m/z calculated for $C_{18}H_{30}N_4O_6$ $[M+H]^+$ requires 398.46, found 398.04 (-0.42 ppm).

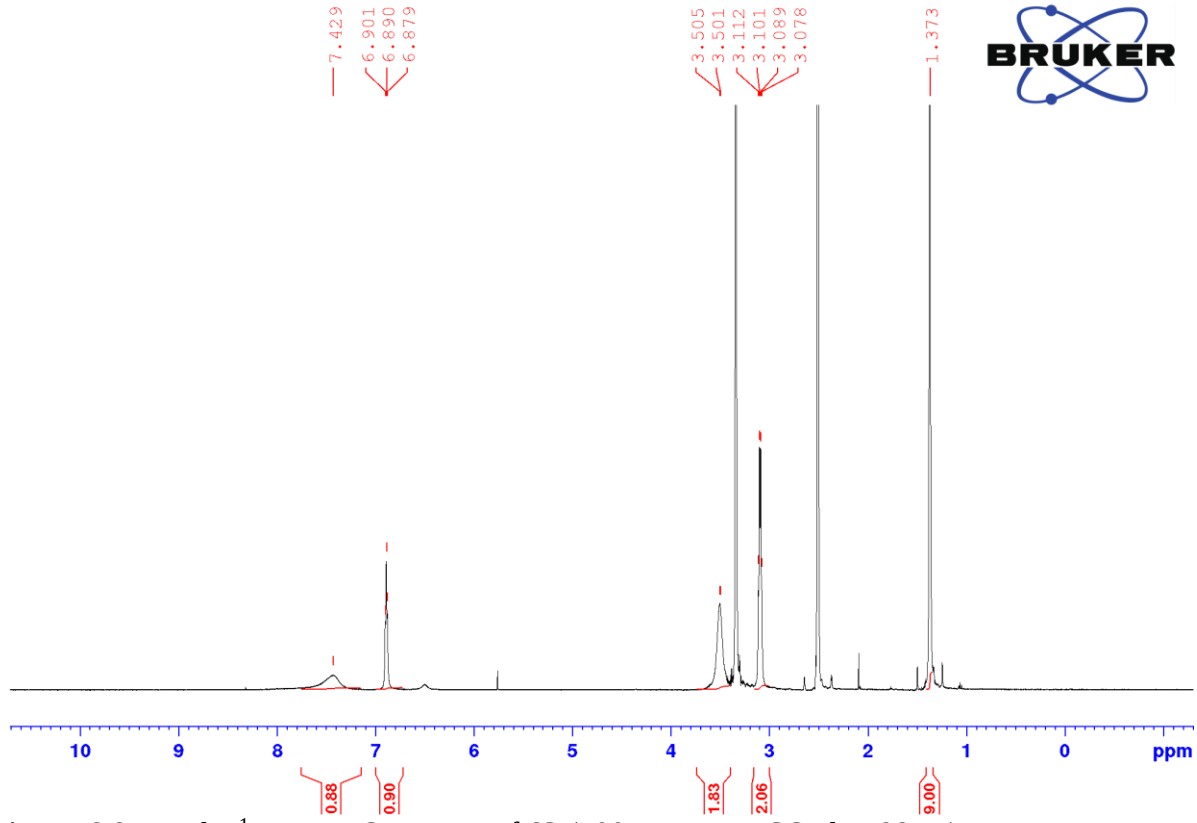

Figure 6.9: The ^1H NMR Spectrum of **63** (500 MHz, DMSO-d_6, 298 K.)

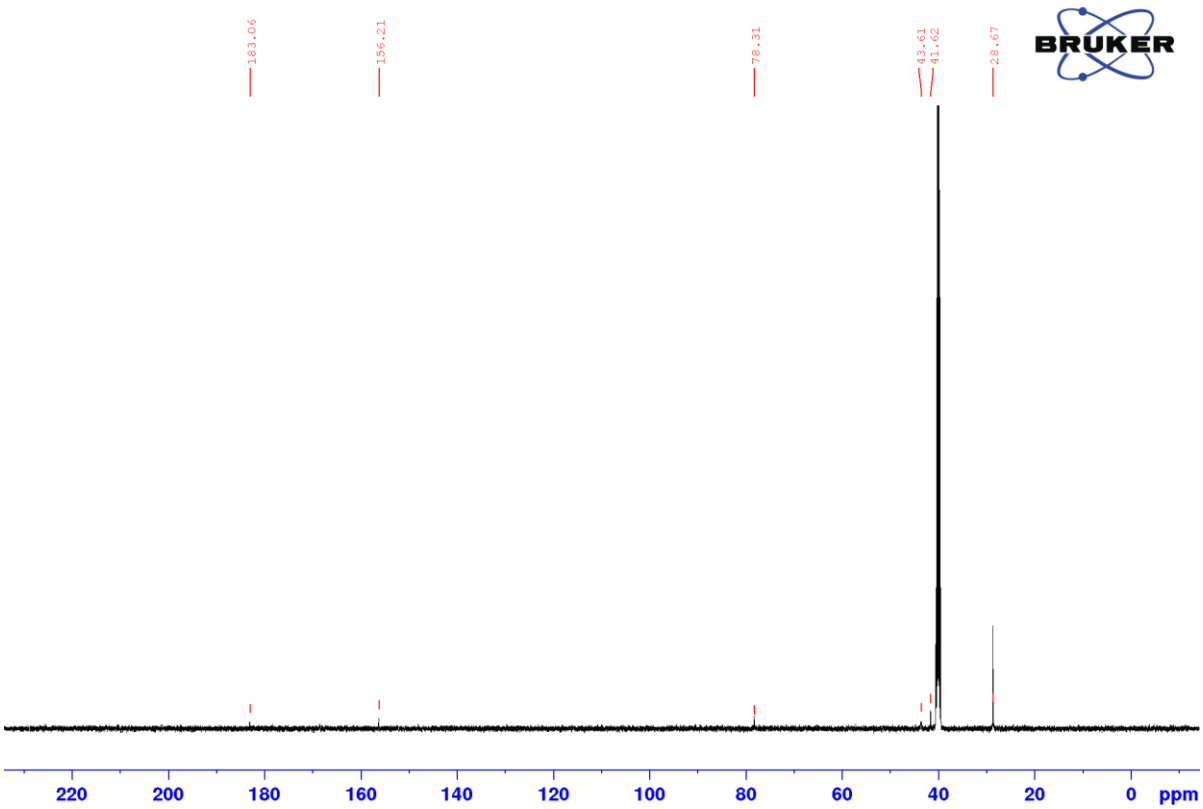

Figure 6.10: The ^{13}C NMR Spectrum of **63** (126 MHz, DMSO-d_6, 298 K.)

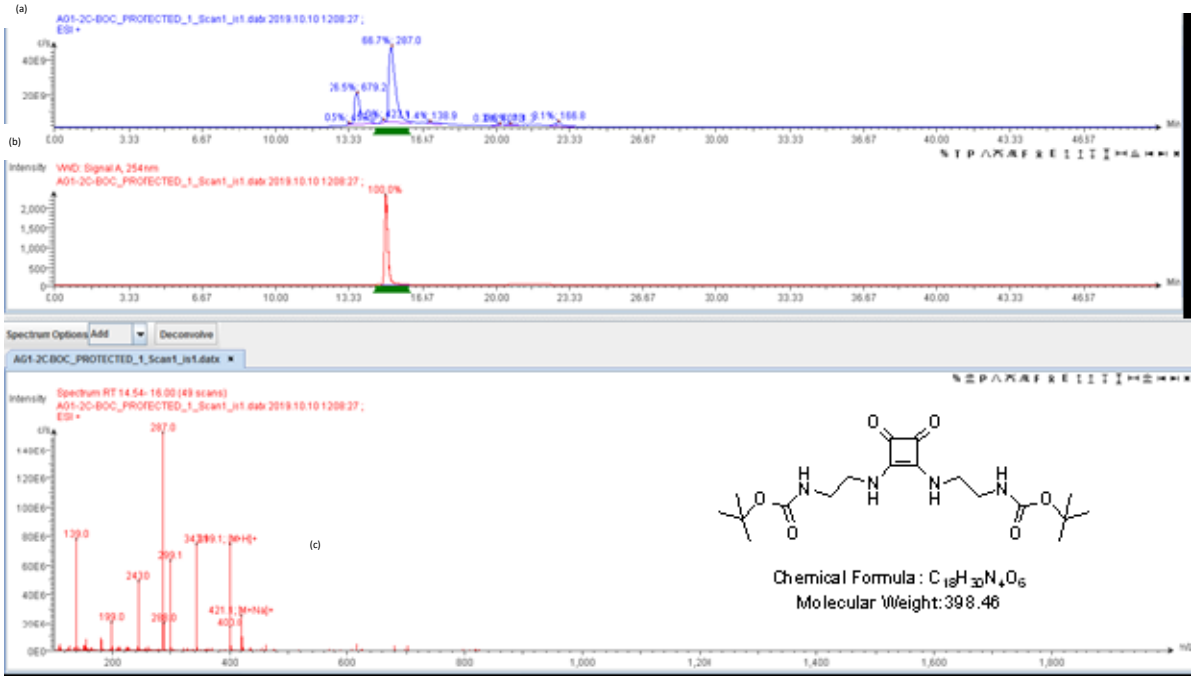

Figure 6.11: LCMS Characterisation of 63: (a) Analytical HPLC trace of purified 63; R_t = 15.0 mins (0-100% MeCN over 30 mins, λ = 254 nm). (b) Extracted Ion Chromatogram for 298.1 $[M + H]^+$. (c) Mass Spectrum detected between R_t = 14.6-16 mins (157 scans); Calculated for $[M + H]^+$ = 399.4; Mass Found (ESI^+) = 399.1. Also Found 421.1 $[M + MeCN + H]^+$.

5-{2-[5-(*tert*-Butoxycarbonylamino)pentylamino]-3,4-dioxo-1-cyclobuten-1-ylamino}pentylamino-*tert*-butylformylate (64)

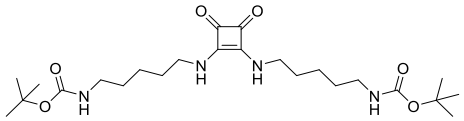

tert-butyl (5-aminopentyl)carbamate) (0.64 g, 3.18 mmol) was dissolved in EtOH (50 mL) followed by a dropwise addition of 3,4-diethoxycyclobut-3-ene-1,2-dione (97 µL, 0.64 mmol) dissolved in 2 mL of EtOH. The reaction mixture was allowed to reflux at 85 °C for 12 hrs. The product was concentrated in-vacuo to afford the crude material. The title compound was purified *via* column chromatography with 94% DCM & 6% MeOH to afford a white solid (0.25 g, 0.52 mmol, 81 %). **^{1}H NMR** (500 MHz, DMSO-d_6, 298 K, ppm) δ 7.33 (br s, 1H), 6.77 (br t, *J* = 10.5 Hz, 1H), 3.48 (s, 2H), 2.90 (q, *J* = 13 Hz, 2H), 1.50 (m, 2H), 1.40 (t, J = 15 Hz, 2H, 3H), 1.27 (q, J = 15.5 Hz, 2H). **^{13}C NMR** (126 MHz, DMSO-d_6, 298 K, ppm) δ 182.8, 168.2, 156.1, 77.8, 43.7, 31.1, 31.0, 29.6, 28.7, 23.6, with DMSO-d6 at 40 ppm. **IR** (film) ν_{max} (cm^{-1}): 3364, 3172, 2935, 2861, 1799, 1685, 1641, 1564 (C=O stretch), 1518 (C=O stretch), 1441, 1456, 1441, 1387, 1364, 1352, 1327, 1310, 1278, 1249, 1169, 1105, 1038, 995, 948, 872, 820, 757, 607, 541, 531, 507, 504, 496, 493, 489, 487, 481, 476, 473, 465, 457, 454. **HRMS** (ESI^+): m/z calculated for $C_{24}H_{42}N_4O_6$ $[M+H]^+$ requires 482.62, found 482.24 (-0.38 ppm).

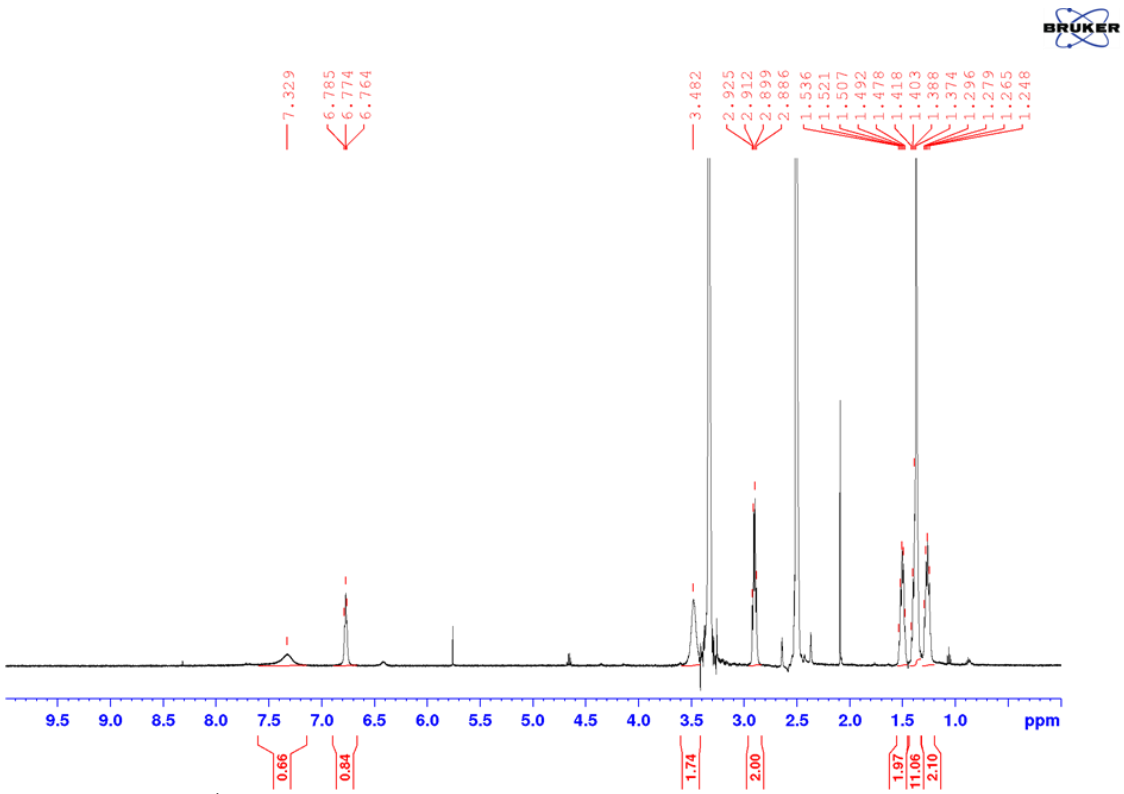

Figure 6.12: The ^{1}H NMR Spectrum of **64** (500 MHz, DMSO-d_6, 298 K.)

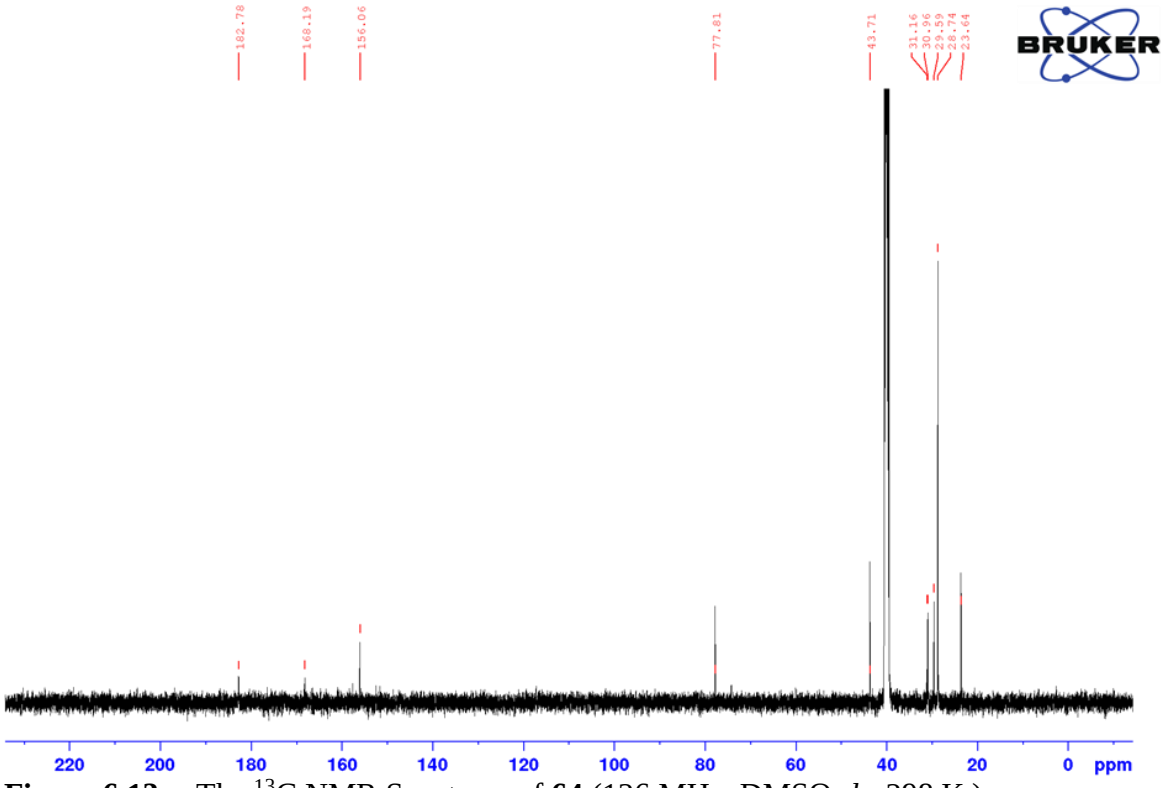

Figure 6.13: The ^{13}C NMR Spectrum of **64** (126 MHz, DMSO-d_6, 298 K.)

8-{2-[8-(*tert*-Butoxycarbonylamino)octylamino]-3,4-dioxo-1-cyclobuten-1 ylamino}octylamino-*tert*-butylformylate (65)

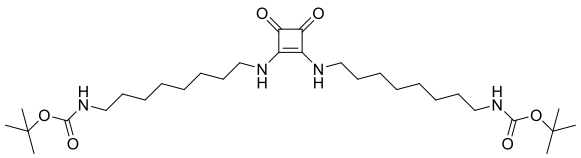

tert-butyl (8-aminooctyl)carbamate) (4.81 g, 19.69 mmol) was dissolved in EtOH (50 mL) followed by a dropwise addition of 3,4-diethoxycyclobut-3-ene-1,2-dione (583 µL, 3.94 mmol) dissolved in 2 mL of EtOH. The reaction mixture was allowed to reflux at 85 °C for 12 hrs. The precipitated product was filtered to afford the crude material. The title compound was a pure product and appeared as a yellow solid (1.77 g, 3.12 mmol, 79 %). The deprotection of the *N*-Boc groups was carried out in separate reactions, where 10 equivalents of both dichloromethane and trifluoroacetic acid have been used in order to progress with the reaction pathways. **^{1}H NMR** (500 MHz, DMSO-d_6, 298 K, ppm) δ 7.40 (br s, 1H), 3.49 (s, 2x2H), 2.88 (q, J = 13 Hz, 2x2H), 1.50 (d, *J* = 6.5 Hz, 2H), 1.37 (m, 3x2H, 3H). **^{13}C NMR** (126 MHz, DMSO-d_6, 298 K, ppm) δ 182.8, 43.7, 42.0, 33.7, 33.7, 31.2, 29.5, 29.4, 29.1, 28.7, 26.9, 26.9, 26.2, with DMSO-d6 at 40 ppm. **IR** (film) ν_{max} (cm^{-1}): 3159, 2923, 2848, (1799, 1644, 1563, 1487 C=O stretch), 1434, 1356, 1311, 1171, 1033, 724, 610, 564, 542, 525, 513, 508, 504, 500. **HRMS** (ESI^{+}): m/z calculated for $C_{30}H_{54}N_4O_6$ [M+H]$^{+}$ requires 566.78, found 566.26 (-0.52 ppm).

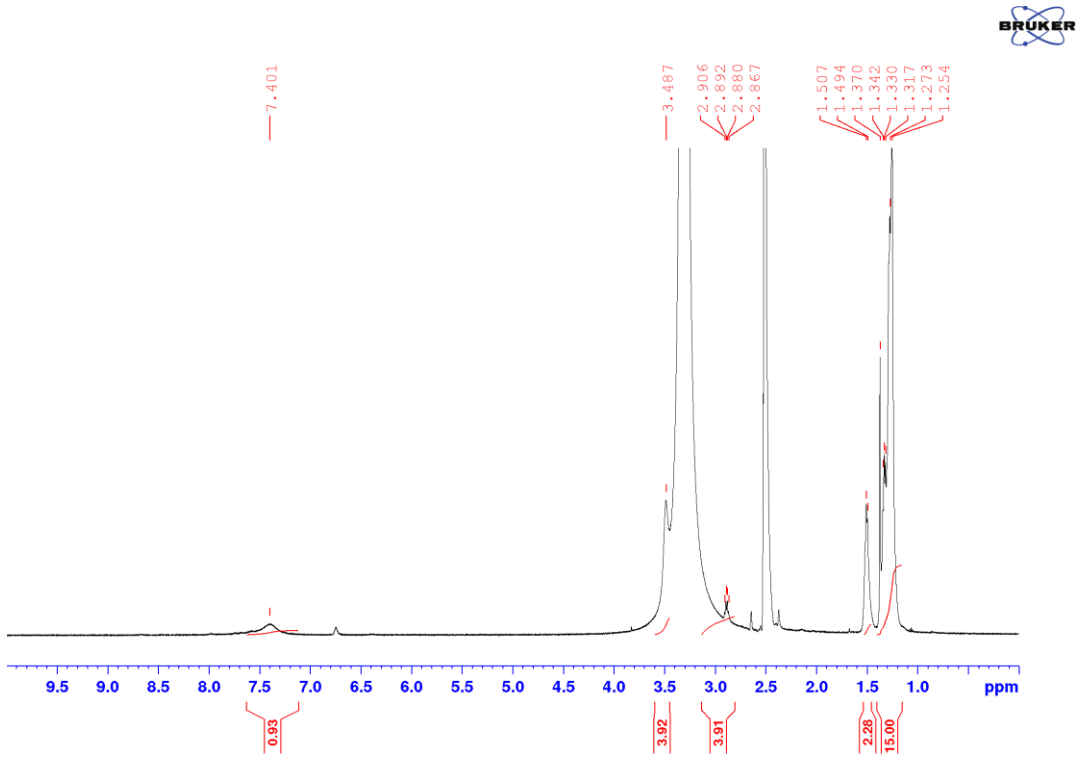

Figure 6.14: The ^{1}H NMR Spectrum of **65** (500 MHz, DMSO-d_6, 298 K.)

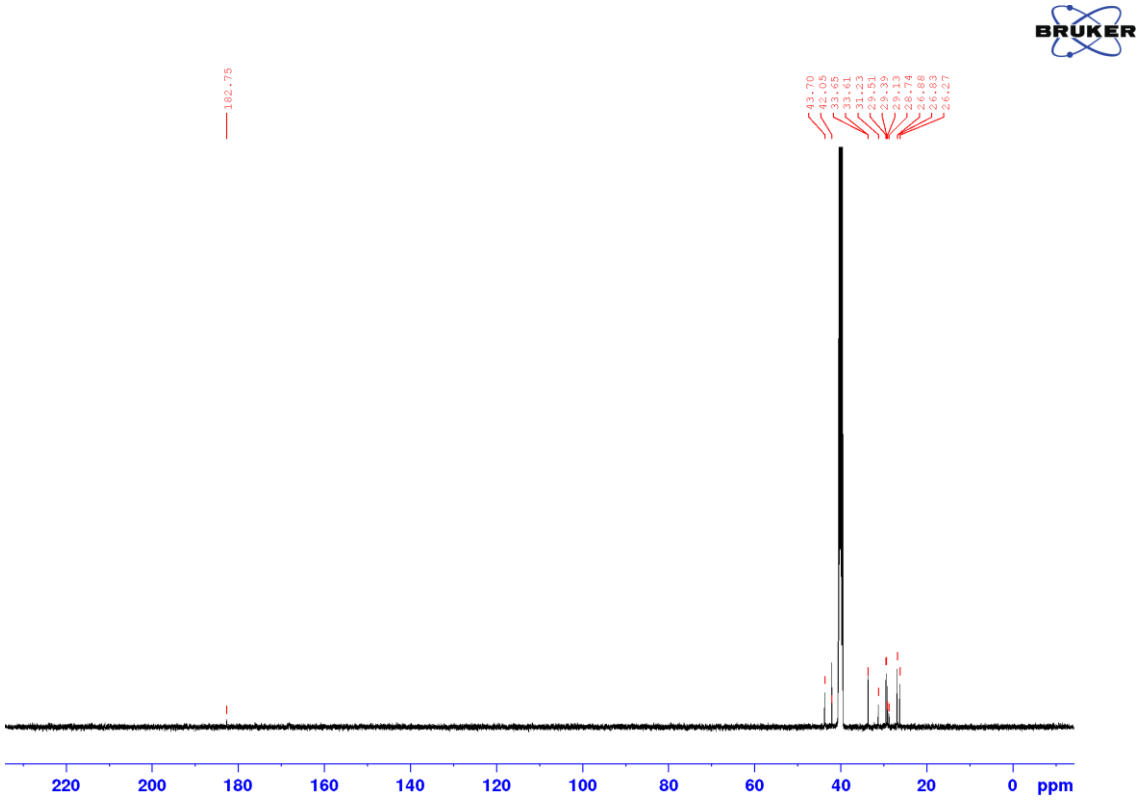

Figure 6.15: The ^{13}C NMR Spectrum of **65** (126 MHz, DMSO-d_6, 298 K.)

2-(2-{2-[2-(1,3-Dioxo-2*H*-2-azaphenalen-2-yl)ethylamino]-3,4-dioxo-1-cyclobuten-1-ylamino}ethyl)-2*H*-2-azaphenalene-1,3-dione (38)

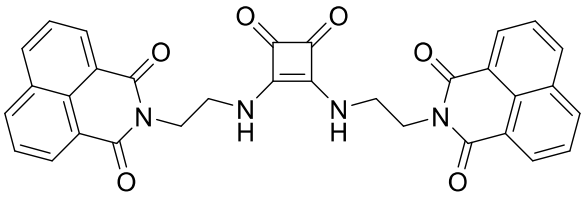

Naphthalene-1,8-dicarboxylic anhydride (0.28 g, 1.4 mmol) was dissolved in ethanol (20 mL) and triethylamine (355 µL, 2.5 mmol) followed by a dropwise addition of **57** (0.20 g, 0.6 mmol) in 2 mL of ethanol. The reaction mixture was allowed to reflux at 85 °C for 12 hrs. The title compound was a precipitate. (0.27 g, 0.48 mmol, 84 %). **^{1}H NMR** (500 MHz, DMSO-d_6, 358 K, ppm) δ 8.26 (d, *J* = 7 Hz, 1H), 8.19 (d, *J* = 8 Hz, 1H), 7.65 (t, *J* = 15.5 Hz, 1H), 7.43 (br s, 1H), 4.15 (t, J = 11 Hz, 2H), 3.67 (d, J = 4 Hz, 2H). **^{13}C NMR** (126 MHz, DMSO-d_6, 298 K, ppm) δ 183.4, 168.7, 164.1, 134.7, 131.5, 131.0, 127.7, 127.5, 122.4, 56.5, 49.1, 19.0, with DMSO-d6 at 40 ppm. **IR** (film) ν_{max} (cm^{-1}): 3302, 1795 (C=O stretch), 1691 (C=O stretch), 1651, 1625, 1583, 1537, 1463, 1441, 1416, 1385, 1339, 1315, 1280, 1233, 1168, 1143, 1120, 1102, 1043, 877, 855, 844, 788, 774, 739, 669, 617, 567, 542, 522. **HRMS** (ESI^+): m/z calculated for $C_{38}H_{34}N_4O_6$ $[M+H]^+$ requires 642.2509, found 642.2367 (-0.014 ppm).

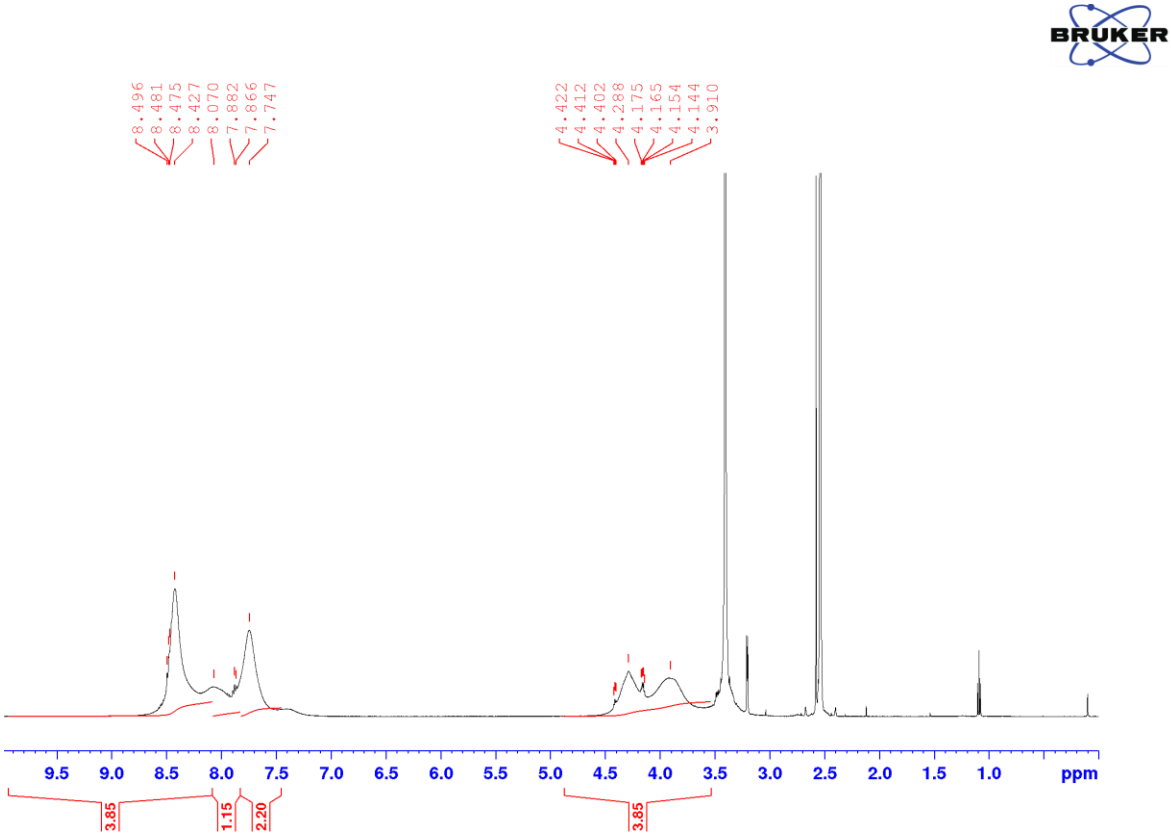

Figure 6.16: The ^{1}H NMR Spectrum of **38** (500 MHz, DMSO-d_6, 298 K.)

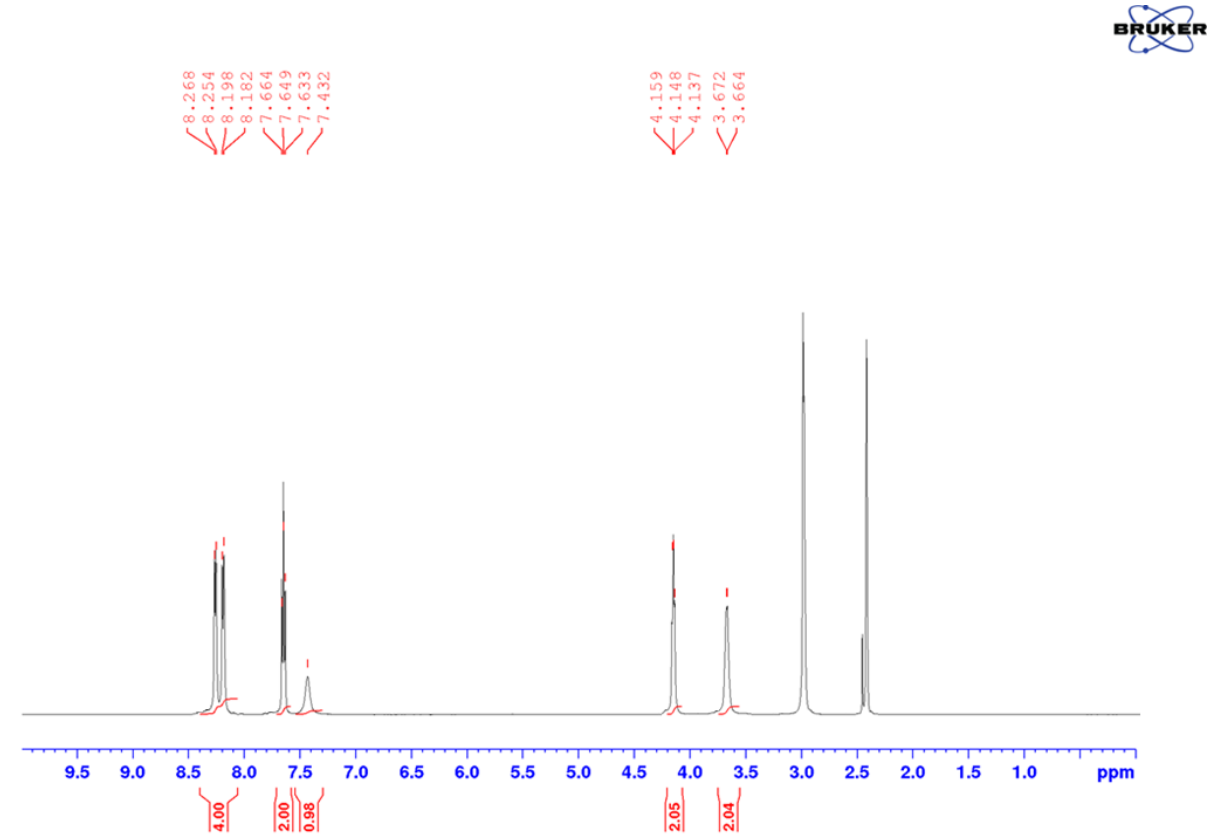

Figure 6.17: The ^{1}H NMR Spectrum of **38** at **358 K** (500 MHz, DMSO-d_6, 358 K.)

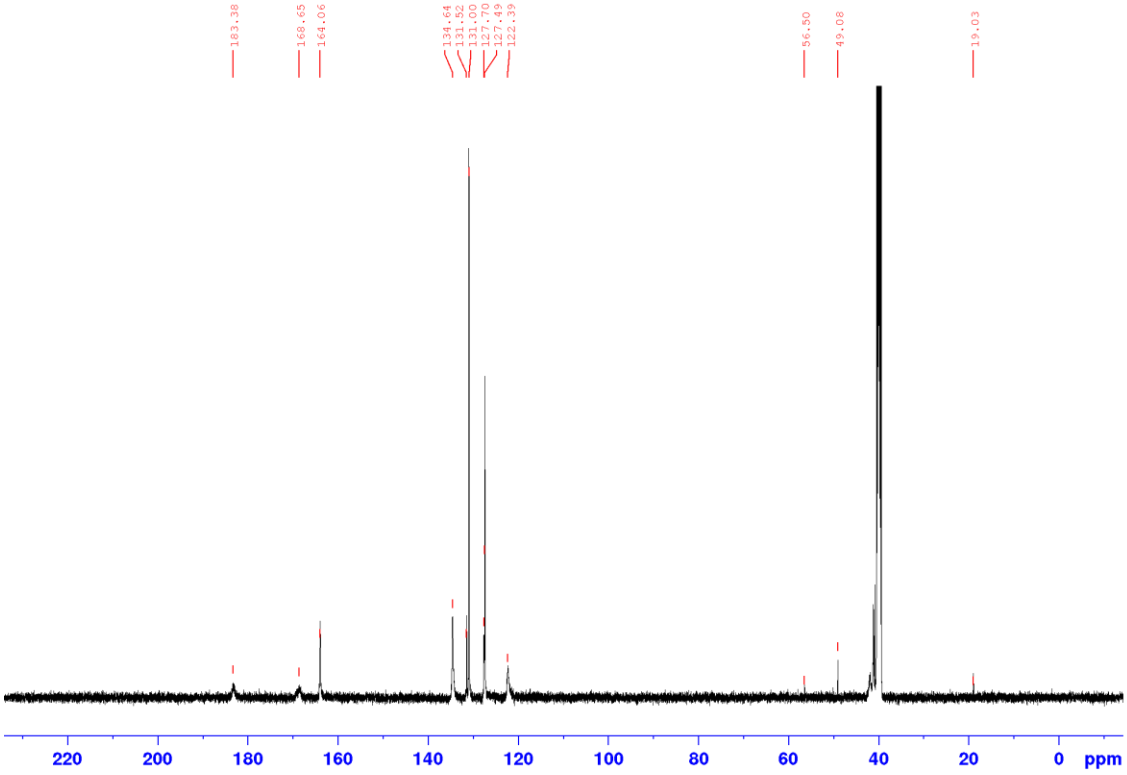

Figure 6.18: The ^{13}C NMR Spectrum of **38** (126 MHz, DMSO-d_6, 298 K.)

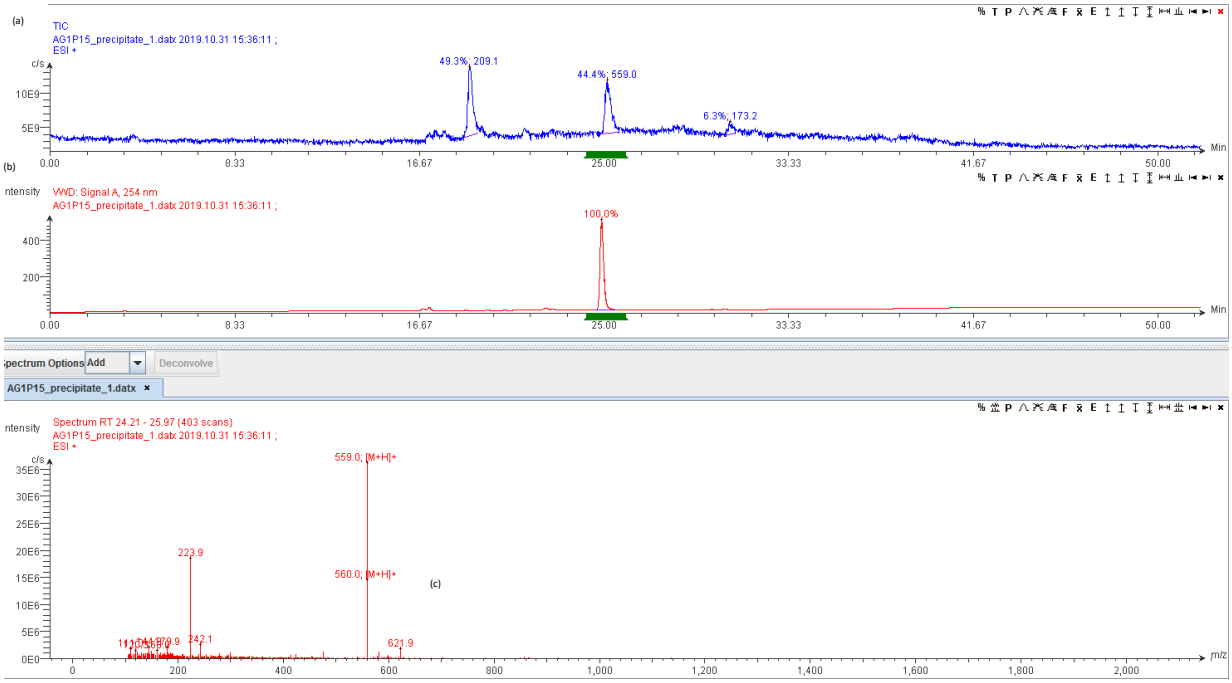

Figure 6.19: LCMS Characterisation of 38: (a) Analytical HPLC trace of precipitate 38; R_t = 25.0 mins (0-100% MeCN over 26 mins, λ = 254 nm). (b) Extracted Ion Chromatogram for 558.58 $[M + H]^+$. (c) Mass Spectrum detected between R_t = 24.0-26.0 mins (354 scans); Calculated for $[M + H]^+$ = 559.1; Mass Found (ESI^+) = 559.0, Also Found 560.0 $[M + H + H]^+$.

2-(5-{2-[5-(1,3-Dioxo-2*H*-2-azaphenalen-2-yl)pentylamino]-3,4-dioxo-1-cyclobuten-1-ylamino}pentyl)-2*H*-2-azaphenalene-1,3-dione (39)

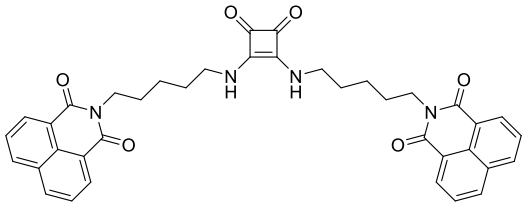

Naphthalene-1,8-dicarboxylic anhydride (0.22 g, 1.1 mmol) was dissolved in ethanol (20 mL) and triethylamine (280 µL, 2.0 mmol) followed by a dropwise addition of dissolved 5,5'-((3,4-dioxocyclobut-1-ene-1,2-diyl)bis(azanediyl))bis(pentan-1-aminium) (0.24 g, 0.5 mmol) in 2 mL of ethanol. The reaction mixture was allowed to reflux at 85 °C for 12 hrs. The title compound was a precipitate. (0.140 g, 0.22 mmol, 89 %). **^{1}H NMR** (500 MHz, DMSO-d_6, 358 K, ppm) δ 8.47 (d, *J* = 7 Hz, 1H), 8.37 (d, *J* = 8 Hz, 1H), 7.82 (t, *J* = 15.5 Hz, 1H), 7.09 (br s, 1H), 4.08 (d, *J* = 6 Hz, 2H), 3.51 (d, *J* = 6 Hz, 2H), 1.71 (d, *J* = 6 Hz, 2H), 1.62 (d, *J* = 6.5 Hz, 2H), 1.43 (t, *J* = 14 Hz, 2H). **^{13}C NMR** (126 MHz, DMSO-d_6, 298 K, ppm) δ 182.8, 168.2, 163.8, 134.7, 131.7, 131.1, 127.8, 127.7, 122.5, 43.6, 31.2, 31.0, 27.7, 23.9, with DMSO-d6 at 40 ppm. **IR** (film) ν_{max} (cm^{-1}): 3249, 2931, 2854, 1794 (C=O stretch), 1695 (C=O stretch), 1656, 1625, 1547, 1463, 1427, 1387, 1339, 1275, 1245, 1173, 1095, 1068, 1045, 996, 960, 911, 848, 815, 800, 778, 738, 686, 652, 608, 591, 573, 544, 534, 528. **HRMS** (ESI^+): m/z calculated for $C_{38}H_{34}N_4O_6$ $[M+H]^+$ requires 642.2509, found 642.2367 (-0.48 ppm).

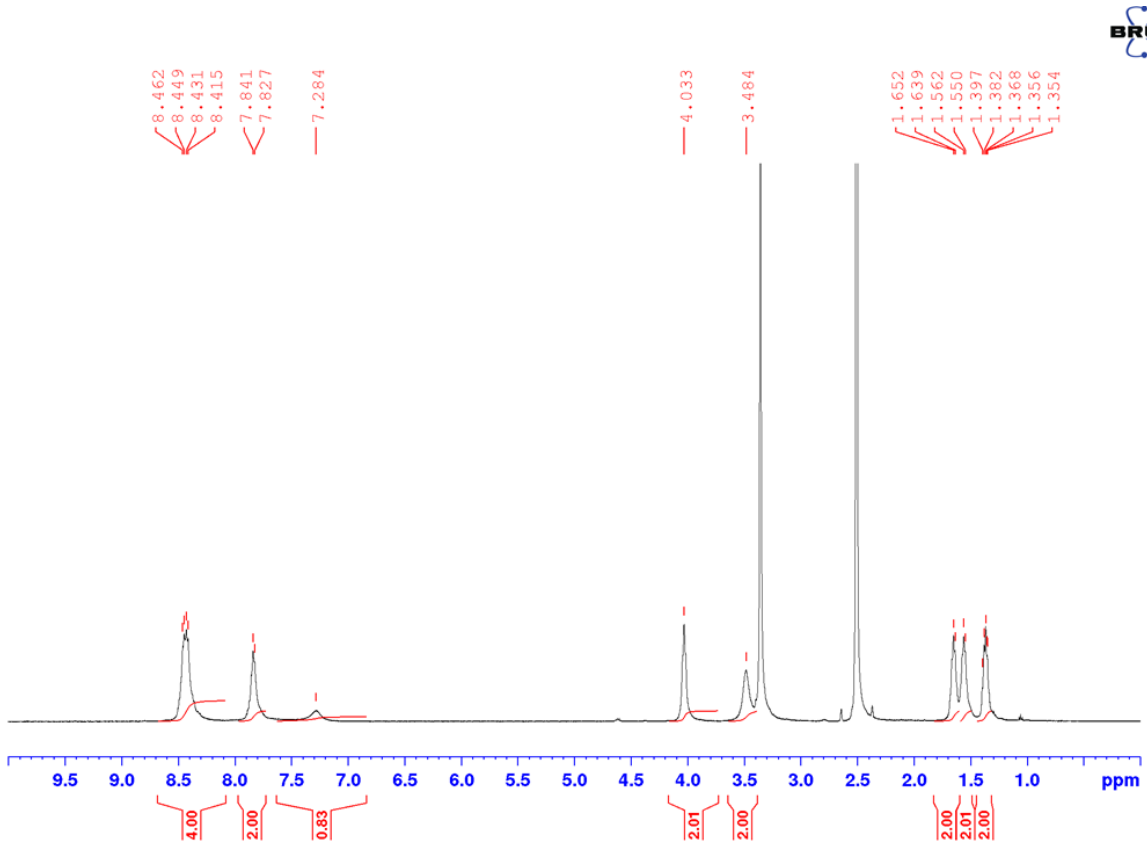

Figure 6.20: The ^{1}H NMR Spectrum of **39** (500 MHz, DMSO-d_6, 298 K.)

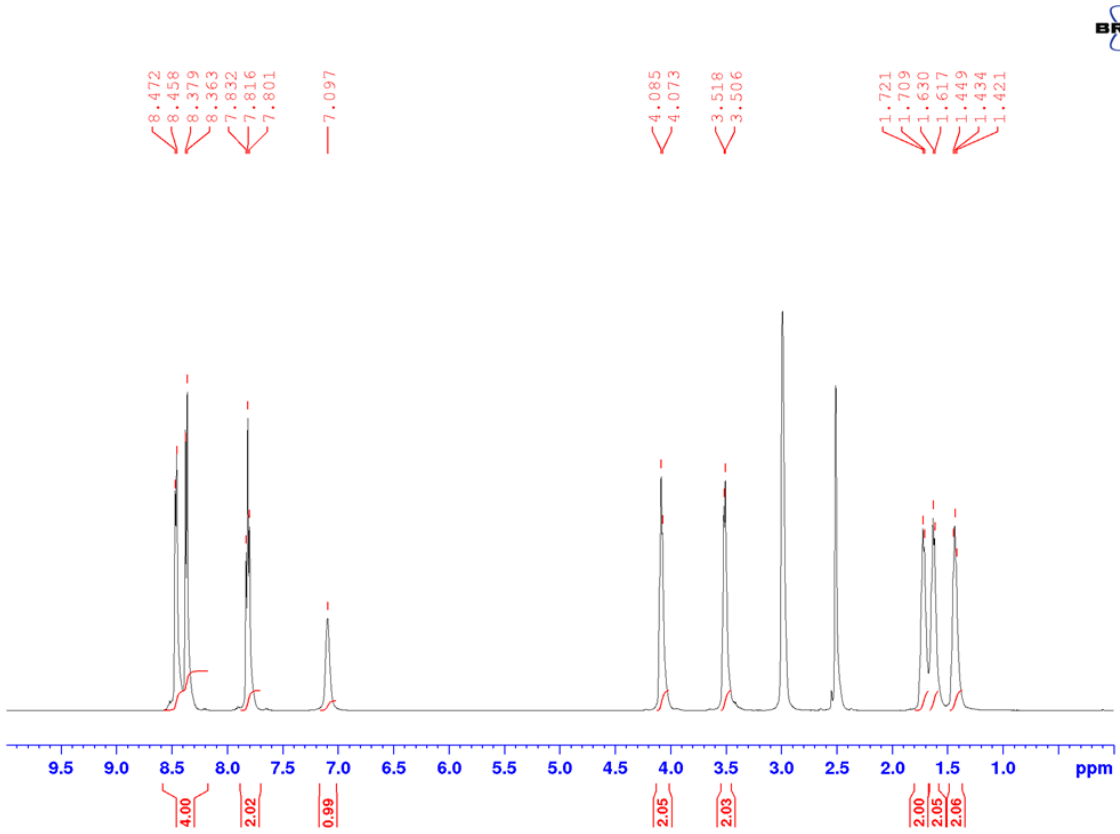

Figure 6.21: The ^{1}H NMR Spectrum of **39** at **358 K** (500 MHz, DMSO-d_6, 358 K.)

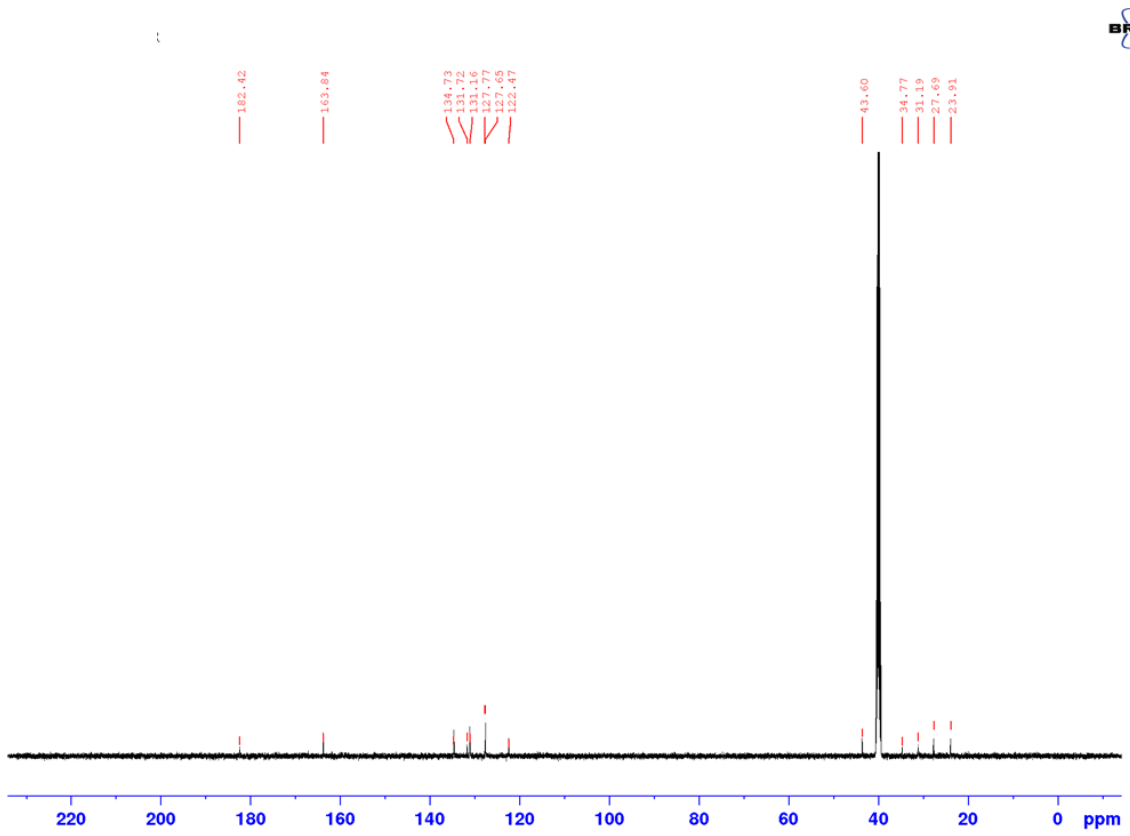

Figure 6.22: The ^{13}C NMR Spectrum of **39** (126 MHz, DMSO-d_6, 298 K.)

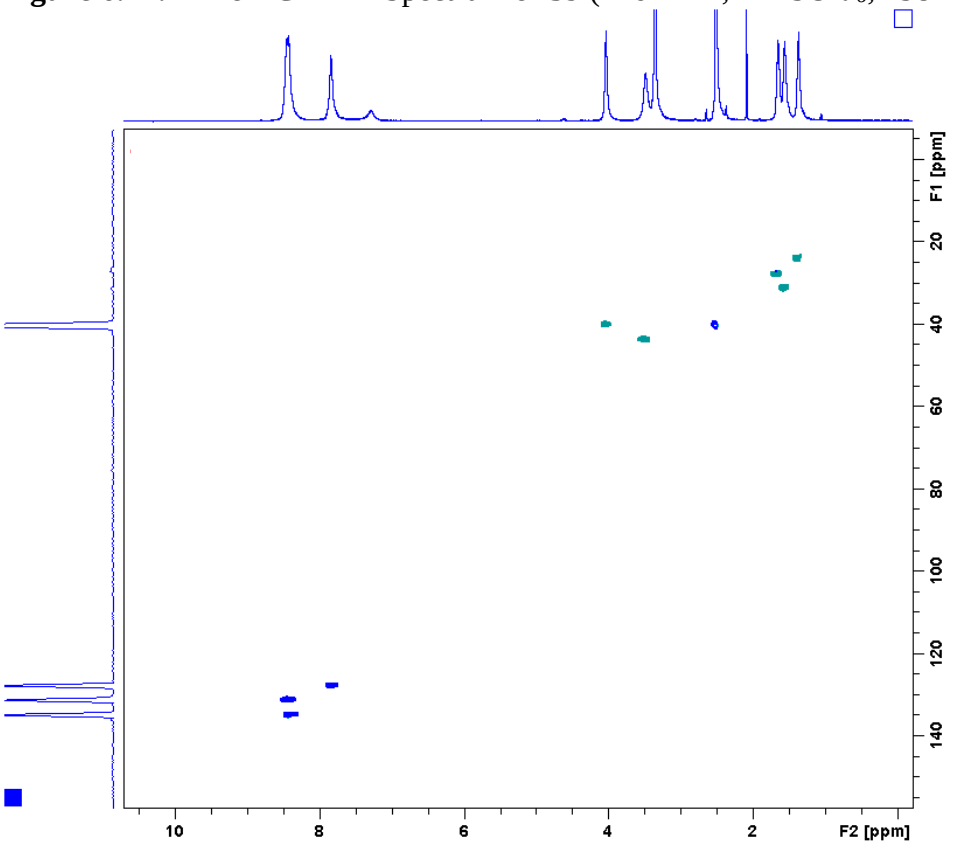

Figure 6.23: The HSQC Spectrum of **39** (126 MHz, DMSO-d_6, 298 K.)

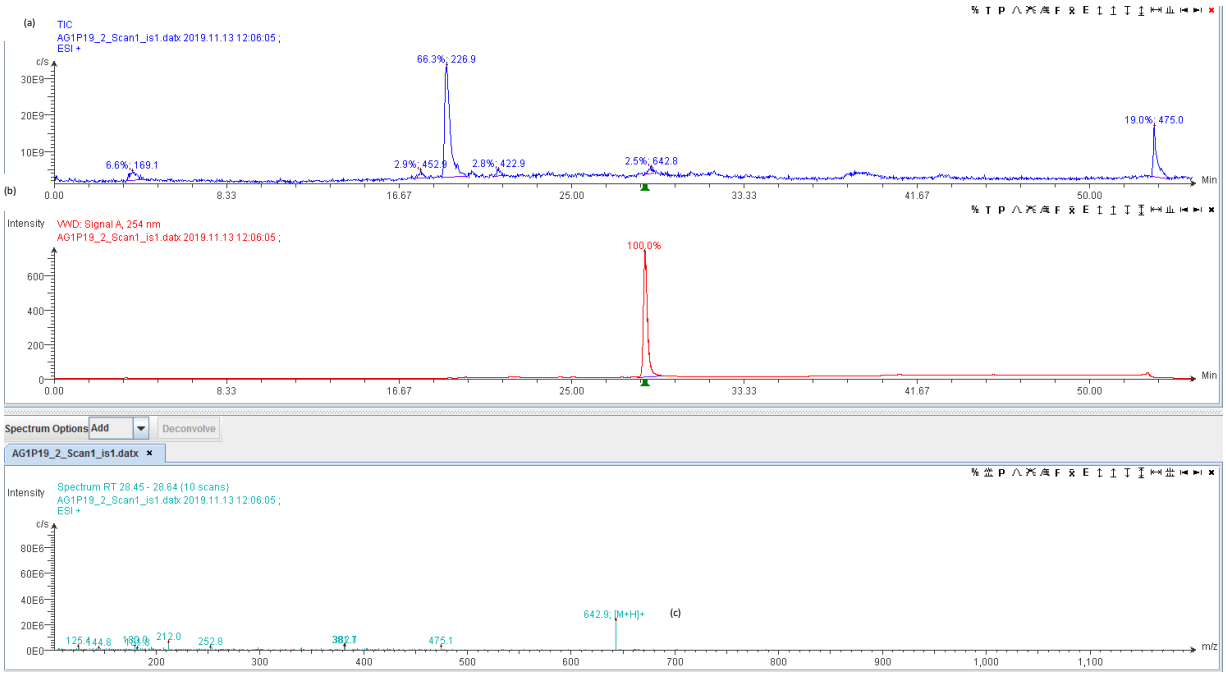

Figure 6.24: LCMS Characterisation of 39: (a) Analytical HPLC trace of precipitate 39; R_t = 29.0 mins (0-100% MeCN over 30 mins, λ = 254 nm). (b) Extracted Ion Chromatogram for 642.7 $[M + H]^+$. (c) Mass Spectrum detected between R_t = 28.0-29.5 mins (354 scans); Calculated for $[M + H]^+$ = 642.9; Mass Found (ESI^+) = 642.9.

2-(8-{2-[8-(1,3-Dioxo-2*H*-2-azaphenalen-2-yl)octylamino]-3,4-dioxo-1-cyclobuten-1-ylamino}octyl)-2*H*-2-azaphenalene-1,3-dione (40)

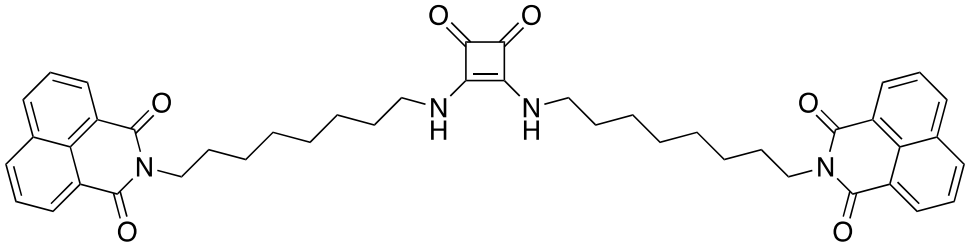

Naphthalene-1,8-dicarboxylic anhydride (0.181 g, 0.41 mmol) was dissolved in ethanol (20 mL) and triethylamine (232 µL, 1.66 mmol) followed by a dropwise addition of dissolved 8,8'-((3,4-dioxocyclobut-1-ene-1,2-diyl)bis(azanediyl))bis(octan-1-aminium) (0.2 g, 0.41 mmol) in 2 mL of ethanol. The reaction mixture was allowed to reflux at 85 °C for 12 hrs. The title compound was a precipitate. (0.135 g, 0.19 mmol, 77 %). **^{1}H NMR** (500 MHz, DMSO-d_6, 358 K, ppm) δ 8.54 (d, J = 6 Hz, 1H), 8.45 (d, J = 8 Hz, 1H), 7.89 (t, J = 14 Hz, 1H), 7.13 (br s, 1H), 4.123 (m, 2H), 3.54 (m, 3x2H), 1.58 (m, 2H), 1.36 (m, 3x2H). **^{13}C NMR** (126 MHz, DMSO-d_6, 298 K, ppm) δ 190.9, 163.9, 134.8, 131.8, 131.2, 128.0, 127.7, 122.5, 56.5, 43.7, 29.1, 29.0, 27.9, 26.9, 26.3, 19.0, 1.6, with DMSO-d6 at 40 ppm. **IR** (film) ν_{max} (cm^{-1}): 3165,

2925, 2852, 1799 (C=O stretch), 1698 (C=O stretch), 1641, 1575, 1432, 1388, 1355, 1236, 1201, 1173, 1132, 1078, 1030, 846, 779, 720, 603, 546, 535, 521, 516, 509, 505. **HRMS** (ESI^+): m/z calculated for $C_{44}H_{46}N_4O_6$ $[M+H]^+$ requires 726.87, found 726.34 (-0.53 ppm).

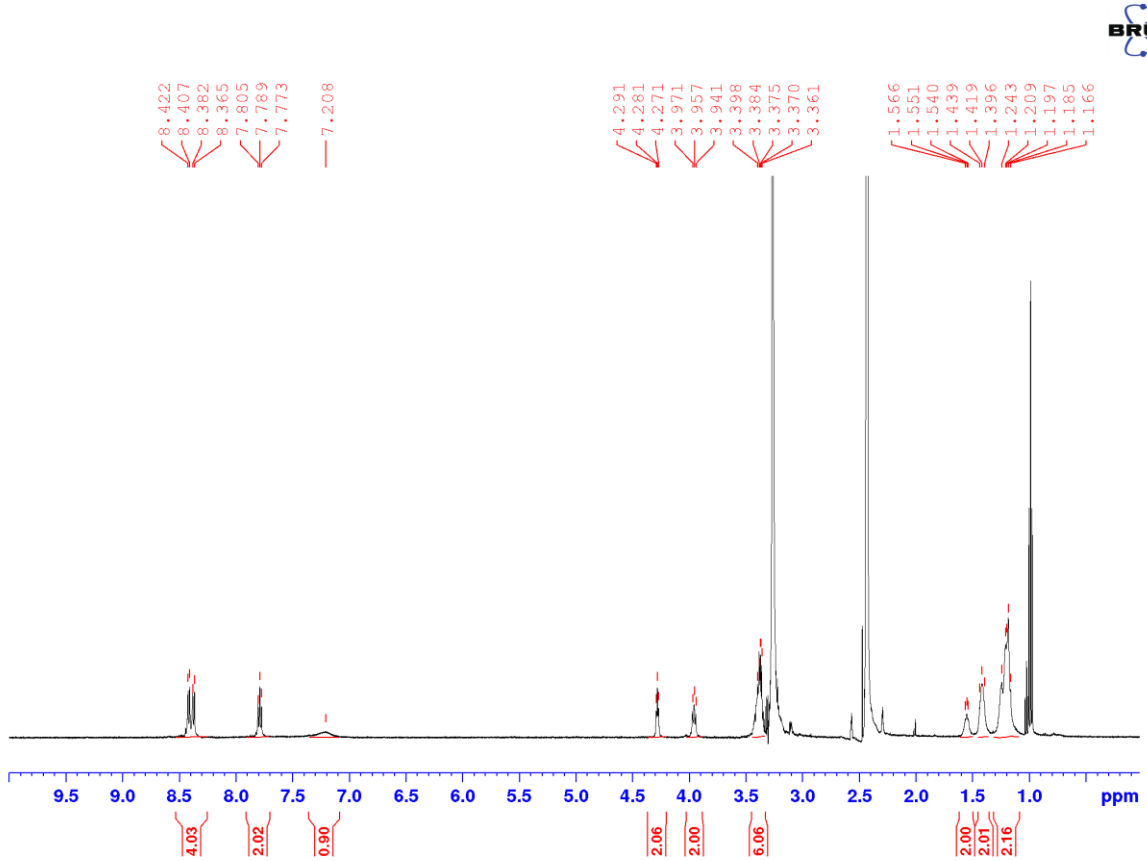

Figure 6.25: The ^{1}H NMR Spectrum of **40** (500 MHz, DMSO-d_6, 298 K.)

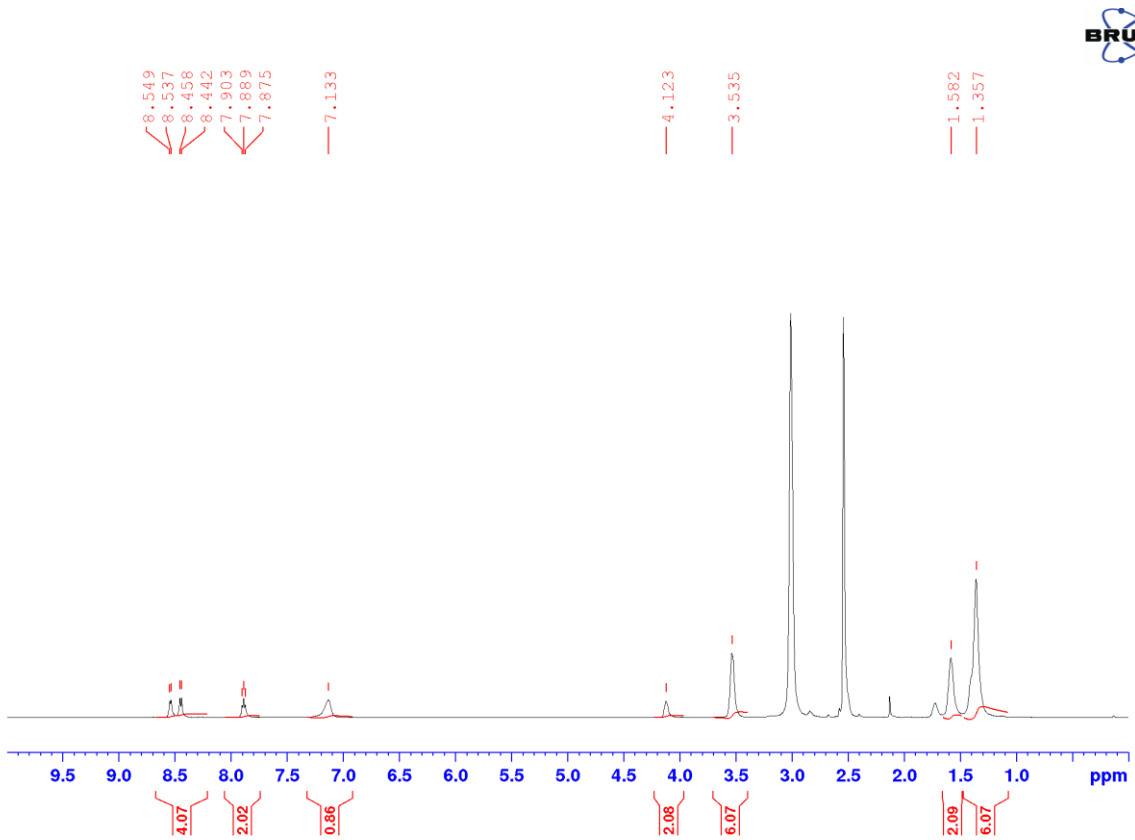

Figure 6.26: The ^{1}H NMR Spectrum of **40 at 358 K** (500 MHz, DMSO-d_6, 358 K.)

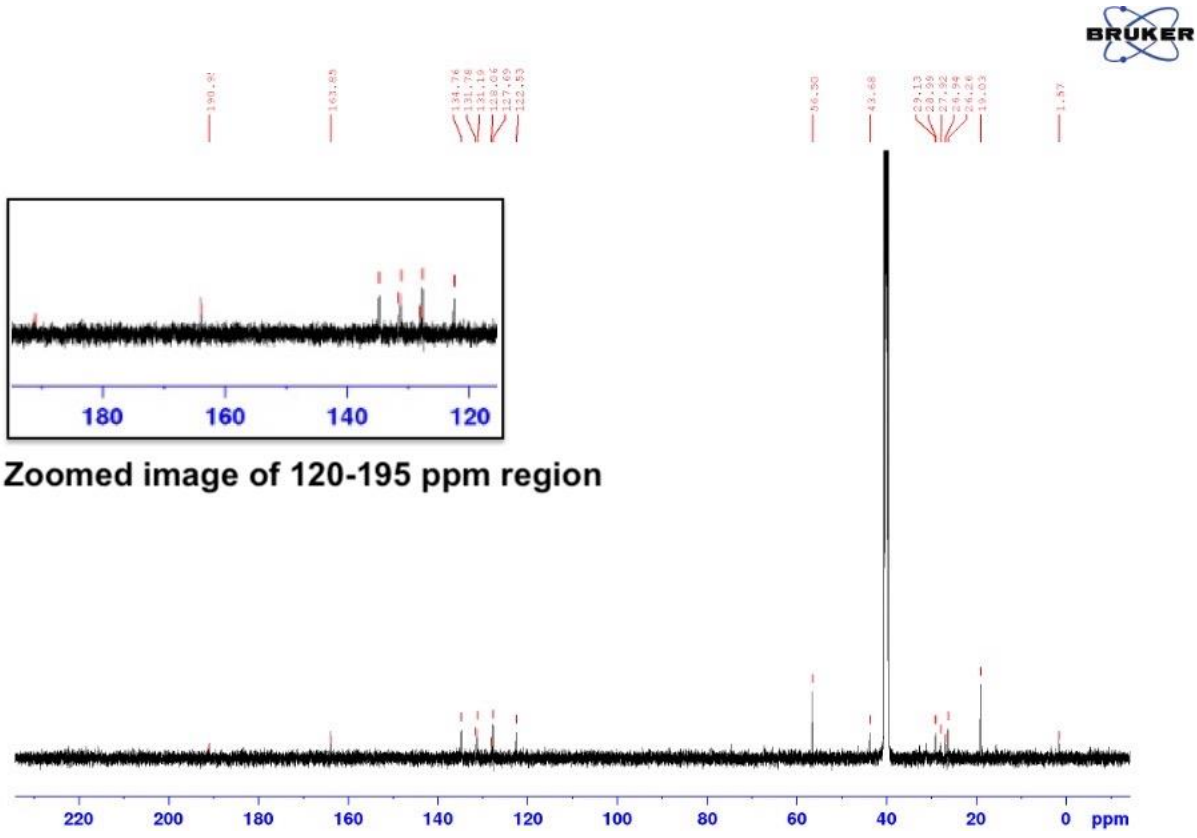

Figure 6.27: The ^{13}C NMR Spectrum of **40** (126 MHz, DMSO-d_6, 298 K.)

6-Nitro-2-(2-{2-[2-(6-nitro-1,3-dioxo-2*H*-2-azaphenalen-2-yl)ethylamino]-3,4-dioxo-1-cyclobuten-1-ylamino}ethyl)-2*H*-2-azaphenalene-1,3-dione (47)

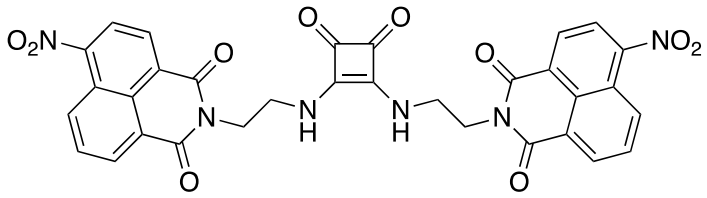

4-Nitronaphthalene-1,8-dicarboxylic anhydride (0.27 g, 1.1 mmol) was dissolved in ethanol (20 mL) and triethylamine (280 µL, 2.0 mmol) followed by a dropwise addition of dissolved 2,2'-((3,4-dioxocyclobut-1-ene-1,2-diyl)bis(azanediyl))bis(ethan-1-aminium) (0.20 g, 0.5 mmol) in 2 mL of ethanol. The reaction mixture was allowed to reflux at 85 °C for 12 hrs. The title compound was a precipitate. (0.172 g, 0.26 mmol, 86 %). **^{1}H NMR** (500 MHz, DMSO-d_6, 358 K, ppm) δ 8.59 (m, 1H), 8.01 (t, J = 15.5 Hz, 1H), 7.53 (br s, 1H), 4.25 (m, 2H), 3.77 (m, 2H). **^{13}C NMR** (126 MHz, DMSO-d_6, 298 K, ppm) δ 183.4, 168.7, 164.1, 134.7, 131.5, 131.0, 127.7, 127.5, 122.4, 56.5, 49.1, 19.0, with DMSO-d6 at 40 ppm. **IR** (film) ν_{max} (cm^{-1}): 3302, 1795 (C=O stretch), 1691 (C=O stretch), 1651, 1625, 1583, 1537, 1463, 1441, 1416, 1385, 1339, 1315, 1280, 1233, 1168, 1143, 1120, 1102, 1043, 877, 855, 844, 788, 774, 739, 669, 617, 567, 542, 522. **HRMS** (ESI^{+}): m/z calculated for $C_{38}H_{34}N_4O_6$ $[M+H]^+$ requires 642.2509, found 642.2367 (-0.48 ppm).

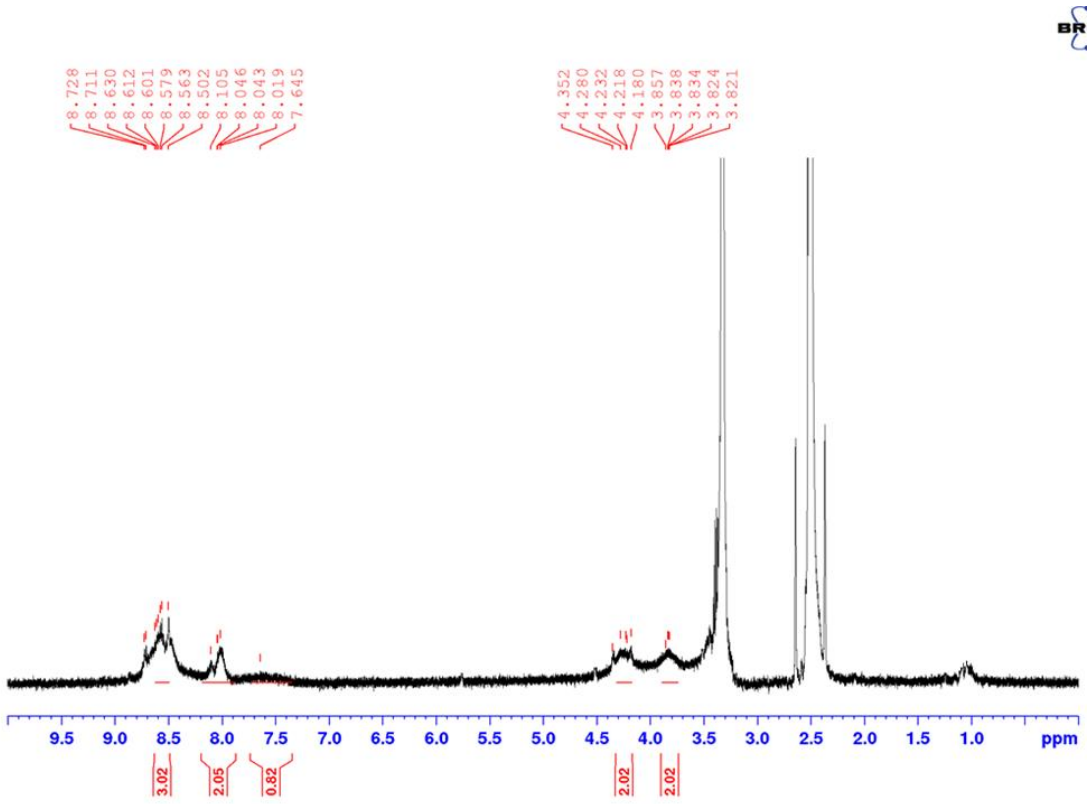

Figure 6.28: The ^{1}H NMR Spectrum of **47** (500 MHz, DMSO-d_6, 298 K.)

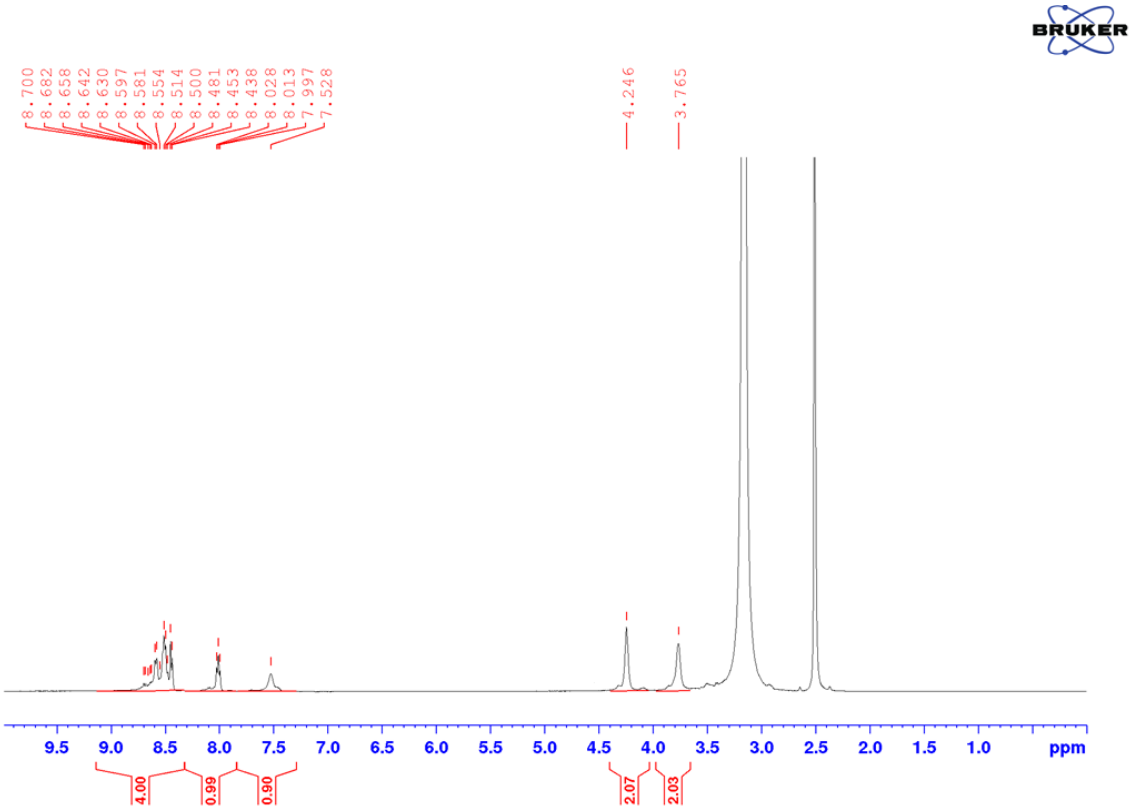

Figure 6.29: The ^{1}H NMR Spectrum of **47 at 358 K** (500 MHz, DMSO-d_6, 358 K.)

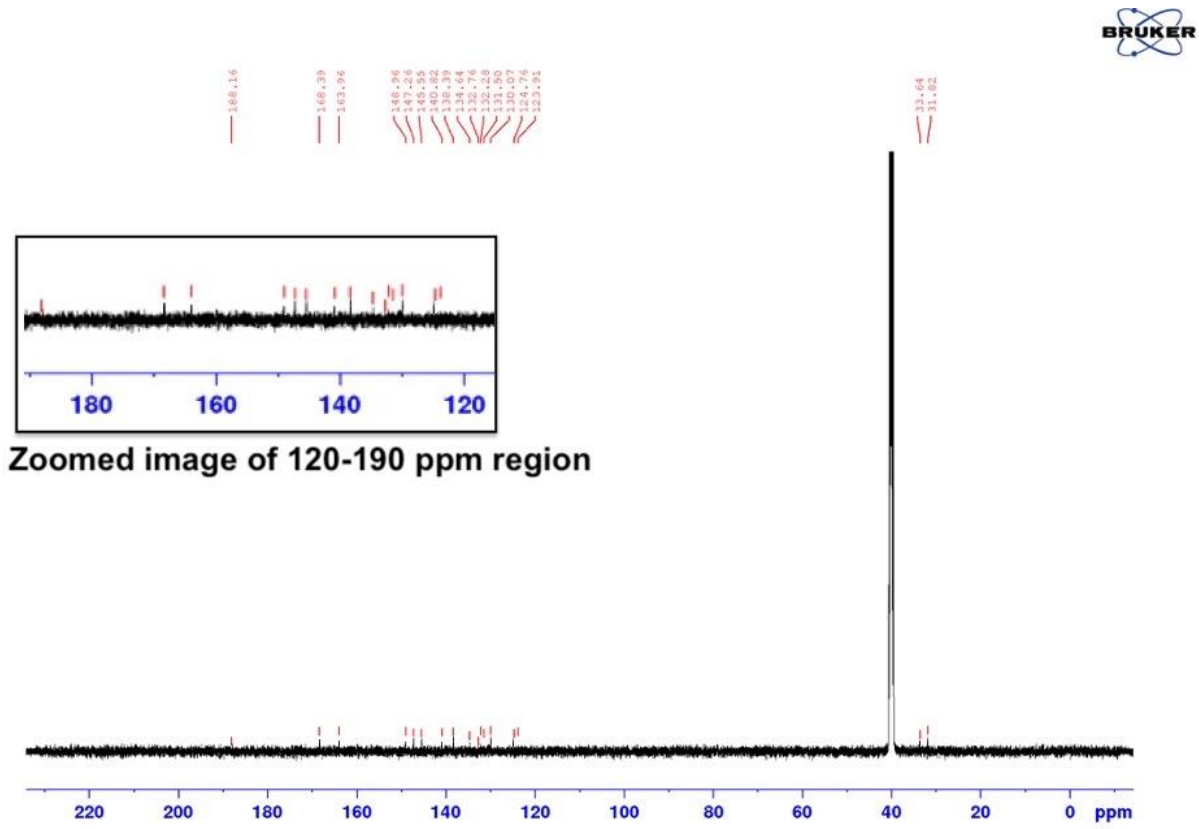

Figure 6.30: The ^{13}C NMR Spectrum of **47** (126 MHz, DMSO-d_6, 298 K.)

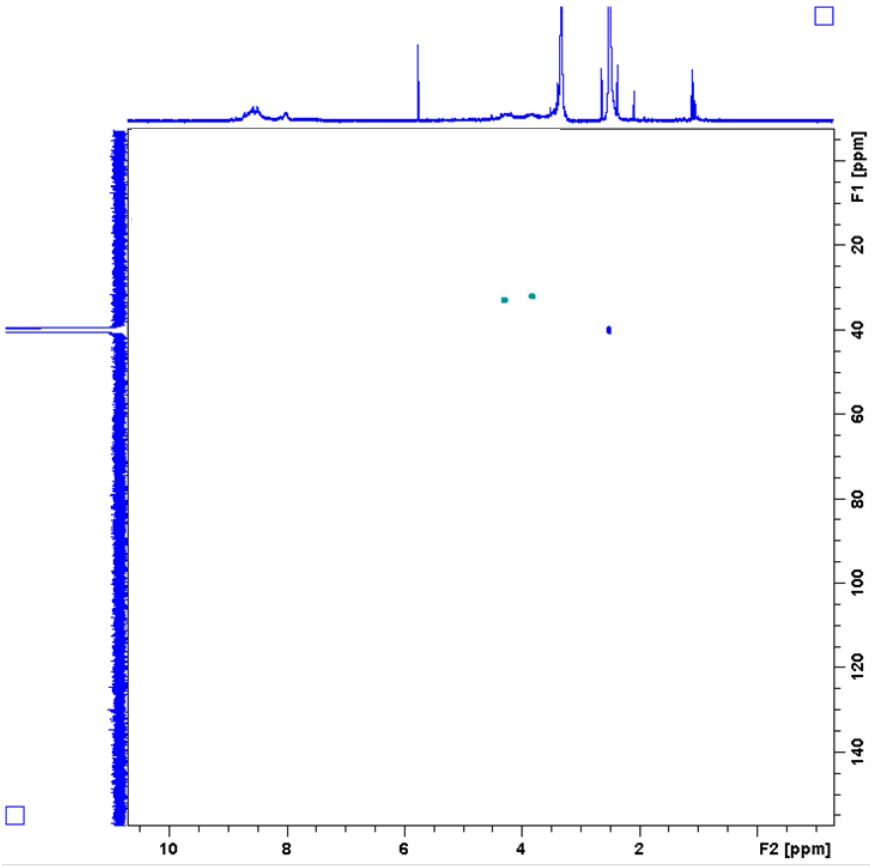

Figure 6.31: The HSQC Spectrum of **47** (126 MHz, DMSO-d_6, 298 K.)

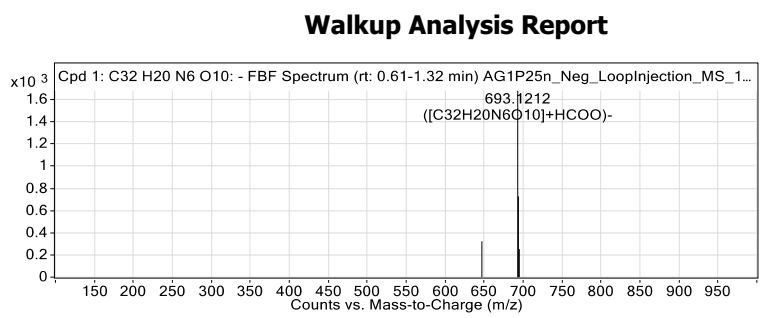

Figure 6.32: HRMS spectrum of **47**.

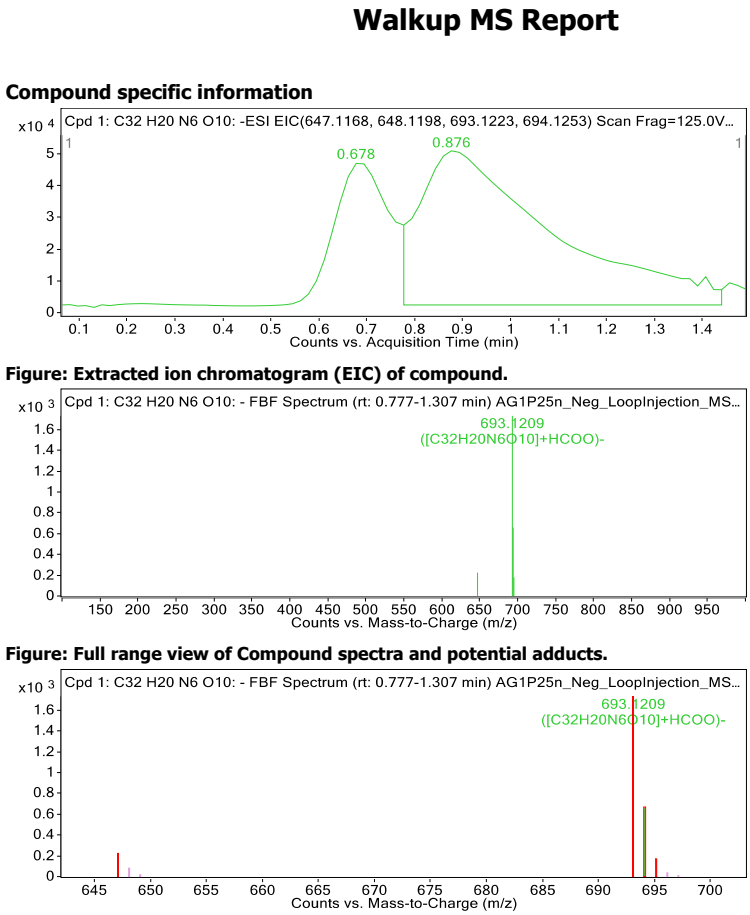

Figure 6.33: HRMS spectrum of **47.**

6-Nitro-2-(5-{2-[5-(6-nitro-1,3-dioxo-2*H*-2-azaphenalen-2-yl)pentylamino]-3,4-dioxo-1-cyclobuten-1-ylamino}pentyl)-2*H*-2-azaphenalene-1,3-dione (48)

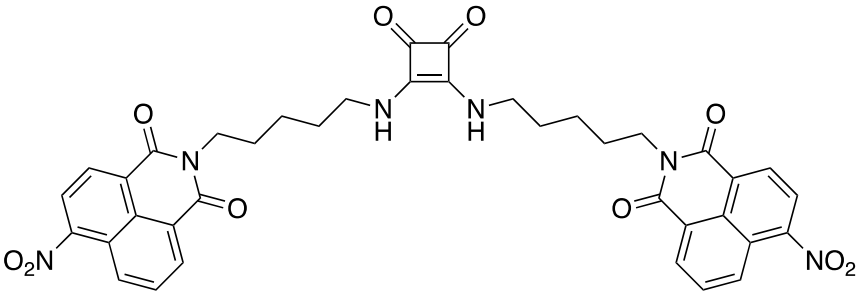

4-Nitronaphthalene-1,8-dicarboxylic anhydride (0.22 g, 0.91 mmol) was dissolved in ethanol (20 mL) and triethylamine (232 µL, 1.65 mmol) followed by a dropwise addition of dissolved 5,5'-(3,4-dioxocyclobut-1-ene-1,2-diyl)bis(azanediyl))bis(pentan-1-aminium) (0.2 g, 0.41 mmol) in 2 mL of ethanol. The reaction mixture was allowed to reflux at 85 °C for 12 hrs. The title compound was a precipitate. (0.162 g, 0.22 mmol, 88 %). **^{1}H NMR** (500 MHz, DMSO-d_6, 358 K, ppm) δ 8.60 (m, 1H), 8.07 (t, J = 16 Hz, 1H), 7.19 (br s, 1H), 4.10 (m, 2H), 3.499 (q, J = 14 Hz, 2H), 1.76 (m, 2H), 1.61 (t, J = 14 Hz, 2H), 1.46 (m, 2H). **^{13}C NMR** (126 MHz, DMSO-d_6, 298 K, ppm) δ 181.0, 163.5, 162.7, 149.6, 132.0, 130.5, 130.0, 130.0, 129.2, 128.8, 127.1, 124.7, 123.2, 123.2, 55.4, 43.6, 27.5, 24.5, 24.4, 23.9, with DMSO-d6 at 40 ppm. **IR** (film) ν_{max} (cm^{-1}): (2936, 1801 (C=O stretch), 1702 (C=O stretch), 1656, 1623, 1583, 1524, 1436, 1409, 1339, 1229, 1183, 1064, 871, 835, 786, 760, 732, 711, 582, 568, 544, 538, 526. **HRMS** (ESI^+): m/z calculated for $C_{38}H_{34}N_4O_6$ $[M+H]^+$ requires 732.71, found 732.21 (-0.50 ppm).

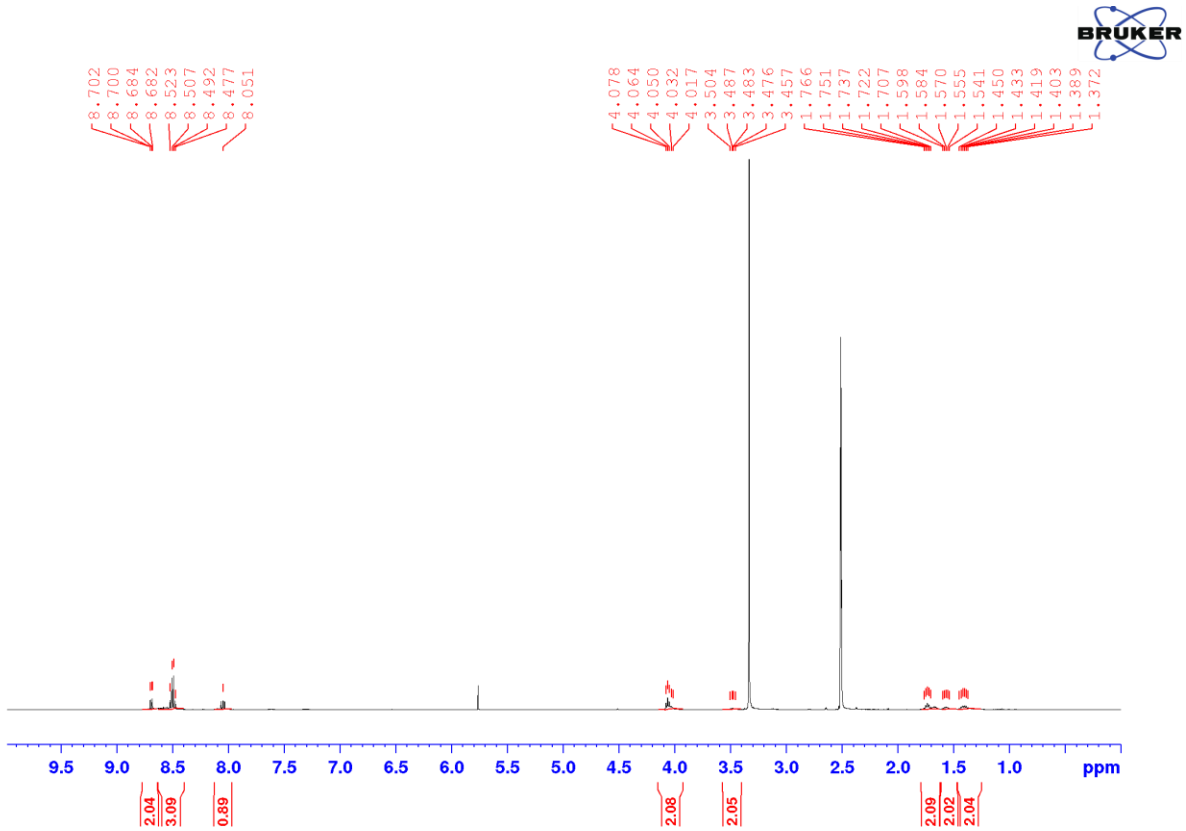

Figure 6.34: The ^{1}H NMR Spectrum of **48** (500 MHz, DMSO-d_6, 298 K.)

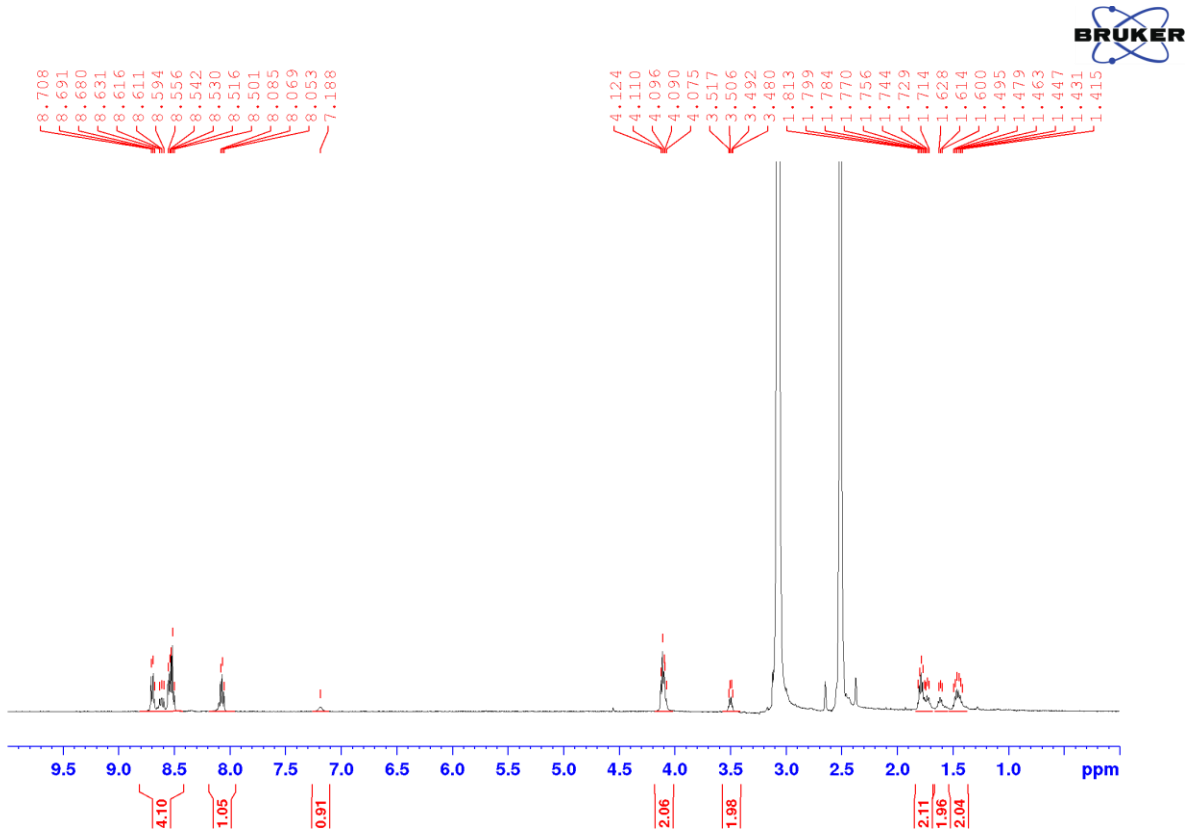

Figure 6.35: The ^{1}H NMR Spectrum of **48 at 358 K** (500 MHz, DMSO-d_6, 358 K.)

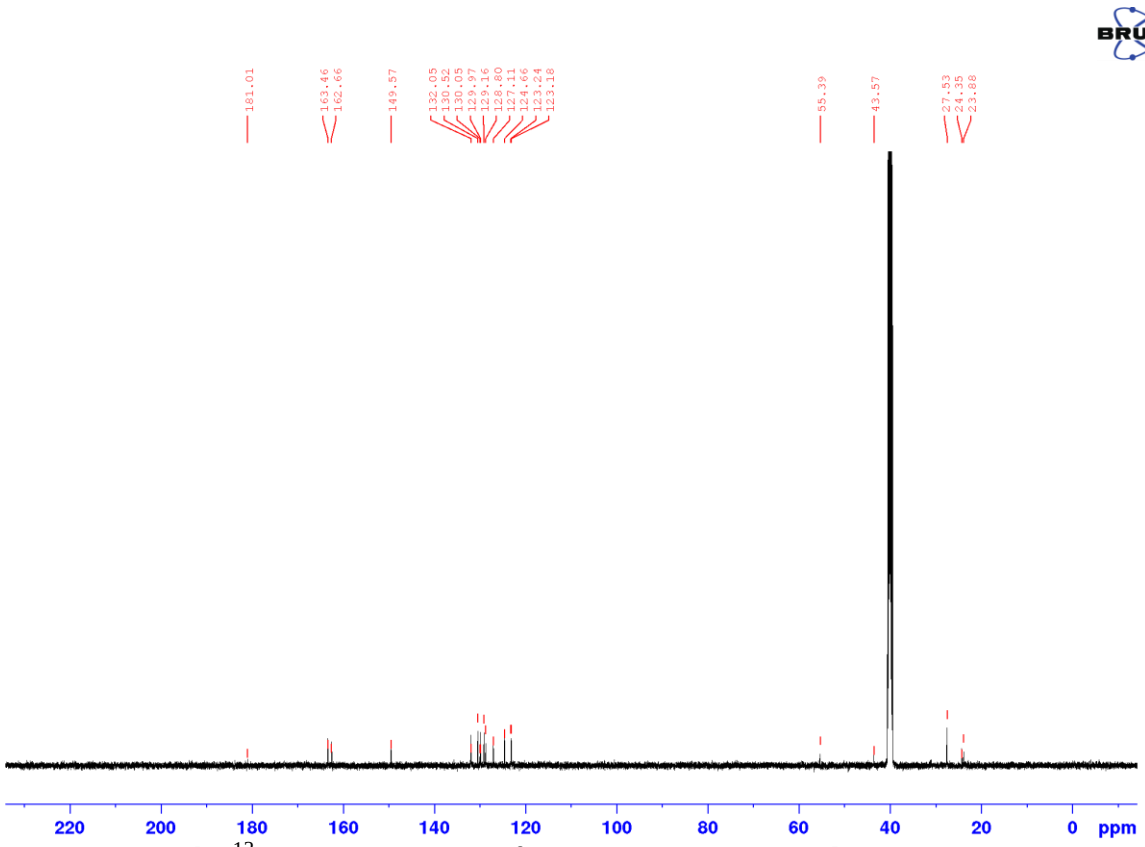

Figure 6.36: The ^{13}C NMR Spectrum of **48** (126 MHz, DMSO-d_6, 298 K.)

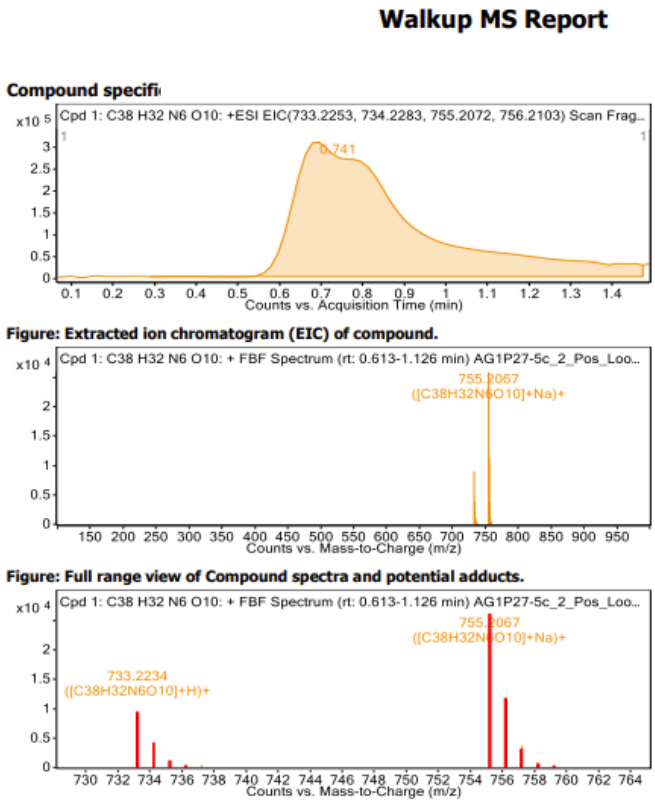

Figure 6.37: HRMS spectrum of **48.**

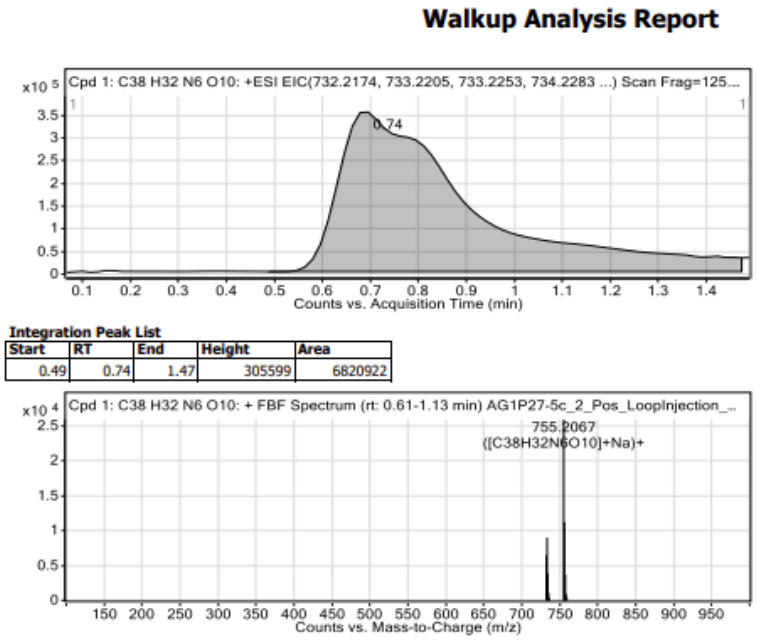

Figure 6.38: HRMS spectrum of **48.**

6-Nitro-2-(8-{2-[8-(6-nitro-1,3-dioxo-2*H*-2-azaphenalen-2-yl)octylamino]-3,4-dioxo-1-cyclobuten-1-ylamino}octyl)-2*H*-2-azaphenalene-1,3-dione (49)

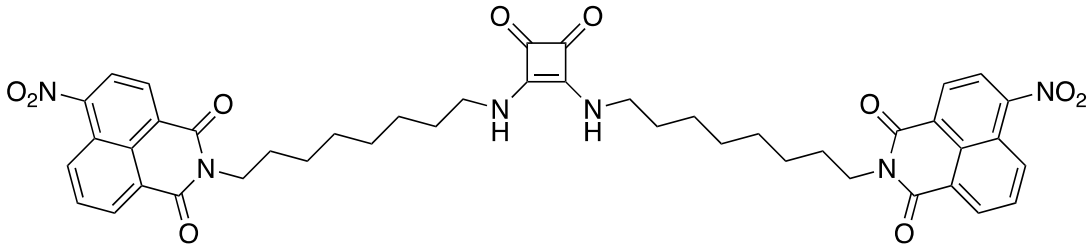

4-Nitronaphthalene-1,8-dicarboxylic anhydride (0.189 g, 0.77 mmol) was dissolved in ethanol (20 mL) and triethylamine (197 µL, 1.41 mmol) followed by a dropwise addition of dissolved 8,8'-((3,4-dioxocyclobut-1-ene-1,2-diyl)bis(azanediyl))bis(octan-1-aminium) (0.2 g, 0.35 mmol) in 2 mL of ethanol. The reaction mixture was allowed to reflux at 85 °C for 12 hrs. The title compound was a precipitate. (0.158 g, 0.19 mmol, 79 %). **^{1}H NMR** (500 MHz, DMSO-d_6, 358 K, ppm) δ 8.59 (m, 1H), 8.07 (m, 1H), 7.18 (br s, 1H), 4.052 (q, J = 20.5 Hz, 2H), 1.67 (t, J = 11 Hz, 2H), 1.53 (t, J = 11 Hz, 2H), 1.344 (m, 5x2H). **^{13}C NMR** (126 MHz, DMSO-d_6, 298 K, ppm) δ 188.2, 168.4, 163.3, 149.5, 133.7, 132.1, 131.6, 130.8, 130.5, 130.3, 130.0, 129.1, 124.8, 124.7, 123.1, 43.7, 34.4, 31.2, 29.1, 28.9, 27.7, 26.9, 26.2, with DMSO-d6 at 40 ppm. **IR** (film) ν_{max} (cm^{-1}): (3168, 2926, 2851, 1797 (C=O stretch), 1704 (C=O stretch), 1663, 1568, 1527, 1435, 1347, 1231, 1087, 1035, 1027, 835, 785, 761, 728, 615, 574, 563, 549, 539,

511. **HRMS** (ESI$^+$): m/z calculated for $C_{44}H_{44}N_6O_{10}$ $[M+H]^+$ requires 816.87, found 816.31 (-0.56 ppm).

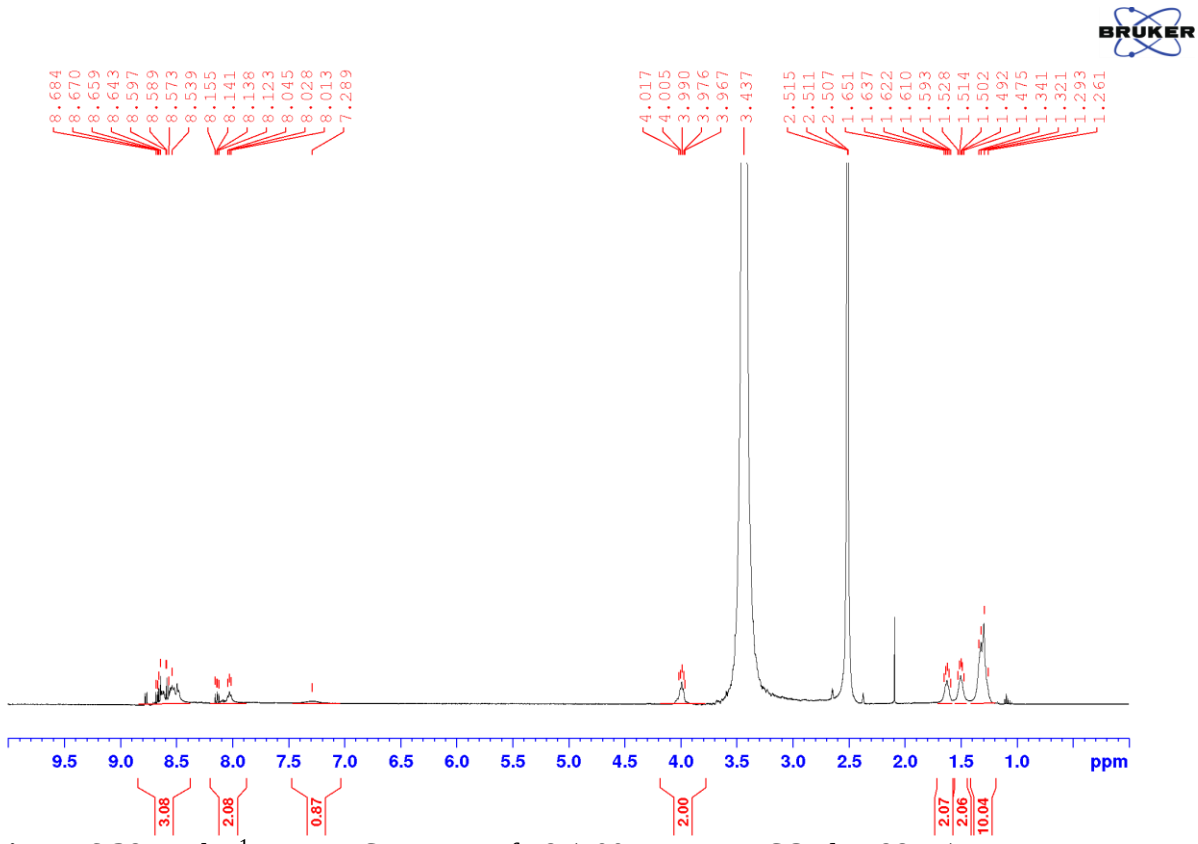

Figure 6.39: The ^{1}H NMR Spectrum of **49** (500 MHz, DMSO-d_6, 298 K.)

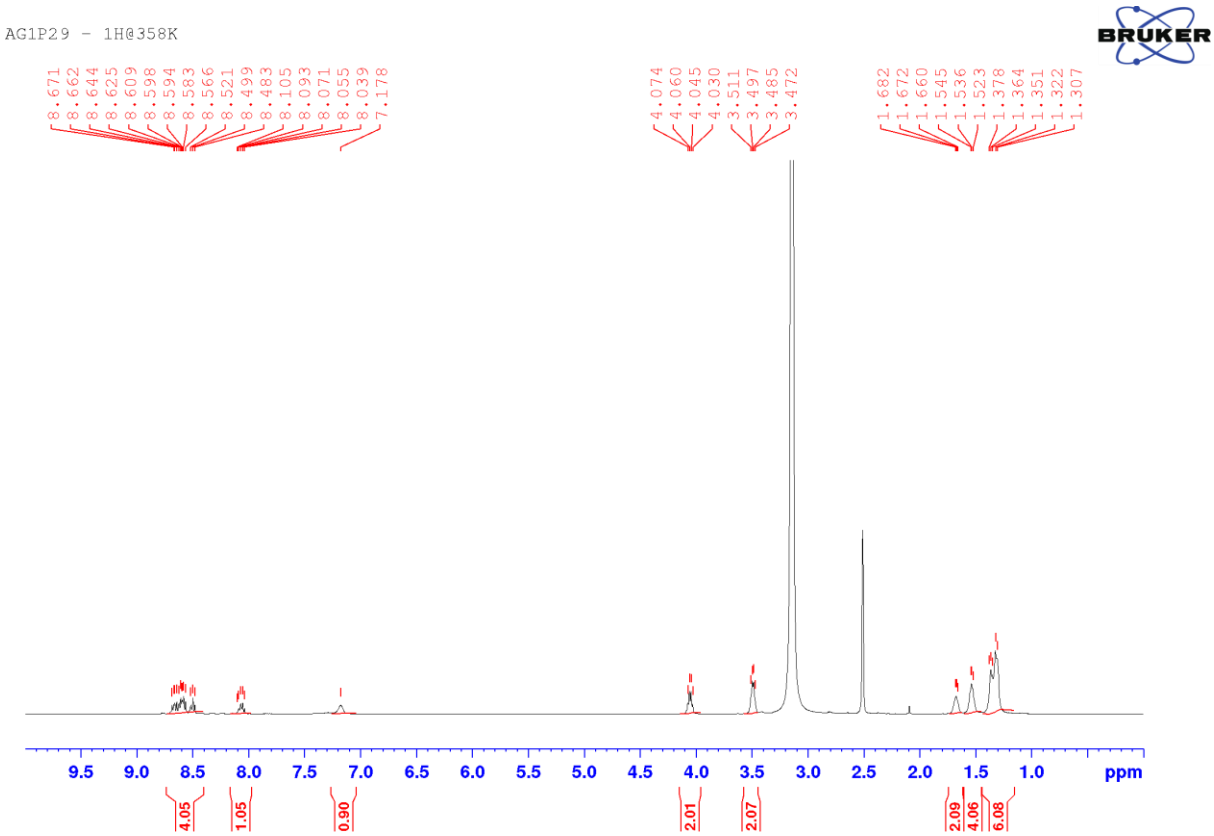

Figure 6.40: The ^{1}H NMR Spectrum of **49 at 358 K** (500 MHz, DMSO-d_6, 358 K.)

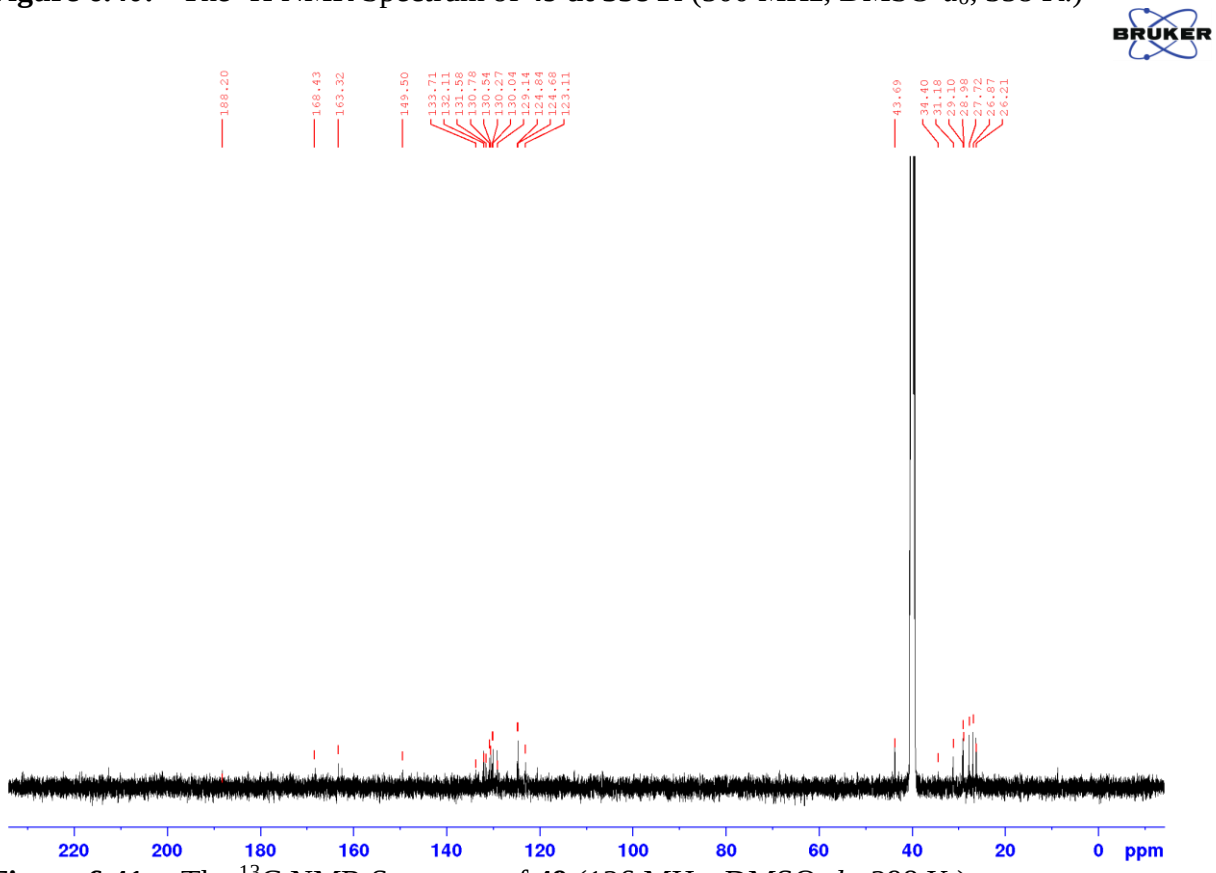

Figure 6.41: The ^{13}C NMR Spectrum of **49** (126 MHz, DMSO-d_6, 298 K.)

Compound specific information

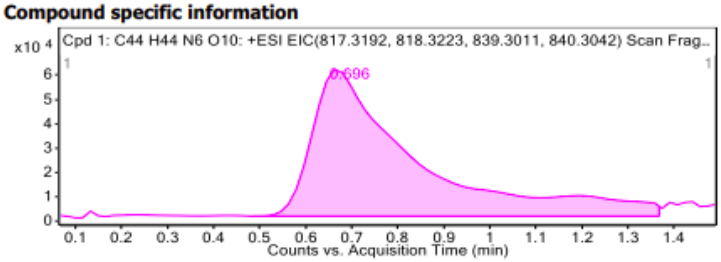

Figure: Extracted ion chromatogram (EIC) of compound.

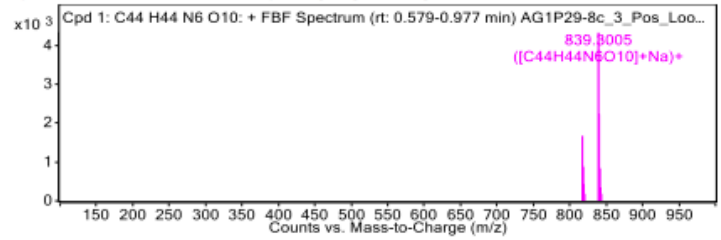

Figure: Full range view of Compound spectra and potential adducts.

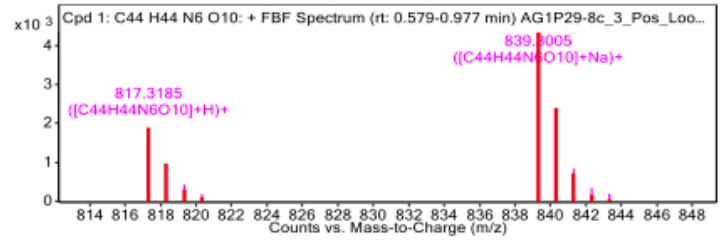

Figure 6.42: HRMS spectrum of **49.**

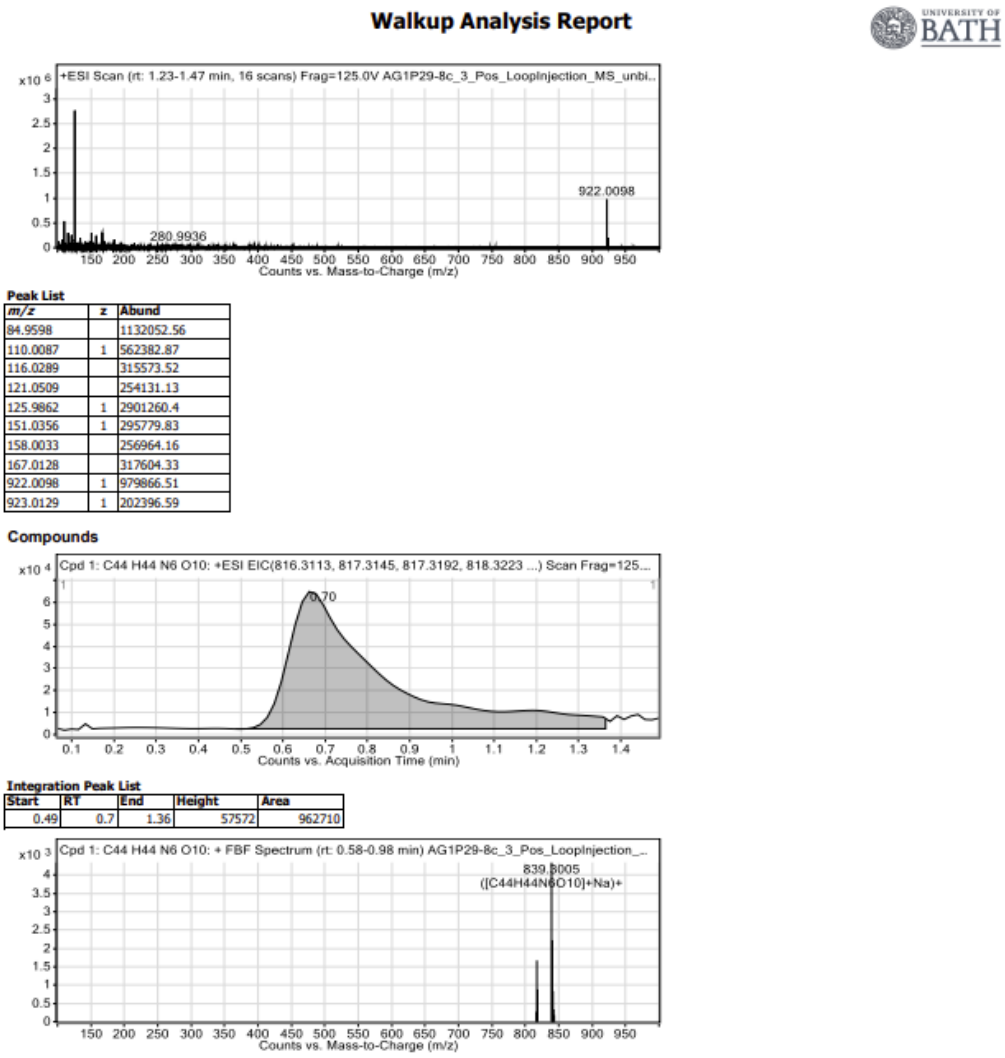

Figure 6.43: HRMS spectrum of **49.**

2-[8-(1,3-Dioxo-2*H*-2-azaphenalen-2-yl)octyl]-2*H*-2-azaphenalene-1,3-dione (97)

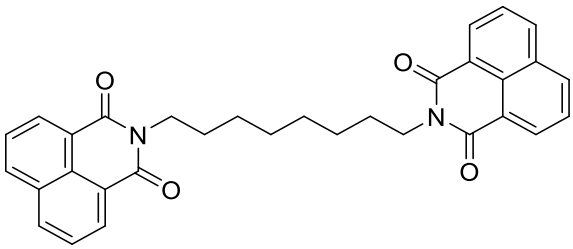

Naphthalene-1,8-dicarboxylic anhydride (0.60 g, 3.0 mmol) was dissolved in ethanol (20 mL) and triethylamine (775 µL, 5.5 mmol) followed by a dropwise addition of dissolved 1,8-octanediamine (0.20 g, 1.4 mmol) in 2 mL of ethanol. The reaction mixture was allowed to reflux at 85 °C for 12 hrs. The title compound was concentrated in-vacuo, which afforded a precipitate. The product was purified from column chromatography with 90% DCM, 10% MeOH. (0.17 g, 0.37 mmol, 84 %). **^{1}H NMR** (500 MHz, DMSO-d_6, 358 K, ppm) δ 8.50 (s, 1H), 8.42 (s, 1H), 4.07 (s, 2x2H), 1.67 (s, 2x2H), 1.36 (s, 4x2H). **^{13}C NMR** (126 MHz, DMSO-d_6, 298 K, ppm) δ 163.6, 162.7, 162.0, 138.1, 136.5, 134.8, 132.9, 132.0, 130.4, 129.1, 125.1, 122.5, 120.7, 55.3, 45.2, 43.9, 36.3, 31.2, 30.5, 19.1, 14.0, with DMSO-d6 at 40 ppm. **IR** (film) ν_{max} (cm^{-1}): 2929, 2865, 1688 (C=O stretch), 1651, 1624, 1586, 1514, 1474, 1458, 1437, 1414, 1386, 1340, 1320, 1266, 1240, 1230, 1197, 1184, 1163, 1138, 1101, 1075, 1033, 1007, 952, 899, 877, 845, 800, 774, 732, 689, 630, 606, 594, 583, 570, 558, 546, m544, 536, 534, 521, 495. **HRMS** (ESI^{+}): m/z calculated for $C_{32}H_{28}N_2O_4$ $[M+H]^+$ requires 505.59, found 505.07 (-0.52 ppm).

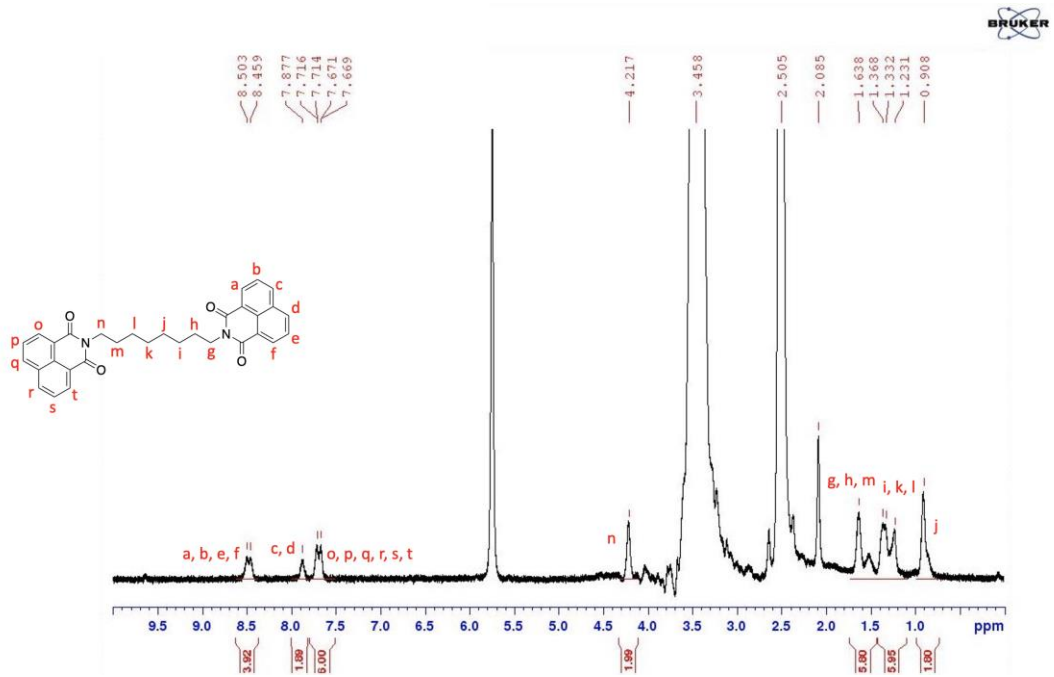

Figure 6.44: The ^{1}H NMR Spectrum of **97** (500 MHz, DMSO-d_6, 298 K.)

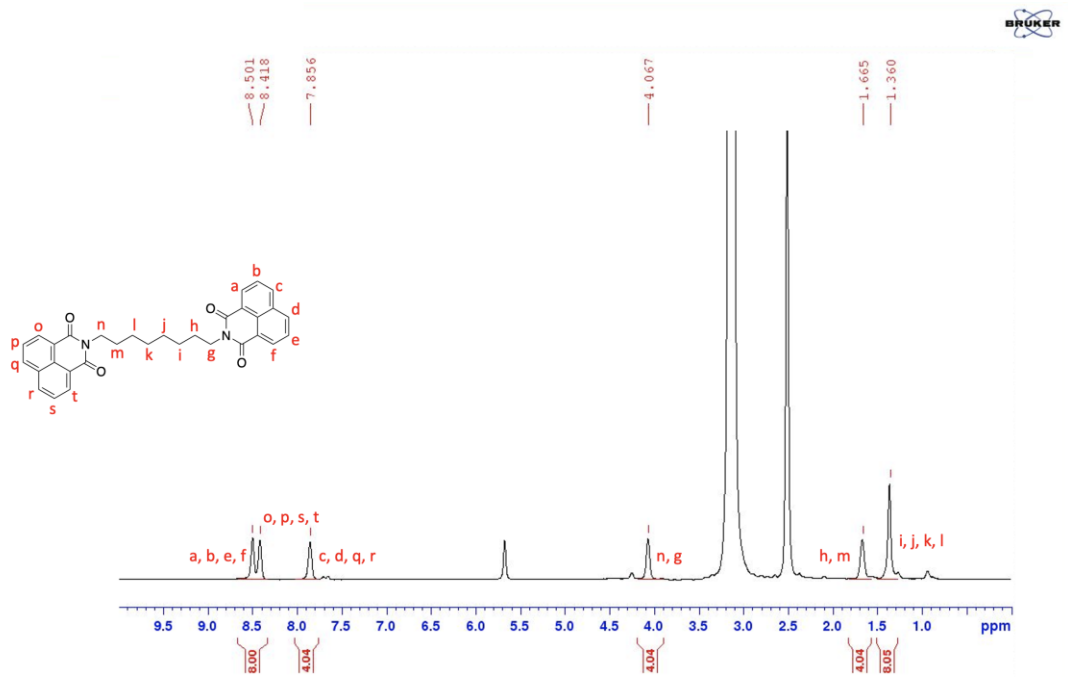

Figure 6.45: The ^{1}H NMR Spectrum of **97 at 358 K** (500 MHz, DMSO-d_6, 358 K.)

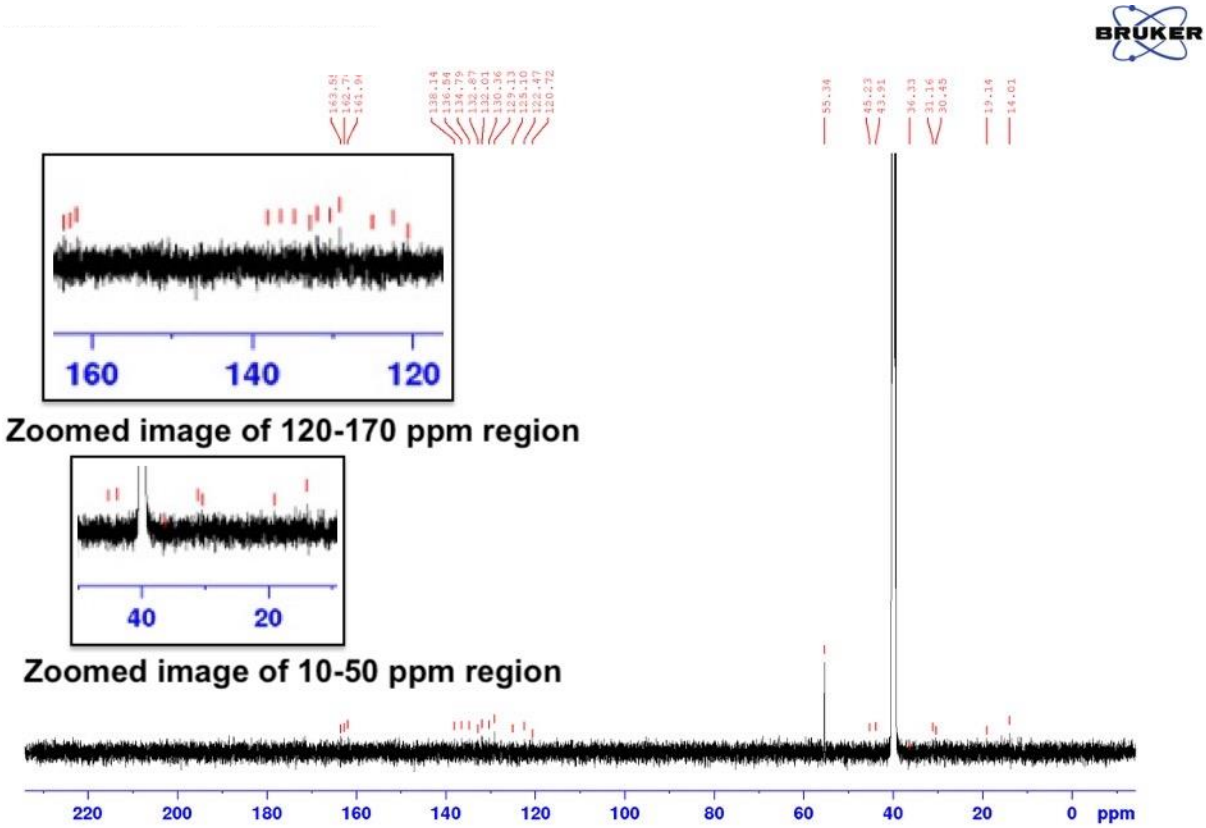

Figure 6.46: The ^{13}C NMR Spectrum of **97** (126 MHz, DMSO-d_6, 298 K.)

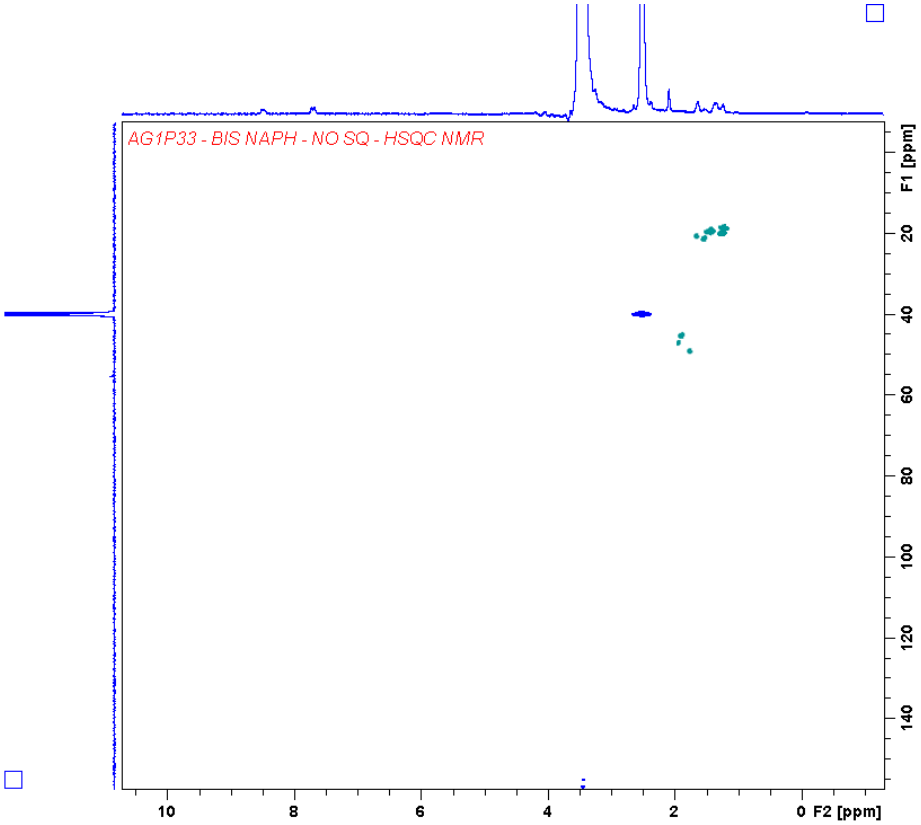

Figure 6.47: The HSQC Spectrum of **97** (126 MHz, DMSO-d_6, 298 K.).

2-Butyl-2*H*-2-azaphenalene-1,3-dione (98)

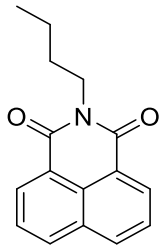

Naphthalene-1,8-dicarboxylic anhydride (0.60 g, 3.0 mmol) was dissolved in ethanol (20 mL) and triethylamine (775 µL, 5.5 mmol) followed by a dropwise addition of 1-aminobutane (0.20 g, 1.4 mmol) in 2 mL of ethanol. The reaction mixture was allowed to reflux at 85 °C for 12 hrs. The product was purified from column chromatography with 95% DCM, 5% MeOH. The title compound was a precipitate (0.17 g, 0.37 mmol, 83 %). **^{1}H NMR** (500 MHz, DMSO-d_6, 298 K, ppm) δ 8.41 (m, 1H), 7.82 (q, J = 15.5 Hz, 1H), 4.00 (t, J = 15 Hz, 2H), 1.58 (m, 2H), 1.33 (m, 2H), 0.91 (t, J = 15 Hz, 3H). **^{13}C NMR** (126 MHz, DMSO-d_6, 298 K, ppm) δ 163.8, 134.7, 131.7, 131.1, 127.7, 127.6, 122.4, 55.4, 30.1, 20.3, 14.2, with DMSO-d6 at 40 ppm. **IR** (film) ν_{max} (cm^{-1}): 3706, 3680, 3665, 2972, 2949, 2922, 2866, 2844, 2826, 2076, 2053,

1696 (C=O stretch), 1654, 1623, 1590, 1511, 1466, 1454, 1437, 1414, 1386, 1346, 1260, 1234, 1204, 1194, 1136, 1115, 1063, 1057, 1051, 1032, 1016, 936, 869, 846, 797, 779, 737, 686, 651, 565, 556, 550, 546, 539, 530, 523, 500. **HRMS** (ESI^+): m/z calculated for $C_{16}H_{15}NO_2$ $[M+H]^+$ requires 254.11, found 253.67 (-0.44 ppm).

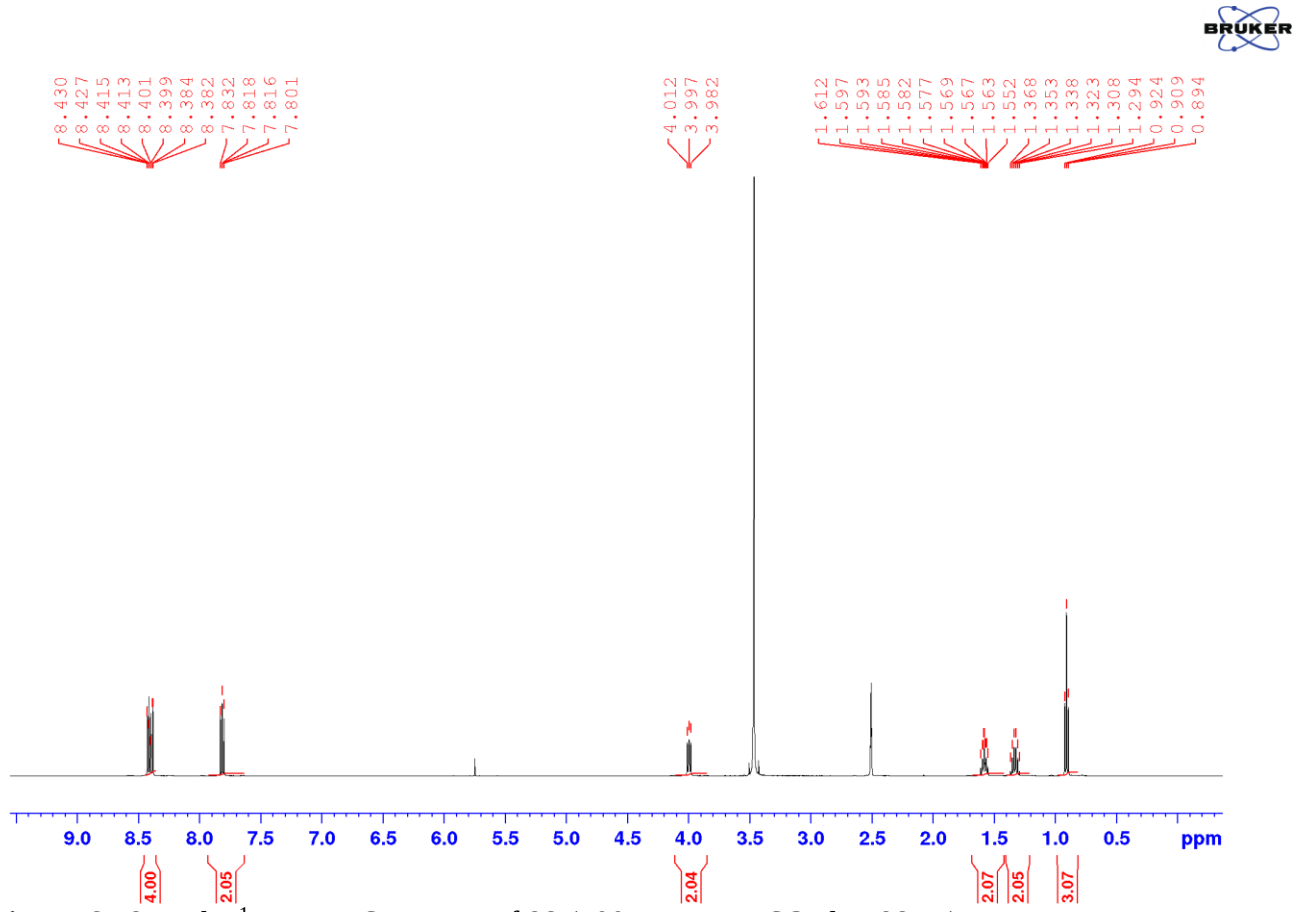

Figure 6.48: The ^{1}H NMR Spectrum of **98** (500 MHz, DMSO-d_6, 298 K.)

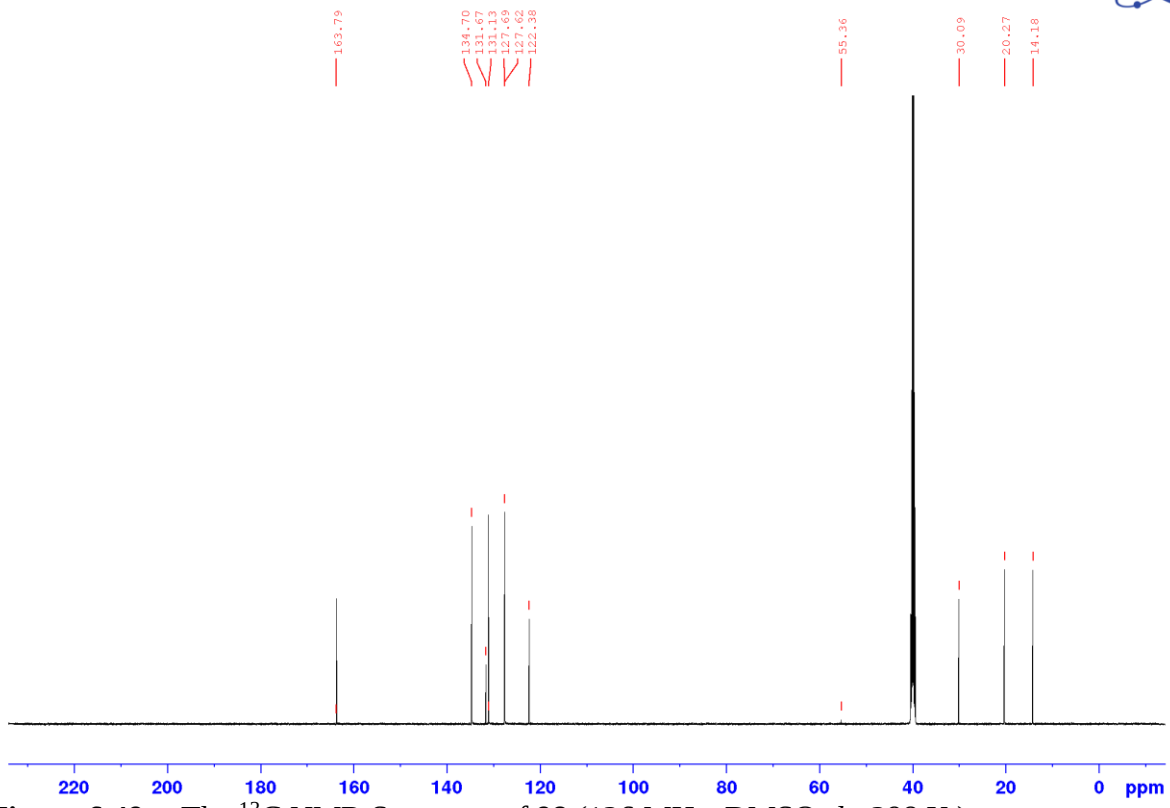

Figure 6.49: The ^{13}C NMR Spectrum of **98** (126 MHz, DMSO-d_6, 298 K.)

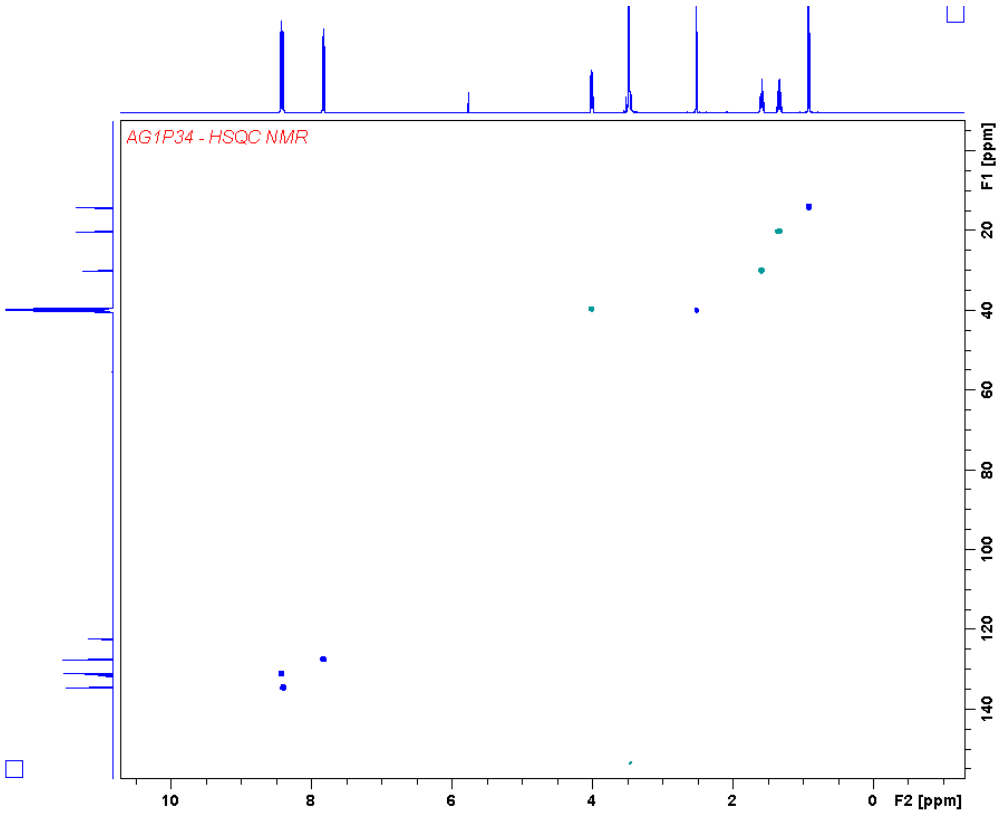

Figure 6.50: The HSQC Spectrum of **98** (126 MHz, DMSO-d_6, 298 K.)

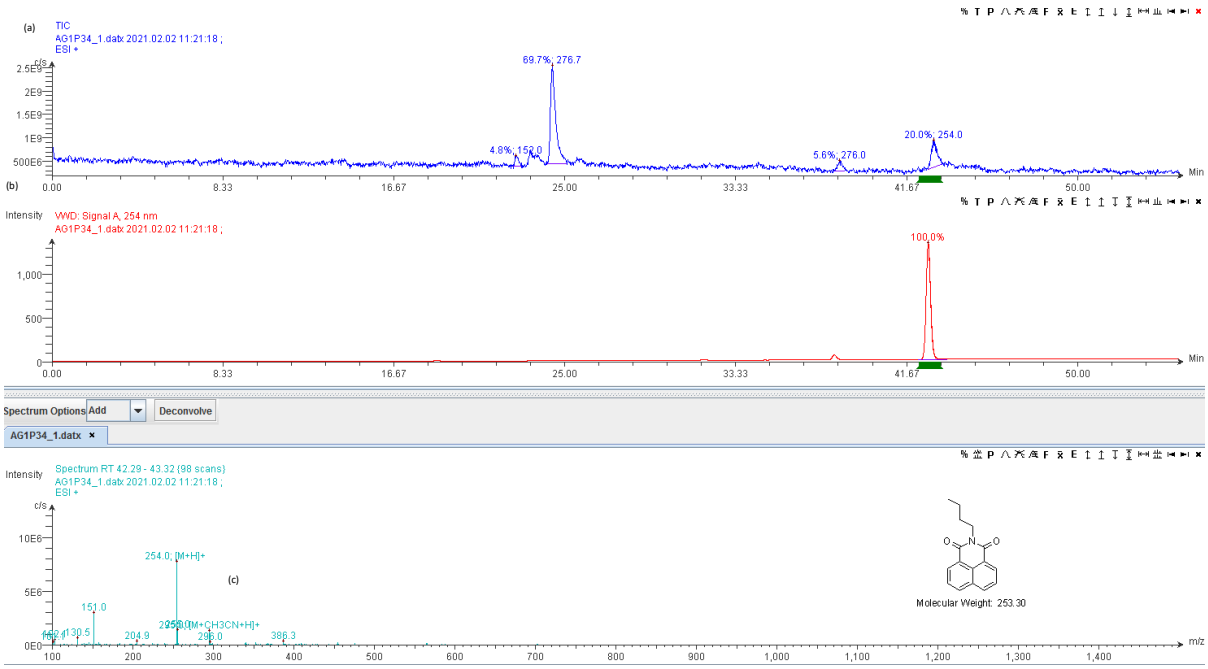

Figure 6.51: LCMS Characterisation of 98: (a) Analytical HPLC trace of precipitate 98; R_t = 43.0 mins (0-100% MeCN over 30 mins, λ = 254 nm). (b) Extracted Ion Chromatogram for 254.3 $[M + H]^+$. (c) Mass Spectrum detected between R_t = 43.0-45.0 mins (354 scans); Calculated for $[M + H]^+$ = 254.3; Mass Found (ESI^+) = 254.0 [M + H]+. Also found 295.0 [M + CH3CN + H]+.

Chapter 7 References

1. Watson, J. D.; Crick, F. H., Genetical implications of the structure of deoxyribonucleic acid. *Nature* **1953,** *171* (4361), 964-967.
2. Doynova, M.; Berretta, A.; Jones, M. B.; Jasoni, C.; Vickers, M.; O'Sullivan, J., Interactions between mitochondrial and nuclear DNA in mammalian cells are non-random. *Mitochondrion* **2016,** *30*, 187-196.
3. Alberts, B.; Johnson, A.; Lewis, J.; Raff, M.; Roberts, K.; Walter, P., The structure and function of DNA. In *Molecular Biology of the Cell. 4th edition*, Garland Science: 2002.
4. Britten, R. J.; Davidson, E. H., Gene regulation for higher cells: a theory. *Science* **1969,** *165* (3891), 349-357.
5. Travers, A.; Muskhelishvili, G.; Thompson, J., DNA information: from digital code to analogue structure. *Philosophical Transactions of the Royal Society A: Mathematical, Physical and Engineering Sciences* **2012,** *370* (1969), 2960-2986.
6. Kool, E. T.; Morales, J. C.; Guckian, K. M., Mimicking the structure and function of DNA: insights into DNA stability and replication. *Angewandte Chemie International Edition* **2000,** *39* (6), 990-1009.
7. Dragoman, D.; Dragoman, M., Real-time detection of deoxyribonucleic acid bases via their negative differential conductance signature. *Physical Review E* **2009,** *80* (2), 022901.
8. Sinden, R. R., *DNA structure and function*. Elsevier: 2012.
9. Szabat, M.; Pedzinski, T.; Czapik, T.; Kierzek, E.; Kierzek, R., Structural Aspects of the Antiparallel and Parallel Duplexes Formed by DNA, 2'-O-Methyl RNA and RNA Oligonucleotides. *PloS one* **2015,** *10* (11).
10. Pray, L., Discovery of DNA structure and function: Watson and Crick. *Nature Education* **2008,** *1* (1), 100.
11. Bryce, C. F.; Pacini, D., *The structure and function of nucleic acids*. Biochemical Society: 1994.
12. Alberts, B.; Johnson, A.; Lewis, J.; Morgan, D.; Raff, M.; Roberts, K.; Walter, P., MBOC6 Custom Textbook-University of Toronto-BIO230H: Molecular Biology of the Cell, Custom E-book Rental. **2015**.
13. Alberts, B., Molecular Biology of the Cell in Cell 4th. Figure: 2002.
14. Minchin, S.; Lodge, J., Understanding biochemistry: structure and function of nucleic acids. *Essays in biochemistry* **2019,** *63* (4), 433-456.
15. Saier, M. H., Understanding the genetic code. *Journal of bacteriology* **2019,** *201* (15), e00091-19.
16. Travers, A.; Muskhelishvili, G., DNA structure and function. *The FEBS journal* **2015,** *282* (12), 2279-2295.
17. Cozzarelli, N.; Boles, T.; White, J. H., Primer on the topology and geometry of DNA supercoiling. *DNA topology and its biological Effects* **1990**, 139-184.
18. Levitt, M., How many base-pairs per turn does DNA have in solution and in chromatin? Some theoretical calculations. *Proceedings of the National Academy of Sciences* **1978,** *75* (2), 640-644.
19. Poltev, V.; Anisimov, V. M.; Danilov, V. I.; Garcia, D.; Sanchez, C.; Deriabina, A.; Gonzalez, E.; Rivas, F.; Polteva, N., The role of molecular structure of sugar-phosphate backbone and nucleic acid bases in the formation of single-stranded and double-stranded DNA structures. *Biopolymers* **2014,** *101* (6), 640-650.
20. Šponer, J.; Mládek, A.; Šponer, J. E.; Svozil, D.; Zgarbová, M.; Banáš, P.; Jurečka, P.; Otyepka, M., The DNA and RNA sugar–phosphate backbone emerges as the key player. An overview of quantum-chemical, structural biology and simulation studies. *Physical Chemistry Chemical Physics* **2012,** *14* (44), 15257-15277.

21. Fortin, C. H.; Schulze, K. V.; Babbitt, G. A., TRX-LOGOS-a graphical tool to demonstrate DNA information content dependent upon backbone dynamics in addition to base sequence. *Source code for biology and medicine* **2015,** *10* (1), 10.
22. Yanagi, K.; Privé, G. G.; Dickerson, R. E., Analysis of local helix geometry in three B-DNA decamers and eight dodecamers. *Journal of molecular biology* **1991,** *217* (1), 201-214.
23. Roberts, M. A., Recombinant DNA technology and DNA sequencing. *Essays in biochemistry* **2019,** *63* (4), 457-468.
24. Dubey, R., *Advanced biotechnology*. S. Chand Publishing: 2014.
25. Lilley, D. M. J., *DNA-protein: structural interactions*. Oxford University Press, USA: 1995; Vol. 7.
26. Heiderscheit, E. A.; Eguchi, A.; Spurgat, M. C.; Ansari, A. Z., Reprogramming cell fate with artificial transcription factors. *FEBS letters* **2018,** *592* (6), 888-900.
27. Goverdhana, S.; Puntel, M.; Xiong, W.; Zirger, J.; Barcia, C.; Curtin, J.; Soffer, E.; Mondkar, S.; King, G.; Hu, J., Regulatable gene expression systems for gene therapy applications: progress and future challenges. *Molecular Therapy* **2005,** *12* (2), 189-211.
28. Kurmis, A. A.; Yang, F.; Welch, T. R.; Nickols, N. G.; Dervan, P. B., A pyrrole-imidazole polyamide is active against enzalutamide-resistant prostate cancer. *Cancer research* **2017,** *77* (9), 2207-2212.
29. Eckel, R.; Ros, R.; Ros, A.; Wilking, S. D.; Sewald, N.; Anselmetti, D., Identification of binding mechanisms in single molecule–DNA complexes. *Biophysical journal* **2003,** *85* (3), 1968-1973.
30. Krautbauer, R.; Pope, L. H.; Schrader, T. E.; Allen, S.; Gaub, H. E., Discriminating small molecule DNA binding modes by single molecule force spectroscopy. *FEBS letters* **2002,** *510* (3), 154-158.
31. Wanunu, M.; Tor, Y., *Methods for studying nucleic acid/drug interactions*. CRC Press: 2016.
32. Vladescu, I. D.; McCauley, M. J.; Nuñez, M. E.; Rouzina, I.; Williams, M. C., Quantifying force-dependent and zero-force DNA intercalation by single-molecule stretching. *Nature methods* **2007,** *4* (6), 517-522.
33. Almaqwashi, A. A.; Paramanathan, T.; Rouzina, I.; Williams, M. C., Mechanisms of small molecule–DNA interactions probed by single-molecule force spectroscopy. *Nucleic acids research* **2016,** *44* (9), 3971-3988.
34. Blackburn, G. M.; Gait, M. J.; Loakes, D.; Williams, D. M.; Grasby, J. A.; Egli, M.; Flavell, A.; Allen, S.; Fisher, J.; Pyle, A. M., *Nucleic acids in chemistry and biology*. Royal Society of Chemistry: 2006.
35. Fox, K. R.; Pommier, Y.; Nordén, B.; Chaires, J.; Gago, F.; Ho, M.-H.; Sheh, L.; Cardin, C.; Nielsen, P. E.; Graves, D., *DNA-targeting Molecules as Therapeutic Agents*. Royal Society of Chemistry: 2018.
36. Yang, X.-L.; Wang, A. H.-J., Structural studies of atom-specific anticancer drugs acting on DNA. *Pharmacology & therapeutics* **1999,** *83* (3), 181-215.
37. van Dam, L.; Korolev, N.; Nordenskiöld, L., Polyamine–nucleic acid interactions and the effects on structure in oriented DNA fibers. *Nucleic acids research* **2002,** *30* (2), 419-428.
38. Eichhorn, G. L.; Shin, Y. A., Interaction of metal ions with polynucleotides and related compounds. XII. The relative effect of various metal ions on DNA helicity. *Journal of the American Chemical Society* **1968,** *90* (26), 7323-7328.
39. Ozsoz, M. S., *Electrochemical DNA biosensors*. CRC Press: 2012.
40. Gessner, R. V.; Quigley, G. J.; Wang, A. H.; Van der Marel, G. A.; Van Boom, J. H.; Rich, A., Structural basis for stabilization of Z-DNA by cobalt hexaammine and magnesium cations. *Biochemistry* **1985,** *24* (2), 237-240.

41. Potyrailo, R. A.; Mirsky, V. M., Combinatorial methods for chemical and biological sensors: Outlook. In *Combinatorial Methods for Chemical and Biological Sensors*, Springer: 2009; pp 483-488.
42. Tongu, C.; Kenmotsu, T.; Yoshikawa, Y.; Zinchenko, A.; Chen, N.; Yoshikawa, K., Competitive Effects of 2+ and 3+ Cations on DNA Compaction. *arXiv preprint arXiv:1601.01392* **2016**.
43. Podestà, A.; Indrieri, M.; Brogioli, D.; Manning, G. S.; Milani, P.; Guerra, R.; Finzi, L.; Dunlap, D., Positively charged surfaces increase the flexibility of DNA. *Biophysical journal* **2005,** *89* (4), 2558-2563.
44. Gill, M. R.; Thomas, J. A., Ruthenium (II) polypyridyl complexes and DNA—from structural probes to cellular imaging and therapeutics. *Chemical Society Reviews* **2012,** *41* (8), 3179-3192.
45. Zeng, L.; Gupta, P.; Chen, Y.; Wang, E.; Ji, L.; Chao, H.; Chen, Z.-S., The development of anticancer ruthenium (II) complexes: from single molecule compounds to nanomaterials. *Chemical Society Reviews* **2017,** *46* (19), 5771-5804.
46. Barton, J. K., Metal/nucleic-acid interactions. *Bioinorganic Chemistry* **1994**, 455-504.
47. Kellett, A.; Molphy, Z.; Slator, C.; McKee, V.; Farrell, N. P., Molecular methods for assessment of non-covalent metallodrug–DNA interactions. *Chemical Society Reviews* **2019,** *48* (4), 971-988.
48. Cardin, C. J.; Kelly, J. M.; Quinn, S. J., Photochemically active DNA-intercalating ruthenium and related complexes–insights by combining crystallography and transient spectroscopy. *Chemical science* **2017,** *8* (7), 4705-4723.
49. Cloonan, S. M.; Elmes, R. B.; Erby, M.; Bright, S. A.; Poynton, F. E.; Nolan, D. E.; Quinn, S. J.; Gunnlaugsson, T.; Williams, D. C., Detailed biological profiling of a photoactivated and apoptosis inducing pdppz ruthenium (II) polypyridyl complex in cancer cells. *Journal of medicinal chemistry* **2015,** *58* (11), 4494-4505.
50. Christopoulos, A.; Lanzafame, A.; Mitchelson, F., Allosteric interactions at muscarinic cholinoceptors. *Clinical and experimental pharmacology and physiology* **1998,** *25* (3-4), 185-194.
51. DeDecker, B. S., Allosteric drugs: thinking outside the active-site box. *Chemistry & Biology* **2000,** *7* (5), R103-R107.
52. Kunig, V.; Potowski, M.; Gohla, A.; Brunschweiger, A., DNA-encoded libraries–an efficient small molecule discovery technology for the biomedical sciences. *Biological chemistry* **2018,** *399* (7), 691-710.
53. Ahn, S.; Pani, B.; Kahsai, A. W.; Olsen, E. K.; Husemoen, G.; Vestergaard, M.; Jin, L.; Zhao, S.; Wingler, L. M.; Rambarat, P. K., Small-molecule positive allosteric modulators of the β2-adrenoceptor isolated from DNA-encoded libraries. *Molecular Pharmacology* **2018,** *94* (2), 850-861.
54. Petersen, L.; Blakskjær, P.; Chaikuad, A.; Christensen, A.; Dietvorst, J.; Holmkvist, J.; Knapp, S.; Kořínek, M.; Larsen, L.; Pedersen, A., Novel p38α MAP kinase inhibitors identified from yoctoReactor DNA-encoded small molecule library. *MedChemComm* **2016,** *7* (7), 1332-1339.
55. Yang, H.; Medeiros, P. F.; Raha, K.; Elkins, P.; Lind, K. E.; Lehr, R.; Adams, N. D.; Burgess, J. L.; Schmidt, S. J.; Knight, S. D., Discovery of a potent class of PI3Kα inhibitors with unique binding mode via encoded library technology (ELT). *ACS medicinal chemistry letters* **2015,** *6* (5), 531-536.
56. Kleiner, R. E.; Dumelin, C. E.; Tiu, G. C.; Sakurai, K.; Liu, D. R., In vitro selection of a DNA-templated small-molecule library reveals a class of macrocyclic kinase inhibitors. *Journal of the American Chemical Society* **2010,** *132* (33), 11779-11791.

57. Georghiou, G.; Kleiner, R. E.; Pulkoski-Gross, M.; Liu, D. R.; Seeliger, M. A., Highly specific, bisubstrate-competitive Src inhibitors from DNA-templated macrocycles. *Nature chemical biology* **2012,** *8* (4), 366-374.
58. Du, M.; Yang, L.; Gu, J.; Wu, J.; Ma, Y.; Wang, T., Inhibition of Peptidyl Arginine Deiminase-4 Prevents Renal Ischemia-Reperfusion-Induced Remote Lung Injury. *Mediators of Inflammation* **2020,** *2020*.
59. Arcamone, F.; Penco, S.; Orezzi, P.; Nicolella, V.; Pirelli, A., Structure and synthesis of distamycin A. *Nature* **1964,** *203* (4949), 1064-1065.
60. Marchini, S.; Broggini, M.; Sessa, C.; D'Incalci, M., Development of distamycin-related DNA binding anticancer drugs. *Expert opinion on investigational drugs* **2001,** *10* (9), 1703-1714.
61. Barrett, M. P.; Gemmell, C. G.; Suckling, C. J., Minor groove binders as anti-infective agents. *Pharmacology & therapeutics* **2013,** *139* (1), 12-23.
62. Baraldi, P. G.; Preti, D.; Fruttarolo, F.; Tabrizi, M. A.; Romagnoli, R., Hybrid molecules between distamycin A and active moieties of antitumor agents. *Bioorganic & medicinal chemistry* **2007,** *15* (1), 17-35.
63. Brown, T., Nucleic Acids Book. *AtdBio Ltd* **2015**.
64. Madkour, L. H., *Nucleic Acids as Gene Anticancer Drug Delivery Therapy*. Academic Press: 2019.
65. Hochster, R., *Metabolic Inhibitors V1: A Comprehensive Treatise*. Elsevier: 2012.
66. Lin, S.-q.; Jia, F.-j.; Zhang, C.-y.; Liu, F.-y.; Ma, J.-h.; Han, Z.; Xie, W.-d.; Li, X., Actinomycin V suppresses human non-small-cell lung carcinoma A549 cells by inducing G2/M phase arrest and apoptosis via the p53-dependent pathway. *Marine drugs* **2019,** *17* (10), 572.
67. Cerami, A.; Reich, E.; Ward, D.; Goldberg, I., The interaction of actinomycin with DNA: requirement for the 2-amino group of purines. *Proceedings of the National Academy of Sciences of the United States of America* **1967,** *57* (4), 1036.
68. Robinson, H.; Gao, Y.-G.; Sanishvili, R.; Joachimiak, A.; Wang, A. H.-J., Hexahydrated magnesium ions bind in the deep major groove and at the outer mouth of A-form nucleic acid duplexes. *Nucleic acids research* **2000,** *28* (8), 1760-1766.
69. Sigel, A.; Sigel, H.; Sigel, R. K., *Interplay between metal ions and nucleic acids*. Springer Science & Business Media: 2012; Vol. 10.
70. Barcellona, M.; Cardiel, G.; Gratton, E., Time-resolved fluorescence of DAPI in solution and bound to polydeoxynucleotides. *Biochemical and biophysical research communications* **1990,** *170* (1), 270-280.
71. Japaridze, A.; Benke, A.; Renevey, S.; Benadiba, C.; Dietler, G., Influence of DNA binding dyes on bare DNA structure studied with atomic force microscopy. *Macromolecules* **2015,** *48* (6), 1860-1865.
72. Eriksson, S.; Kim, S. K.; Kubista, M.; Norden, B., Binding of 4', 6-diamidino-2-phenylindole (DAPI) to AT regions of DNA: evidence for an allosteric conformational change. *Biochemistry* **1993,** *32* (12), 2987-2998.
73. Tanious, F. A.; Veal, J. M.; Buczak, H.; Ratmeyer, L. S.; Wilson, W. D., DAPI (4', 6-diamidino-2-phenylindole) binds differently to DNA and RNA: minor-groove binding at AT sites and intercalation at AU sites. *Biochemistry* **1992,** *31* (12), 3103-3112.
74. Pilch, D. S.; Kirolos, M. A.; Liu, X.; Plum, G. E.; Breslauer, K. J., Berenil [1, 3-bis (4'-amidinophenyl) triazene] binding to DNA duplexes and to a RNA duplex: evidence for both intercalative and minor groove binding properties. *Biochemistry* **1995,** *34* (31), 9962-9976.
75. Sands, M.; Kron, M. A.; Brown, R. B., Pentamidine: a review. *Reviews of infectious diseases* **1985,** *7* (5), 625-6344.

76. Edwards, K. J.; Jenkins, T. C.; Neidle, S., Crystal structure of a pentamidine-oligonucleotide complex: implications for DNA-binding properties. *Biochemistry* **1992,** *31* (31), 7104-7109.
77. Jenkins, T. C.; Lane, A. N., AT selectivity and DNA minor groove binding: modelling, NMR and structural studies of the interactions of propamidine and pentamidine with d (CGCGAATTCGCG) 2. *Biochimica et Biophysica Acta (BBA)-Gene Structure and Expression* **1997,** *1350* (2), 189-204.
78. Nunn, C. M.; Jenkins, T. C.; Neidle, S., Crystal structure of d (CGCGAATTCGCG) complexed with propamidine, a short-chain homolog of the drug pentamidine. *Biochemistry* **1993,** *32* (50), 13838-13843.
79. Issar, U.; Kakkar, R., DNA minor groove binder Hoechst 33258 and its analogues: A review. *Int. Rev. Biophys. Chem.(IREBIC)* **2013,** *4*, 49-66.
80. Sheng, J.; Gan, J.; Huang, Z., Structure-based DNA-targeting strategies with small molecule ligands for drug discovery. *Medicinal research reviews* **2013,** *33* (5), 1119-1173.
81. Neidle, S., DNA minor-groove recognition by small molecules. *Natural product reports* **2001,** *18* (3), 291-309.
82. Sischka, A.; Toensing, K.; Eckel, R.; Wilking, S. D.; Sewald, N.; Ros, R.; Anselmetti, D., Molecular mechanisms and kinetics between DNA and DNA binding ligands. *Biophysical journal* **2005,** *88* (1), 404-411.
83. Husale, S.; Grange, W.; Hegner, M., DNA mechanics affected by small DNA interacting ligands. *Single Molecules* **2002,** *3* (2-3), 91-96.
84. Kuddus, M.; Arif, J. M.; Yunus, G.; Jamal, Q. M., THEORETICAL AND IN SILICO ANALYSIS OF MOLECULAR INTERACTION OF ANTI-TRYPANOSOMAL DRUG BERENIL AND ITS ANALOG WITH CALF THYMUS DNA.
85. Almaqwashi, A. A.; Paramanathan, T.; Lincoln, P.; Rouzina, I.; Westerlund, F.; Williams, M. C., Strong DNA deformation required for extremely slow DNA threading intercalation by a binuclear ruthenium complex. *Nucleic acids research* **2014,** *42* (18), 11634-11641.
86. Rocha, M.; Viana, N.; Mesquita, O., DNA-psoralen interaction: A single molecule experiment. *The Journal of chemical physics* **2004,** *121* (19), 9679-9683.
87. Broude, N.; Budowsky, E., The reaction of glyoxal with nucleic acid components: V. Denaturation of DNA under the action of glyoxal. *Biochimica et Biophysica Acta (BBA)-Nucleic Acids and Protein Synthesis* **1973,** *294* (3), 378-384.
88. Lyubchenko, Y. L.; Kalambet, Y. A.; Lyamichev, V.; Borovik, A., A comparison of experimental and theoretical melting maps for replicative form of φ X174 DNA. *Nucleic acids research* **1982,** *10* (6), 1867-1876.
89. Hannon, M. J., Supramolecular DNA recognition. *Chemical Society Reviews* **2007,** *36* (2), 280-295.
90. Yesudhas, D.; Batool, M.; Anwar, M. A.; Panneerselvam, S.; Choi, S., Proteins recognizing DNA: Structural uniqueness and versatility of DNA-binding domains in stem cell transcription factors. *Genes* **2017,** *8* (8), 192.
91. Hamilton, P. L.; Arya, D. P., Natural product DNA major groove binders. *Natural product reports* **2012,** *29* (2), 134-143.
92. Balazy, M.; Fausto, A.; Voskanian, C.; Chavez, B.; Panesar, H.; Minehan, T. G., Dimeric and trimeric derivatives of the azinomycin B chromophore show enhanced DNA binding. *Organic & biomolecular chemistry* **2017,** *15* (21), 4522-4526.
93. Bhaduri, S.; Ranjan, N.; Arya, D. P., An overview of recent advances in duplex DNA recognition by small molecules. *Beilstein journal of organic chemistry* **2018,** *14* (1), 1051-1086.

94. Takeuchi, T.; Nitta, K.; Umezawa, H., Antitumor Effect of Pluramycin Crude Powder on Ehrlich Carcinoma of Mice (Studies on Antitumor Substances Produced by Microorganisms. X). *The Journal of Antibiotics, Series A* **1956,** *9* (1), 22-30.
95. Joel, P. B.; Goldberg, I. H., The inhibition of RNA and DNA polymerases by hedamycin. *Biochimica et Biophysica Acta (BBA)-Nucleic Acids and Protein Synthesis* **1970,** *224* (2), 361-370.
96. Sun, D.; Hansen, M.; Clement, J. J.; Hurley, L. H., Structure of the altromycin B (N7-guanine)-DNA adduct. A proposed prototypic DNA adduct structure for the pluramycin antitumor antibiotics. *Biochemistry* **1993,** *32* (32), 8068-8074.
97. Kwok, Y.; Zeng, Q.; Hurley, L. H., Topoisomerase II-mediated site-directed alkylation of DNA by psorospermin and its use in mapping other topoisomerase II poison binding sites. *Proceedings of the National Academy of Sciences* **1998,** *95* (23), 13531-13536.
98. Hansen, M.; Hurley, L., Altromycin B Threads the DNA Helix Interacting with Both the Major and the Minor Grooves to Position Itself for Site-directed Alkylation and Guanine N7. *Journal of the American Chemical Society* **1995,** *117* (9), 2421-2429.
99. Bililign, T.; Hyun, C.-G.; Williams, J. S.; Czisny, A. M.; Thorson, J. S., The hedamycin locus implicates a novel aromatic PKS priming mechanism. *Chemistry & biology* **2004,** *11* (7), 959-969.
100. Sun, D.; Hansen, M.; Hurley, L., Molecular basis for the DNA sequence specificity of the pluramycins. A novel mechanism involving groove interactions transmitted through the helix via intercalation to achieve sequence selectivity at the covalent bonding step. *Journal of the American Chemical Society* **1995,** *117* (9), 2430-2440.
101. Rhoads, R. E., *Proceedings of the Research Symposium on Complexes of Biologically Active Substances with Nucleic Acids and Their Modes of Action: Held at the Walter Reed Army Institute of Research Washington, 16–19 March 1970*. Springer Science & Business Media: 2012; Vol. 2.
102. Shaikh, S. A.; Jayaram, B., DNA drug interaction. *Supercomputing Facility for Bioinformatics and Computational Biology*.
103. Hurley, L. H., DNA and its associated processes as targets for cancer therapy. *Nature Reviews Cancer* **2002,** *2* (3), 188-200.
104. Ralhan, R.; Kaur, J., Alkylating agents and cancer therapy. *Expert Opinion on Therapeutic Patents* **2007,** *17* (9), 1061-1075.
105. Ye, J.; Farrington, C. R.; Millard, J. T., Polymerase bypass of N7-guanine monoadducts of cisplatin, diepoxybutane, and epichlorohydrin. *Mutation Research/Fundamental and Molecular Mechanisms of Mutagenesis* **2018,** *809*, 6-12.
106. Rocha, C. R. R.; Silva, M. M.; Quinet, A.; Cabral-Neto, J. B.; Menck, C. F. M., DNA repair pathways and cisplatin resistance: an intimate relationship. *Clinics* **2018,** *73*.
107. International journal of medical and biological frontiers. *Int. j. med. biol. front.* **1995**.
108. Bancroft, D. P.; Lepre, C. A.; Lippard, S. J., Platinum-195 NMR kinetic and mechanistic studies of cis-and trans-diamminedichloroplatinum (II) binding to DNA. *Journal of the American Chemical Society* **1990,** *112* (19), 6860-6871.
109. Avendaño, C.; Menendez, J. C., *Medicinal chemistry of anticancer drugs*. Elsevier: 2015.
110. Todd, R. C.; Lippard, S. J., Inhibition of transcription by platinum antitumor compounds. *Metallomics* **2009,** *1* (4), 280-291.
111. Wang, Z.; Zhu, G., DNA Damage Repair Pathways and Repair of Cisplatin-Induced DNA Damage. **2018**.
112. Kelland, L., The resurgence of platinum-based cancer chemotherapy. *Nature Reviews Cancer* **2007,** *7* (8), 573-584.

113. Reedijk, J., New clues for platinum antitumor chemistry: kinetically controlled metal binding to DNA. *Proceedings of the National Academy of Sciences* **2003,** *100* (7), 3611-3616.
114. Dospivova, D.; Smerkova, K.; Ryvolova, M.; Hynek, D.; Adam, V.; Kopel, P.; Stiborova, M.; Eckschlager, T.; Hubalek, J.; Kizek, R., Catalytic electrochemical analysis of platinum in Pt-DNA adducts. *Int. J. Electrochem. Sci* **2012,** *7* (4), 3072-3088.
115. Ndagi, U.; Mhlongo, N.; Soliman, M. E., Metal complexes in cancer therapy–an update from drug design perspective. *Drug design, development and therapy* **2017,** *11*, 599.
116. Takezawa, Y.; Shionoya, M., Metal-mediated DNA base pairing: alternatives to hydrogen-bonded Watson–Crick base pairs. *Accounts of Chemical Research* **2012,** *45* (12), 2066-2076.
117. Lee, J. S.; Latimer, L. J.; Reid, R. S., A cooperative conformational change in duplex DNA induced by Zn2+ and other divalent metal ions. *Biochemistry and cell biology* **1993,** *71* (3-4), 162-168.
118. Taherpour, S., Metal-Ion-Binding Oligonucleotides: High-Affinity Probes for Nucleic Acid Sequences. **2015**.
119. Galindo-Murillo, R.; Ruíz-Azuara, L.; Moreno-Esparza, R.; Cortés-Guzmán, F., Molecular recognition between DNA and a copper-based anticancer complex. *Physical Chemistry Chemical Physics* **2012,** *14* (44), 15539-15546.
120. Krasnovskaya, O.; Naumov, A.; Guk, D.; Gorelkin, P.; Erofeev, A.; Beloglazkina, E.; Majouga, A., Copper Coordination Compounds as Biologically Active Agents. *International Journal of Molecular Sciences* **2020,** *21* (11), 3965.
121. Hussain, A.; AlAjmi, M. F.; Rehman, M. T.; Amir, S.; Husain, F. M.; Alsalme, A.; Siddiqui, M. A.; AlKhedhairy, A. A.; Khan, R. A., Copper (II) complexes as potential anticancer and Nonsteroidal anti-inflammatory agents: In vitro and in vivo studies. *Scientific reports* **2019,** *9* (1), 1-17.
122. Ueda, J.-i.; Takai, M.; Shimazu, Y.; Ozawa, T., Reactive oxygen species generated from the reaction of copper (II) complexes with biological reductants cause DNA strand scission. *Archives of biochemistry and biophysics* **1998,** *357* (2), 231-239.
123. Sissi, C.; Mancin, F.; Gatos, M.; Palumbo, M.; Tecilla, P.; Tonellato, U., Efficient plasmid DNA cleavage by a mononuclear copper (II) complex. *Inorganic chemistry* **2005,** *44* (7), 2310-2317.
124. García-Ramos, J. C.; Gutiérrez, A. G.; Vázquez-Aguirre, A.; Toledano-Magaña, Y.; Alonso-Sáenz, A. L.; Gómez-Vidales, V.; Flores-Alamo, M.; Mejía, C.; Ruiz-Azuara, L., The mitochondrial apoptotic pathway is induced by Cu (II) antineoplastic compounds (Casiopeínas®) in SK-N-SH neuroblastoma cells after short exposure times. *Biometals* **2017,** *30* (1), 43-58.
125. De Vizcaya-Ruiz, A.; Rivero-Müller, A.; Ruiz-Ramirez, L.; Howarth, J.; Dobrota, M., Hematotoxicity response in rats by the novel copper-based anticancer agent: casiopeina II. *Toxicology* **2003,** *194* (1-2), 103-113.
126. Bravo-Gómez, M. E.; García-Ramos, J. C.; Gracia-Mora, I.; Ruiz-Azuara, L., Antiproliferative activity and QSAR study of copper (II) mixed chelate [Cu (N–N)(acetylacetonato)] NO3 and [Cu (N–N)(glycinato)] NO3 complexes,(Casiopeínas®). *Journal of inorganic biochemistry* **2009,** *103* (2), 299-309.
127. Serment-Guerrero, J.; Cano-Sanchez, P.; Reyes-Perez, E.; Velazquez-Garcia, F.; Bravo-Gomez, M.; Ruiz-Azuara, L., Genotoxicity of the copper antineoplastic coordination complexes casiopeinas®. *Toxicology in Vitro* **2011,** *25* (7), 1376-1384.
128. Silva-Platas, C.; Villegas, C. A.; Oropeza-Almazan, Y.; Carranca, M.; Torres-Quintanilla, A.; Lozano, O.; Valero-Elizondo, J.; Castillo, E. C.; Bernal-Ramírez, J.; Fernandez-Sada, E., Ex vivo Cardiotoxicity of antineoplastic Casiopeinas is mediated through

energetic dysfunction and triggered mitochondrial-dependent apoptosis. *Oxidative medicine and cellular longevity* **2018,** *2018*.
129. Bravo-Gómez, M. E.; Dávila-Manzanilla, S.; Flood-Garibay, J.; Muciño-Hernández, M. Á.; Mendoza, Á.; García Ramos, J. C.; Moreno-Esparza, R.; Ruiz-Azuara, L., Secondary ligand effects on the cytotoxicity of several Casiopeina's group II compounds. *Journal of the Mexican Chemical Society* **2012,** *56* (1), 85-92.
130. Wang, M.; Yu, Y.; Liang, C.; Lu, A.; Zhang, G., Recent advances in developing small molecules targeting nucleic acid. *International journal of molecular sciences* **2016,** *17* (6), 779.
131. Rohs, R.; Jin, X.; West, S. M.; Joshi, R.; Honig, B.; Mann, R. S., Origins of specificity in protein-DNA recognition. *Annual review of biochemistry* **2010,** *79*, 233-269.
132. Mondal, M.; Mukherjee, S.; Bhattacharyya, D., Contribution of phenylalanine side chain intercalation to the TATA-box binding protein–DNA interaction: molecular dynamics and dispersion-corrected density functional theory studies. *Journal of molecular modeling* **2014,** *20* (11), 2499.
133. Bell, C. E.; Lewis, M., A closer view of the conformation of the Lac repressor bound to operator. *Nature structural biology* **2000,** *7* (3), 209-214.
134. Romanuka, J.; Folkers, G. E.; Biris, N.; Tishchenko, E.; Wienk, H.; Bonvin, A. M.; Kaptein, R.; Boelens, R., Specificity and affinity of Lac repressor for the auxiliary operators O2 and O3 are explained by the structures of their protein–DNA complexes. *Journal of molecular biology* **2009,** *390* (3), 478-489.
135. Maaloum, M.; Muller, P.; Harlepp, S., DNA-intercalator interactions: structural and physical analysis using atomic force microscopy in solution. *Soft Matter* **2013,** *9* (47), 11233-11240.
136. Lin, C.; Yang, D., DNA recognition by a novel bis-intercalator, potent anticancer drug XR5944. *Current topics in medicinal chemistry* **2015,** *15* (14), 1385-1397.
137. Harris, S. M.; Scott, J. A.; Brown, J. L.; Charlton, P. A.; Mistry, P., Preclinical anti-tumor activity of XR5944 in combination with carboplatin or doxorubicin in non-small-cell lung carcinoma. *Anti-cancer drugs* **2005,** *16* (9), 945-951.
138. Gamage, S. A.; Spicer, J. A.; Finlay, G. J.; Stewart, A. J.; Charlton, P.; Baguley, B. C.; Denny, W. A., Dicationic bis (9-methylphenazine-1-carboxamides): relationships between biological activity and linker chain structure for a series of potent topoisomerase targeted anticancer drugs. *Journal of medicinal chemistry* **2001,** *44* (9), 1407-1415.
139. Byers, S. A.; Schafer, B.; Sappal, D. S.; Brown, J.; Price, D. H., The antiproliferative agent MLN944 preferentially inhibits transcription. *Molecular cancer therapeutics* **2005,** *4* (8), 1260-1267.
140. Finlay, G.; Riou, J.-F.; Baguley, B., From amsacrine to DACA (N-[2-(dimethylamino) ethyl] acridine-4-carboxamide): selectivity for topoisomerases I and II among acridine derivatives. *European Journal of Cancer* **1996,** *32* (4), 708-714.
141. Mistry, P.; Stewart, A. J.; Dangerfield, W.; Baker, M.; Liddle, C.; Bootle, D.; Kofler, B.; Laurie, D.; Denny, W. A.; Baguley, B., In vitro and in vivo characterization of XR11576, a novel, orally active, dual inhibitor of topoisomerase I and II. *Anti-cancer drugs* **2002,** *13* (1), 15-28.
142. Vicker, N.; Burgess, L.; Chuckowree, I. S.; Dodd, R.; Folkes, A. J.; Hardick, D. J.; Hancox, T. C.; Miller, W.; Milton, J.; Sohal, S., Novel angular benzophenazines: dual topoisomerase I and topoisomerase II inhibitors as potential anticancer agents. *Journal of medicinal chemistry* **2002,** *45* (3), 721-739.
143. Sappal, D. S.; McClendon, A. K.; Fleming, J. A.; Thoroddsen, V.; Connolly, K.; Reimer, C.; Blackman, R. K.; Bulawa, C. E.; Osheroff, N.; Charlton, P., Biological characterization of MLN944: a potent DNA binding agent. *Molecular Cancer Therapeutics* **2004,** *3* (1), 47-58.

144. Stewart, A. J.; Mistry, P.; Dangerfield, W.; Bootle, D.; Baker, M.; Kofler, B.; Okiji, S.; Baguley, B. C.; Denny, W. A.; Charlton, P. A., Antitumor activity of XR5944, a novel and potent topoisomerase poison. *Anti-cancer drugs* **2001,** *12* (4), 359-367.
145. Di Nicolantonio, F.; Knight, L. A.; Whitehouse, P. A.; Mercer, S. J.; Sharma, S.; Charlton, P. A.; Norris, D.; Cree, I. A., The ex vivo characterization of XR5944 (MLN944) against a panel of human clinical tumor samples. *Molecular cancer therapeutics* **2004,** *3* (12), 1631-1637.
146. Harris, S.; Mistry, P.; Freathy, C.; Brown, J.; Charlton, P., Antitumour activity of XR5944 in vitro and in vivo in combination with 5-fluorouracil and irinotecan in colon cancer cell lines. *British journal of cancer* **2005,** *92* (4), 722-728.
147. Lin, C. DNA and its secondary structures as targets for small molecule anticancer drugs-an NMR structural study. The University of Arizona, 2016.
148. Chaires, J. B.; Leng, F.; Przewloka, T.; Fokt, I.; Ling, Y.-H.; Perez-Soler, R.; Priebe, W., Structure-based design of a new bisintercalating anthracycline antibiotic. *Journal of medicinal chemistry* **1997,** *40* (3), 261-266.
149. Ross, D. D., Cellular and pharmacologic aspects of drug resistance in acute myeloid leukemia. *Current Opinion in Oncology* **1991,** *3* (1), 21-29.
150. Hu, G. G.; Shui, X.; Leng, F.; Priebe, W.; Chaires, J. B.; Williams, L. D., Structure of a DNA− bisdaunomycin complex. *Biochemistry* **1997,** *36* (20), 5940-5946.
151. Portugal, J.; Martin, B.; Vaquero, A.; Ferrer, N.; Villamarin, S.; Priebe, W., Analysis of the effects of daunorubicin and WP631 on transcription. *Current medicinal chemistry* **2001,** *8* (1), 1-8.
152. Alberts, B.; Johnson, A.; Lewis, J.; Raff, M.; Roberts, K.; Walter, P., DNA-binding motifs in gene regulatory proteins. In *Molecular Biology of the Cell. 4th edition*, Garland Science: 2002.
153. Baraldi, P. G.; Bovero, A.; Fruttarolo, F.; Preti, D.; Tabrizi, M. A.; Pavani, M. G.; Romagnoli, R., DNA minor groove binders as potential antitumor and antimicrobial agents. *Medicinal research reviews* **2004,** *24* (4), 475-528.
154. Kapuscinski, J., DAPI: a DNA-specific fluorescent probe. *Biotechnic & Histochemistry* **1995,** *70* (5), 220-233.
155. Mishra, A. K.; Mishra, L., *Ruthenium chemistry*. CRC Press: 2018.
156. Larsen, T. A.; Goodsell, D. S.; Cascio, D.; Grzeskowiak, K.; Dickerson, R. E., The structure of DAPI bound to DNA. *Journal of Biomolecular Structure and Dynamics* **1989,** *7* (3), 477-491.
157. Tidwell, R. R.; Boykin, D. W., Dicationic DNA minor groove binders as antimicrobial agents. *Small molecule DNA and RNA binders: from synthesis to nucleic acid complexes* **2002**, 414-460.
158. Biebricher, A. S.; Heller, I.; Roijmans, R. F.; Hoekstra, T. P.; Peterman, E. J.; Wuite, G. J., The impact of DNA intercalators on DNA and DNA-processing enzymes elucidated through force-dependent binding kinetics. *Nature communications* **2015,** *6*, 7304.
159. Lerman, L., Structural considerations in the interaction of DNA and acridines. *Journal of molecular biology* **1961,** *3* (1), 18-IN14.
160. Li, H. J.; Crothers, D. M., Relaxation studies of the proflavine-DNA complex: the kinetics of an intercalation reaction. *Journal of molecular biology* **1969,** *39* (3), 461-477.
161. Waring, M., Variation of the supercoils in closed circular DNA by binding of antibiotics and drugs: evidence for molecular models involving intercalation. *Journal of molecular biology* **1970,** *54* (2), 247-279.
162. Berman, H. M.; Young, P. R., The interaction of intercalating drugs with nucleic acids. *Annual review of biophysics and bioengineering* **1981,** *10* (1), 87-114.

163. Denny, W. A., Acridine derivatives as chemotherapeutic agents. *Current Medicinal Chemistry* **2002,** *9* (18), 1655-1665.
164. Waring, M. J., DNA modification and cancer. *Annual review of biochemistry* **1981,** *50* (1), 159-192.
165. Lenglet, G.; David-Cordonnier, M.-H., DNA-destabilizing agents as an alternative approach for targeting DNA: mechanisms of action and cellular consequences. *Journal of nucleic acids* **2010,** *2010*.
166. Syed, S. N.; Schulze, H.; Macdonald, D.; Crain, J.; Mount, A. R.; Bachmann, T. T., Cyclic denaturation and renaturation of double-stranded DNA by redox-state switching of DNA intercalators. *Journal of the American Chemical Society* **2013,** *135* (14), 5399-5407.
167. Wilson, W., DNA and RNA intercalators. *DNA and Aspects of Molecular Biology* **1999,** *7*.
168. Karabencheva-Christova, T., *Dynamics of proteins and nucleic acids*. Elsevier: 2013.
169. Tomczyk, M. D.; Walczak, K. Z., l, 8-Naphthalimide based DNA intercalators and anticancer agents. A systematic review from 2007 to 2017. *European Journal of Medicinal Chemistry* **2018,** *159*, 393-422.
170. Palhares, D. R. Synthesis and biological evaluation of mono and bis-naphthalimide derivatives against SH-SY5Y, human brain cancer cells. 2015.
171. Kamal, A.; Bolla, N. R.; Srikanth, P. S.; Srivastava, A. K., Naphthalimide derivatives with therapeutic characteristics: a patent review. *Expert opinion on therapeutic patents* **2013,** *23* (3), 299-317.
172. Cao, X.; Meng, L.; Li, Z.; Mao, Y.; Lan, H.; Chen, L.; Fan, Y.; Yi, T., Large red-shifted fluorescent emission via intermolecular π–π stacking in 4-ethynyl-1, 8-naphthalimide-based supramolecular assemblies. *Langmuir* **2014,** *30* (39), 11753-11760.
173. Alami, N.; Paterson, J.; Belanger, S.; Juste, S.; Grieshaber, C.; Leyland-Jones, B., Comparative analysis of xanafide cytotoxicity in breast cancer cell lines. *British journal of cancer* **2007,** *97* (1), 58-64.
174. Brana, M.; Ramos, A., Naphthalimides as anticancer agents: synthesis and biological activity. *Current Medicinal Chemistry-Anti-Cancer Agents* **2001,** *1* (3), 237-255.
175. Peters, A.; Bide, M., Amino derivatives of 1, 8-naphthalic anhydride and derived dyes for synthetic-polymer fibres. *Dyes and Pigments* **1985,** *6* (5), 349-375.
176. Bardajee, G. R.; Li, A. Y.; Haley, J. C.; Winnik, M. A., The synthesis and spectroscopic properties of novel, functional fluorescent naphthalimide dyes. *Dyes and Pigments* **2008,** *79* (1), 24-32.
177. Xuhong, Q.; Jim, T.; Jiandong, Z.; Yulan, Z., Synthesis of furonaphthalimides with potential photosensitizing biological activity. *Dyes and pigments* **1994,** *25* (2), 109-114.
178. Wolarz, E.; Moryson, H.; Bauman, D., Dichroic fluorescent dyes for 'guest-host'liquid crystal displays. *Displays* **1992,** *13* (4), 171-178.
179. Tao, Z.-F.; Qian, X.; Tang, J., Synthesis of furonaphthalimides as novel DNA intercalators. *Dyes and pigments* **1996,** *30* (4), 247-252.
180. Martin, E.; Weigand, R.; Pardo, A., Solvent dependence of the inhibition of intramolecular charge-transfer in N-substituted 1, 8-naphthalimide derivatives as dye lasers. *Journal of luminescence* **1996,** *68* (2-4), 157-164.
181. Chang, S.-C.; Archer, B. J.; Utecht, R. E.; Lewis, D. E.; Judy, M. M.; Matthews, J. L., 4-Alkylamino-3-bromo-N-alkyl-1, 8-naphthalimides: New photochemically activatable antiviral compounds. *Bioorganic & Medicinal Chemistry Letters* **1993,** *3* (4), 555-556.
182. Ingrassia, L.; Lefranc, F.; Kiss, R.; Mijatovic, T., Naphthalimides and azonafides as promising anti-cancer agents. *Current medicinal chemistry* **2009,** *16* (10), 1192-1213.
183. Thomas, S. W.; Joly, G. D.; Swager, T. M., Chemical sensors based on amplifying fluorescent conjugated polymers. *Chemical reviews* **2007,** *107* (4), 1339-1386.

184. Ruedas-Rama, M. J.; Walters, J. D.; Orte, A.; Hall, E. A., Fluorescent nanoparticles for intracellular sensing: a review. *Analytica chimica acta* **2012,** *751*, 1-23.
185. Duke, R. M.; Veale, E. B.; Pfeffer, F. M.; Kruger, P. E.; Gunnlaugsson, T., Colorimetric and fluorescent anion sensors: an overview of recent developments in the use of 1, 8-naphthalimide-based chemosensors. *Chemical Society Reviews* **2010,** *39* (10), 3936-3953.
186. Qian, X.; Li, Y.; Xu, Y.; Liu, Y.; Qu, B., Highly-efficient DNA photocleavers with long wavelength absorptions: thio-heterocyclic fused naphthalimides containing aminoalkyl side chains. *Bioorganic & medicinal chemistry letters* **2004,** *14* (10), 2665-2668.
187. Li, Y.; Xu, Y.; Qian, X.; Qu, B., Naphthalimide–thiazoles as novel photonucleases: molecular design, synthesis, and evaluation. *Tetrahedron letters* **2004,** *45* (6), 1247-1251.
188. Tandon, R.; Luxami, V.; Kaur, H.; Tandon, N.; Paul, K., 1, 8-Naphthalimide: A Potent DNA Intercalator and Target for Cancer Therapy. *The Chemical Record* **2017,** *17* (10), 956-993.
189. Gellerman, G., Recent developments in the synthesis and applications of anticancer amonafide derivatives. A mini review. *Letters in Drug Design & Discovery* **2016,** *13* (1), 47-63.
190. Banerjee, S.; Veale, E. B.; Phelan, C. M.; Murphy, S. A.; Tocci, G. M.; Gillespie, L. J.; Frimannsson, D. O.; Kelly, J. M.; Gunnlaugsson, T., Recent advances in the development of 1, 8-naphthalimide based DNA targeting binders, anticancer and fluorescent cellular imaging agents. *Chemical Society reviews* **2013,** *42* (4), 1601-1618.
191. Norton, J. T.; Witschi, M. A.; Luong, L.; Kawamura, A.; Ghosh, S.; Stack, M. S.; Sim, E.; Avram, M. J.; Appella, D. H.; Huang, S., Synthesis and anticancer activities of 6-amino amonafide derivatives. *Anti-cancer drugs* **2008,** *19* (1), 23-36.
192. Lv, M.; Xu, H., Overview of naphthalimide analogs as anticancer agents. *Current medicinal chemistry* **2009,** *16* (36), 4797-4813.
193. Freeman, C. L.; Swords, R.; Giles, F. J., Amonafide: a future in treatment of resistant and secondary acute myeloid leukemia? *Expert review of hematology* **2012,** *5* (1), 17-26.
194. Lu, Y.-T.; Chen, T.-L.; Chang, K.-S.; Chang, C.-M.; Wei, T.-Y.; Liu, J.-W.; Hsiao, C.-A.; Shih, T.-L., Synthesis of novel C4-benzazole naphthalimide derivatives with potent anti-tumor properties against murine melanoma. *Bioorganic & medicinal chemistry* **2017,** *25* (2), 789-794.
195. Wang, Y.; Zhang, J.; Li, M.; Li, M.; Xie, S.; Wang, C., Synthesis and evaluation of novel amonafide–polyamine conjugates as anticancer agents. *Chemical biology & drug design* **2017,** *89* (5), 670-680.
196. Ge, C.; Chang, L.; Zhao, Y.; Chang, C.; Xu, X.; He, H.; Wang, Y.; Dai, F.; Xie, S.; Wang, C., Design, synthesis and evaluation of naphthalimide derivatives as potential anticancer agents for hepatocellular carcinoma. *Molecules* **2017,** *22* (2), 342.
197. Brider, T.; Redko, B.; Oron-Herman, M.; Cohen-Matzlich, A.; Gerlitz, G.; Gellerman, G.; Grynszpan, F., Synthesis and in vitro anticancer evaluation of 1, 8-naphthalimide N (4) and S (4)-derivatives combining DNA intercalation and alkylation capabilities. *Research on Chemical Intermediates* **2016,** *42* (3), 1741-1757.
198. Bousquet, P. F.; Braña, M. F.; Conlon, D.; Fitzgerald, K. M.; Perron, D.; Cocchiaro, C.; Miller, R.; Moran, M.; George, J.; Qian, X.-D., Preclinical evaluation of LU 79553: a novel bis-naphthalimide with potent antitumor activity. *Cancer research* **1995,** *55* (5), 1176-1180.
199. Veale, E. B.; Frimannsson, D. O.; Lawler, M.; Gunnlaugsson, T., 4-Amino-1, 8-naphthalimide-Based Troger's bases As high affinity DNA targeting fluorescent supramolecular scaffolds. *Organic letters* **2009,** *11* (18), 4040-4043.

200. Veale, E. B.; Gunnlaugsson, T., Synthesis, photophysical, and DNA binding studies of fluorescent Troger's base derived 4-amino-1, 8-naphthalimide supramolecular clefts. *The Journal of organic chemistry* **2010,** *75* (16), 5513-5525.
201. Antonini, I.; Santoni, G.; Lucciarini, R.; Amantini, C.; Sparapani, S.; Magnano, A., Synthesis and biological evaluation of new asymmetrical bisintercalators as potential antitumor drugs. *Journal of medicinal chemistry* **2006,** *49* (24), 7198-7207.
202. Ott, I.; Xu, Y.; Qian, X., Fluorescence properties and antiproliferative effects of mono-, bis-, and tris-thiophenylnaphthalimides: Results of a comparative pilot study. *Journal of Photochemistry and Photobiology B: Biology* **2011,** *105* (1), 75-80.
203. Pavlov, V.; Lin, P. K. T.; Rodilla, V., Cytotoxicity, DNA binding and localisation of novel bis-naphthalimidopropyl polyamine derivatives. *Chemico-biological interactions* **2001,** *137* (1), 15-24.
204. Lin, P. K. T.; Pavlov, V. A., The synthesis and in vitro cytotoxic studies of novel bis-naphthalimidopropyl polyamine derivatives. *Bioorganic & medicinal chemistry letters* **2000,** *10* (14), 1609-1612.
205. Ralton, L. D.; Bestwick, C. S.; Milne, L.; Duthie, S.; Lin, P. K. T., Bisnaphthalimidopropyl spermidine induces apoptosis within colon carcinoma cells. *Chemico-biological interactions* **2009,** *177* (1), 1-6.
206. Leng, F.; Priebe, W.; Chaires, J. B., Ultratight DNA binding of a new bisintercalating anthracycline antibiotic. *Biochemistry* **1998,** *37* (7), 1743-1753.
207. Brana, M.; Castellano, J.; Roldan, C.; Santos, A.; Vazquez, D.; Jimenez, A., Synthesis and mode (s) of action of a new series of imide derivatives of 3-nitro-1, 8 naphthalic acid. *Cancer chemotherapy and pharmacology* **1980,** *4* (1), 61-66.
208. Shankaraiah, N.; Kumar, N. P.; Tokala, R.; Gayatri, B. S.; Talla, V.; Santos, L. S., Synthesis of New 1, 2, 3-Triazolo-naphthalimide/phthalimide Conjugates via 'Click'Reaction: DNA Intercalation and Cytotoxic Studies. *Journal of the Brazilian Chemical Society* **2019,** *30* (3), 454-461.
209. Jiang, W.; Sun, Y.; Wang, X.; Wang, Q.; Xu, W., Synthesis and photochemical properties of novel 4-diarylamine-1, 8-naphthalimide derivatives. *Dyes and Pigments* **2008,** *77* (1), 125-128.
210. Yang, J.-X.; Wang, X.-L.; Xu, L.-H., Studies on the synthesis and spectral properties of novel 4-benzofuranyl-1, 8-naphthalimide derivatives. *Dyes and pigments* **2005,** *67* (1), 27-33.
211. Havlík, M.; Talianová, V.; Kaplánek, R.; Bříza, T.; Dolenský, B.; Králová, J.; Martásek, P.; Král, V., Versatile fluorophores for bioimaging applications: π-expanded naphthalimide derivatives with skeletal and appendage diversity. *Chemical communications* **2019,** *55* (18), 2696-2699.
212. Fernandez, H. F., New trends in the standard of care for initial therapy of acute myeloid leukemia. *Hematology 2010, the American Society of Hematology Education Program Book* **2010,** *2010* (1), 56-61.
213. Capranico, G.; Binaschi, M., DNA sequence selectivity of topoisomerases and topoisomerase poisons. *Biochimica et Biophysica Acta (BBA)-Gene Structure and Expression* **1998,** *1400* (1-3), 185-194.
214. Chau, M.; Christensen, J. L.; Ajami, A. M.; Capizzi, R. L., Amonafide, a topoisomerase II inhibitor, is unaffected by P-glycoprotein-mediated efflux. *Leukemia research* **2008,** *32* (3), 465-473.
215. Leith, C. P.; Chen, I.-M.; Kopecky, K. J.; Appelbaum, F. R.; Head, D. R.; Godwin, J. E.; Weick, J.; Willman, C., Correlation of multidrug resistance (MDR1) protein expression with functional dye/drug efflux in acute myeloid leukemia by multiparameter flow cytometry: identification of discordant MDR-/efflux+ and MDR1+/efflux-cases. **1995**.

216. Legha, S. S.; Ring, S.; Raber, M.; Felder, T. B.; Newman, R. A.; Krakoff, I. H., Phase I clinical investigation of benzisoquinolinedione. *Cancer Treat. Rep.* **1987,** *71* (12), 1165-1169.
217. Feigon, J.; Denny, W. A.; Leupin, W.; Kearns, D. R., Interactions of antitumor drugs with natural DNA: proton NMR study of binding mode and kinetics. *Journal of medicinal chemistry* **1984,** *27* (4), 450-465.
218. Hsiang, Y.-H.; Jiang, J. B.; Liu, L.-F., Topoisomerase II-mediated DNA cleavage by amonafide and its structural analogs. *Molecular pharmacology* **1989,** *36* (3), 371-376.
219. Goftar, M. K.; Kor, N. M.; Kor, Z. M., DNA intercalators and using them as anticancer drugs. *Int. J. Adv. Biol. Biomed. Res* **2014,** *2*, 811-822.
220. Bailly, C.; Braña, M.; Waring, M. J., Sequence-Selective Intercalation of Antitumour Bis-Naphthalimides into DNA: Evidence for an Approach Via the Major Groove. *European journal of biochemistry* **1996,** *240* (1), 195-208.
221. Gallego, J.; Reid, B. R., Solution structure and dynamics of a complex between DNA and the antitumor bisnaphthalimide LU-79553: intercalated ring flipping on the millisecond time scale. *Biochemistry* **1999,** *38* (46), 15104-15115.
222. Brana, M.; Castellano, J.; Moran, M.; Perez de Vega, M.; Romerdahl, C.; Qian, X.; Bousquet, P.; Emling, F.; Schlick, E.; Keilhauer, G., Bis-naphthalimides: a new class of antitumor agents. *Anti-cancer drug design* **1993,** *8* (4), 257-268.
223. Cohen, S. M.; Lippard, S. J., Cisplatin: from DNA damage to cancer chemotherapy. **2001**.
224. Pérez, J. M.; López-Solera, I.; Montero, E. I.; Braña, M. F.; Alonso, C.; Robinson, S. P.; Navarro-Ranninger, C., Combined effect of platination and intercalation upon DNA binding of novel cytotoxic Pt− Bis (naphthalimide) complexes. *Journal of medicinal chemistry* **1999,** *42* (26), 5482-5486.
225. Murphy, S.; Bright, S. A.; Poynton, F. E.; McCabe, T.; Kitchen, J. A.; Veale, E. B.; Williams, D. C.; Gunnlaugsson, T., Synthesis, photophysical and cytotoxicity evaluations of DNA targeting agents based on 3-amino-1, 8-naphthalimide derived Tröger's bases. *Organic & biomolecular chemistry* **2014,** *12* (34), 6610-6623.
226. Metcalfe, C.; Thomas, J. A., Kinetically inert transition metal complexes that reversibly bind to DNA. *Chemical Society Reviews* **2003,** *32* (4), 215-224.
227. Moucheron, C.; Kirsch-De Mesmaeker, A.; Kelly, J. M., Photoreactions of ruthenium (II) and osmium (II) complexes with deoxyribonucleic acid (DNA). *Journal of Photochemistry and Photobiology B: Biology* **1997,** *40* (2), 91-106.
228. Haq, I.; Lincoln, P.; Suh, D.; Norden, B.; Chowdhry, B. Z.; Chaires, J. B., Interaction of. delta.-and. lambda.-[Ru (phen) 2DPPZ] 2+ with DNA: a calorimetric and equilibrium binding study. *Journal of the American Chemical Society* **1995,** *117* (17), 4788-4796.
229. Hall, J. P.; O'Sullivan, K.; Naseer, A.; Smith, J. A.; Kelly, J. M.; Cardin, C. J., Structure determination of an intercalating ruthenium dipyridophenazine complex which kinks DNA by semiintercalation of a tetraazaphenanthrene ligand. *Proceedings of the National Academy of Sciences* **2011,** *108* (43), 17610-17614.
230. Niyazi, H.; Hall, J. P.; O'sullivan, K.; Winter, G.; Sorensen, T.; Kelly, J. M.; Cardin, C. J., Crystal structures of Λ-[Ru (phen) 2 dppz] 2+ with oligonucleotides containing TA/TA and AT/AT steps show two intercalation modes. *Nature Chemistry* **2012,** *4* (8), 621-628.
231. Song, H.; Kaiser, J. T.; Barton, J. K., Crystal structure of Δ-[Ru (bpy) 2 dppz] 2+ bound to mismatched DNA reveals side-by-side metalloinsertion and intercalation. *Nature chemistry* **2012,** *4* (8), 615-620.
232. Neidle, S., Into the minor groove. *Nature Chemistry* **2012,** *4* (8), 594-595.
233. Ghosh, A.; Das, P.; Gill, M. R.; Kar, P.; Walker, M. G.; Thomas, J. A.; Das, A., Photoactive RuII–Polypyridyl Complexes that Display Sequence Selectivity and High-Affinity

Binding to Duplex DNA through Groove Binding. *Chemistry–A European Journal* **2011,** *17* (7), 2089-2098.
234. Tian, X.; Gill, M. R.; Cantón, I.; Thomas, J. A.; Battaglia, G., Live cell luminescence imaging as a function of delivery mechanism. *ChemBioChem* **2011,** *12* (4), 548-551.
235. Wilson, T.; Williamson, M. P.; Thomas, J. A., Differentiating quadruplexes: binding preferences of a luminescent dinuclear ruthenium (II) complex with four-stranded DNA structures. *Organic & Biomolecular Chemistry* **2010,** *8* (11), 2617-2621.
236. Kelly, J. M.; Tossi, A. B.; McConnell, D. J.; OhUigin, C., A study of the interactions of some polypyridylruthenium (II) complexes with DNA using fluorescence spectroscopy, topoisomerisation and thermal denaturation. *Nucleic Acids Research* **1985,** *13* (17), 6017-6034.
237. Zeglis, B. M.; Pierre, V. C.; Barton, J. K., Metallo-intercalators and metallo-insertors. *Chemical Communications* **2007,** (44), 4565-4579.
238. Ortmans, I.; Content, S.; Boutonnet, N.; Kirsch-De Mesmaeker, A.; Bannwarth, W.; Constant, J. F.; Defrancq, E., and; Lhomme, J., Ru-Labeled Oligonucleotides for Photoinduced Reactions on Targeted DNA Guanines. *Chemistry–A European Journal* **1999,** *5* (9), 2712-2721.
239. Ryan, G. J.; Poynton, F. E.; Elmes, R. B.; Erby, M.; Williams, D. C.; Quinn, S. J.; Gunnlaugsson, T., Unexpected DNA binding properties with correlated downstream biological applications in mono vs. bis-1, 8-naphthalimide Ru (ii)-polypyridyl conjugates. *Dalton Transactions* **2015,** *44* (37), 16332-16344.
240. Marchetti, L. A.; Kumawat, L. K.; Mao, N.; Stephens, J. C.; Elmes, R. B., The Versatility of Squaramides: From Supramolecular Chemistry to Chemical Biology. *Chem* **2019**.
241. Storer, R. I.; Aciro, C.; Jones, L. H., Squaramides: physical properties, synthesis and applications. *Chemical Society Reviews* **2011,** *40* (5), 2330-2346.
242. Wurm, F. R.; Klok, H.-A., Be squared: expanding the horizon of squaric acid-mediated conjugations. *Chemical Society Reviews* **2013,** *42* (21), 8220-8236.
243. Cai, X.-J.; Li, Z.; Chen, W.-H., Synthesis, anion recognition and transmembrane anion-transport properties of squaramides and their derivatives. *Mini-Reviews in Organic Chemistry* **2018,** *15* (2), 148-156.
244. Saez Talens, V.; Englebienne, P.; Trinh, T. T.; Noteborn, W. E.; Voets, I. K.; Kieltyka, R. E., Aromatic gain in a supramolecular polymer. *Angewandte Chemie International Edition* **2015,** *54* (36), 10502-10506.
245. Prohens, R.; Portell, A.; Font-Bardia, M.; Bauzá, A.; Frontera, A., Experimental and theoretical study of aromaticity effects in the solid state architecture on squaric acid derivatives. *Crystal growth & design* **2014,** *14* (5), 2578-2587.
246. Malerich, J. P.; Hagihara, K.; Rawal, V. H., Chiral squaramide derivatives are excellent hydrogen bond donor catalysts. *Journal of the American Chemical Society* **2008,** *130* (44), 14416-14417.
247. Zhao, B. L.; Li, J. H.; Du, D. M., Squaramide-Catalyzed Asymmetric Reactions. *The Chemical Record* **2017,** *17* (10), 994-1018.
248. Karahan, S.; Tanyeli, C., Squaramide catalyzed α-chiral amine synthesis. *Tetrahedron Letters* **2018,** *59* (42), 3725-3737.
249. Brandão, P.; Burke, A. J., Recent advances in the asymmetric catalytic synthesis of chiral 3-hydroxy and 3-aminooxindoles and derivatives: Medicinally relevant compounds. *Tetrahedron* **2018,** *74* (38), 4927-4957.
250. Dwyer, M. P.; Yu, Y.; Chao, J.; Aki, C.; Chao, J.; Biju, P.; Girijavallabhan, V.; Rindgen, D.; Bond, R.; Mayer-Ezel, R., Discovery of 2-hydroxy-N, N-dimethyl-3-{2-[[(R)-1-(5-methylfuran-2-yl) propyl] amino]-3, 4-dioxocyclobut-1-enylamino} benzamide (SCH

527123): a potent, orally bioavailable CXCR2/CXCR1 receptor antagonist. *Journal of medicinal chemistry* **2006,** *49* (26), 7603-7606.
251. Kinney, W. A.; Abou-Gharbia, M.; Garrison, D. T.; Schmid, J.; Kowal, D. M.; Bramlett, D. R.; Miller, T. L.; Tasse, R. P.; Zaleska, M. M.; Moyer, J. A., Design and Synthesis of [2-(8, 9-Dioxo-2, 6-diazabicyclo [5.2. 0] non-1 (7)-en-2-yl)-ethyl] phosphonic Acid (EAA-090), a Potent N-Methyl-d-aspartate Antagonist, via the Use of 3-Cyclobutene-1, 2-dione as an Achiral α-Amino Acid Bioisostere. *Journal of medicinal chemistry* **1998,** *41* (2), 236-246.
252. Ribeiro, C. J.; Espadinha, M.; Machado, M.; Gut, J.; Gonçalves, L. M.; Rosenthal, P. J.; Prudêncio, M.; Moreira, R.; Santos, M. M., Novel squaramides with in vitro liver stage antiplasmodial activity. *Bioorganic & medicinal chemistry* **2016,** *24* (8), 1786-1792.
253. Martín-Escolano, R.; Marín, C.; Vega, M.; Martin-Montes, Á.; Medina-Carmona, E.; López, C.; Rotger, C.; Costa, A.; Sánchez-Moreno, M., Synthesis and biological evaluation of new long-chain squaramides as anti-chagasic agents in the BALB/c mouse model. *Bioorganic & medicinal chemistry* **2019,** *27* (5), 865-879.
254. Marín, C.; Ximenis, M.; Ramirez-Macías, I.; Rotger, C.; Urbanova, K.; Olmo, F.; Martín-Escolano, R.; Rosales, M. J.; Cañas, R.; Gutierrez-Sánchez, R., Effective anti-leishmanial activity of minimalist squaramide-based compounds. *Experimental parasitology* **2016,** *170*, 36-49.
255. Amendola, V.; Bergamaschi, G.; Boiocchi, M.; Fabbrizzi, L.; Milani, M., The squaramide versus urea contest for anion recognition. *Chemistry–A European Journal* **2010,** *16* (14), 4368-4380.
256. Andrés, J. M.; Maestro, A.; Valle, M. a.; Pedrosa, R., Chiral Bifunctional Thioureas and Squaramides and Their Copolymers as Recoverable Organocatalysts. Stereoselective Synthesis of 2-Substituted 4-Amino-3-nitrobenzopyrans and 3-Functionalized 3, 4-Diamino-4 H-Chromenes. *The Journal of organic chemistry* **2018,** *83* (10), 5546-5557.
257. Nagy, S.; Kisszékelyi, P.; Kupai, J., Synthesis and Application of Thiosquaramides and Their Derivatives: A Review. *Periodica Polytechnica Chemical Engineering* **2018,** *62* (4), 467–475-467–475.
258. Aletti, A. B.; Gillen, D. M.; Gunnlaugsson, T., Luminescent/colorimetric probes and (chemo-) sensors for detecting anions based on transition and lanthanide ion receptor/binding complexes. *Coordination Chemistry Reviews* **2018,** *354*, 98-120.
259. Gale, P. A.; Caltagirone, C., Fluorescent and colorimetric sensors for anionic species. *Coordination Chemistry Reviews* **2018,** *354*, 2-27.
260. Gale, P. A.; Howe, E. N.; Wu, X., Anion receptor chemistry. *Chem* **2016,** *1* (3), 351-422.
261. Prohens, R.; Tomàs, S.; Morey, J.; Deyà, P. M.; Ballester, P.; Costa, A., Squaramido-based receptors: Molecular recognition of carboxylate anions in highly competitive media. *Tetrahedron letters* **1998,** *39* (9), 1063-1066.
262. Prohens, R.; Martorell, G.; Ballester, P.; Costa, A., A squaramide fluorescent ensemble for monitoring sulfate in water. *Chemical Communications* **2001,** (16), 1456-1457.
263. van Binst, G.; Katzir, E.; Prelog, V., *Design and synthesis of organic molecules based on molecular recognition*. Springer: 1986.
264. Boyd, N. D.; Cohen, J. B., Kinetics of binding of [3H] acetylcholine and [3H] carbamoylcholine to Torpedo postsynaptic membranes: slow conformational transitions of the cholinergic receptor. *Biochemistry* **1980,** *19* (23), 5344-5353.
265. Zwicker, V. E.; Yuen, K. K.; Smith, D. G.; Ho, J.; Qin, L.; Turner, P.; Jolliffe, K. A., Deltamides and Croconamides: Expanding the Range of Dual H-bond Donors for Selective Anion Recognition. *Chemistry–A European Journal* **2018,** *24* (5), 1140-1150.

266. Elmes, R.; Schroeder, M.; Kumawat, L. K.; Abogunrin, A. A.; Kickham, M.; Pardeshi, J.; Fenelon, O., Squaramide–Napthalimide Conjugates as 'Turn-On'Fluorescent Sensors for Bromide Through an Aggregation-Disaggregation Approach. *Frontiers in Chemistry* **2019,** *7*, 354.
267. Kumawat, L. K.; Abogunrin, A. A.; Kickham, M.; Pardeshi, J.; Fenelon, O.; Schroeder, M.; Elmes, R. B., Squaramide—Naphthalimide Conjugates as "Turn-On" Fluorescent Sensors for Bromide Through an Aggregation-Disaggregation Approach. *Frontiers in chemistry* **2019,** *7*.
268. Veale, E. B.; Tocci, G. M.; Pfeffer, F. M.; Kruger, P. E.; Gunnlaugsson, T., Demonstration of bidirectional photoinduced electron transfer (PET) sensing in 4-amino-1, 8-naphthalimide based thiourea anion sensors. *Organic & biomolecular chemistry* **2009,** *7* (17), 3447-3454.
269. Brana, M.; Cacho, M.; Gradillas, A.; Pascual-Teresa, B. d.; Ramos, A., Intercalators as anticancer drugs. *Current pharmaceutical design* **2001,** *7* (17), 1745-1780.
270. Wang, L.; Fujii, M.; Yamaji, M.; Okamoto, H., Fluorescence behaviour of 2-, 3-and 4-amino-1, 8-naphthalimides: effects of the substitution positions of the amino functionality on the photophysical properties. *Photochemical & Photobiological Sciences* **2018,** *17* (10), 1319-1328.
271. Jia, X.; Yang, Y.; Xu, Y.; Qian, X., Naphthalimides for labeling and sensing applications. *Pure and Applied Chemistry* **2014,** *86* (7), 1237-1246.
272. Jin, R.; Tang, S., Theoretical investigation into optical and electronic properties of 1, 8-naphthalimide derivatives. *Journal of molecular modeling* **2013,** *19* (4), 1685-1693.
273. Zhou, E.; Zhang, J.; Lu, Y.; Dong, C., *Design and Synthesis of Novel C2-symmetric Chiral Shift Reagents Derived from Squaramide and their Recognition of Anions and Chiral Carboxylate Anions*. Ann Arbor, MI: Michigan Publishing, University of Michigan Library: 2014.
274. Minagawa, H.; Shimizu, A.; Kataoka, Y.; Kuwahara, M.; Kato, S.; Horii, K.; Shiratori, I.; Waga, I., Fluorescence polarization-based rapid detection system for salivary biomarkers using modified DNA aptamers containing base-appended bases. *Analytical chemistry* **2019,** *92* (2), 1780-1787.
275. Devi, K.; Sarma, R. J., Naphthalimide-Containing Isomeric Urea Derivatives: Mechanoluminescence and Fluoride Recognition. *ChemPhotoChem* **2017,** *1* (11), 524-531.
276. Kamal, A.; Srinivas, O.; Ramulu, P.; Ramesh, G.; Kumar, P. P., Synthesis of novel C2 and C2–C8 linked pyrrolo [2, 1-c][1, 4] benzodiazepine-naphthalimide hybrids as DNA-binding agents. *Bioorganic & medicinal chemistry letters* **2003,** *13* (20), 3577-3581.
277. Abdel-Hamid, M. K.; Macgregor, K. A.; Odell, L. R.; Chau, N.; Mariana, A.; Whiting, A.; Robinson, P. J.; McCluskey, A., 1, 8-Naphthalimide derivatives: new leads against dynamin I GTPase activity. *Organic & biomolecular chemistry* **2015,** *13* (29), 8016-8028.
278. Guo, P.; Chen, Q.; Liu, T.; Xu, L.; Yang, Q.; Qian, X., Development of unsymmetrical dyads as potent noncarbohydrate-based inhibitors against human β-N-acetyl-D-hexosaminidase. *ACS medicinal chemistry letters* **2013,** *4* (6), 527-531.
279. Patra, J. K.; Das, G.; Fraceto, L. F.; Campos, E. V. R.; del Pilar Rodriguez-Torres, M.; Acosta-Torres, L. S.; Diaz-Torres, L. A.; Grillo, R.; Swamy, M. K.; Sharma, S., Nano based drug delivery systems: recent developments and future prospects. *Journal of nanobiotechnology* **2018,** *16* (1), 1-33.
280. O'Malley, W. I.; Rubbiani, R.; Aulsebrook, M. L.; Grace, M. R.; Spiccia, L.; Tuck, K. L.; Gasser, G.; Graham, B., Cellular uptake and photo-cytotoxicity of a Gadolinium (III)-DOTA-Naphthalimide complex "clicked" to a lipidated tat peptide. *Molecules* **2016,** *21* (2), 194.

281. Cho, D. W.; Fujitsuka, M.; Sugimoto, A.; Majima, T., Intramolecular excimer formation and photoinduced electron-transfer process in bis-1, 8-naphthalimide dyads depending on the linker length. *The Journal of Physical Chemistry A* **2008,** *112* (31), 7208-7213.
282. Ye, Z.; Kai, W.; Xianghui, Y.; Wen, Q.; Hengshan, W., Synthesis of 1, 8-Naphthalimide Derivative under Ultrasound. *CHINESE JOURNAL OF ORGANIC CHEMISTRY* **2011,** *31* (4), 557-562.
283. Grabchev, I.; Petkov, C.; Bojinov, V., Synthesis and absorption properties of some new bis-1, 8-naphthalimides. *Dyes and pigments* **2001,** *48* (3), 239-244.
284. Huang, Y.; Wu, C.-X.; Song, Y.; Huang, M.; Tian, D.-N.; Yang, X.-B.; Fan, Y.-R., Synthesis, DNA binding, and anticancer properties of bis-naphthalimide derivatives with lysine-modified polyamine linkers. *Molecules* **2018,** *23* (2), 266.
285. Hardesty, J. H.; Attili, B., Spectrophotometry and the Beer-Lambert Law: An Important Analytical Technique in Chemistry. *Collin College, Department of Chemistry* **2010**.
286. Shao, Y.; Yin, G.-Z.; Ren, X.; Zhang, X.; Wang, J.; Guo, K.; Li, X.; Wesdemiotis, C.; Zhang, W.-B.; Yang, S., Engineering π–π interactions for enhanced photoluminescent properties: unique discrete dimeric packing of perylene diimides. *RSC advances* **2017,** *7* (11), 6530-6537.
287. Propst, C., *Nucleic acid targeted drug design*. Informa Health Care: 1992.
288. Tse, W. C.; Boger, D. L., A fluorescent intercalator displacement assay for establishing DNA binding selectivity and affinity. *Accounts of chemical research* **2004,** *37* (1), 61-69.
289. LePecq, J.-B.; Paoletti, C., A fluorescent complex between ethidium bromide and nucleic acids: physical—chemical characterization. *Journal of molecular biology* **1967,** *27* (1), 87-106.
290. Boger, D. L.; Fink, B. E.; Hedrick, M. P., Total synthesis of distamycin A and 2640 analogues: a solution-phase combinatorial approach to the discovery of new, bioactive DNA binding agents and development of a rapid, high-throughput screen for determining relative DNA binding affinity or DNA binding sequence selectivity. *Journal of the American Chemical Society* **2000,** *122* (27), 6382-6394.
291. Veale, E. B. Design, synthesis, photophysical and biological evaluation of Novel 1, 8-naphthalimide derivatives as DNA binders and potential anti-cancer agents. Trinity College (Dublin, Ireland). School of Chemistry, 2008.
292. Hermann, A.; Mohamed, S.; Sadawe, I.; Meiqal, N.; Alshoushan, A.; Aboud, A.; Aboulqasim, S.; Issa, A.; Bensaber, S.; Gbaj, A., DNA Interaction Study of Some Symmetrical 1, 2-Phenylenediamine Schiff's Base Derivatives as New Potential DNA Intercalators Using Ethidium Bromide Competition Fluorescent Assay. *Archives in Biomedical Engineering & Biotechnology* **2019,** (2 (2)), 1-7.

Appendix

Appendix 1

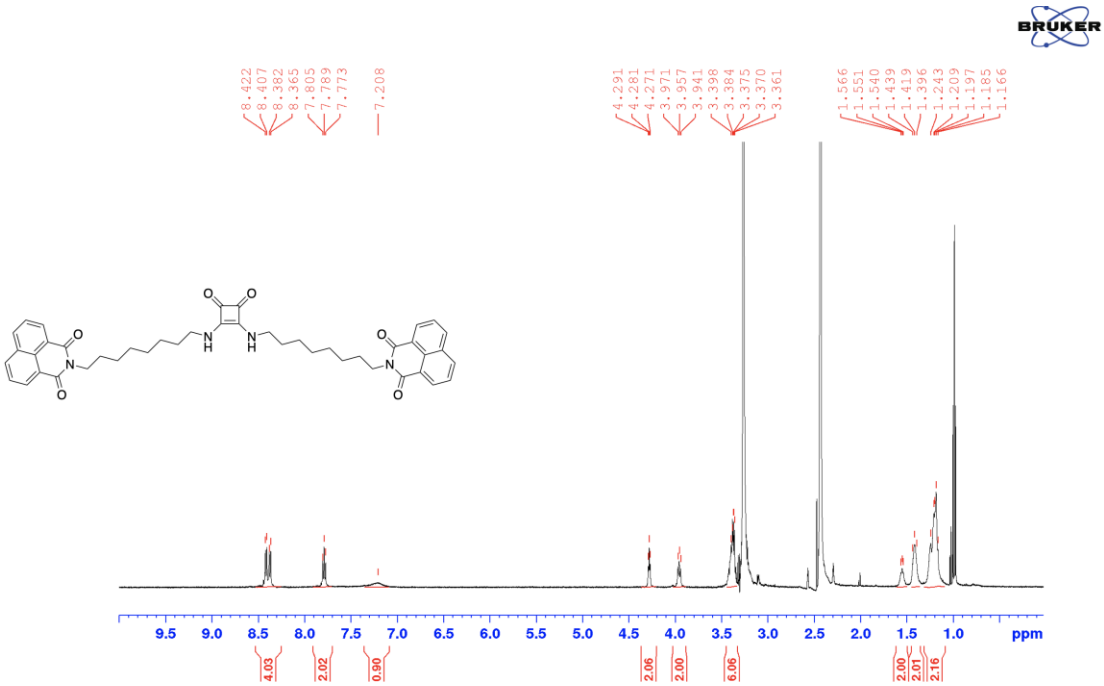

Figure A1.1: ^{1}H NMR (500 MHz, DMSO-d6) of **40** at 298 K.

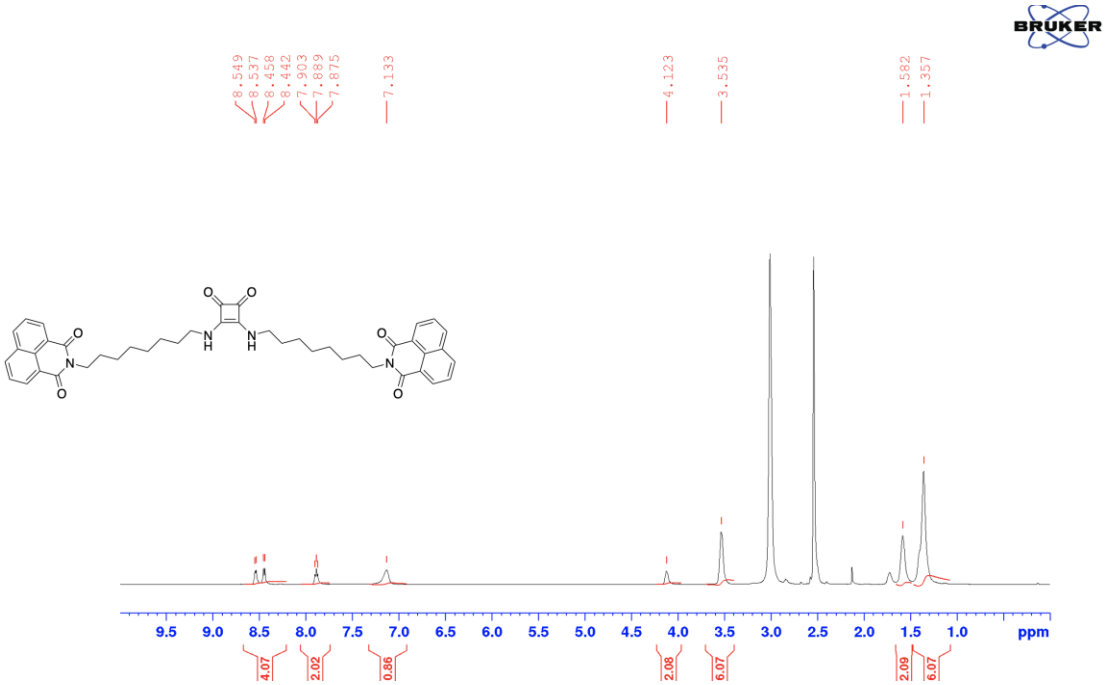

Figure A1.2: ^{1}H NMR (500 MHz, DMSO-d6) of **40** at 358 K.

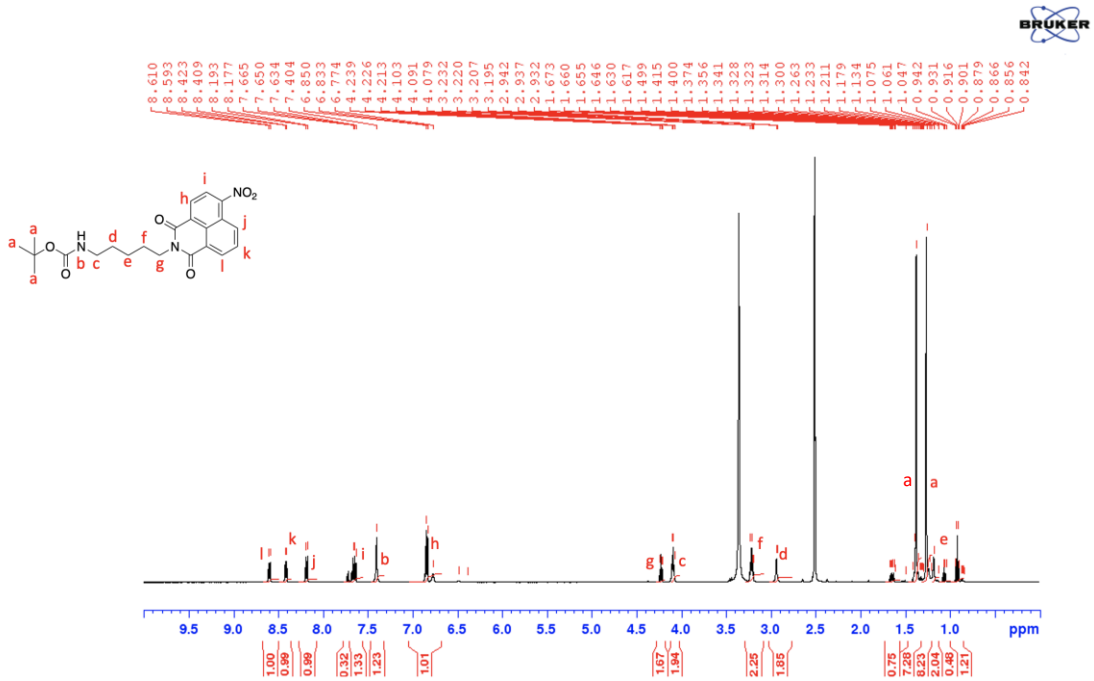

Figure A1.3: ^{1}H NMR (500 MHz, DMSO-d6) of **74** at 298 K.

Appendix 2

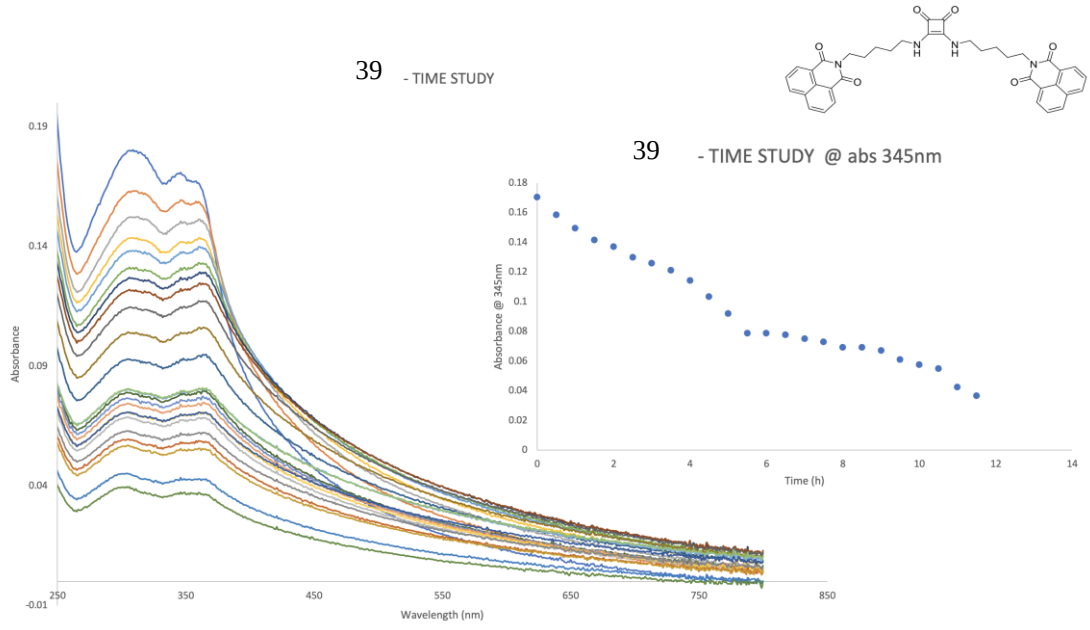

Figure 2.1: UV-VIS absorbance time study of **39** over the course of 12 hours in DMSO and its absorbance at 345nm vs the concentration (mg/mL) of **39**.

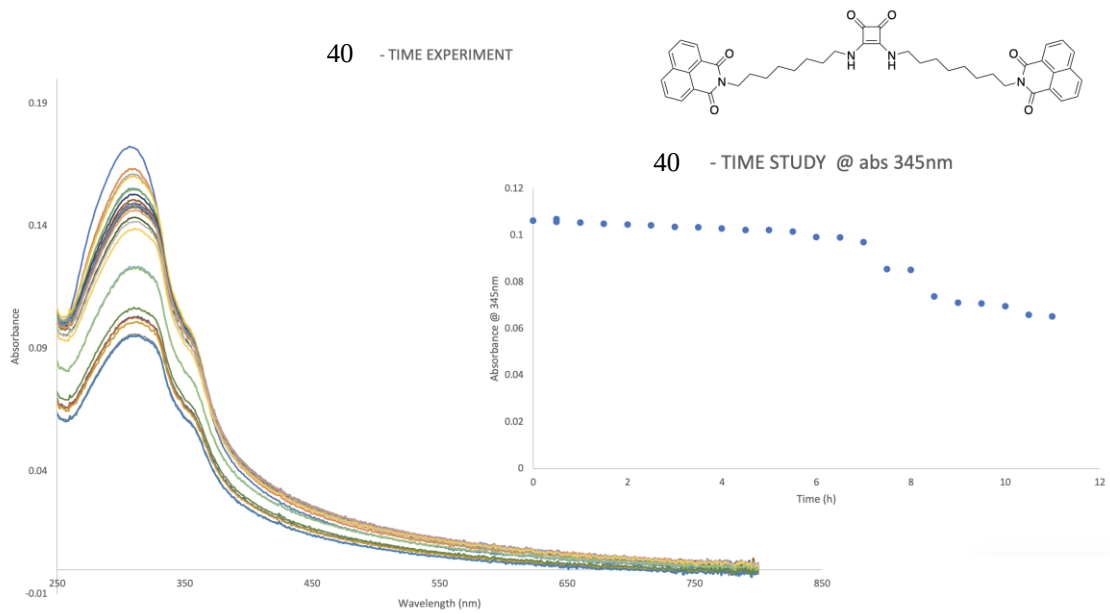

Figure A2.2: UV-VIS absorbance time study of **40** over the course of 12 hours in DMSO, and its absorbance at 345nm vs the concentration (mg/mL) of **40**.

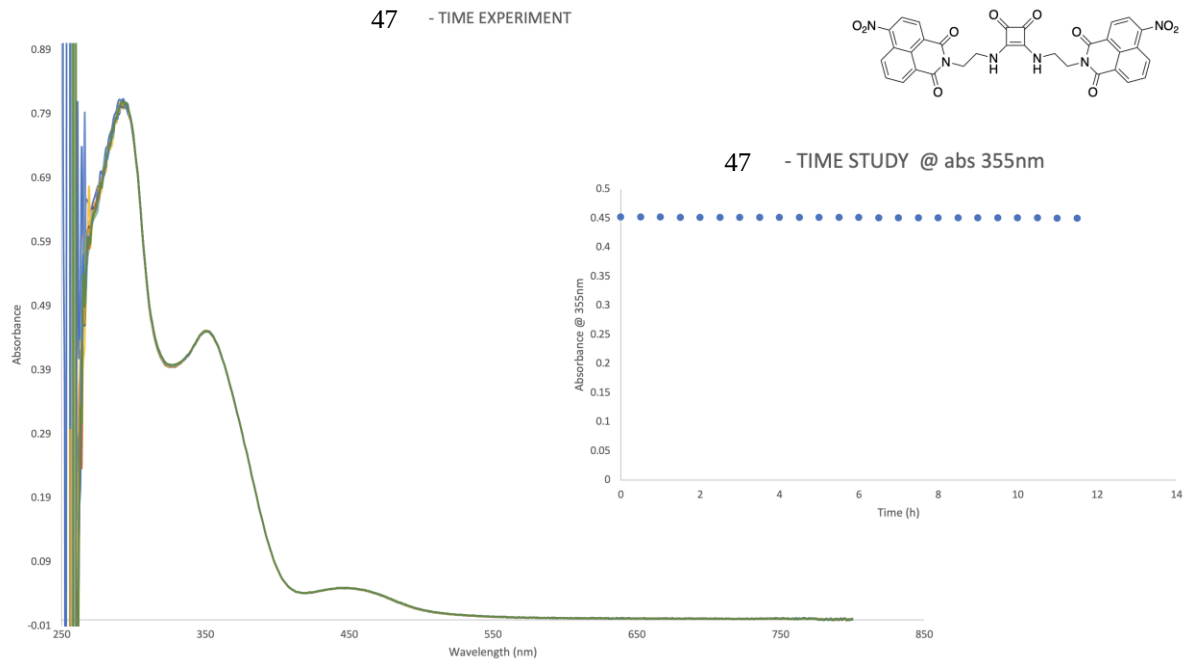

Figure A2.3: UV-VIS absorbance time study of **47** over the course of 12 hours in DMSO, and its absorbance at 345nm vs the concentration (mg/mL) of **47**.

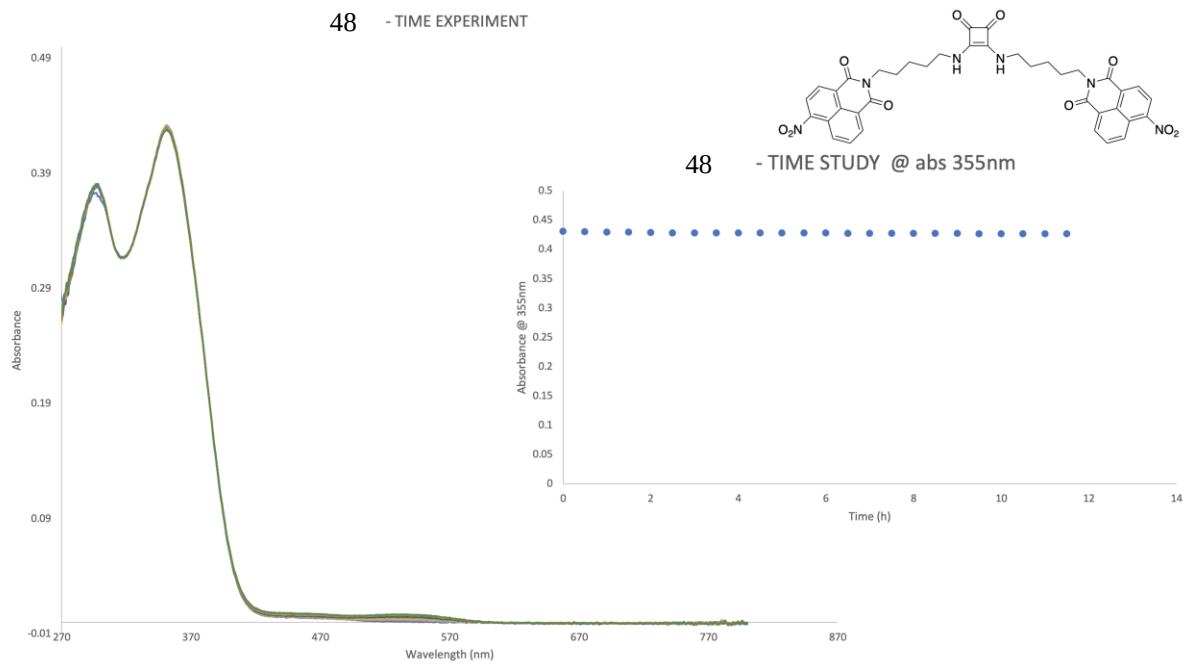

Figure A2.4: UV-VIS absorbance time study of **48** over the course of 12 hours in DMSO and its absorbance at 345nm vs the concentration (mg/mL) of **48**.

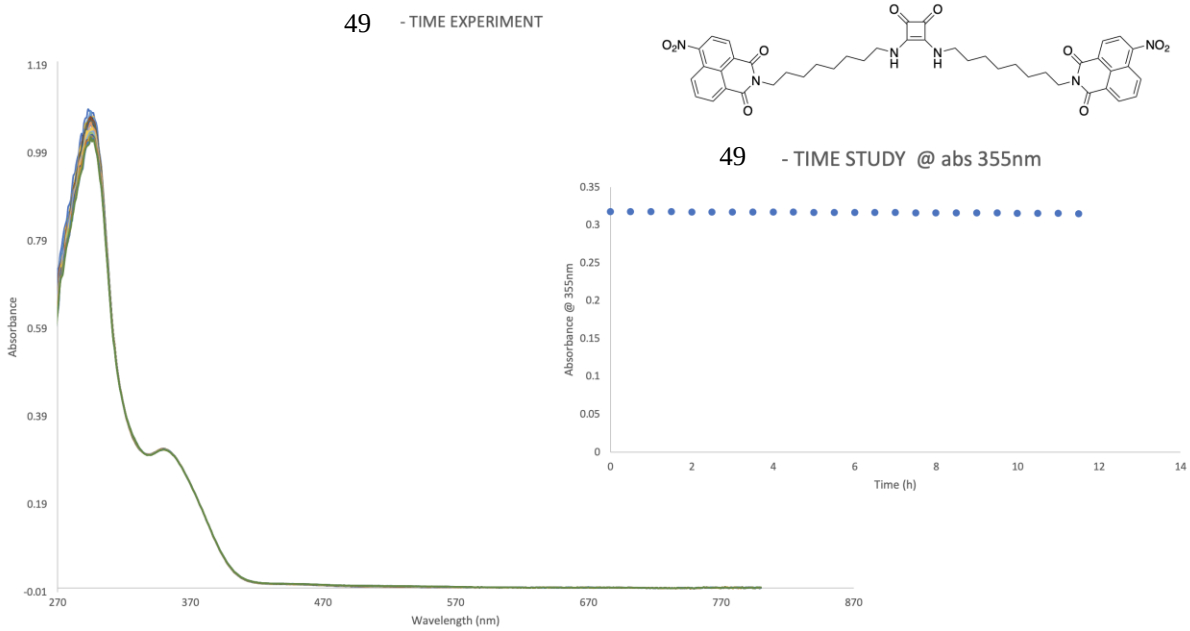

Figure A2.5: UV-VIS absorbance time study of **49** over the course of 12 hours in DMSO, and its absorbance at 345nm vs the concentration (mg/mL) of **49**.

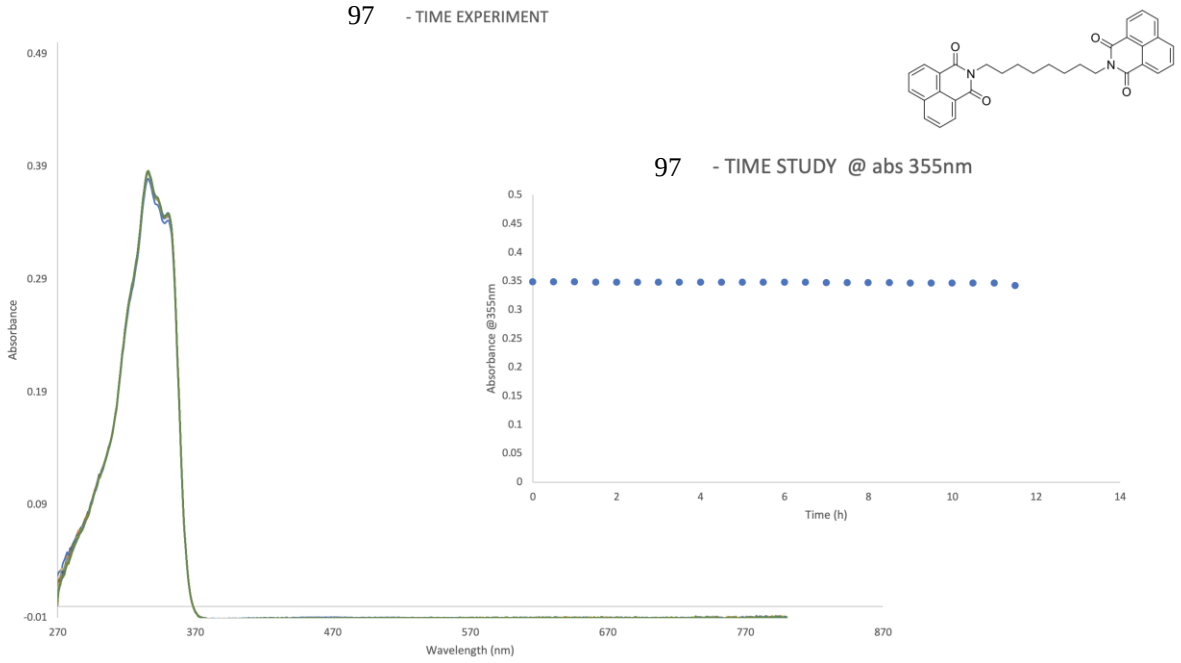

Figure A2.6: UV-VIS absorbance time study of **97** over the course of 12 hours in DMSO, and its absorbance at 345nm vs the concentration (mg/mL) of **97**.

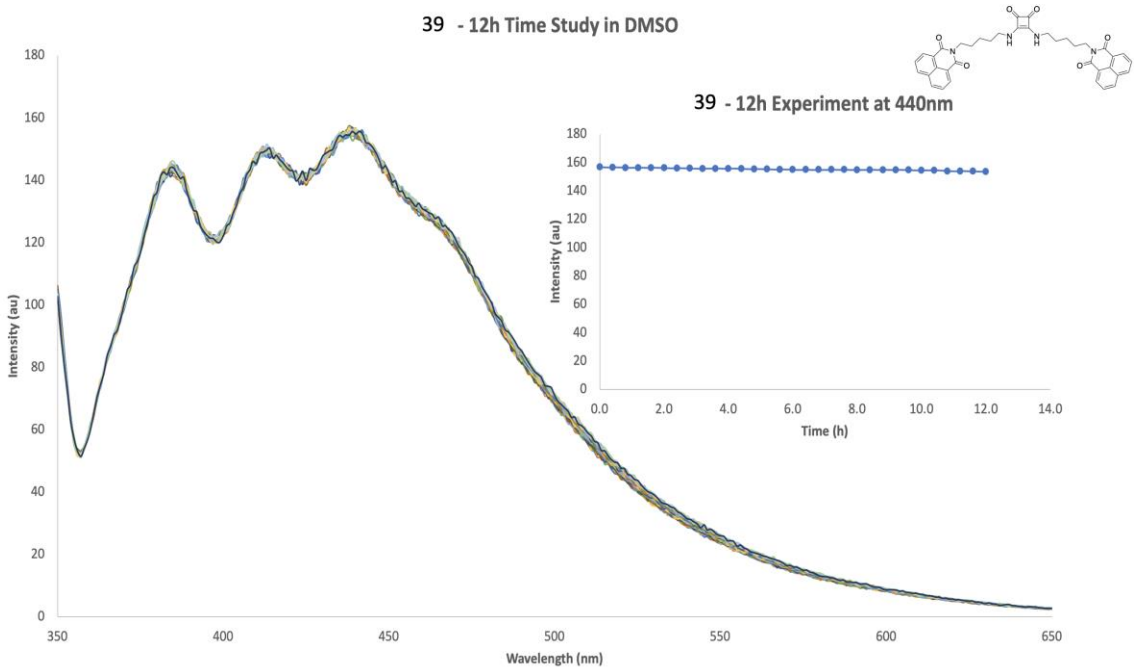

Figure A2.7: Fluorescence intensity (au) time study of **39**, with an excitation wavelength at 440 nm over the course of 12 hours in DMSO.

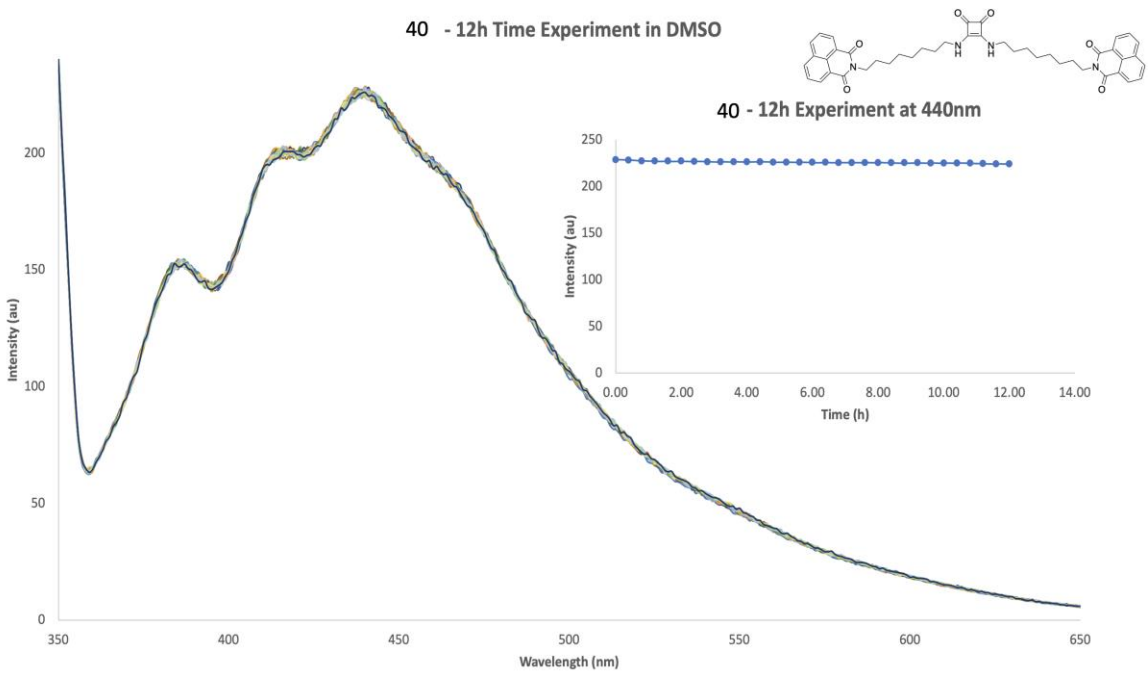

Figure A2.8: Fluorescence intensity (au) time study of **40**, with an excitation wavelength at 440 nm over the course of 12 hours in DMSO.

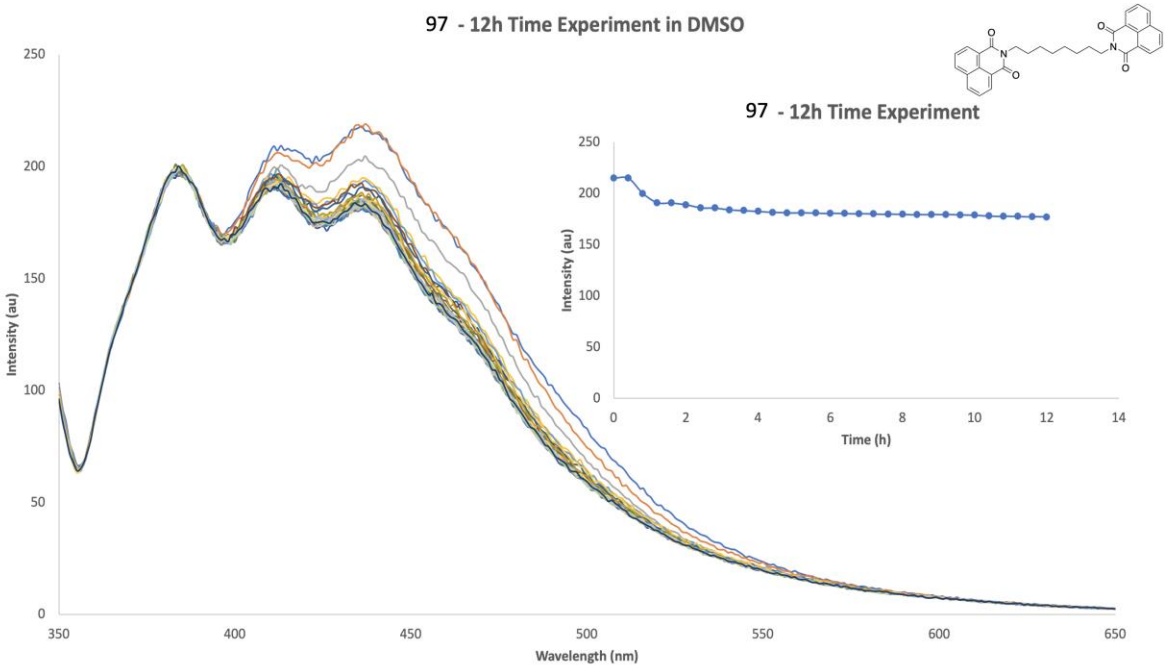

Figure A2.9: Fluorescence intensity (au) time study of **97**, with an excitation wavelength at 440 nm over the course of 12 hours in DMSO.

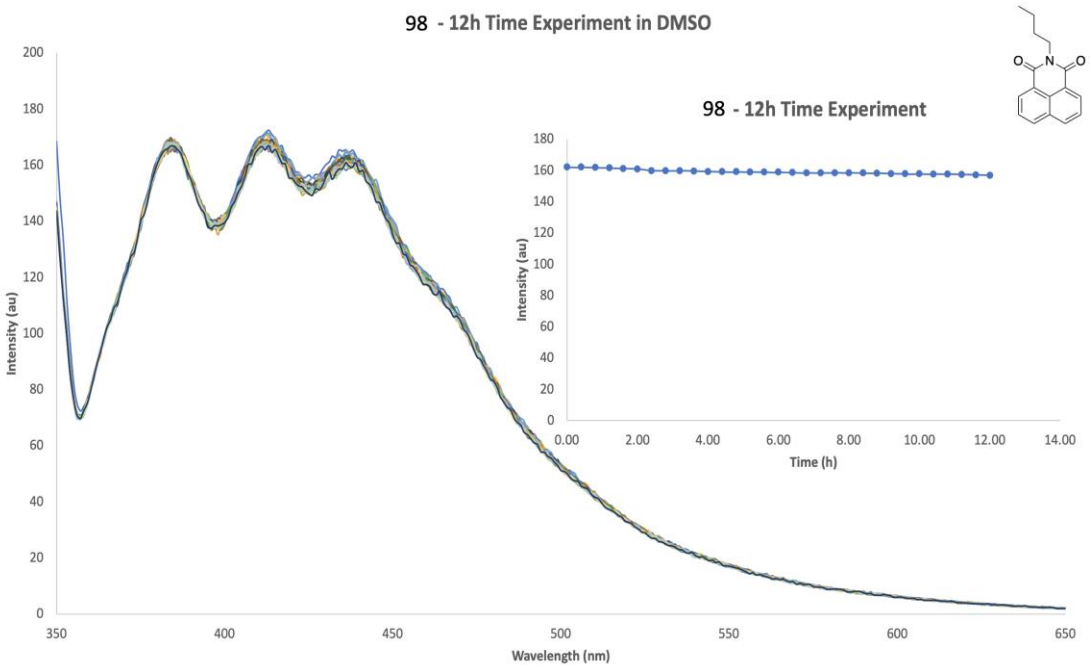

Figure A2.10: Fluorescence intensity (au) time study of **98**, with an excitation wavelength at 450 nm over the course of 12 hours in DMSO.

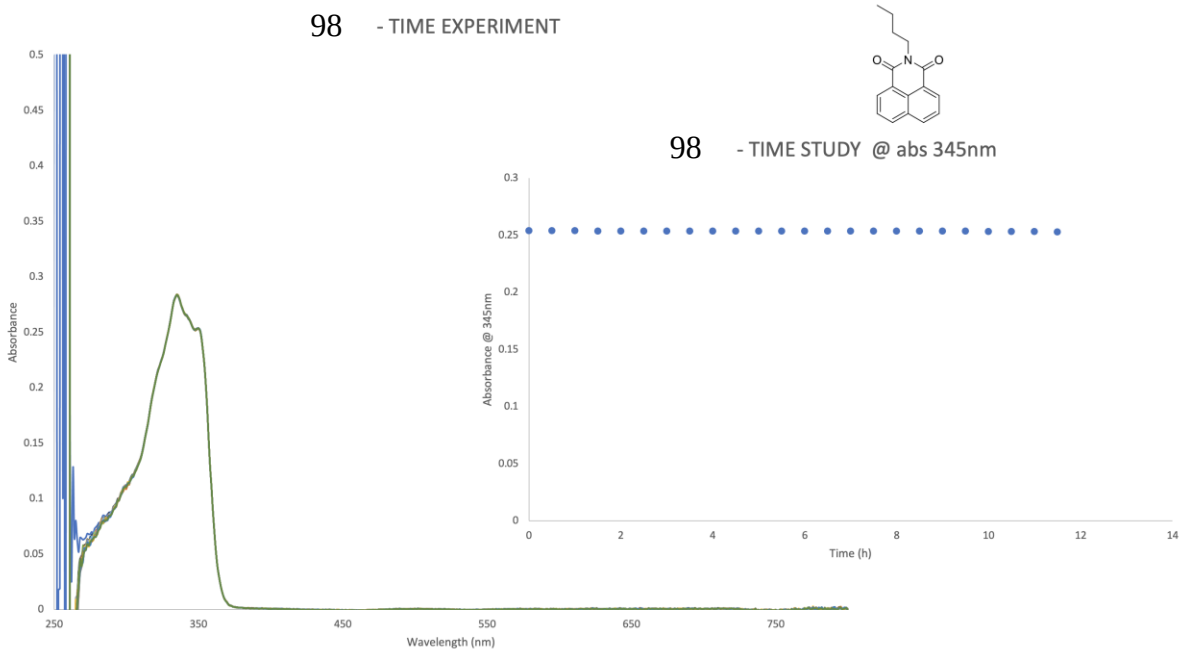

Figure A2.11: UV-VIS absorbance time study of **98** over the course of 12 hours in DMSO.

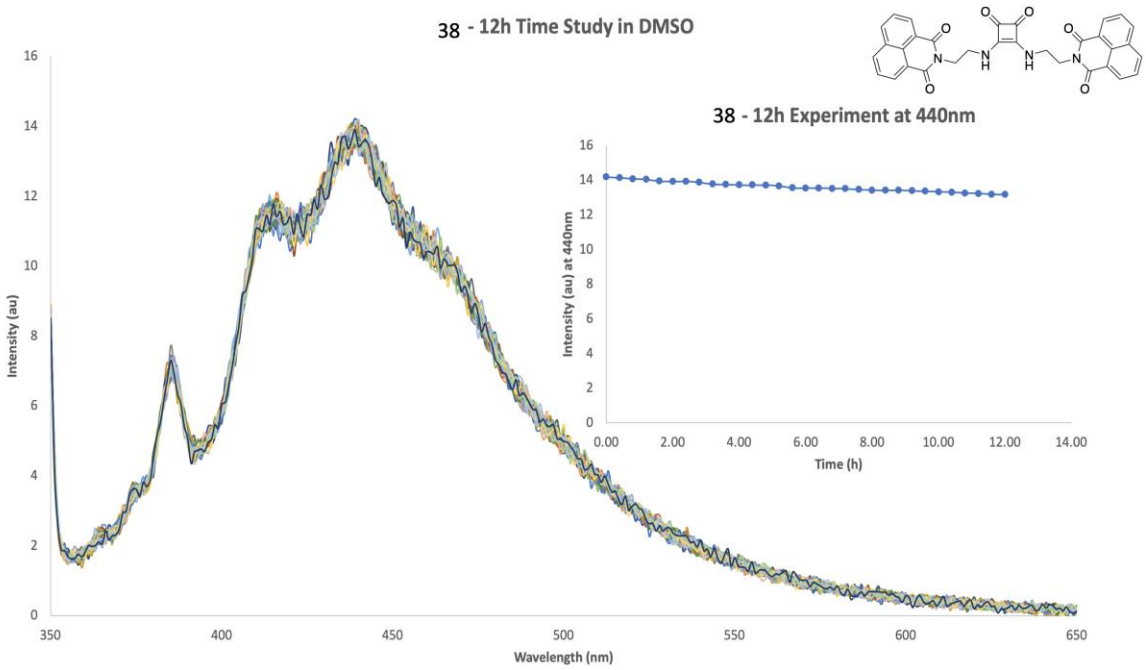

Figure A2.12: Fluorescence intensity (au) time study of **38**, with an excitation wavelength at 440 nm over the course of 12 hours in DMSO.

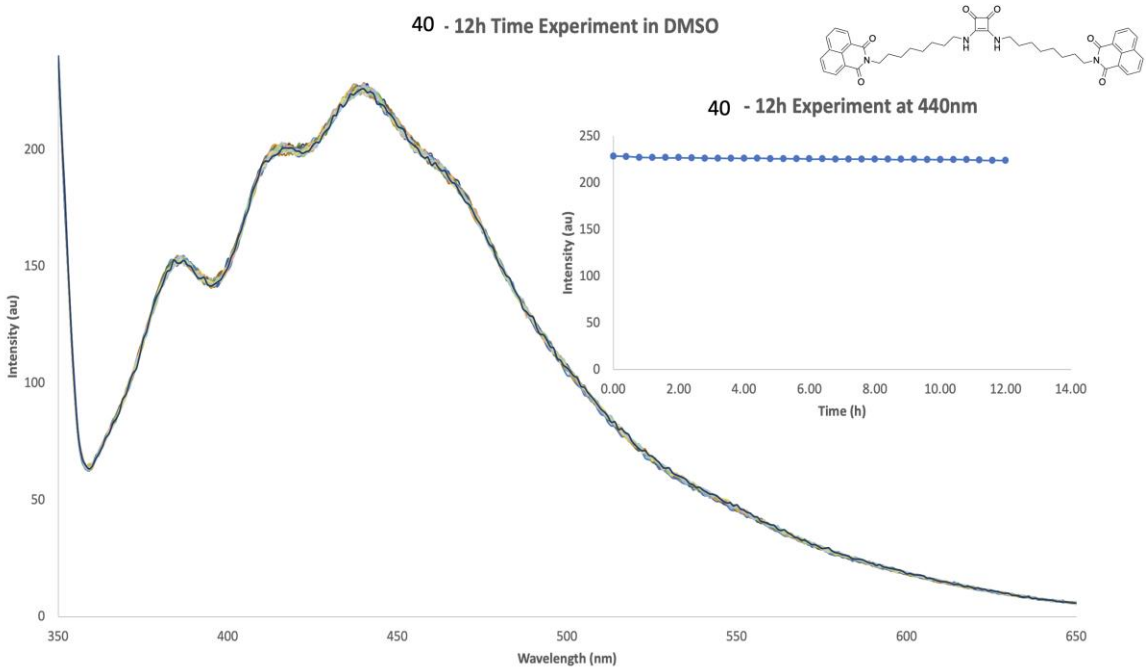

Figure A2.13: Fluorescence intensity (au) time study of **40** with an excitation wavelength at 440 nm over the course of 12 hours in DMSO.

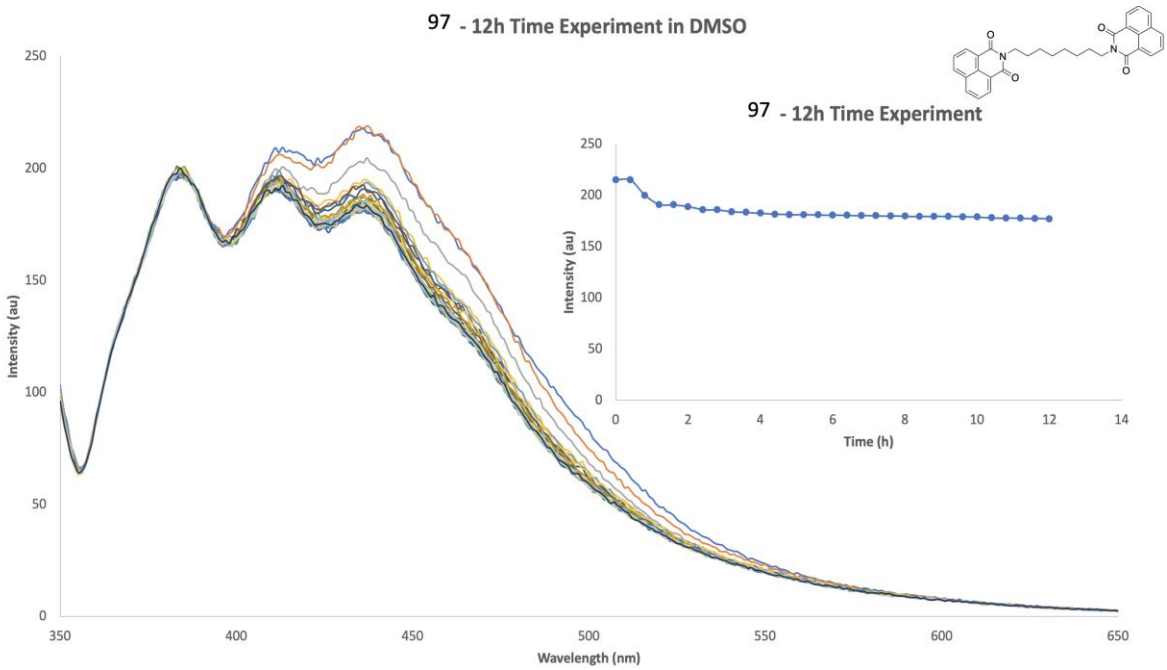

Figure A2.14: Fluorescence intensity (au) time study of **97**, with an excitation wavelength at 440 nm over the course of 12 hours in DMSO.

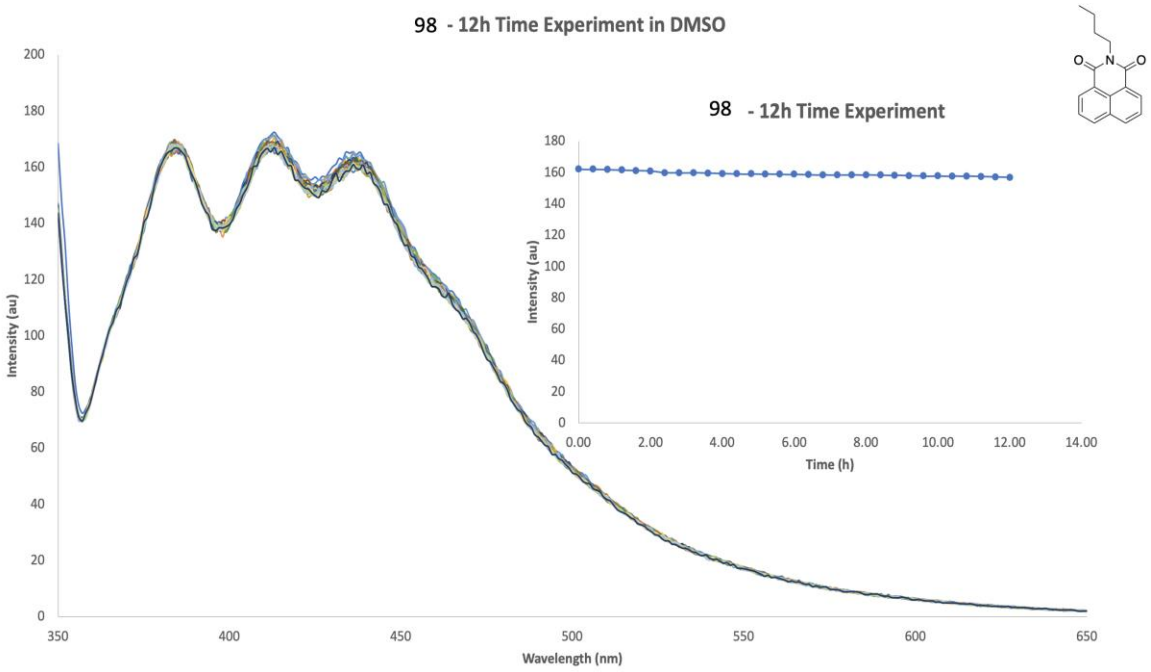

Figure A2.15: Fluorescence intensity (au) time study of **98**, with an excitation wavelength at 440 nm over the course of 12 hours in DMSO.

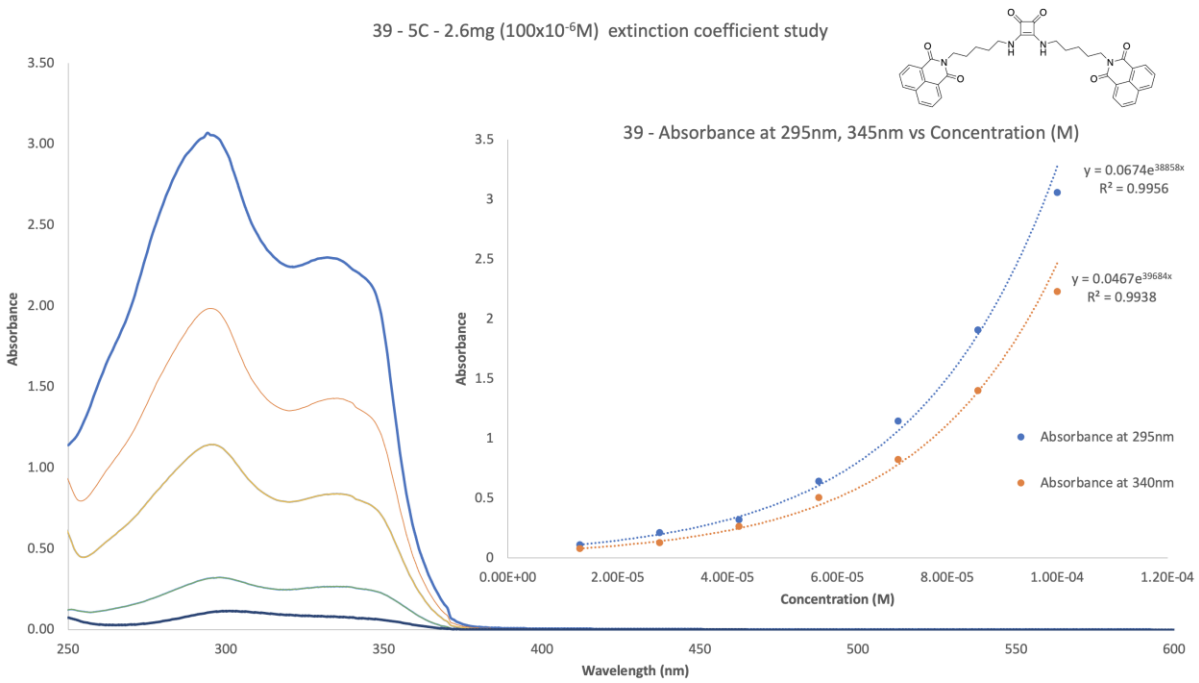

Figure A2.16: UV-Vis Absorbance of 2.6mg of **39** and its absorbance at 345nm vs the concentration (M) of **39**.

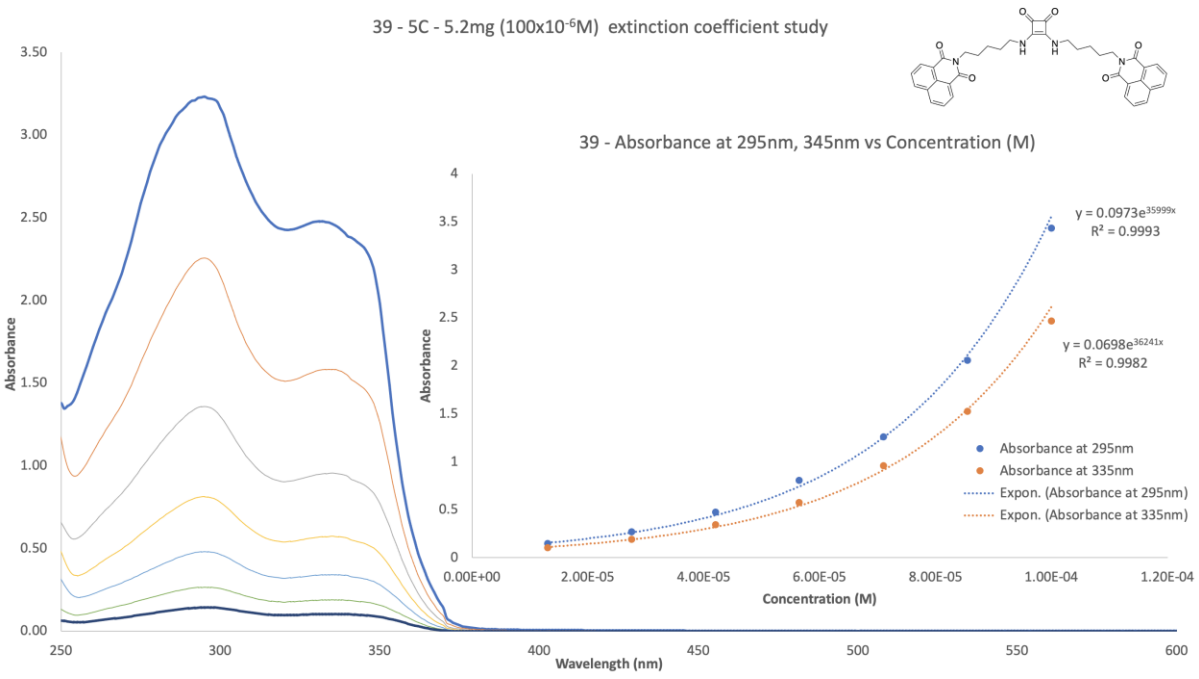

Figure A2.17: UV-Vis Absorbance of 5.2mg of **39** and its absorbance at 345nm vs the concentration (M) of **39**.

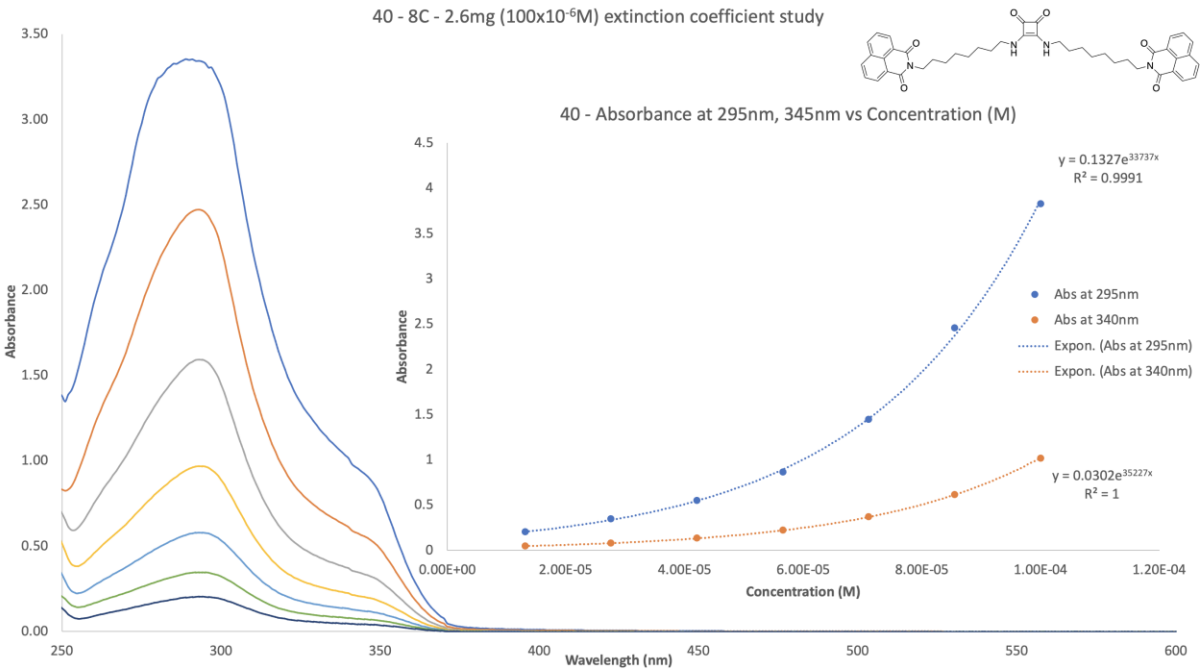

Figure A2.18: UV-Vis Absorbance of 2.6mg of **40** and its absorbance at 345nm vs the concentration (M) of **40**.

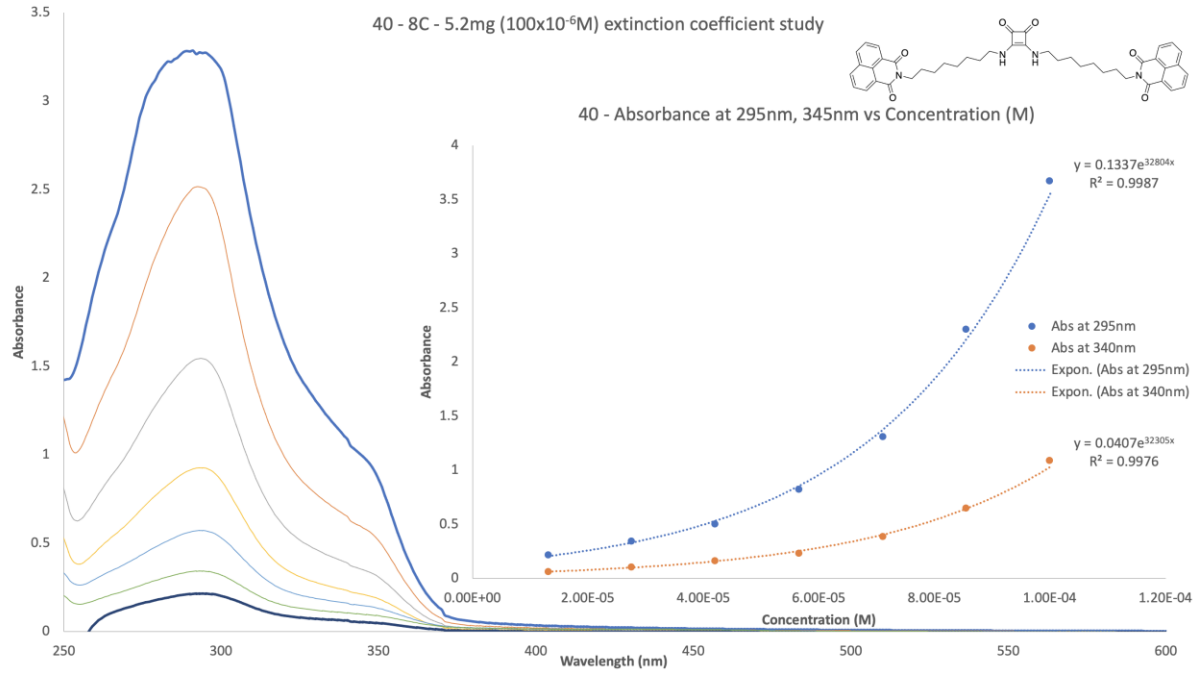

Figure A2.19: UV-Vis Absorbance of 5.2mg of **40** and its absorbance at 345nm vs the concentration (M) of **40**.

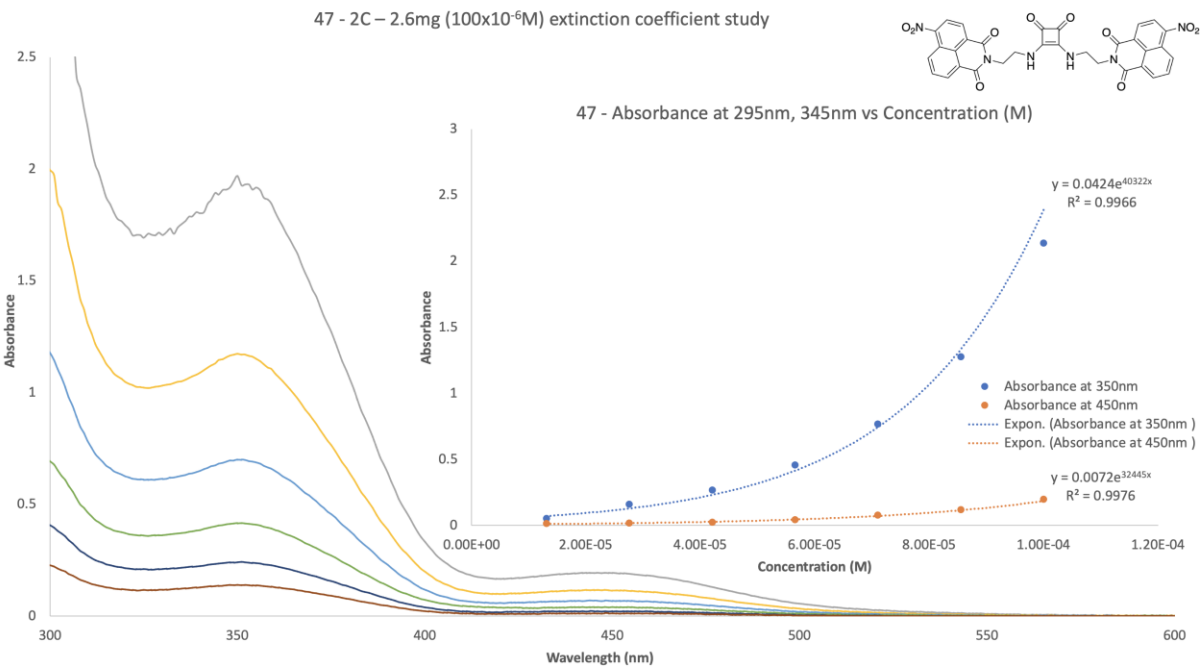

Figure A2.20: UV-Vis Absorbance of 2.6mg of **47** and its absorbance at 345nm vs the concentration (M) of **47**.

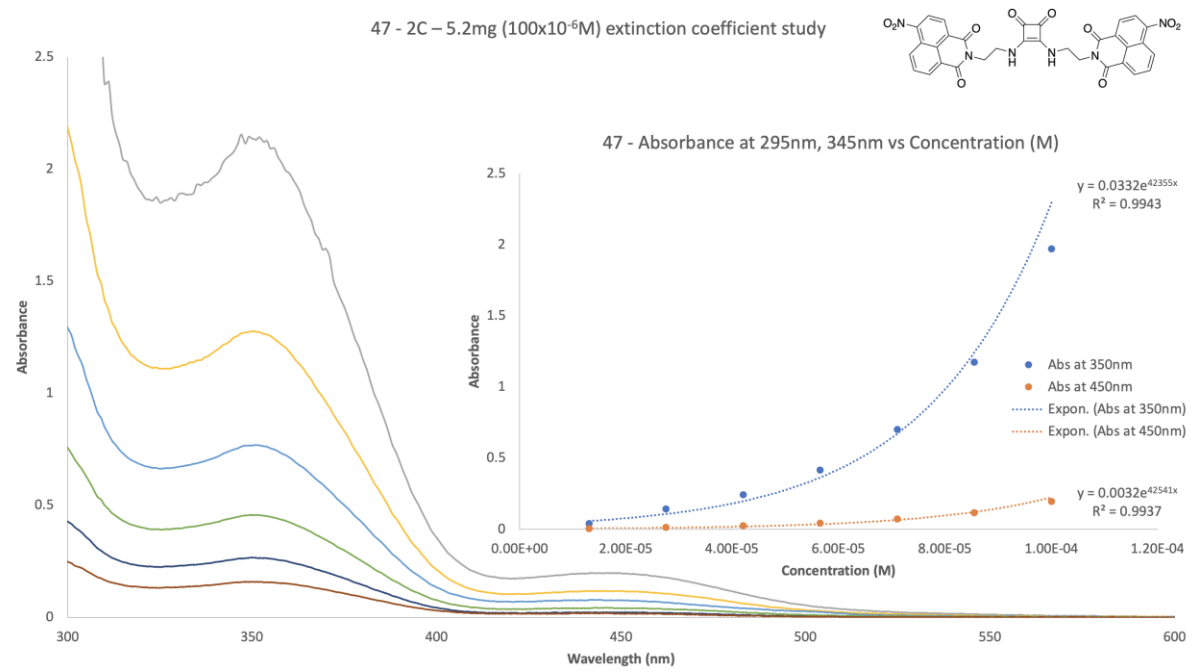

Figure A2.21: UV-Vis Absorbance of 5.2mg of **47** and its absorbance at 345nm vs the concentration (M) of **47**.

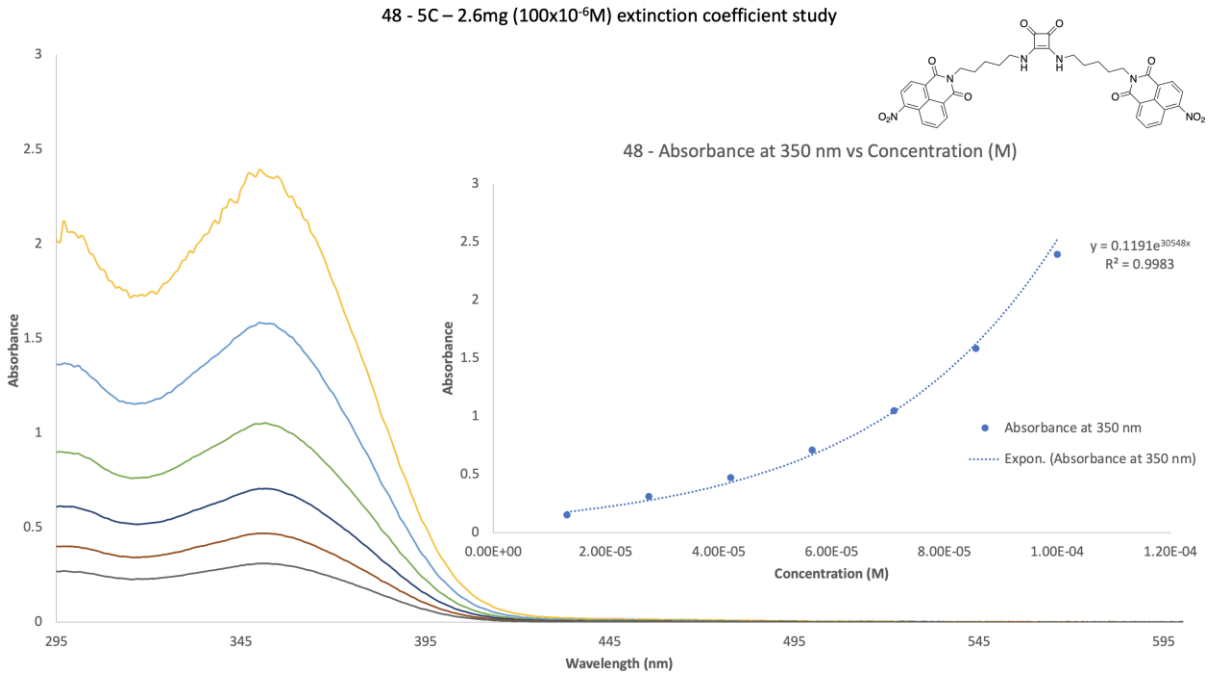

Figure A2.22: UV-Vis Absorbance of 2.6mg of **48** and its absorbance at 345nm vs the concentration (M) of **48**.

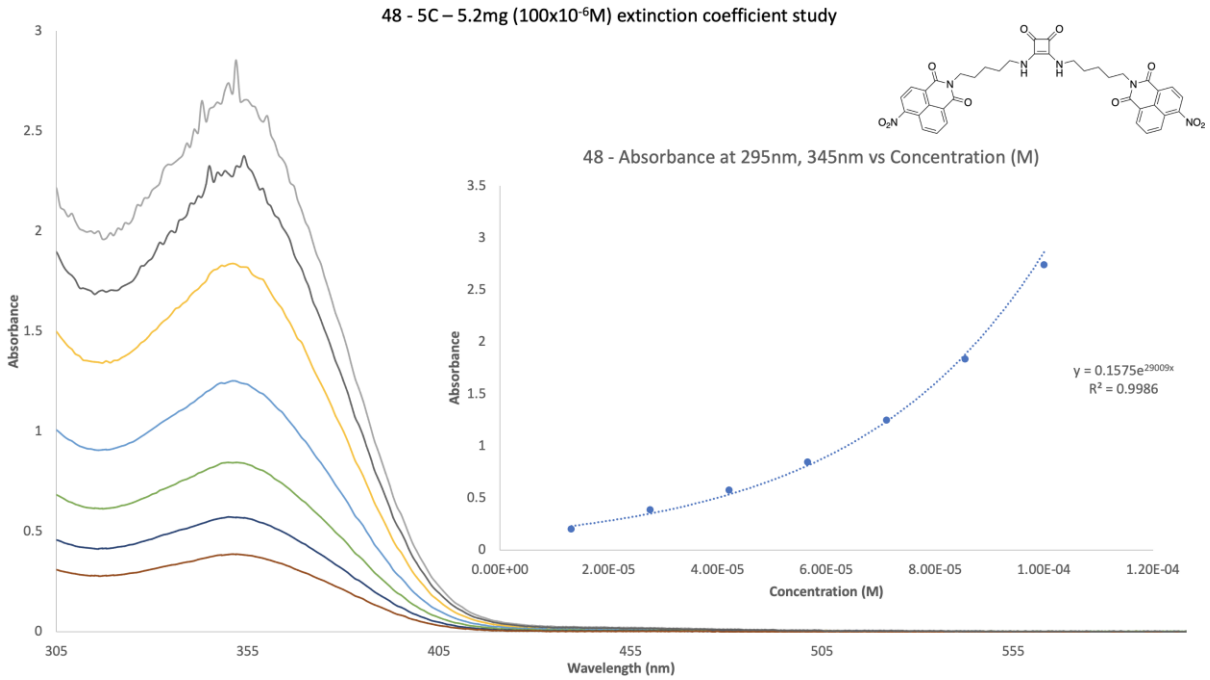

Figure A2.23: UV-Vis Absorbance of 5.2mg of **48** and its absorbance at 345nm vs the concentration (M) of **48**.

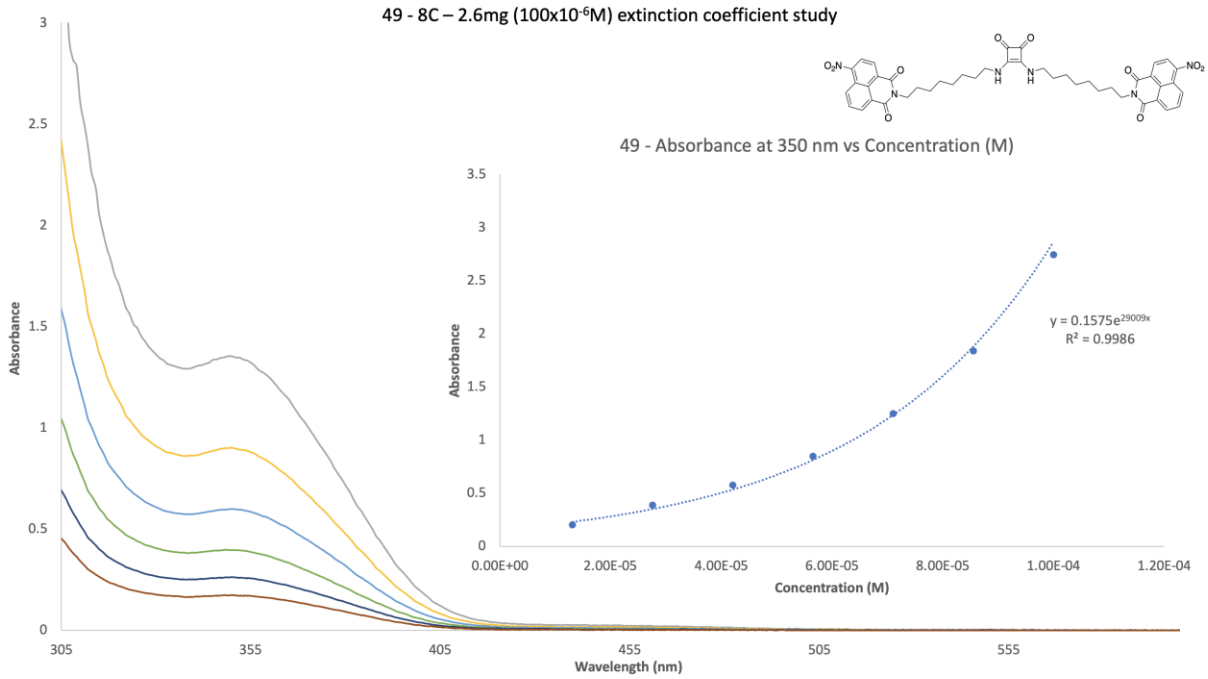

Figure A2.24: UV-Vis Absorbance of 2.6mg of **49** and its absorbance at 345nm vs the concentration (M) of **49**.

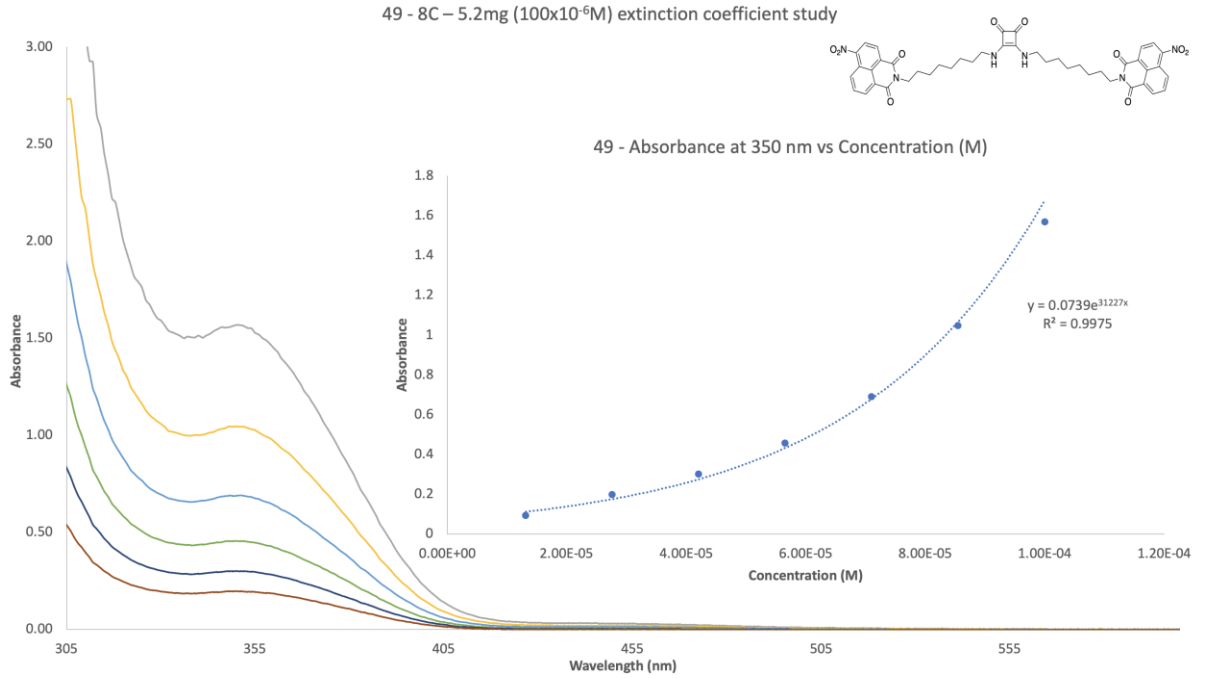

Figure A2.25: UV-Vis Absorbance of 5.2mg of **49** and its absorbance at 345nm vs the concentration (M) of **49**.

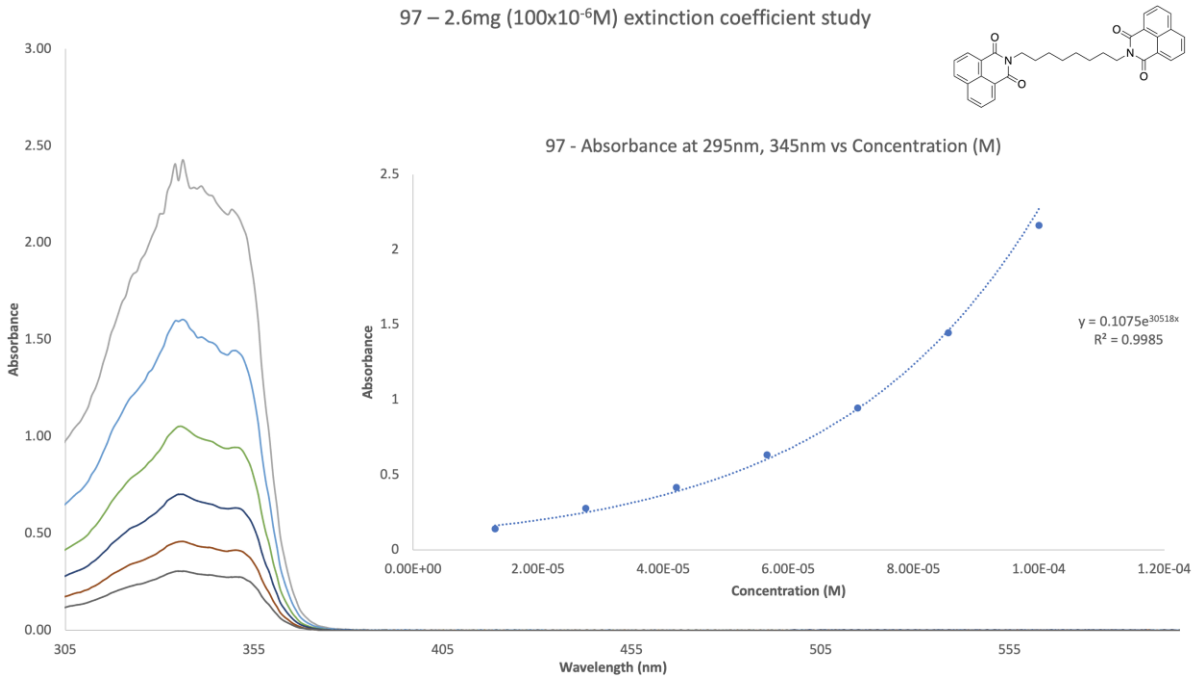

Figure A2.26: UV-Vis Absorbance of 2.6mg of **97** and its absorbance at 345nm vs the concentration (M) of **97**.

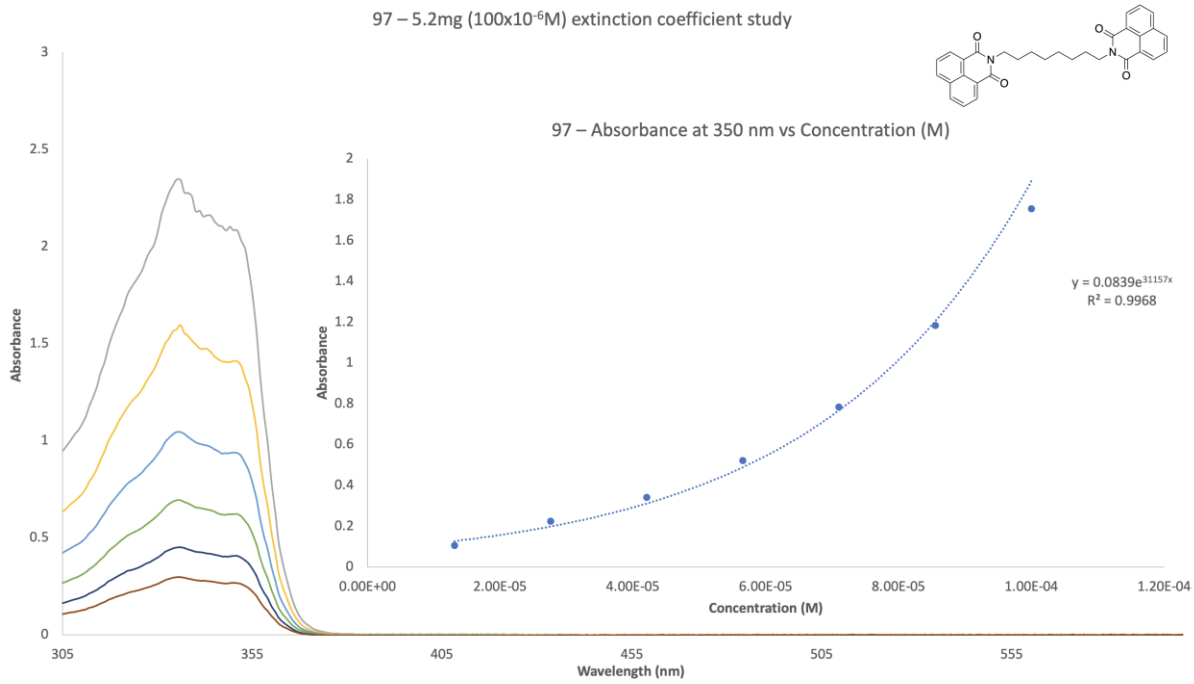

Figure A2.27: UV-Vis Absorbance of 5.2mg of **97** and its absorbance at 345nm vs the concentration (M) of **97**.

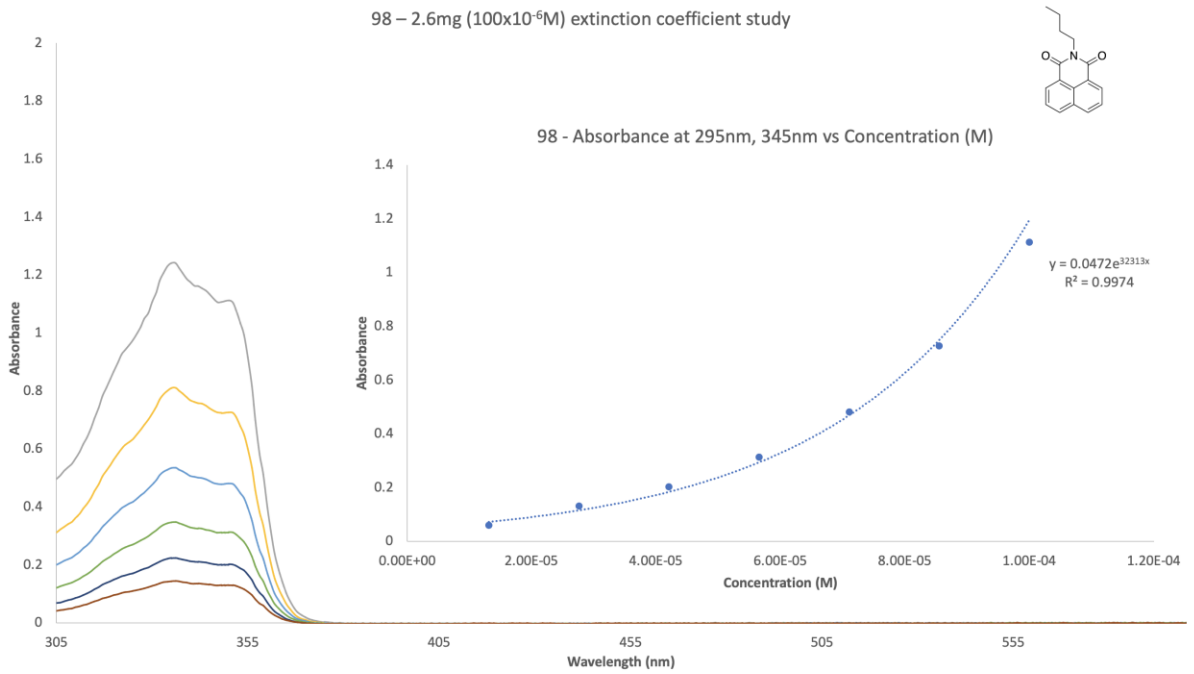

Figure A2.28: UV-Vis Absorbance of 2.6mg of **98** and its absorbance at 345nm vs the concentration (M) of **98**.

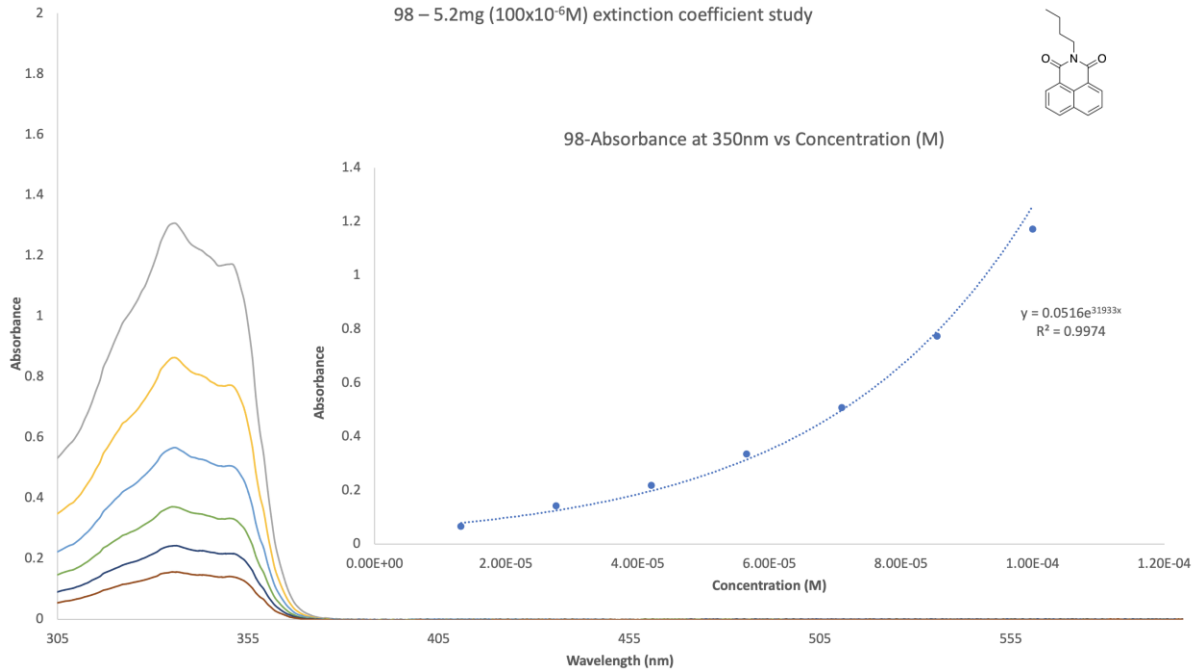

Figure A2.29: UV-Vis Absorbance of 5.2mg of **98** and its absorbance at 345nm vs the concentration (M) of **98**.

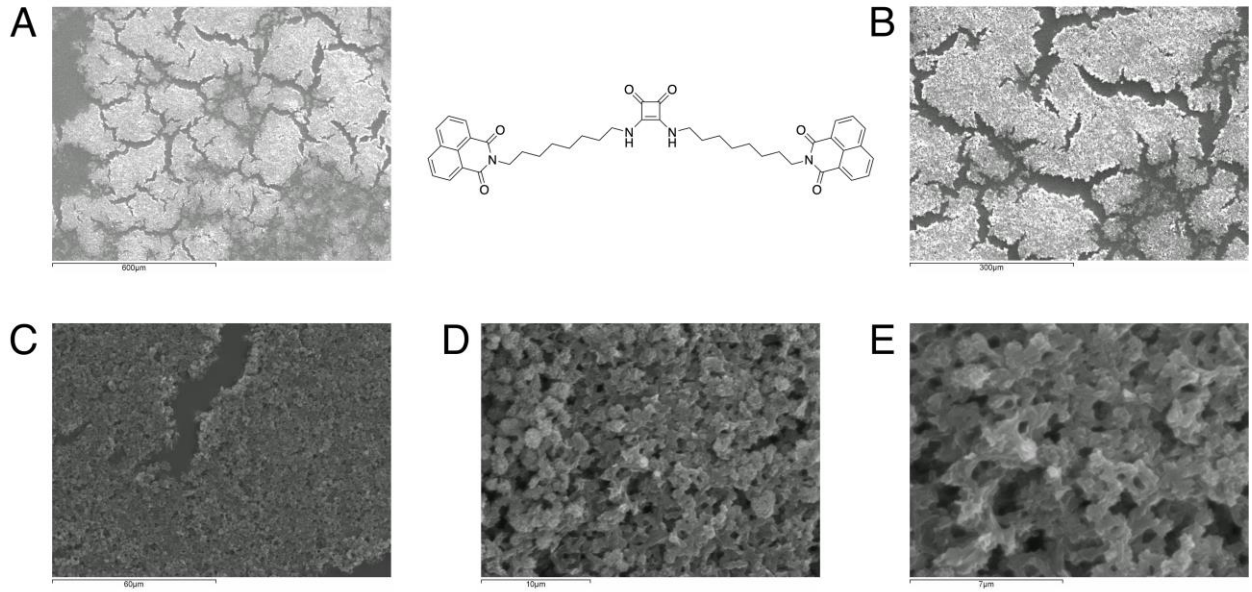

Figure A2.30: Scanning electron microscopy (SEM) images of compound **40** spotted with Au, **(A):** Mag x 100; **(B):** Mag x 200; **(C):** Mag x 1000; **(D):** Mag x 4000; **(E):** Mag x 8000.

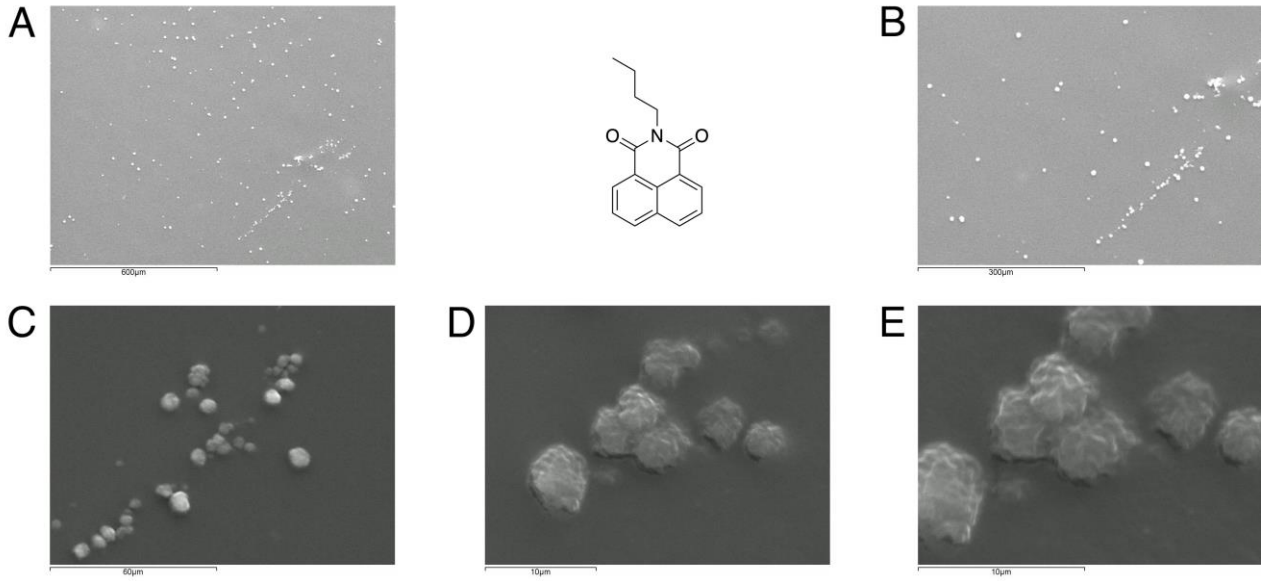

Figure A2.31: Scanning electron microscopy (SEM) images of compound **98** spotted with Au in DMSO, **(A):** Mag x 100; **(B):** Mag x 200; **(C):** Mag x 1000; **(D):** Mag x 4000; **(E):** Mag x 6000.

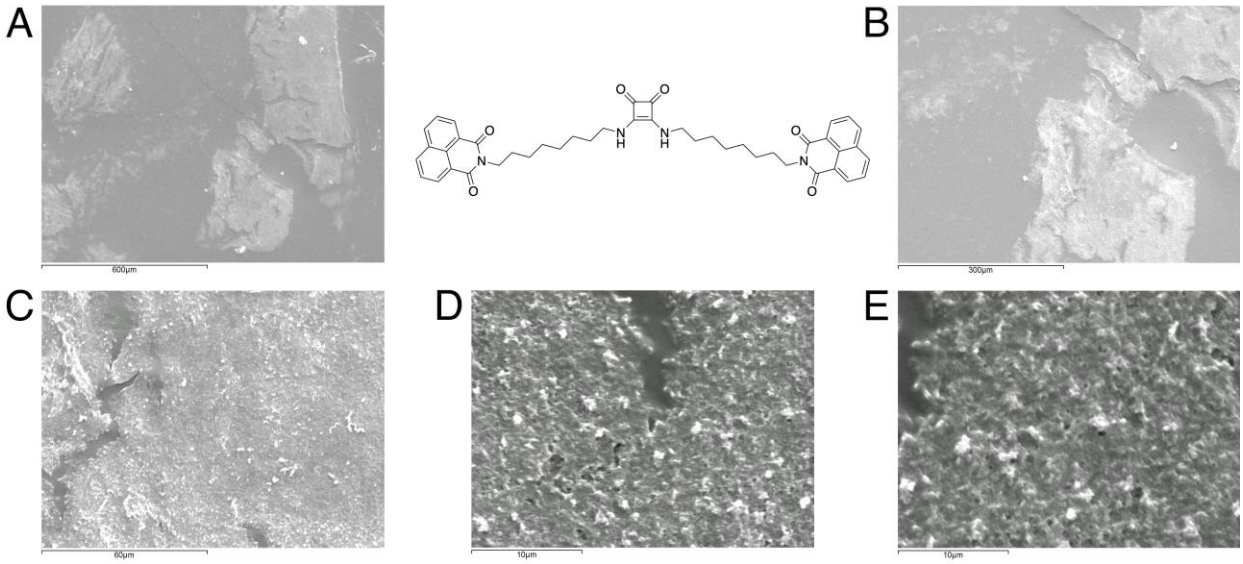

Figure A2.32: Scanning electron microscopy (SEM) images of compound **40** spotted with Au in DMSO:H_2O 50:50, **(A):** Mag x 100; **(B):** Mag x 200; **(C):** Mag x 1000; **(D):** Mag x 4000; **(E):** Mag x 6000.

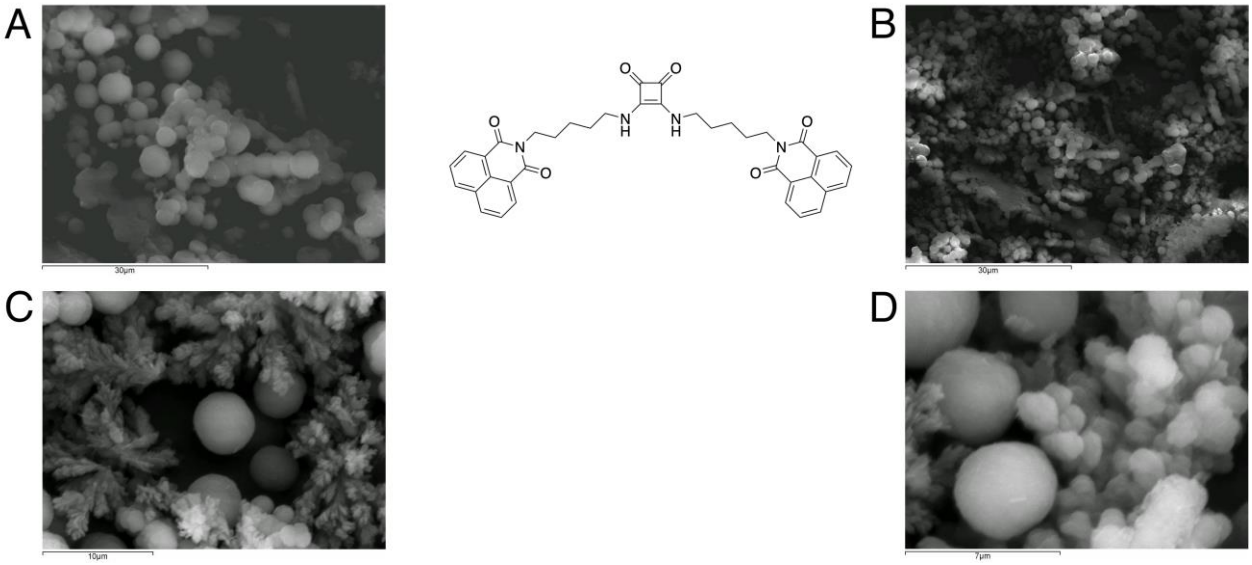

Figure A2.33: Scanning electron microscopy (SEM) images of compound **39** in DMSO:H_2O 50:50 (tilted), **(A):** Mag x 200; **(B):** Mag x 800; **(C):** Mag x 4000; **(D):** Mag x 8000.

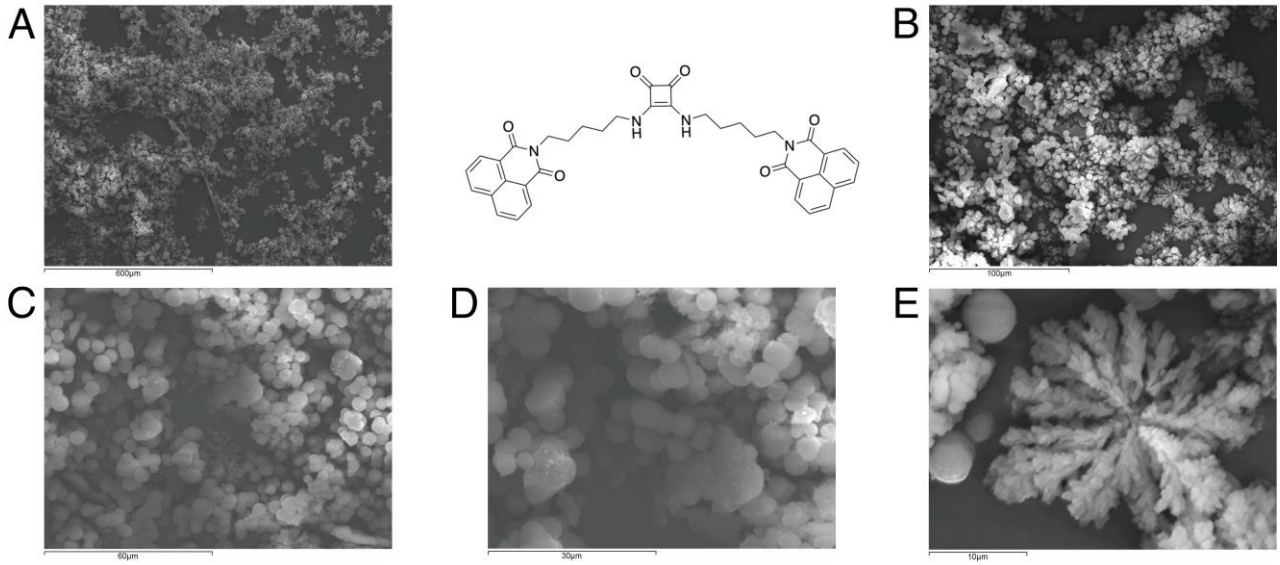

Figure A2.34: Scanning electron microscopy (SEM) images of compound **39** in DMSO:H_2O 50:50, **(A):** Mag x 100; **(B):** Mag x 500; **(C):** Mag x 1000; **(D):** Mag x 2000; **(E):** Mag x 3500.

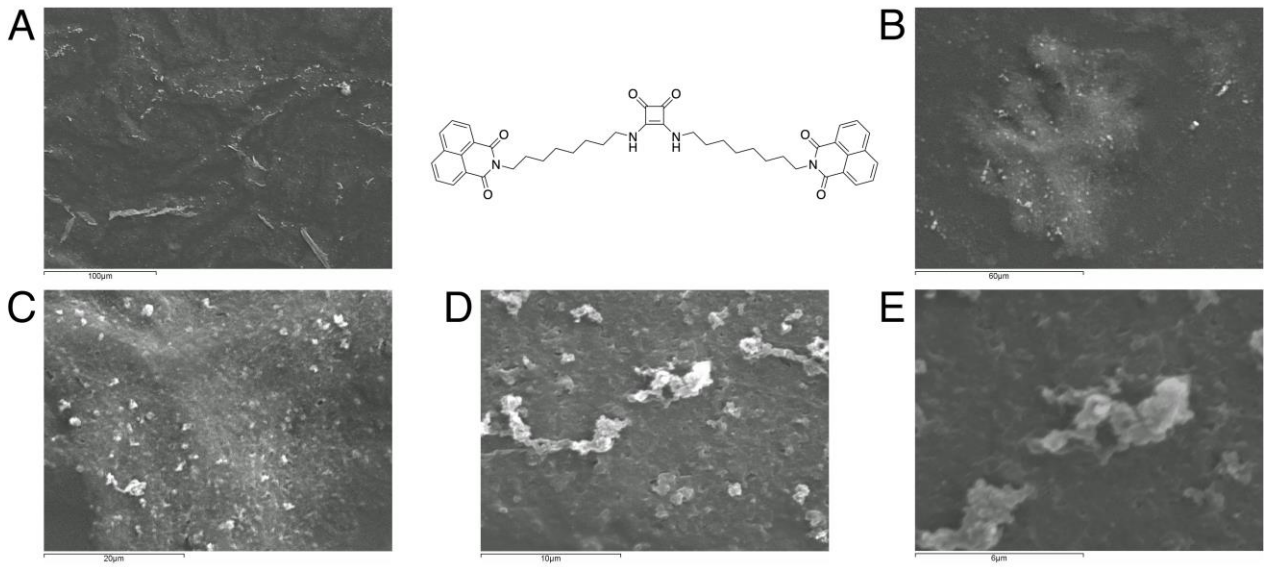

Figure A2.35: Scanning electron microscopy (SEM) images of compound **40** in DMSO:H_2O 50:50, **(A):** Mag x 400; **(B):** Mag x 1000; **(C):** Mag x 2500; **(D):** Mag x 5000; **(E):** Mag x 10000.

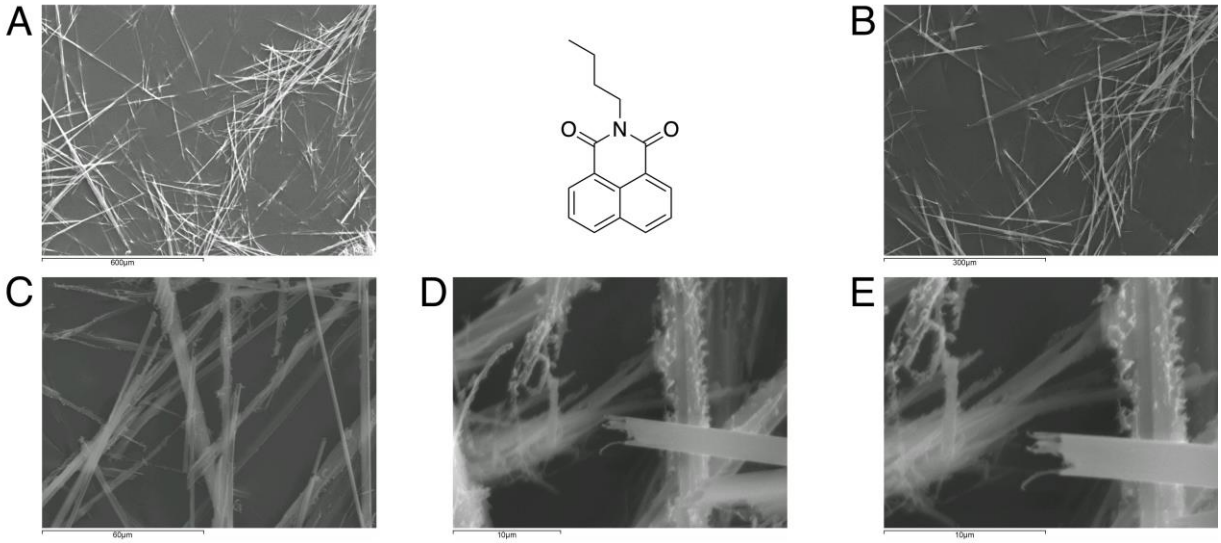

Figure A2.36: Scanning electron microscopy (SEM) images of compound **98** spotted with Au in DMSO:H_2O 50:50, **(A):** Mag x 100; **(B):** Mag x 200; **(C):** Mag x 1000; **(D):** Mag x 4000; **(E):** Mag x 6000.

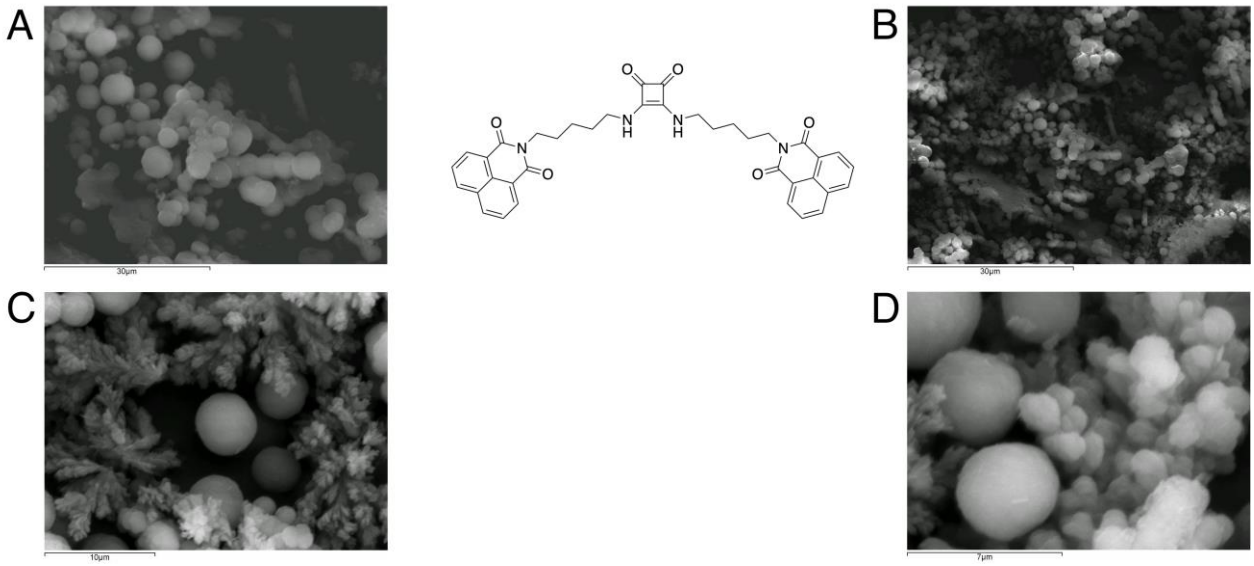

Figure A2.37: Scanning electron microscopy (SEM) images of compound **39** in DMSO:H_2O 50:50 (tilted), **(A):** Mag x 200; **(B):** Mag x 800; **(C):** Mag x 4000; **(D):** Mag x 8000.

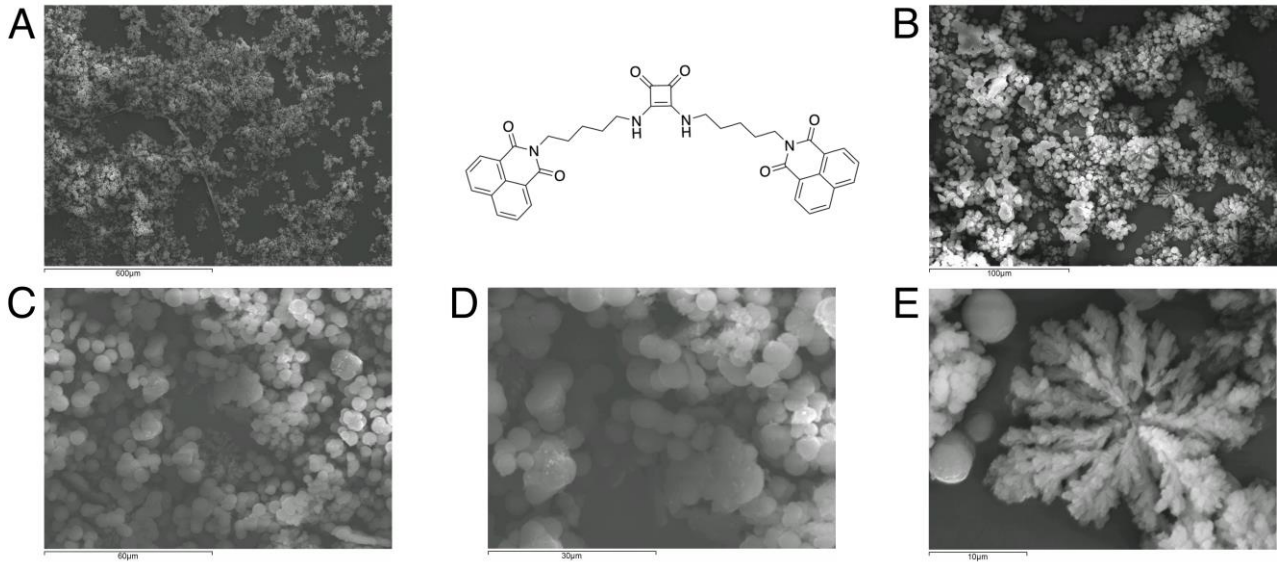

Figure A2.38: Scanning electron microscopy (SEM) images of compound **39** in DMSO:H_2O 50:50, **(A):** Mag x 100; **(B):** Mag x 500; **(C):** Mag x 1000; **(D):** Mag x 2000; **(E):** Mag x 3500.

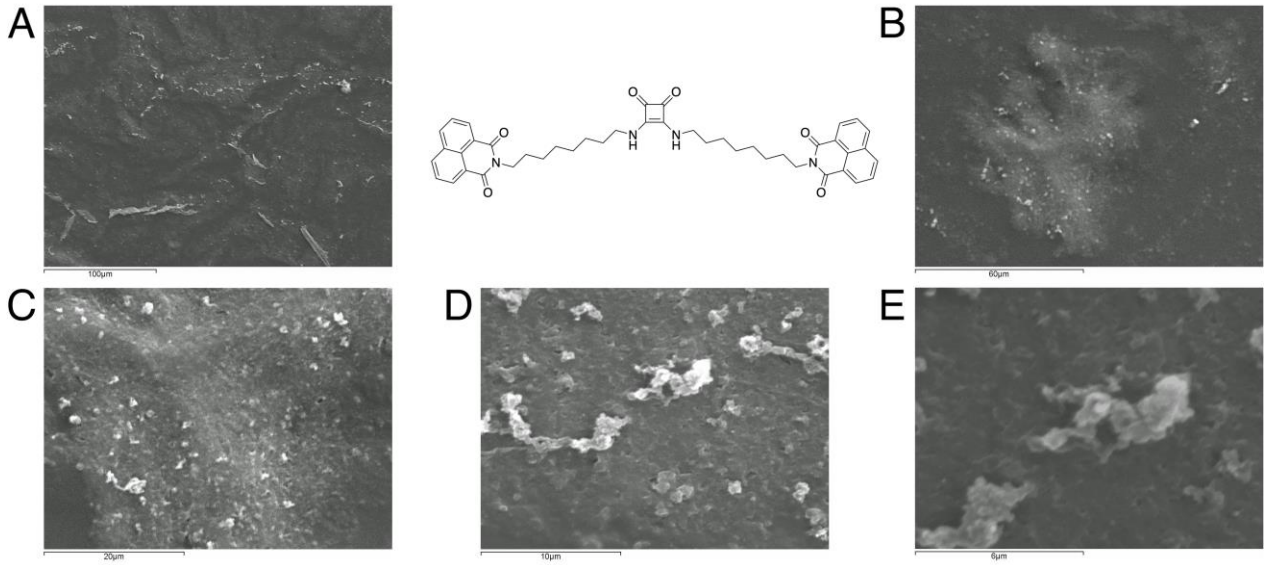

Figure A2.39: Scanning electron microscopy (SEM) images of compound **40** in DMSO:H_2O 50:50, **(A):** Mag x 400; **(B):** Mag x 1000; **(C):** Mag x 2500; **(D):** Mag x 5000; **(E):** Mag x 10000.

Appendix 3

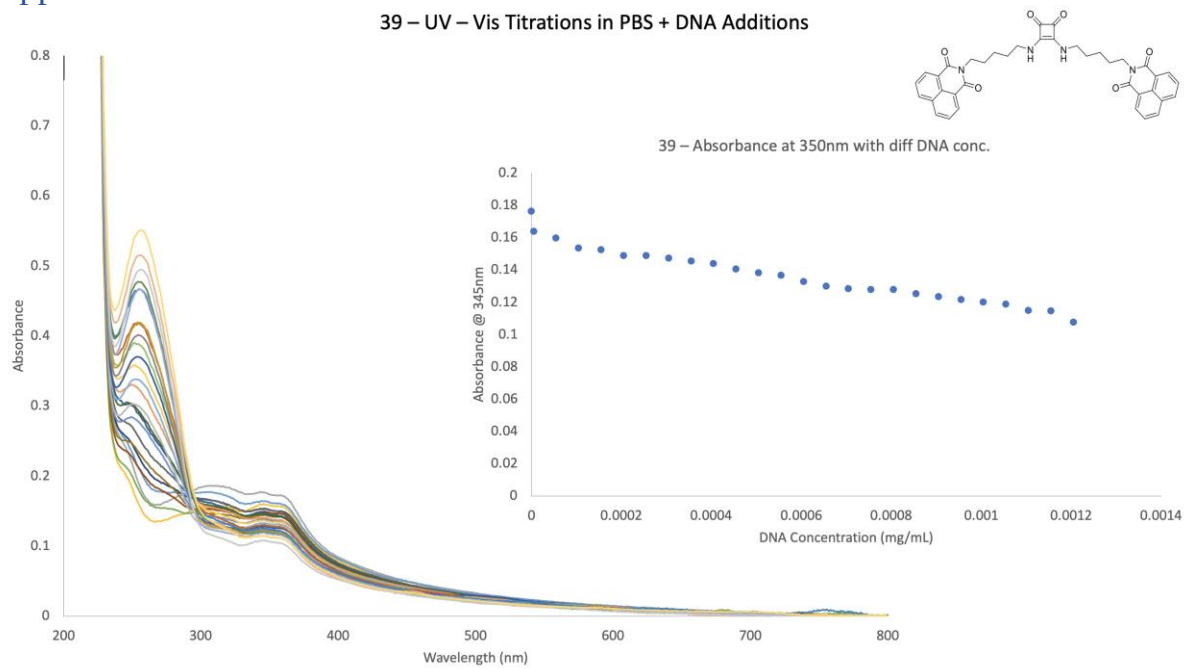

Figure A3.1: UV-VIS absorbance of **39**, with DNA concentration increases of (0.00005 mg/mL) for a total of 25 runs with DNA.

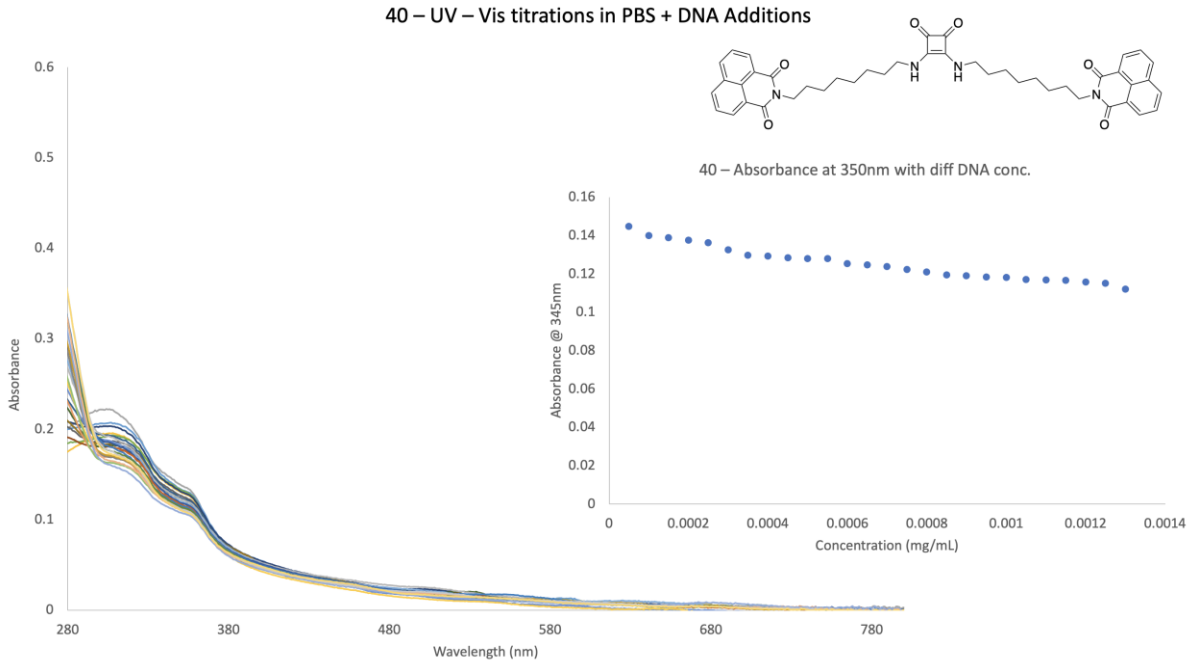

Figure A3.2: UV-VIS absorbance of **40**, with DNA concentration increases of (0.00005 mg/mL) for a total of 25 runs with DNA.

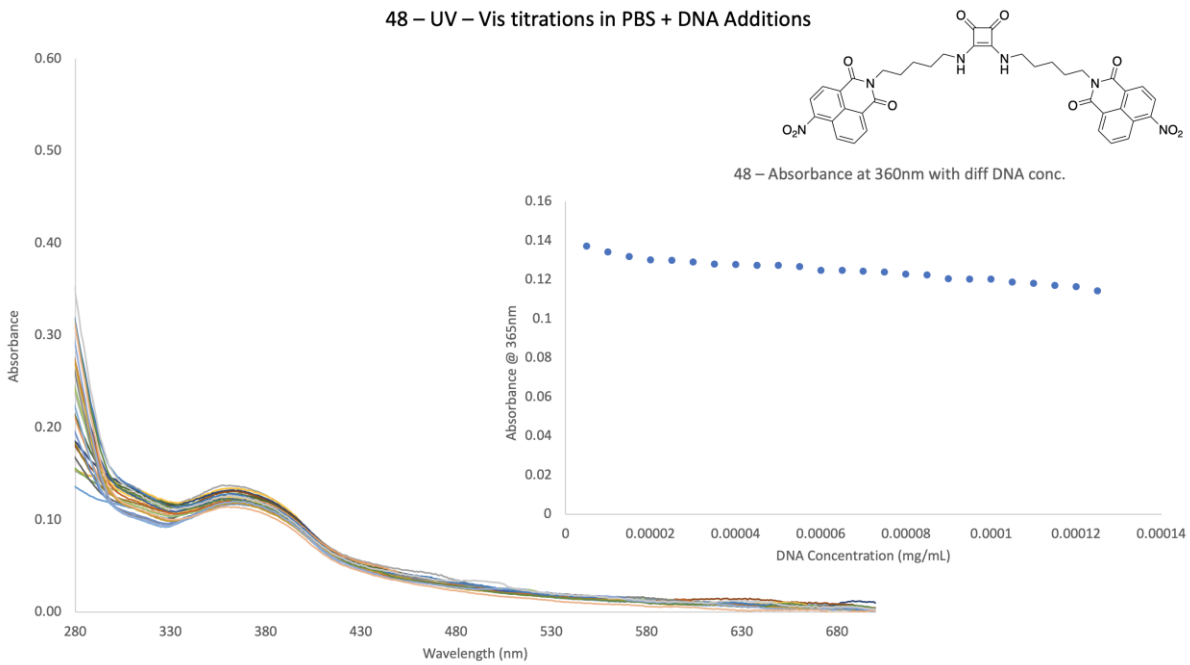

Figure A3.3: UV-VIS absorbance of **48**, with DNA concentration increases of (0.00005 mg/mL) for a total of 25 runs with DNA.

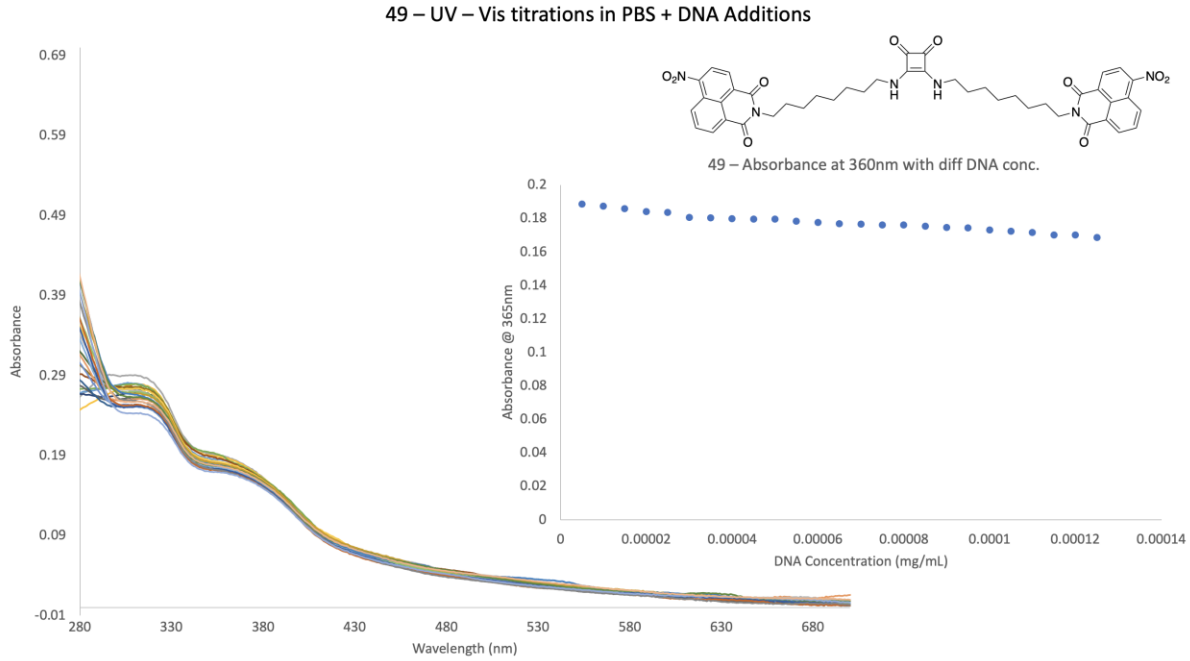

Figure A3.4: UV-VIS absorbance of **49**, with DNA concentration increases of (0.00005 mg/mL) for a total of 25 runs with DNA.

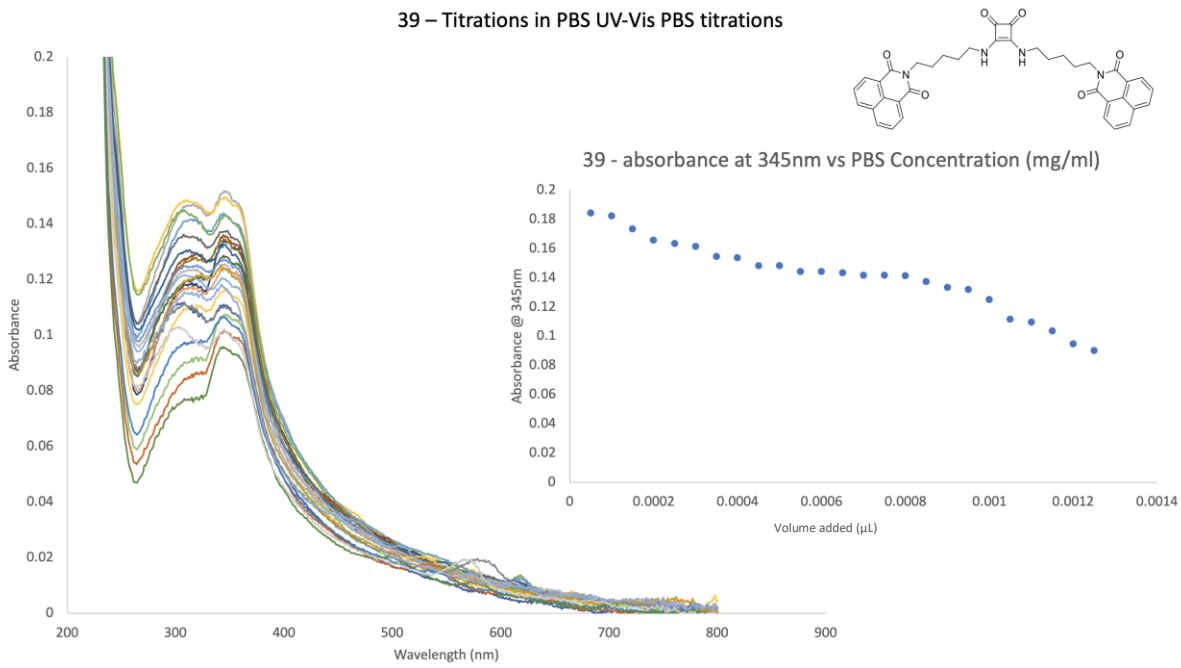

Figure A3.5: UV-VIS absorbance of **39**, with PBS equivalents of DNA concentration increases of (0.00005 mL) for a total of 25 runs with PBS.

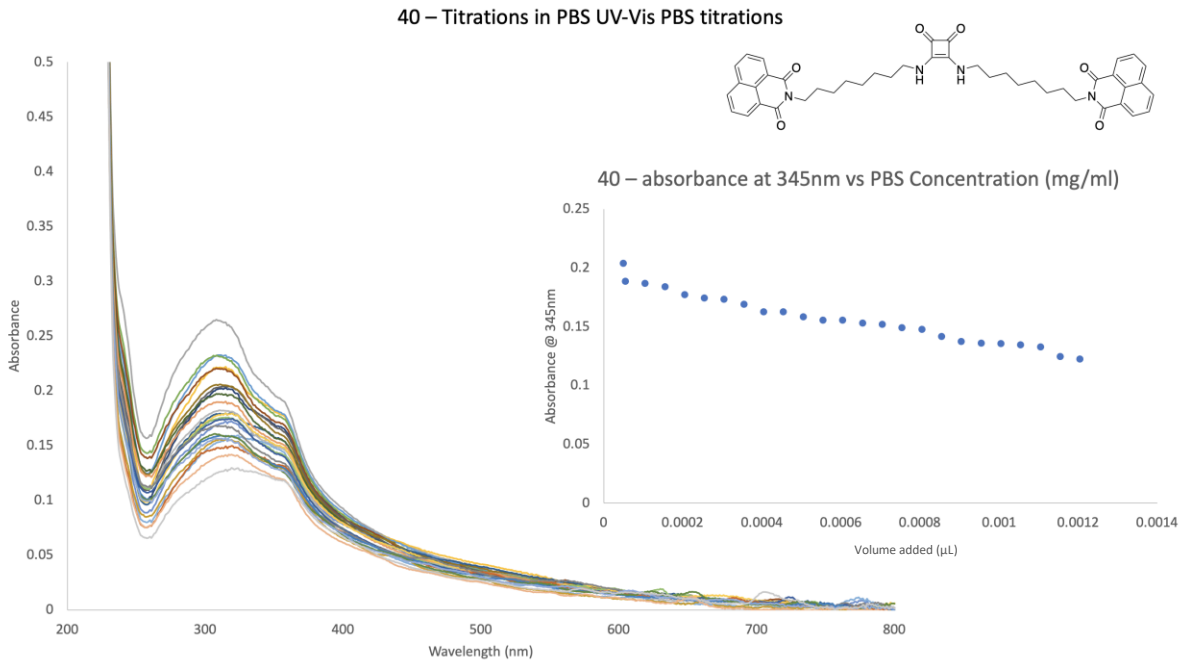

Figure A3.6: UV-VIS absorbance of **40**, with PBS equivalents of DNA concentration increases of (0.00005 mL) for a total of 25 runs with PBS.

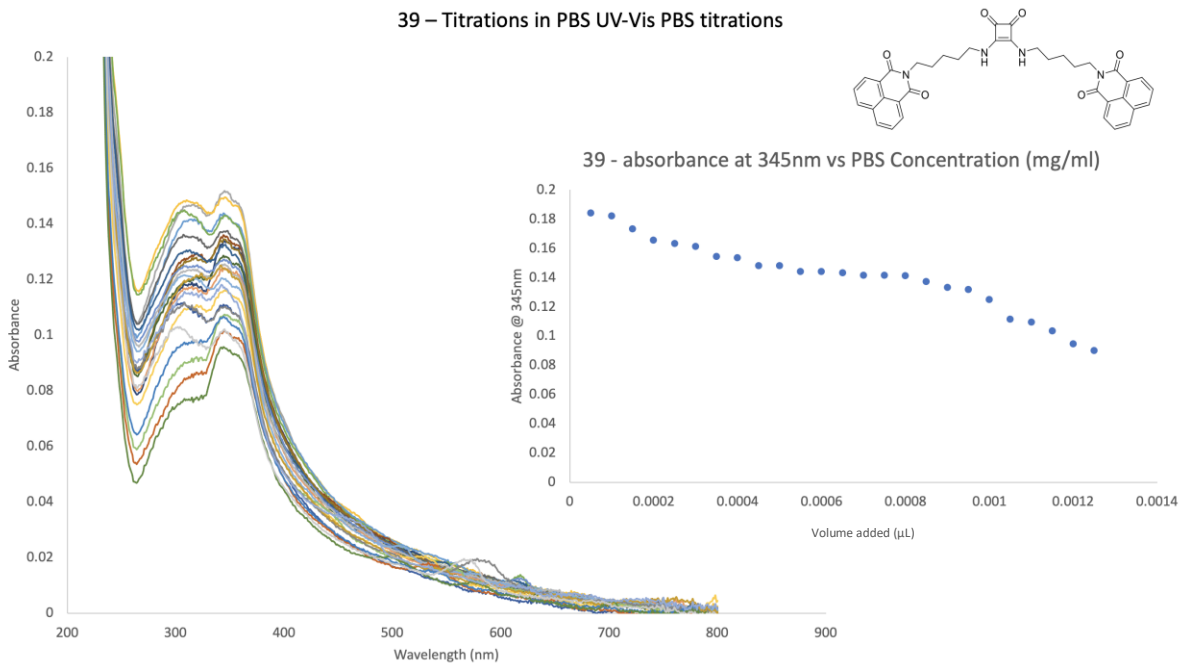

Figure A3.7: UV-VIS absorbance of **39**, with PBS equivalents of DNA concentration increases of (0.00005 mL) for a total of 25 runs with PBS.

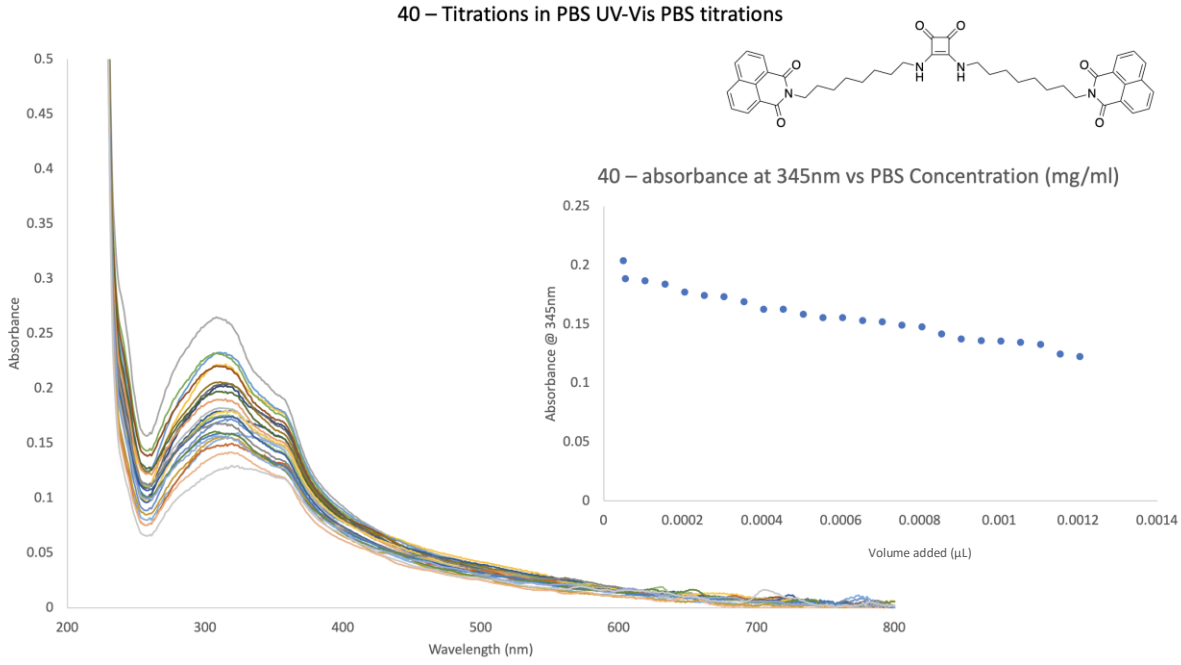

Figure A3.8: UV-VIS absorbance of **40**, with PBS equivalents of DNA concentration increases of (0.00005 mL) for a total of 25 runs with PBS.

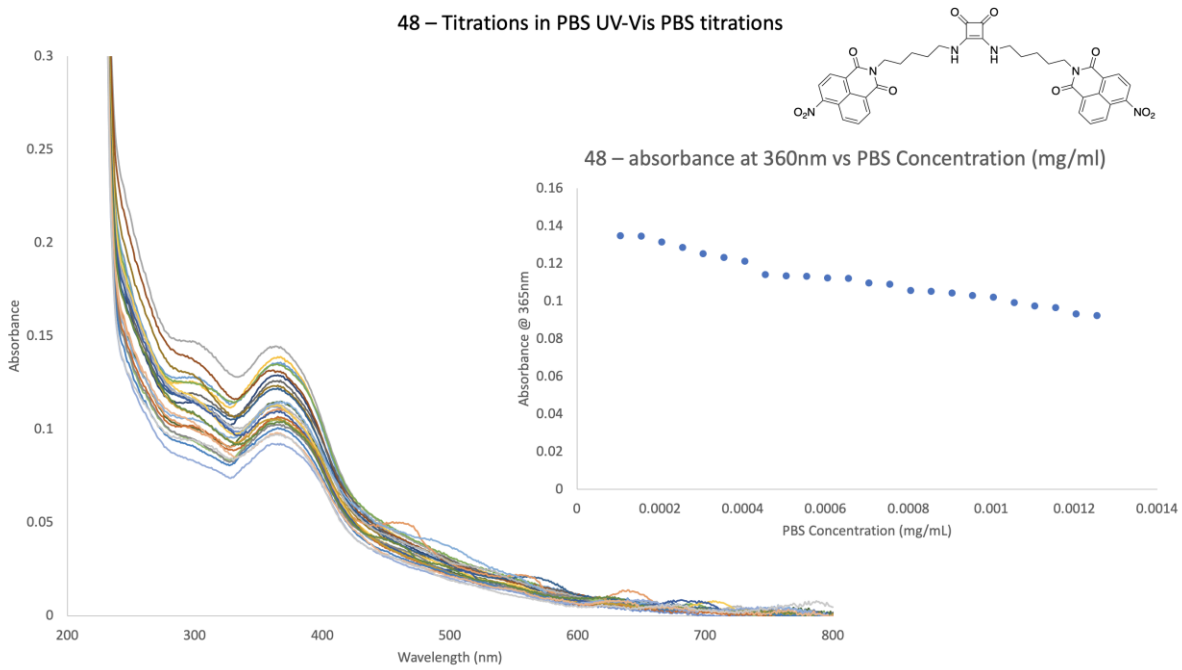

Figure A3.9: UV-VIS absorbance of **48**, with PBS equivalents of DNA concentration increases of (0.00005 mL) for a total of 25 runs with PBS.

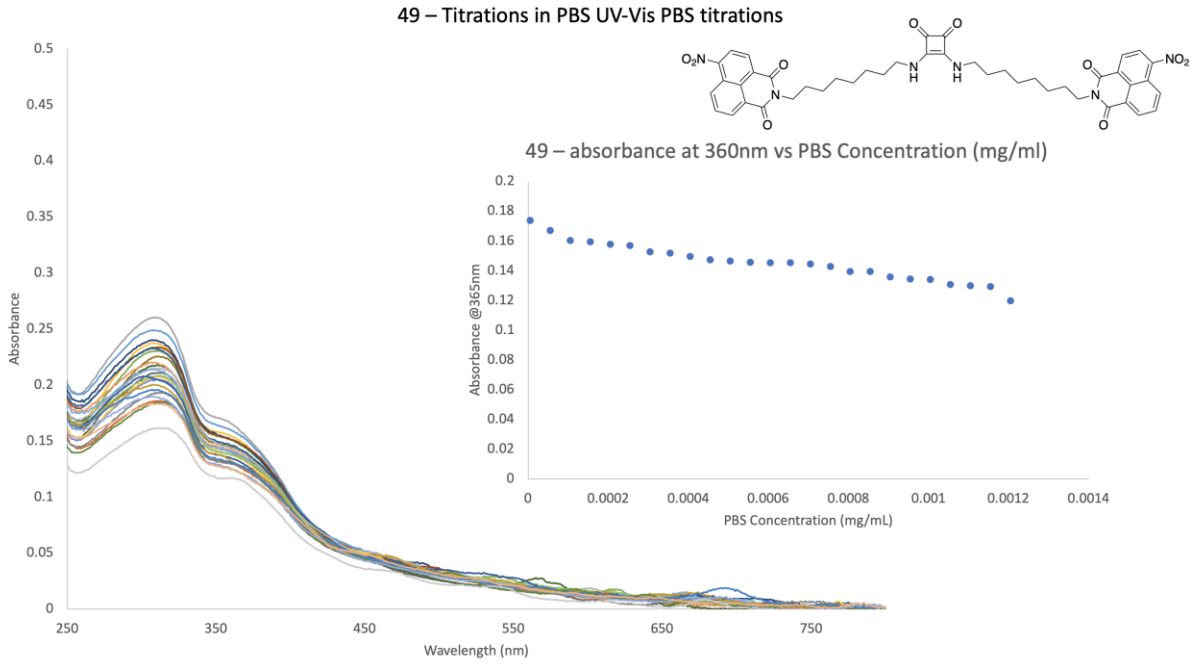

Figure A3.10: UV-VIS absorbance of **49**, with PBS equivalents of DNA concentration increases of (0.00005 mL) for a total of 25 runs with PBS.

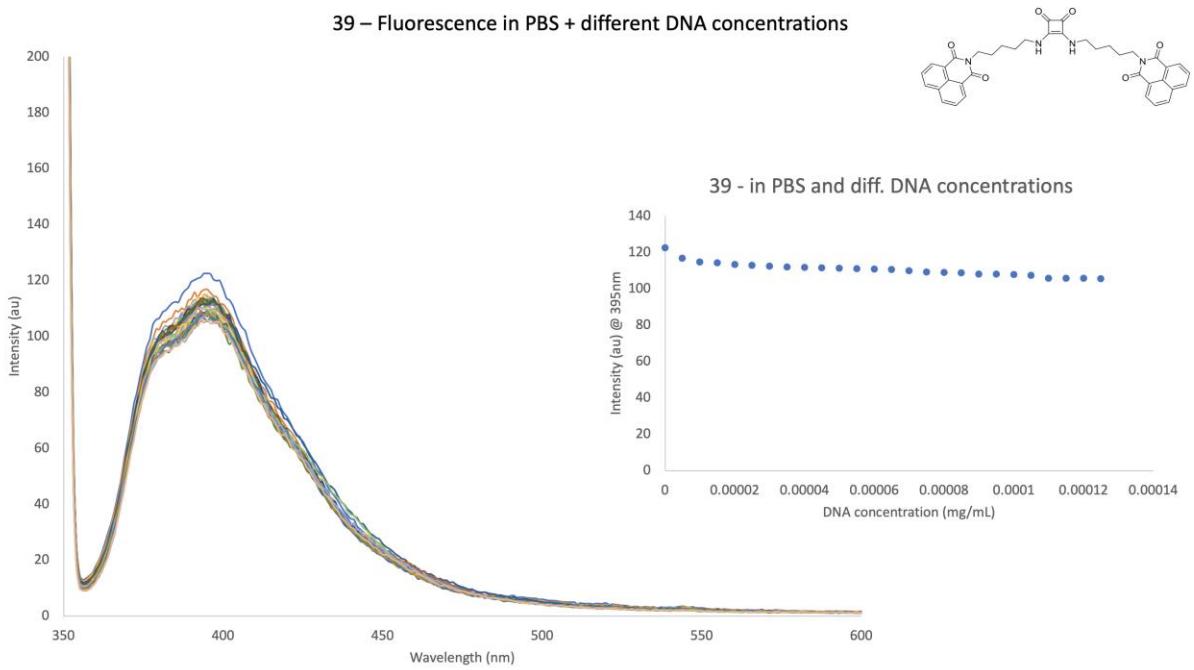

Figure A3.11: Fluorescence intensity of **39**, with an excitation wavelength at 400 nm, with an increased DNA concentration of (0.00005 mL) for a total of 25 runs in PBS.

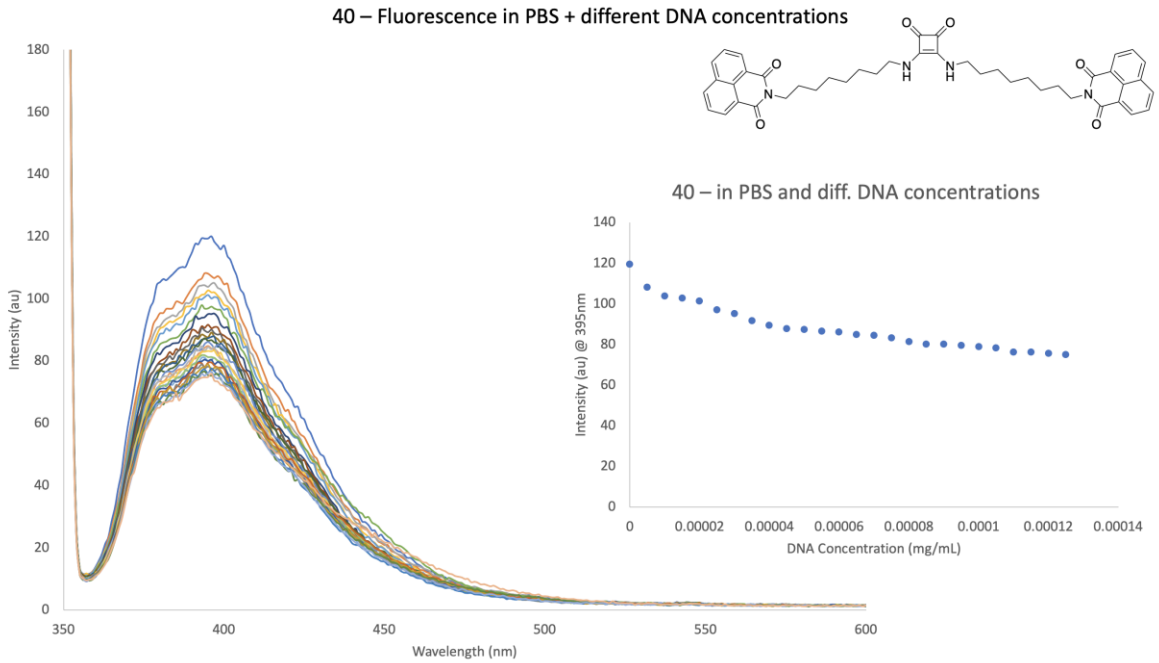

Figure A3.12: Fluorescence intensity of **40**, with an excitation wavelength at 400 nm, with an increased DNA concentration of (0.00005 mL) for a total of 25 runs in PBS.

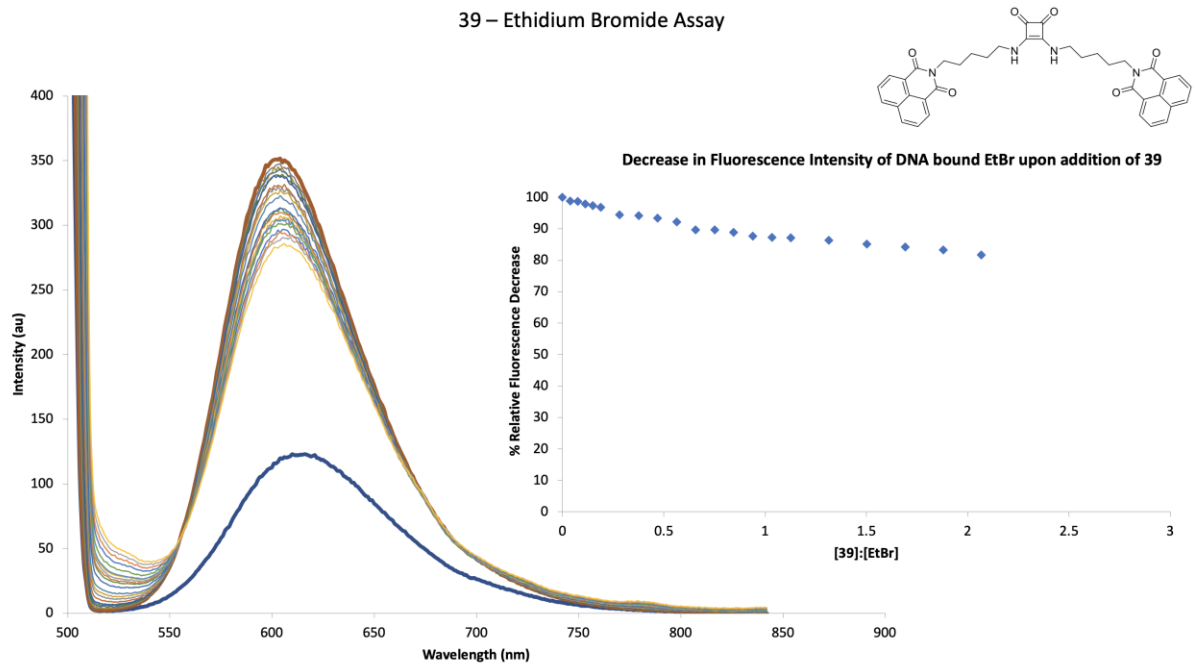

Figure A3.13: Ethidium Bromide displacement of various concentration of **39**, in DMSO with DNA, where the blue trace indicates the EtBr and DMSO solution without DNA and **39**.

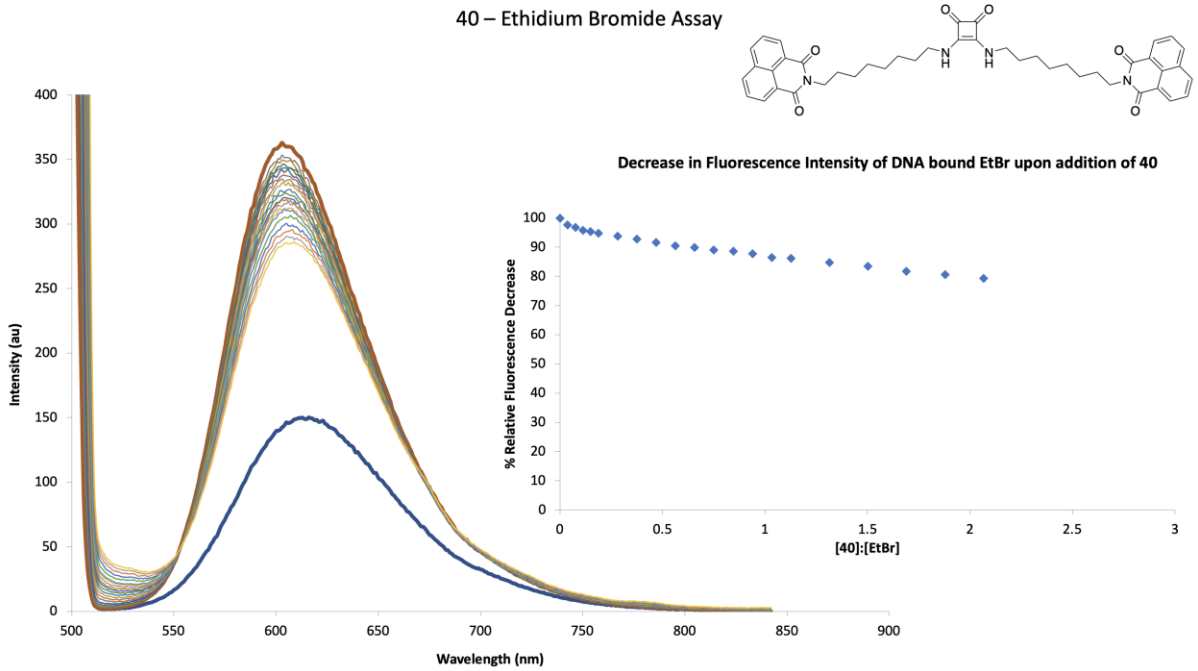

Figure A3.14: Ethidium Bromide displacement of various concentration of **40**, in DMSO with DNA, where the blue trace indicates the EtBr and DMSO solution without DNA and **40**.

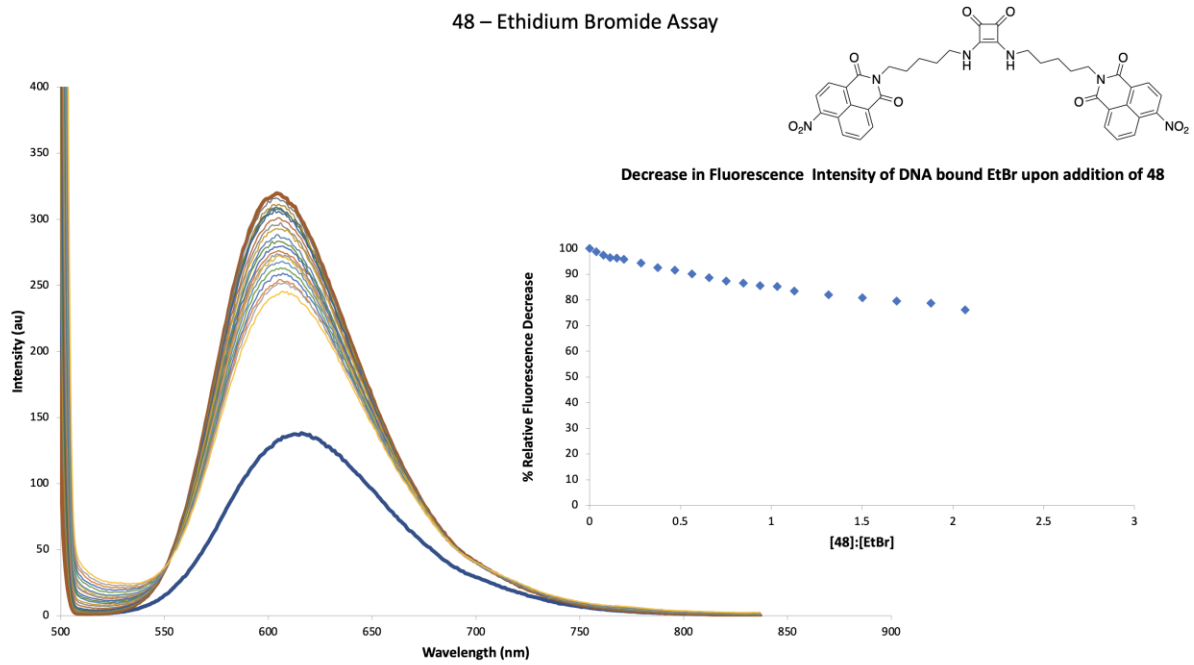

Figure A3.15: Ethidium Bromide displacement of various concentration of **48**, in DMSO with DNA, where the blue trace indicates the EtBr and DMSO solution without DNA and **48**.

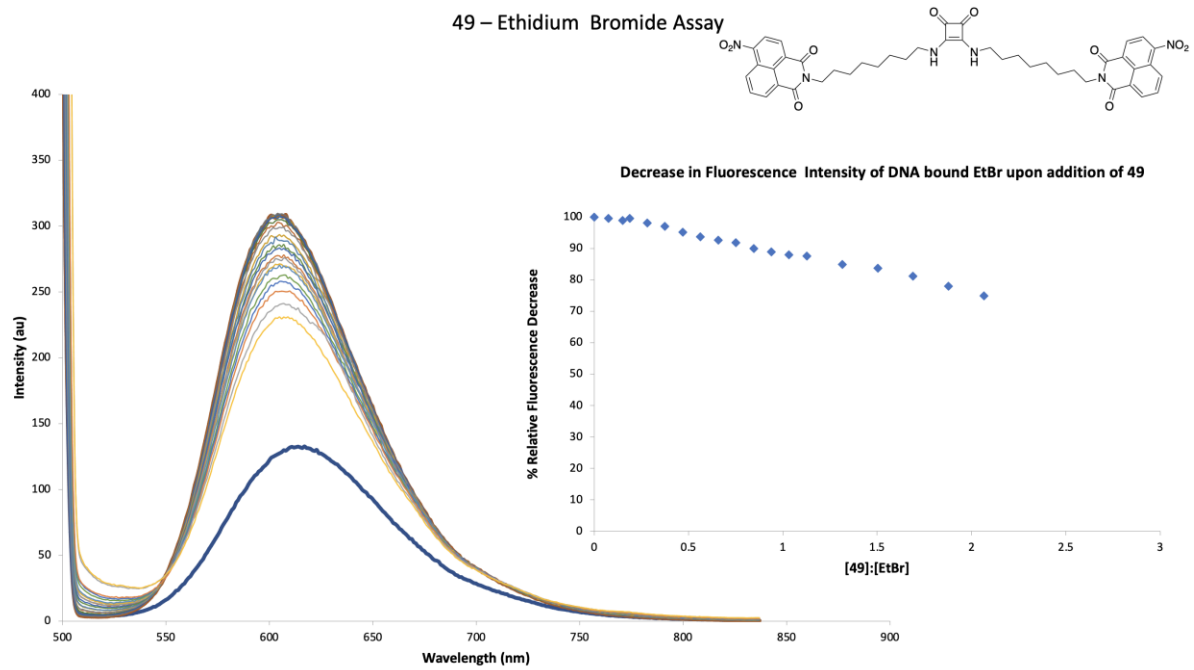

Figure A3.16: Ethidium Bromide displacement of various concentration of **49**, in DMSO with DNA, where the blue trace indicates the EtBr and DMSO solution without DNA and **49**.